LUND UNIVERSITY

Optimization of Low-Level Controllers and High-Level Polymer Grade Changes

Larsson, Per-Ola

2011

Document Version:
Publisher's PDF, also known as Version of record

Optimization of Low-Level Controllers and High-Level Polymer Grade Changes

Optimization of Low-Level Controllers and High-Level Polymer Grade Changes

Per-Ola Larsson

Department of Automatic Control
Lund University
Lund, November 2011

Department of Automatic Control
Lund University
Box 118
SE-221 00 LUND
Sweden

ISSN 0280–5316
ISRN LUTFD2/TFRT--1088--SE

Printed in Sweden by Media-Tryck.
Lund 2011

Till min familj

Abstract

Two design problems at different levels in the control hierarchy are considered; optimization of robust low-level controllers with constrained control signal activity and optimization of economical high-level polyethylene grade changes.

As for the first design problem, a constraint on control signal activity due to measurement noise is presented and used when optimizing and comparing PI/PID controllers with measurement filters of different orders. The results show increased performance when roll-off is present in the feedback loop and that similarities exist between PID and high-order Youla-parametrized controllers.

Robustness margins separating the dead-time uncertainty from other process uncertainties are presented. Methods to compute the margins, posed as optimization problems based on Nyquist diagram interpretations, are given.

PID and predictive PI (PPI) controllers with measurement filters are optimized and compared using the presented control signal activity constraint and robustness margins. The two controllers show similar performance on industrially representative processes, with a few exceptions where the PID controller outperforms the PPI controller.

Concerning the second design problem mentioned above, a cost function for optimization of economical polyethylene grade changes is proposed. It considers inflow costs, on- and off-grade polymer production revenues and polymer quality variable intervals to define on-grade production as well as economical incentives for on-target production.

Using the JModelica.org platform, several stationary operating points and dynamic grade changes are optimized with regards to economy. The optimizations are based on Modelica models of both a gas-phase polyethylene reactor and the polyethylene plant PE3 at Borealis AB. The results show that economically optimal grade changes can be divided into three phases with distinguishing features, and that the synchronization of control flows and the usage of recycle area off-gas flows are important.

A Modelica library for the plant PE3 at Borealis AB, including three reactors and three distillation columns, is presented.

Acknowledgments

First of all, I would like to thank my main supervisor Tore Hägglund and my co-supervisor Johan Åkesson. Both Tore and Johan have supported and guided me with great skills and I have thoroughly enjoyed working together with them.

Tore gave me the optimal amount of freedom, which I am most grateful for, when finding my own research directions as a fresh Ph.D. student. He was always very supportive of my ideas and his ability of finding simple solutions that are highly applicable in practice has been inspiring, not only for my research.

It is hard to find a more organized, thorough and enthusiastic supervisor than Johan. With great knowledge of optimization, he could always find a solution that gave us time for rewarding discussions on modeling and optimization, even with constraints on department time. His structured way of working has influenced me significantly and will definitely benefit me in the future.

I would like to acknowledge everyone who was involved in the PIC-LU project. In particular, I would like to thank Niklas Andersson at the Department of Chemical Engineering for great cooperation throughout the project, especially when constructing the Modelica library. Thanks also to Niclas Carlsson and Staffan Haugwitz at Borealis AB for answering numerous questions regarding polyethylene reactors and production.

I am most grateful for the comments and suggestions by Bo Bernhardsson, Per Hagander, Maria Henningsson and Anders Widd at my Thesis workshop. They influenced my research and work resulting in two of the papers in my thesis.

Parts of my thesis have been proof-read by Niclas Carlsson, Olof Garpinger, Staffan Haugwitz, Tore Hägglund, Bernt Lie, Eva Westin, Anders Widd and Johan Åkesson, and they are thanked for all the comments that have helped me improve the thesis' readability.

My time at the department has been joyful and rewarding in so many

ways. The social, creative and stimulating atmosphere engendered by this talented group of people will make you succeed and reach your goals. I will be very proud when I say that I received my Ph.D. from the Department of Automatic Control at Lund University.

The administrative and technical personnel at the department as well as the department board deserve special acknowledgments for making the department run so smoothly and successfully.

My fellow Ph.D. students are thanked for giving me many enjoyable lunches, coffee breaks, discussions and conference experiences. Special thanks go to: Erik Johannesson, for inspiring me with his sense of initiative and forward spirit. Karl Mårtensson, for sharing with me the experience of completing the Swedish classic circuit and the training behind it. Anders Widd, for the crucial C-sharing and for being a great neighbor, i.e., not getting tired of all my door-knocking and many questions.

It was a pleasure sharing office with Olof Garpinger during my first couple of years as a Ph.D. student and he is thanked for all the PID-related and unrelated discussions we had, also after he left the department.

Finally, I would like to thank my family and my friends for their support and encouragement and Martina for her love and understanding during the writing of this thesis.

Per-Ola

Financial Support

The Swedish Foundation for Strategic Research in the framework of Process Industry Centre at Lund University (PIC-LU) is gratefully acknowledged for financial support.

Contents

Preface

Contents and Contributions of the Thesis

This thesis consists of two introductory chapters, six papers and one supplement. This section describes mainly the two chapters, the contributions of each paper and the contributions made by each author of the papers. It also gives a brief description of the supplement and provides a list of additional publications by the author of the thesis.

Chapter 1 – Optimization of Low-Level Controllers

This chapter provides brief overviews of the PID controller and the predictive PI controller. Measures of performance, robustness and noise sensitivity, useful at optimization of low-level controllers and measurement filters, are reviewed to give a background to the contributions of papers I–III. This chapter gives also a more detailed overview of the contributions of the papers I–III and suggestions on future work.

Chapter 2 – Optimization of High-Level Polymer Grade Changes

An introduction to why and how grade changes are performed by polymer producers today is given in this chapter. An overview of the modeling language, optimization methodology and tools used when optimizing grade changes in papers IV–VI is also provided. This chapter gives also a more detailed overview of the contributions of the papers IV–VI and suggestions on future work.

Paper I

Larsson, P. and T. Hägglund (2011): "Control Signal Constraints and Filter Order Selection for PI and PID Controllers." In *Proceedings of the 2011 American Control Conference*, San Francisco, USA.

This paper presents a constraint on the control signal activity due to measurement noise. PI and PID controllers, together with measurement filters of different orders, are designed via optimization with regards to load disturbance attenuation, the presented constraint and robustness requirements related to process uncertainties. The implications of using measurement filters of different orders are presented. For performance comparison, optimal linear controllers of high orders are designed via Youla parametrization.

The control signal constraint was derived by P. Larsson. The optimization framework for PI and PID controllers and measurement filters is work of P. Larsson, while the optimization framework for Youla parametrized controllers is work of A. Wernrud, see citation in the paper. The optimizations of PI, PID and Youla parametrized controllers and measurement filters, and the analysis of the results, were performed by P. Larsson. T. Hägglund provided valuable comments during the work.

Paper II

Larsson, P. and T. Hägglund (2009): "Robustness Margins Separating Process Dynamics Uncertainties." In *Proceedings of the 2009 European Control Conference*, Budapest, Hungary.

This paper presents robustness margins that separate the process dead-time uncertainty from other process uncertainties. The robustness margins are based on extended sensitivity functions that depend on the dead-time uncertainty. The margins can be shown graphically in a Nyquist diagram as frequency dependent prohibited areas for the Nyquist curve. Methods to calculate the robustness margins are presented and based on the graphical interpretations.

The derivations of the robustness margins were performed by P. Larsson. The graphical interpretations and the methods to calculate the margins are also work by P. Larsson. T. Hägglund provided support and insight on process uncertainties during the work.

Paper III

Larsson, P. and T. Hägglund (2011): "Comparison Between Robust PID and Predictive PI Controllers with Constrained Control Signal Activity." Submitted to the *2012 IFAC Conference on Advances in PID*, Brescia, Italy.

This paper presents a comparison between PID and predictive PI controllers with associated measurement filters. The controllers and filters are optimized for load disturbance attenuation with constraints on control signal activity due to noise and robustness towards process uncertainties

using the constraint and margins presented in Paper I and II, respectively. The differences between the prediction methods associated with the controllers are shown and the performances of the two controllers on industrially representative processes are compared.

The optimization framework used when designing optimal controllers and filters is work by P. Larsson. The analysis of the results was performed by P. Larsson, while T. Hägglund contributed with support during the work and with his experience of both the controllers.

Paper IV

Larsson, P., J. Åkesson, S. Haugwitz, and N. Andersson (2011): "Modeling and Optimization of Grade Changes for Multistage Polyethylene Reactors." In *Proceedings of the 18th IFAC World Congress*, Milano, Italy.

This paper presents a brief overview of the models representing the three Borealis Borstar® polyethylene reactors, implemented in a Modelica library. DAE initialization problems and a quadratic optimization problem for a grade change are solved using the JModelica.org platform. The optimization results are shown and briefly discussed. The paper provided an important evaluation of the optimization methodology and tools considering the applicability to large-scale systems.

P. Larsson and N. Andersson constructed the Modelica library for the three reactors. Models for solving DAE initialization problems and the quadratic grade change optimization problem were built by P. Larsson. Manual scaling of model variables, optimization of the grade change and discussion of the results were provided by P. Larsson. Development of JModelica.org and helpful comments regarding optimization and Modelica library structuring were given by J. Åkesson. S. Haugwitz provided industrial insight and help regarding the reactor models.

Paper V

Larsson, P., J. Åkesson, and N. Andersson (2011): "Cost Function Design for Economically Optimal Grade Changes for a Polyethylene Gas-Phase Reactor." To appear in *Proceedings of the 50th Conference on Decision and Control and European Control Conference*, Orlando, USA.

This paper presents a cost function that considers inflow costs and revenues from production of on- and off-grade polymer. It uses the polymer quality variable intervals for defining on-grade polymer and adds economical incentives to produce on-target polymer. Additionally, the cost function includes a preparatory time interval prior defined transition time that may be utilized for economical preparations of reactor conditions. Us-

ing JModelica.org, several stationary operating points and grade changes are optimized for a previously published polyethylene gas-phase reactor model. The implications of using the designed cost function are shown and discussed.

P. Larsson implemented the polyethylene gas-phase reactor model in a Modelica library and constructed also the optimization models. The cost function for economical grade changes was designed by P. Larsson. All optimizations, both stationary and dynamic, and analysis of the associated results, were also made by P. Larsson. J. Åkesson and P. Larsson had several discussions concerning the design of the cost function. J. Åkesson provided also with development and support of the JModelica.org platform.

Paper VI

Larsson, P., J. Åkesson, N. Carlsson, and N. Andersson (2011): "Model-Based Optimization of Economical Grade Changes for the Borealis Borstar® Polyethylene Plant." Submitted to *Computers & Chemical Engineering*.

This paper presents grade change optimizations with regards to economy on a model of a Borealis Borstar® polyethylene plant, including three reactors and three distillation columns. More detailed descriptions of the Borealis Borstar® reactor models than in Paper IV are provided together with models of the distillation columns. The plant is modeled using the Modelica language and the Modelica library in Paper IV is extended to also include the distillation columns. The cost function presented in Paper V is extended and optimizations of two stationary operating points and two grade changes with regards to economy are performed. The grade changes are thoroughly reviewed considering characteristics and usage of control flows. The paper shows that the considered models, cost function, optimization methodology and tools are appropriate to use at large-scale optimization.

The implementation of the reactor models in the Modelica library and the library structure are results of joint work of P. Larsson and N. Andersson, while the implementation of the distillation column models was made by P. Larsson. The extension of the cost function in Paper V was made by P. Larsson. Construction of optimization models, optimization of grade changes, and analysis of the optimization results, are work performed by P. Larsson. N. Carlsson helped clarifying the practical operation of the plant and provided an industrial view of the results. Except for development and support of the JModelica.org platform, J. Åkesson gave P. Larsson helpful comments regarding the performed optimizations.

Supplement A – `PE3Lib` – A Modelica Library for the Plant PE3 at Borealis AB

This supplement gives a description of the Modelica library `PE3Lib` for the plant PE3 at Borealis AB. The library is used in Paper IV and VI when optimizing grade changes.

Additional Publications

Below is a list of additional publications by the author of the thesis that were chosen not to be included in the thesis.

Larsson, P. and R. Braun (2008): "Construction and Control of an Educational Lab Process – The Gantry Crane." In *Proceedings of Reglermöte 2008*, Luleå, Sweden.

Larsson, P. and T. Hägglund (2008): "Relations Between Control Signal Properties and Robustness Measures." In *Proceedings of the 17th IFAC World Congress*, Seoul, Korea.

Larsson, P., N. Andersson, J. Åkesson, and S. Haugwitz (2010): "Modelica Based Grade Change Optimization for a Polyethylene Reactor." In *Proceedings of the 9th International Symposium on Dynamics and Control of Process Systems*, Leuven, Belgium.

Larsson, P., N. Andersson, J. Åkesson, and S. Haugwitz (2010): "Modeling and Optimization of Grade Changes for a Polyethylene Reactor." In *Proceedings of Reglermöte 2010*, Lund, Sweden.

Larsson, P., J. Åkesson, S. Haugwitz, and N. Andersson (2010): "Modeling and Optimization of Grade Changes for Multistage Polyethylene Reactors." In *Proceedings of the 16th Nordic Process Control Workshop*, Lund, Sweden

Andersson, N., P. Larsson, J. Åkesson, S. Haugwitz and B. Nilsson (2011): "Calibration of a Polyethylene Plant for Grade Change Optimizations." In *Proceedings of the 21st European Symposium on Computer-Aided Process Engineering*, Chalkidiki, Greece.

Errata and Clarifying Notes

Errata and clarifying notes for Paper II and IV are found on the backs of the corresponding front covers.

1

Optimization of Low-Level Controllers

1.1 Problem Formulation

Many plants today have several hierarchical levels of control. At the top level, plant-wide optimization is performed, finding optimal steady state production of the plant. At a lower level, production unit optimizers are present, considering steady state operation of each single unit, often using more detailed models than at the top level. Set-points are sent from the unit optimizer to the dynamic controller of the unit at a lower level, such as a model predictive controller (MPC). At the lowest level of control, set-points are received by the low-level controllers from the dynamic controller. These set-points can be time varying or constant, i.e., the low-level controllers are in servo or regulatory mode. Additionally, the set-points may e.g., also be set manually or by other low-level control loops. The low-level controllers are most often of simple structure, such as PI, PID, additional lead-lag filters, and dead-time compensating controllers, combined in different control structures and used with e.g., logics, sequential functions and selectors. These control structures are sufficient for most of the low-level control problems.

At each control level, it is often assumed that the control at the underlying levels are perfect. Even though e.g., an MPC is perfectly designed, the performance of the production unit may be poor due to insufficient performance of the low-level controllers. Thus, as expressed in [Åström and Hägglund, 2006], low-level controllers can be viewed as the “bread and butter” of control engineering.

In many plants in for instance pulp and paper and chemical industry, the number of low-level control loops are overwhelming and the controllers

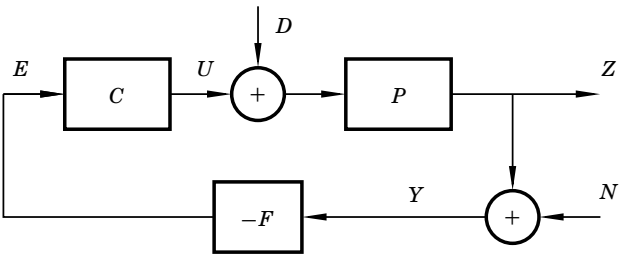

Figure 1.1 Control loop with process P, controller C and measurement filter F.

are tuned by the maintenance personnel and operators. This puts several requirements on the low-level controllers. The maintenance personnel and operators cannot be required to have expertise in control engineering, so the tuning of the controllers must be simple, and desirably, made in an automatic fashion. If the automatic tunings gives non-satisfying results, it should be easy to manually re-tune the low-level controllers. This requires the number of parameters to set in the controller to be small and have intuitive effect on the control. Due to the number of control loops, the time it takes for tuning a low-level controller is also of essence.

In this thesis, only the regulatory problem of the low-level control loop will be considered, that is, keeping the process output at a constant desired value. This is not a restriction as set-point responses can be tuned for by using a feed-forward filter on the set-point before being fed to the controller [Åström and Hägglund, 2006]. Apart from the above mentioned requirements on the controller, the main concerns when designing regulatory low-level controllers are

- disturbance rejection
- robustness towards process uncertainties
- measurement noise sensitivity of the control signal

A block diagram of a low-level control loop in regulatory mode with constant set-point, for simplicity set equal to 0, is found in Figure 1.1. The process P is controlled by the low-level controller C, which has a measurement filter F. The controlled variable, i.e., the process output, is denoted Z and the measurement Y is corrupted with noise N. The input to the controller is the control error E and the output is the control signal U. A load disturbance D is assumed to act on the process input. The design problem of the controller C and the measurement filter F considered in this thesis is to make the process output to be as close as possible to 0, despite the presence of load disturbances, measurement noise and uncertainties in the process.

Robustness towards process uncertainties can be expressed using the sensitivity and complementary sensitivity functions, defined as

$$S = \frac{1}{1 + PCF} \tag{1.1}$$

$$T = \frac{PCF}{1 + PCF}, \tag{1.2}$$

respectively. They are uniquely given by the open loop transfer function PCF. The process output response to load disturbances and the control signal response to measurement noise, are found as

$$Z = \frac{P}{1 + PCF} D = PSD \tag{1.3}$$

$$U = -\frac{CF}{1 + PCF} N = -CFSN. \tag{1.4}$$

Thus, all the three main concerns in a regulatory low-level control loop can be considered by using the transfer functions S, T, PS and CFS, which are all affected by the controller C and the measurement filter F. In fact, as no set-point is considered, the closed loop system is completely characterized by the four transfer functions [Åström and Hägglund, 2006]. In the design problem of C and F, which is the main topics of Paper I and III, properties of the four transfer functions should thus be specified.

The remainder of this chapter will give an overview of two low-level controllers; the PID controller used in Paper I and III and the predictive PI controller used in Paper III. It will also present different measures of the load disturbance rejection performance, i.e., the response of the transfer function PS, robustness towards process uncertainties using S and T, and also the noise sensitivity of the control signal using the transfer function CFS. Some of the measures presented are used directly in the controller and measurement filter designs in Paper I and III, while additional measures are presented in Paper I and II.

1.2 Low-Level Controllers

This section will give a short introduction to the PID and predictive PI controllers. Co-design of PID controllers and measurement filters is considered in Paper I, while both PID and predictive PI controllers are co-designed with measurement filters in Paper III, where also a performance comparison between the two controllers is made.

PID

The PID controller structure considered throughout this thesis is the standard parallel form where the control signal $u(t)$ is given by

$$u(t) = K\left(e(t) + \frac{1}{T_i}\int_{-\infty}^{t} e(\tau)\,d\tau + T_d\frac{de(t)}{dt}\right), \tag{1.5}$$

where K, T_i and T_d are the proportional gain, integral time and derivative time, respectively, and $e(t)$ is the control error. A PI controller is obtained by setting $T_d = 0$. The proportional part considers the current control error, while the integral part considers the history of the control error. The derivative part, together with the proportional part, introduce a linear prediction of the control error with prediction length T_d. This is seen from a Taylor series expansion of the control error $e(t + T_d)$ as

$$e(t + T_d) \approx e(t) + T_d\frac{de(t)}{dt} + \ldots, \tag{1.6}$$

where the two first terms are multiplied by the proportional gain K in the PID controller.

The drawback of high gain for high-frequency signals and noise sensitivity introduced by the ideal derivative in the PID controller is often suppressed to some extent by introducing a filter only on the derivative part. Another common choice, which is used in this thesis, is to filter the measurement signal before it is used by the controller, as in the control loop in Figure 1.1. This is motivated by the noise sensitivity introduced by the proportional gain as well.

Predictive PI

An alternative to the linear prediction in the PID controller is prediction by simulation of an internal model of the process inside the controller, using the control signal applied to the process. Controllers preforming this type of prediction are known as dead-time compensating controllers. The first such structure was presented in [Smith, 1957], now commonly known as the Smith predictor. The predictive PI (PPI) controller is a simplified form of the Smith predictor, and its structure is here described in the light of the Smith predictor structure.

The main idea behind the Smith predictor is to separate the process model $\hat{P}$ into a dead-time free part and a pure dead-time as

$$\hat{P} = \hat{P}_0 e^{-sL}, \tag{1.7}$$

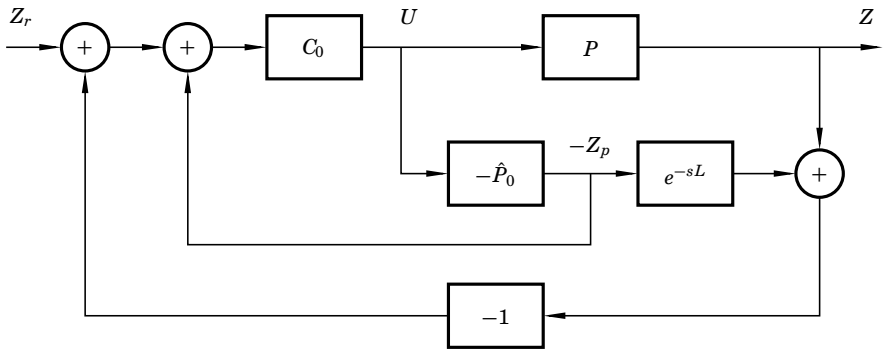

Figure 1.2 Control loop with a Smith predictor.

and to use the simulated output of $\hat{P}_0$ as a prediction of the process output L time units ahead. The Smith predictor structure can be seen in the control loop in Figure 1.2, where C_0 is e.g., an ordinary PI or PID controller and P is the process. If $\hat{P}_0$ is a perfect model of the delay free part of P, then the output z_p is a perfect prediction of the process output z, where z_p and z are the time-domain equivalents of Z_p and Z, respectively. The prediction may thus be used instead of the true process output and is fed back to the controller C_0. However, as $\hat{P}_0$ may not be a perfect model of the delay free part of the process and disturbances may act on the process, an outer feedback loop is also used, comparing the process and model output.

The Smith predictor structure can be interpreted as an ordinary controller C_0 with a feedback structure around it, composed of the difference between the process model and the delay free part of the process model, as

$$C = \frac{C_0}{1 + C_0\hat{P}_0(1 - e^{-sL})}. \tag{1.8}$$

It can also be viewed as a controller in cascade with a predictor as $C = C_0 C_{\text{pred}}$, where the predictor is

$$C_{\text{pred}} = \frac{1}{1 + C_0\hat{P}_0(1 - e^{-sL})}. \tag{1.9}$$

If C_0 is a PI controller, the predictor corresponds to the derivative part in a PID controller, with the difference that the prediction is model-based instead of a linear extrapolation. This is clearly seen in the input-output relation of the Smith predictor, as it may be written as

$$U = C_0\left(E - \hat{P}_0(1 - e^{-sL})U\right), \tag{1.10}$$

where U and E are the control signal and control error, respectively. The term $\hat{P}_0(1 - e^{-sL})U$ can be interpreted as the predicted output due to the control signal during the time interval $(t - L, t)$, and is used by the controller C_0.

The predictor C_{pred} can yield large phase advance which is useful when compensating for process dead-time. However, it may come with the price of unstable poles, and also high sensitivity towards modeling error in the dead-time if the controller C_0 is designed for high bandwidth of the nominal closed-loop system, see for instance [Palmor, 1980]. Thus, designing a Smith predictor requires careful robustness considerations.

The simplest and most used Smith predictor has a PI controller and a first order system with dead-time as process model, i.e.,

$$\hat{P} = \frac{K_p}{sT + 1} e^{-sL}. \tag{1.11}$$

Thus, adding prediction capability to a PI controller, if not considering measurement filter, requires three additional parameters to be determined for the Smith predictor, i.e., K_p, T and L, while for a derivative part only T_d requires to be determined. Hence, the operational complexity of a Smith predictor is significantly higher than for a PID controller.

Simplifications of the Smith predictor structure, yielding fewer parameters to set, have been introduced. One such structure is the PPI controller, also known as the PI_τ controller, see [Hägglund, 1996] and [Shinskey, 1994]. In this structure, the process model parameters K_p and T are related to the parameters of the controller C_0 as

$$K_p = 1/K, \qquad T = T_i. \tag{1.12}$$

This decreases the number of parameters to be determined to three, which is equal to the number of parameters in the PID controller.

The transfer function of the PPI controller can, as for the Smith predictor, be divided into an ordinary PI controller C_0 and predictive part C_{pred} defined as

$$C_{\text{pred}} = \frac{1}{1 + \dfrac{1}{sT_i}\left(1 - e^{-sL}\right)}. \tag{1.13}$$

The controller is easily implemented by adding the dead-time L into the positive feedback in a PI controller, see Figure 1.3. The input-output relation of the predictive PI controller becomes

$$\begin{aligned} U &= K\left(1 + \frac{1}{sT_i}\right)\left(E - \frac{K^{-1}}{sT_i + 1}\left(1 - e^{-sL}\right)U\right) \\ &= K\left(1 + \frac{1}{sT_i}\right)E - \frac{1}{sT_i}\left(1 - e^{-sL}\right)U, \end{aligned} \tag{1.14}$$

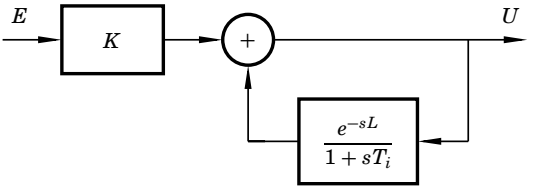

Figure 1.3 Structure of the predictive PI controller.

where U and E are the control signal and control error, respectively.

If K and T_i are not chosen explicitly according to an estimated process model, the prediction is no longer performed using a model of the process, as seen in the input-output relation. The PPI controller is not constrained to model-matching. Instead, the parameters K, T_i, and L can be tuned manually, much like when tuning a conventional PID controller [Shinskey, 2001].

In the time-domain, the input-output relation of the PPI controller is

$$u(t) = K\left(e(t) + \frac{1}{T_i}\int_{-\infty}^{t} e(\tau)\,d\tau\right) - \frac{1}{T_i}\int_{-\infty}^{t}\left(u(\tau) - u(\tau - L)\right)\,d\tau, \quad (1.15)$$

where the first term is an ordinary PI controller and the second term performs the prediction by low-pass filtering the control signal. This can be compared to the PID controller, which uses high-pass filtering of the measurement signal, see Eq. (1.5).

It is interesting to compare the predictor part with the linear prediction performed in a PID controller. Figure 1.4 shows the Bode diagram of a predictor with $T_i = 0.25$ and $L = 1$. A Taylor series expansion of the predictor for small s is, see [Åström and Hägglund, 2006],

$$C_{\text{pred}} \approx \frac{1}{1 + L/T_i}\left(1 + \frac{1}{2}\frac{(L/T_i)^2}{1 + L/T_i}\,T_i s + \ldots\right), \quad (1.16)$$

showing that the static gain of the predictor is $1/(1 + L/T_i)$. A PD controller, with K and T_d set according to the Taylor series expansion of the PPI predictor as

$$K = \frac{1}{1 + L/T_i}, \qquad T_d = \frac{1}{2}\frac{(L/T_i)^2}{1 + L/T_i}\,T_i, \quad (1.17)$$

and the ideal predictor e^{sT_d} are also shown in Figure 1.4 for comparison.

The phase of the predictor C_{pred} follows the ideal predictor well up to a certain frequency but falls rapidly for higher frequencies. The PD

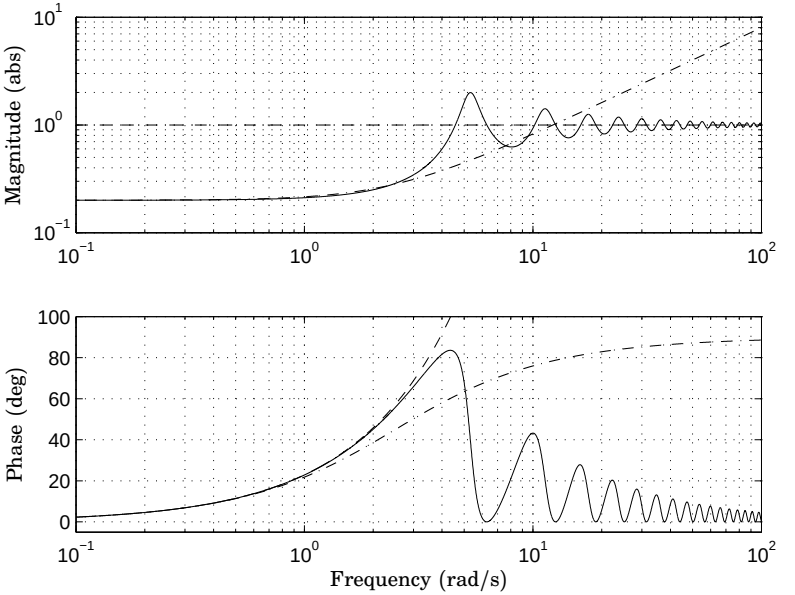

Figure 1.4 The predictor C_{pred} in the predictive PI controller (–), a PD controller (-·-) and an ideal predictor e^{sT_d} (--).

controller, however, cannot follow the ideal predictor but gives instead phase advance in a wider frequency interval. The ideal predictor has a magnitude equal to 1 for all frequencies, while the predictor C_{pred} has several peaks in the magnitude where the phase is advanced. Compared to the PD controller, the magnitude of the predictor C_{pred} increases more rapidly at low frequencies, but the magnitude of the PD controller tends to infinity at high frequencies whereas the magnitude of C_{pred} tends to 1. Hence, for bounded high-frequency gain, the PPI controller does not need a filter, whereas the PID controller needs a first order filter.

A performance comparison between the PPI and PID controllers, and thus a comparison between the predictor C_{pred} and linear prediction by derivative action, is the topic of Paper III. The comparison includes demands on robustness margins and constraints on noise sensitivity of the control signal.

1.3 Performance

Load disturbances yield in general the process output to deviate from its set-point. As most process control systems operate in regulatory mode,

tuning low-level controllers for fast load disturbance rejection is common, both in industry and academia. The transfer function from load disturbance to process output, governing the load disturbance response, is, as noted in Section 1.1,

$$PS = \frac{P}{1 + PCF}. \tag{1.18}$$

Load disturbances often have low-frequency characteristics and it is thus the low-frequency part of PS that essentially will determine the response. For processes with $P(0) \neq 0$, measurement filters with $F(0) = 1$ and controllers with integral action, the following approximation can be made,

$$\frac{P}{1 + PCF} \approx \frac{s}{k_i}, \tag{1.19}$$

where $k_i = K/T_i$ is the integral gain of the controller. Thus, for fast disturbance rejection, a high low-frequency gain of the controller is desired, and hence, k_i is a good measure of the disturbance rejection capability of the controller.

In the design of low-level controllers, a performance measure is selected. Frequency domain measures are for instance the low-frequency controller gain k_i, the open-loop gain cross-over frequency ω_{gc} or, as used in [Kristiansson and Lennartson, 2006b], the peak value J_v defined as

$$J_v = \left\| \frac{1}{s} PS \right\|_\infty. \tag{1.20}$$

Time-domain measures are often based on the process output response to a load disturbance step at time $t = 0$ on the process input. Two measures are the maximum deviation, $z_{\max}$, and the time to reach it, $t_{\max}$, defined as

$$z_{\max} = \max_{t \in [0,\ \infty)} |z(t)|, \qquad t_{\max} = \arg\max |z(t)|, \tag{1.21}$$

where $z(t)$ is the time-domain equivalent to Z in Figure 1.1. More common are the integral criteria of $z(t)$. Two examples are the integrated error (IE) and the integrated absolute error (IAE), defined as

$$\mathrm{IE} = \int_0^\infty z(t)\, dt, \qquad \mathrm{IAE} = \int_0^\infty |z(t)|\, dt. \tag{1.22}$$

These two measures are equal if the response is monotone. It can be shown that $\mathrm{IE} = 1/k_i$, which is appealing. However, IE has the disadvantage of

having a low and misleading value for oscillative responses, while IAE contains an inherent stability criteria as it will steadily increase. Other measures are the integrated time-weighted absolute error (ITAE) and integrated squared error (ISE), defined as

$$\text{ITAE} = \int_0^\infty t|z(t)|\,dt, \qquad \text{ISE} = \int_0^\infty z^2(t)\,dt. \tag{1.23}$$

The ITAE criteria tends to penalize long term deviation from set-point more than short transients. This makes the load response to have a short but high peak, which is generally not desirable, see [Shinskey, 1994]. The ISE criteria has the opposite effect, as it penalizes large errors more than small, yielding the response to a have a small amplitude but a prolonged settling time. When designing low-level controllers in Paper I and III, IAE is used as a performance measure as it penalizes all deviations equally and is considered to be the most useful, see the discussion in [Shinskey, 1994].

1.4 Robustness

The concept of feedback has many advantages, such as making a process follow set-points and rejecting disturbances. However, introducing feedback also comes with the possibility of causing instability. Design of a control system is often made using a model of the process, which contains simplifications and assumptions. Therefore, at the design phase, robustness towards process uncertainties must be considered in order to avoid instability when the control system is used on the process. Notions used for robustness can essentially be divided into specifications on the loop transfer function and specifications on the sensitivity functions.

Loop Transfer Function Specifications

Two classical stability margins are based on the loop transfer function of the system, i.e., $G_l = PCF$, and are well illustrated in a Nyquist diagram, see left part of Figure 1.5. The first one is the gain margin g_m, which is the smallest increase in the process gain that will yield an unstable system and is defined as

$$g_m = \frac{1}{|G_l(\omega_\pi)|}, \tag{1.24}$$

where ω_π is the phase cross-over frequency, i.e., the lowest frequency where the phase lag of G_l is $-\pi$ rad/s. The second one is the phase margin

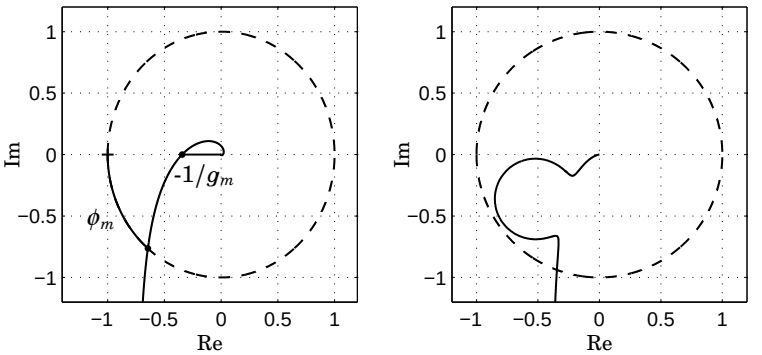

Figure 1.5 *Left*: Definition of phase margin ϕ_m and gain margin g_m. *Right*: Nyquist curve showing the drawbacks of ϕ_m and g_m (Courtesy K.J. Åström and T. Hägglund).

ϕ_m, indicating the increase in phase lag required to reach instability. If using the gain cross-over frequency ω_{gc}, i.e., the lowest frequency where the loop transfer function has unit magnitude, the phase margin may be calculated as

$$\phi_m = \pi + \arg G_l(i\omega_{gc}). \tag{1.25}$$

Both gain and phase margins were originally proposed for the case when the Nyquist curve only intersects the unit circle and negative real axis once. For more complicated loop transfer functions, it is necessary to consider all frequency points where $G_l(i\omega)$ has unit magnitude or a phase of $-\pi \pm 2\pi k$, $k = 1, 2, \ldots$, and then choose the points with worst margins. Additionally, the smallest decrease in phase lag and gain yielding instability should also be considered.

A third classical stability margin, although not seen directly in a Nyquist diagram, is the dead-time margin d_m. It considers how much the process dead-time can increase until the system becomes unstable. Originally, it was defined by using the classical phase margin and gain cross-over frequency as

$$d_m = \frac{\phi_m}{\omega_{gc}}. \tag{1.26}$$

As for the phase margin, it is important to extend the definition to consider all frequency points where the loop transfer function have unit gain, and also consider that a decrease in process dead-time may yield instability. The delay margin is especially important for controllers with dead-time compensating structures, as the Smith predictor and the predictive PI controller in Section 1.2.

There are however some drawbacks with the three margins above. They are computed almost independently of each other, meaning that simultaneous changes in process gain and phase are not considered. The right part of Figure 1.5 shows a Nyquist diagram where the system has good gain and phase margins. However, simultaneous changes, smaller than the computed margins, yield the closed loop system unstable.

Sensitivity Function Specifications

A process may be modeled with a nominal model P and an additive stable transfer function ΔP_T, expressing uncertainties in e.g., process gain, time constants and dead-time, as

$$\tilde{P} = P\left(1 + \frac{\Delta P_T}{P}\right). \tag{1.27}$$

The additive uncertainty ΔP_T changes the nominal Nyquist curve with $C\Delta P_T$. To avoid instability, the Nyquist curve should avoid the critical point -1, that is, the distance between any point on the Nyquist curve and -1 should be greater then 0, i.e.,

$$|1 + \tilde{P}CF| > 0. \tag{1.28}$$

Using Eq. (1.27), this condition can for every frequency ω be expressed as

$$\frac{|\Delta P_T(i\omega)|}{|P(i\omega)|} < \frac{1}{|T(i\omega)|}, \tag{1.29}$$

where T is the complementary sensitivity function of the nominal system. A simple, but conservative, estimate of the allowed relative error is $1/M_T$, where M_T is the maximum value of $|T(i\omega)|$, i.e.,

$$M_T = \|T\|_\infty. \tag{1.30}$$

This quantity can be related to both gain and phase margin as a specific value of M_T guarantees that

$$g_m \geq 1 + \frac{1}{M_T} \tag{1.31}$$

$$\phi_m \geq 2\arcsin\left(\frac{1}{2M_T}\right). \tag{1.32}$$

With the same approach, but now considering an inverse uncertainty of the process, i.e.,

$$\tilde{P} = P\left(1 + \frac{\Delta P_S}{P}\right)^{-1}, \tag{1.33}$$

yields the constraint

$$\frac{|\Delta P_S(i\omega)|}{|P(i\omega)|} < \frac{1}{|S(i\omega)|} \tag{1.34}$$

at every frequency ω, where S is the sensitivity function of the nominal system. Also for this inequality, a simple, but conservative, estimate of the allowed relative process error can be used, i.e., $1/M_S$, where M_S is the maximum value of the sensitivity function,

$$M_S = \|S\|_\infty. \tag{1.35}$$

Analogous to M_T, the quantity M_S can be related to both gain and phase margin as a specific value of M_S guarantees that

$$g_m \geq \frac{M_S}{M_S - 1} \tag{1.36}$$

$$\phi_m \geq 2 \arcsin\left(\frac{1}{2M_S}\right). \tag{1.37}$$

Additionally, if the open loop and closed loop responses to a load disturbance are denoted Y_c and Y_o, respectively, then

$$\frac{Y_c}{Y_o} = S. \tag{1.38}$$

The sensitivity function thus shows which disturbance frequencies are attenuated and which are amplified by feedback, and M_S gives the maximum amplification.

Requirements of the sensitivity functions T and S having peak values less than M_T and M_S, respectively, can be given graphical interpretations in a Nyquist diagram in the form of circles. The circles have centers and radii as given in Table 1.1 and examples of the circles can be found in Figure 1.6. For $\|T\|_\infty < M_T$, with $M_T > 1$, the Nyquist curve should be outside the M_T-circle, while if $M_T < 1$, then the Nyquist curve should be inside the circle. For $M_T = 1$ the circle degenerates to a straight line. For $\|S\|_\infty < M_S$ to be fulfilled, the Nyquist curve should be outside the M_S-circle.

The simple but conservative peak values M_T and M_S have been used successfully as design parameters when designing PI and PID controllers, see [Åström and Hägglund, 2006], and are also used in Paper I as design parameters. However, the simplicity comes with a price. As M_T and M_S are set as upper amplitude limits on T and S, respectively, for all frequencies, all frequency dependent model errors may not be covered. For

Table 1.1 Centers and radii of circles representing constant values $M_T > 1$ and M_S of T and S, respectively.

Peak value	Center	Radius
M_T	$-\frac{M_T^2}{M_T^2-1}$	$\frac{M_T}{M_T^2-1}$
M_S	-1	$1/M_S$

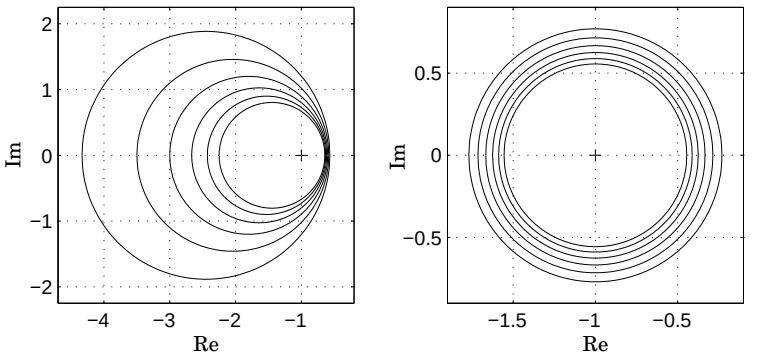

Figure 1.6 *Left*: Circles corresponding to $M_T = 1.3,\ 1.4,\ 1.5,\ 1.6,\ 1.7$ and 1.8. *Right*: Circles corresponding to $M_S = 1.3,\ 1.4,\ 1.5,\ 1.6,\ 1.7$ and 1.8.

PID, this has shown not to be a problem for industrially common processes, see [Åström and Hägglund, 2006]. However, for controllers with dead-time compensating structures, that are inherently sensitive to process dead-time modeling errors, frequency independent constraints on the sensitivity functions have shown not to be sufficient. Paper II gives a procedure to include a guaranteed dead-time margin as well as using M_T and M_S as design parameters for robustness towards other type of uncertainties, e.g., gain and time constant uncertainties. This procedure is used in Paper III when comparing PID and PPI controllers. In the following example, PPI controllers will be designed both using an upper limit on the sensitivity function and the robustness margin presented in Paper II.

Example 1.1—Optimization of the Predictive PI Controller
In this example, optimization of the predictive PI (PPI) controller, considering the integrated absolute error (IAE) as a performance measure, will be made. Optimization results with two different robustness measures will be given, showing the sensitivity towards dead-time modeling error of the PPI controller and the importance of setting adequate robustness

Table 1.2 Optimal predictive PI controller parameters and constraint function values in Example 1.1.

Design constraint	IAE	K	T_i	L	$\|S\|_\infty$	$\|S_\Delta(\Delta L)\|_\infty$
$\|S\|_\infty \leq M_S$	2.30	0.46	0.02	1.04	1.30	∞
$\|S_\Delta(\Delta L)\|_\infty \leq M_S$	3.06	0.37	0.13	0.99	1.22	1.30

constraints. The optimizations will be performed in a discrete time setting on the following first order process with dead-time,

$$P(s) = \frac{1}{0.1s + 1} e^{-s}. \tag{1.39}$$

Both process and PPI controller are discretized using zero-order hold with sampling period $h = 0.02$ and no measurement filter will be considered.

The first robustness constraint is the commonly used amplitude peak of the sensitivity function S. The optimization problem may be stated as

$$\begin{aligned} \min_{K,T_i,L} \quad & h \sum_{k=0}^{\infty} |z(k)| \\ \text{s.t.} \quad & \|S\|_\infty \leq M_S, \end{aligned} \tag{1.40}$$

where $z(k)$ is the time-domain response to a load disturbance step at initial time. The constraint on the sensitivity function is set to $M_S = 1.3$, which is conservative, see [Åström and Hägglund, 2006]. The optimal controller parameters are found in Table 1.2 together with IAE and constraint function values, while the Bode diagram of the controller is shown in Figure 1.7. The controller has a very small integral time, yielding the predictor to have undesirably high amplitude peaks. Figure 1.8 shows the nominal Nyquist curve and sensitivity function of the system, which fulfills the constraint. Hence, the system has a at least a gain and a phase margin of 4.3 and 45°, respectively. The amplitude peaks cause the Nyquist curve to have significant loops in the right half-plane and the sensitivity function to have significant amplitude dips. The resulting closed-loop is sensitive towards modeling errors ΔL of the process dead-time, and approximately $\Delta L = \pm 0.085$, i.e., $\pm 8.5\%$ of nominal process dead-time, yield instability.

Figure 1.8 shows also the implications on the Nyquist curve and sensitivity function as the dead-time is varied in the interval [0.915, 1.085]. It is often implied that it is the loop with highest gain in the right half-plane of the Nyquist diagram that causes the sensitivity towards dead-time uncertainties. However, for the presented design, it is the fourth amplitude

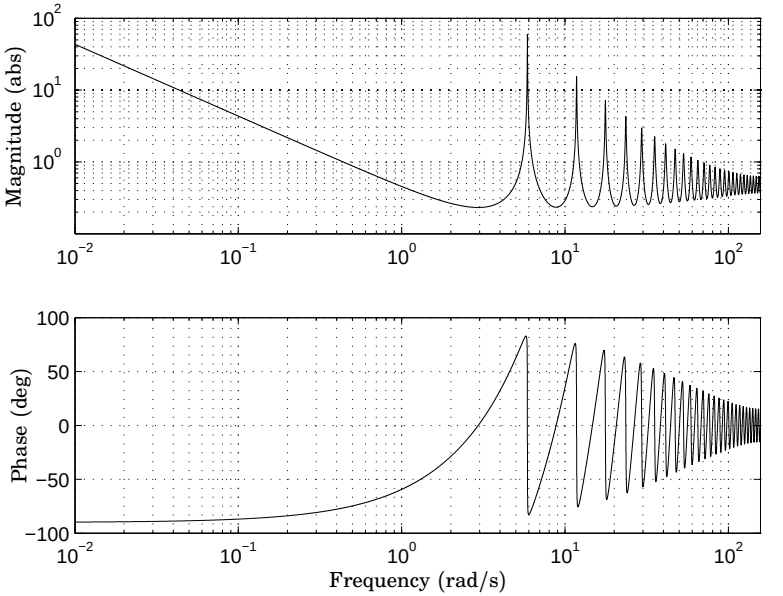

Figure 1.7 Bode diagram of the predictive PI controller from Example 1.1 when using the constraint $\|S\|_\infty \leq M_S$.

peak in the PPI controller that causes the instability for $\Delta L = \pm 0.085$. This peak is considerably smaller than the highest peak, but it is located at a higher frequency yielding larger phase shift for an equal dead-time uncertainty. The presented results show that using only an upper amplitude bound on the sensitivity function is not enough at optimization of PPI controllers.

A more robust system could have been designed if an even lower value of M_S was selected. However, this would e.g., also increase the gain margin to an even more conservative value. Another method is to separate the dead-time uncertainty and other uncertainties, as in the presented robustness margin in Paper II, which was subsequently used in the design of PPI controllers in Paper III. Using the notation from Paper III, the optimization problem may then be expressed as,

$$\begin{aligned} \min_{K,T_i,L} \quad & h\sum_{k=0}^{\infty}|z(k)| \\ \text{s.t.} \quad & \|S_\Delta(\Delta L)\|_\infty \leq M_S, \quad \Delta\underline{L} \leq \Delta L \leq \Delta\overline{L}, \end{aligned} \tag{1.41}$$

where $S_\Delta(\Delta L)$ is the sensitivity function extended to depend on the dead-time uncertainty, which has upper and lower limit $\Delta\underline{L}$ and $\Delta\overline{L}$, respectively. The constraint on $S_\Delta(\Delta L)$ guarantees that any dead-time uncer-

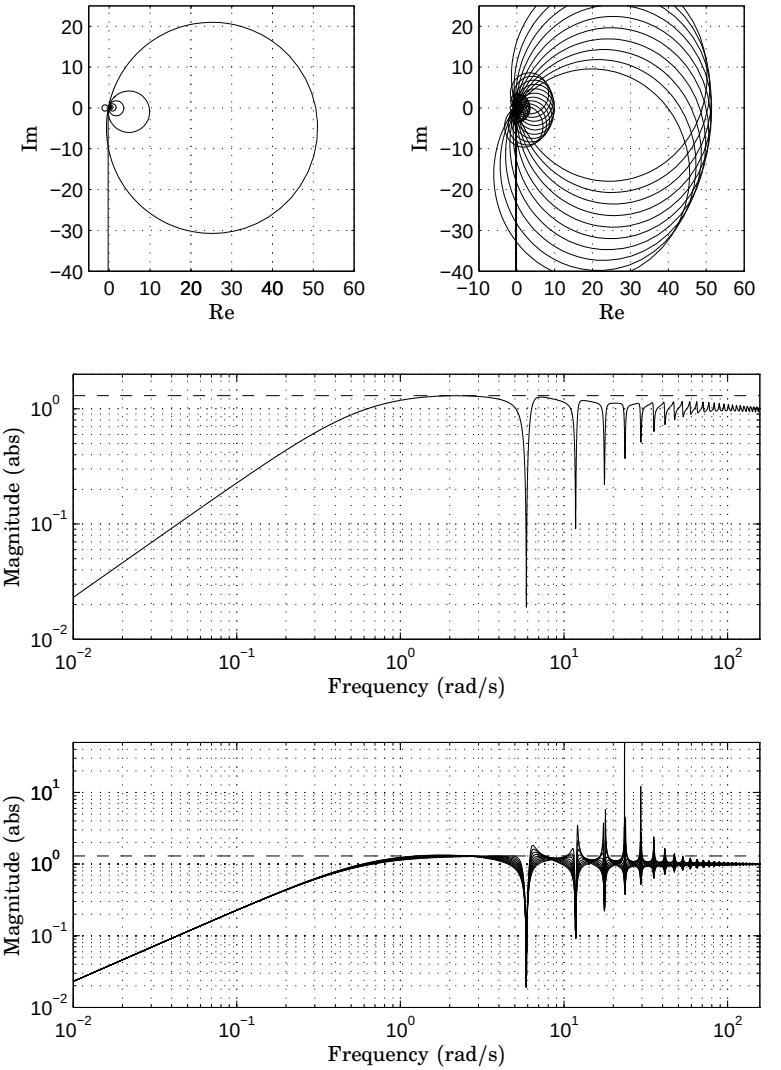

Figure 1.8 Nyquist diagrams and sensitivity function magnitudes from Example 1.1 when using the constraint $\|S\|_\infty \leq M_S$. *Top left:* Nominal Nyquist curve. *Top right:* Nyquist curves when process dead-time is shifted within the interval [0.915, 1.085]. *Middle:* Nominal sensitivity function. *Bottom*: Sensitivity functions when process dead-time is shifted within the interval [0.915, 1.085]. Circles and horizontal lines (--) indicate the limit $\|S\|_\infty = 1.3$.

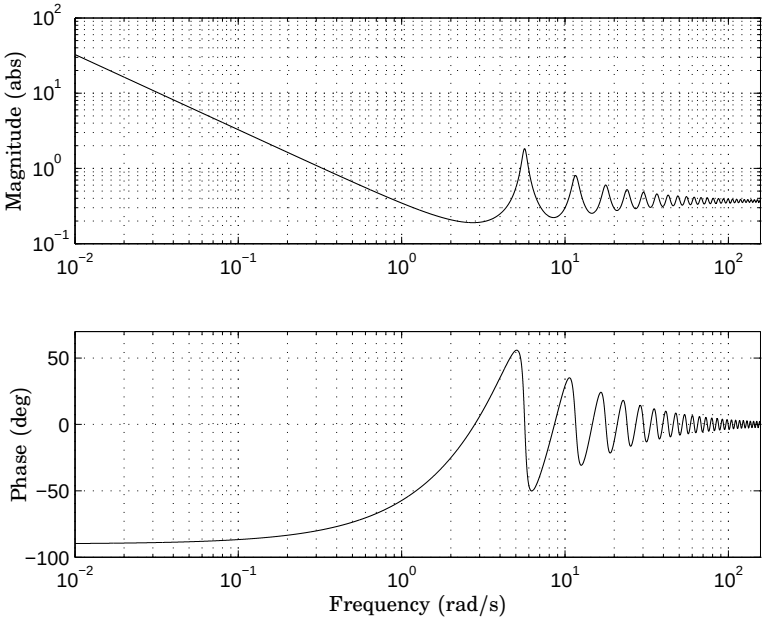

Figure 1.9 Bode diagram of the predictive PI controller from Example 1.1 when using the constraint $\|S_\Delta(\Delta L)\|_\infty \leq M_S$.

tainty in the specified interval cannot yield the ordinary sensitivity function S to have a larger amplitude than M_S. As an example, the dead-time uncertainty interval is set by $\Delta\underline{L} = -0.085$ and $\Delta\overline{L} = 0.085$, while $M_S = 1.3$, yielding at least the same gain margin as in the previous optimization problem.

The resulting controller parameters together with IAE and constraint function values are found in Table 1.2 and a Bode diagram of the controller is found in Figure 1.9. Compared to when using a constraint on $\|S\|_\infty$, the integral time is larger and the proportional gain is smaller, resulting in a less aggressive controller with smaller gain peaks. The IAE is increased and the nominal sensitivity function has a decreased peak value. The robustness properties of the closed-loop system are however considerably improved as seen in Figure 1.10, where Nyquist curves and sensitivity functions are shown for different values of the process dead-time uncertainty within the specified interval. As required by the design, the sensitivity function of the system has a magnitude smaller than or equal to 1.3 for all dead-times in the defined interval, and thus, the Nyquist curves are outside or touch the circle indicating $\|S\|_\infty = 1.3$. Hence, the constraint on $\|S_\Delta(\Delta L)\|_\infty$ presented in Paper II may be used in optimization of robust PPI controllers, guaranteeing robustness towards process dead-time uncertainties without increasing e.g., specified gain margin. □

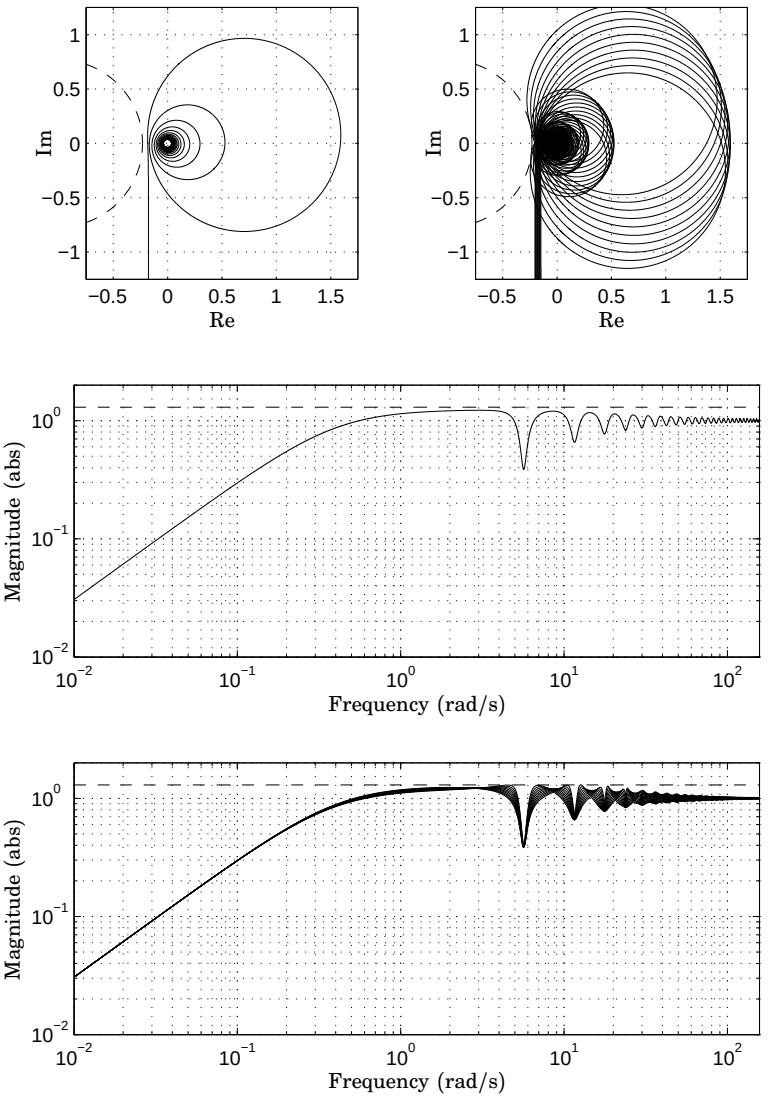

Figure 1.10 Nyquist diagrams and sensitivity function magnitudes from Example 1.1 when using the constraint $\|S_\Delta(\Delta L)\|_\infty \leq M_S$. *Top left:* Nominal Nyquist curve. *Top right:* Nyquist curves when process dead-time is shifted within the interval [0.915, 1.085]. *Middle:* Nominal sensitivity function. *Bottom*: Sensitivity functions when process dead-time is shifted within the interval [0.915, 1.085]. Circles and horizontal lines (--) indicate the limit $\|S\|_\infty = 1.3$.

1.5 Noise Sensitivity

A control system requires measurements of the process to be controlled. In general, the measurements contain noise, and noise is thus fed into the control loop, see Figure 1.1. The control variable affects the process via actuators that often have mechanical parts and the control signal movement due to the noise may cause undesirable wear. These control signal variations depend on the nature of the noise, but also on the transfer function from noise to control signal, i.e., CFS, as seen in Section 1.1.

To remove noise from the measurement signal, the measurement filter F may be designed in an advantageous way and the selection of filter order for PI and PID controllers is the topic of Paper I. In practice, the measurement filter is often inserted after the controller design to obtain desired noise sensitivity, or its settings are related directly to the controller design. In the first case, the outcome is a controller tuned for another system than it will be used in, making in general its performance not follow the design specifications. The second case may yield undesirable control signal variations, yielding re-design of the control system necessary, as pointed out in [Isaksson and Graebe, 2002]. As both the measurement filter F and controller C affect the closed loop behavior, it is thus clear that they should be co-designed and that specifications on CFS should be considered already at the design phase.

Two measures of the noise impact on the control signal are presented in [Åström and Hägglund, 2006]. One is the peak value M_n of the transfer function CFS, i.e.,

$$M_n = \|CFS\|_\infty, \tag{1.42}$$

which in some cases can be related to controller parameters. The second one is the variance σ_u^2 of the control signal calculated by using the power spectrum $\phi_n(\omega)$ of the noise as

$$\sigma_u^2 = \int_{-\infty}^{\infty} |C(i\omega)F(i\omega)S(i\omega)|^2 \phi_n(\omega)\, d\omega. \tag{1.43}$$

The latter measure is used in both Paper I and III for sampled systems, with the addition of also considering the control signal derivative due to the noise.

1.6 Design of Low-Level Controllers

Design of low-level controllers, such as the PID and predictive PI controllers presented in Section 1.2 with associated measurement filters, dif-

fer from the general controller design problem as the structure is fixed.

Design methods for the predictive PI controller (PPI) are rare in the literature, but some guidelines are given in [Hägglund, 1996, Åström and Hägglund, 2006], where the controller parameters are directly related to the step response of the process to be controlled and to the desired closed loop time constant. The design methods do not explicitly address robustness, which was noted and improved on in [Normey-Rico *et al.*, 1997]. However, the noise sensitivity of the PPI controller was not analyzed in the above references.

For the design problem of the PID controller, on the contrary to the PPI controller, an abundance of different tuning methods for the PID parameters and a variety of processes can be found, see for instance [O'Dwyer, 2009]. The first attempt for systematic tuning, and probably most known, is the tuning method by Ziegler and Nichols [Ziegler and Nichols, 1942], from which several extensions have been made, see [Åström and Hägglund, 2006]. However, neither robustness nor noise sensitivity were explicitly considered. This is in general also true for the standard method of pole placement, where specifications are set by closed-loop poles.

During the last two decades, simple design rules for PID controllers have been derived from optimization. One example is the AMIGO method, presented in [Åström and Hägglund, 2006]. For a batch of processes, PI and PID controllers were designed such that the integrated error (IE) at a load disturbance was minimized, while setting robustness by using a combined sensitivity with S and T. Simple tuning rules were then found both for PI and PID controllers by correlating the resulting controller parameters with normalized process parameters. However, noise sensitivity was not considered directly. The controllers have to be de-tuned or re-tuned with a pre-determined measurement filter in the loop if desired noise sensitivity is not obtained.

The noise sensitivity was however considered together with robustness in [Kristiansson and Lennartson, 2006a] and [Kristiansson and Lennartson, 2006b], where minimization of a frequency domain objective, closely related to IE, was performed for a batch of processes. Tuning rules were based on observed relations between the resulting controller parameters and process parameters, which can be estimated in practice by relay experiments and characterize the difficulty of controlling the process.

All the above mentioned tuning rules have at least two points in common. First, the resulting robustness and noise sensitivity have to be analyzed after the design has been performed. Secondly, the tuning rules have been derived using specifications set by the corresponding inventors. If the resulting design does not fulfill the desired specifications, another tuning method must be used or the controller parameters must be tuned manually, requiring knowledge and insight.

Another type of PID controller tuning is based on the internal model control (IMC) principle, where the controller contains an approximate inverse of the process model. The controller also contains a tunable filter that determines the trade-off between robustness and performance, which is hence explicitly considered in the design. With certain model orders and approximations of the process dead-time, the resulting controllers are of PI and PID type, see [Rivera *et al.*, 1986]. The lambda tuning method, see [Dahlin, 1968, Higham, 1968], is a special case of the IMC method, where the closed loop response time is the only design parameter. The IMC method yields satisfying set-point responses, but as process poles and zeros are canceled in the design, load disturbance responses may be slow for processes with lag-dominated dynamics. To overcome this deficiency, the SIMC tuning rule was presented in [Skogestad, 2003], containing an ad hoc modification of the integral time in the controller which yields better responses to load disturbances. Neither of the IMC based methods considers the noise sensitivity explicitly. However, guidelines for the controller gains in the SIMC method that results in smooth control, and thus less noise sensitivity, were presented in [Skogestad, 2006].

A tuning procedure for low-level controllers should be able to explicitly address performance, robustness and noise sensitivity. Additionally, the procedure should be able to handle tuning in different settings. For instance, the robustness specification depends on how detailed and accurate the process model is, while the noise sensitivity should be specified when the noise level of the measurement signal is known. It is hence impossible to find simple tuning rules based on only process model parameters, similar to the tuning rules above, that can handle the performance and all specifications simultaneously for various settings in an optimal manner.

The advances of optimization algorithms, and the limited number of controller and filter parameters, yield model-based controller optimization attractive. A performance measure together with constraints on robustness and noise sensitivity may explicitly be set in each design case. Such optimization problems have recently been posed and solved, see for instance [Kristiansson and Lennartson, 2006a, Garpinger, 2009, Šekara and Mataušek, 2009]. The work presented in Paper I and III in this thesis are along the same lines, where PID or PPI controller parameters are optimized together with measurement filter parameters, while considering both robustness towards process uncertainties and noise sensitivity of the control signal. However, compared to the listed references, additional and different noise sensitivity measures are used. The robustness constraint used in Paper III is also different and is presented in Paper II.

Optimization-based low-level controller design is conceptually simple, but care must be exercised. If the optimization routine terminates successfully, the resulting controller is optimal in some sense. However, it

may still be unsuitable to use due to e.g., lack of significant constraints in the optimization formulation or a local minimum in the objective function has been found. An example of the former was seen in Example 1.1.

1.7 Contributions Overview

The author of the thesis read the paper [Shinskey, 2001] in the beginning of his Ph.D. studies, which was the starting point of the work on low-level controllers. The paper presented a PID controller, which was extended with a predictor transfer function equal to the predictor presented in Section 1.2. The controller showed a much better performance compared to an ordinary PID controller. The predictor structure had a high-frequency gain of 1, indicating that the noise sensitivity was not significantly higher than for the original PID controller, yielding it interesting to analyze. To evaluate the predictor, the work was first directed towards making a comparison between a PI controller extended with a predictor, i.e., the predictive PI (PPI) controller, and an ordinary PID controller. However, designing the controllers by optimization using frequency independent limits on the sensitivity functions, as is common for PID, were not feasible due to the sensitivity of dead-time uncertainties of the PPI. Thus, robustness constraints, considering simultaneous uncertainties in e.g., dead-time, gain and time constants of the process, were needed. Additionally, the robustness constraints were also supposed to be easy to use and interpret. The resulting work on robustness constraints is presented in Paper II, where the uncertainty in process dead-time is separated from other uncertainties. The margins use sensitivity functions that are extended to depend on the dead-time uncertainty. Amplitude limits on the extended sensitivity functions are specified and should hold for all dead-time uncertainties in a specified interval. Hence, the ordinary sensitivity functions are guaranteed to have peak values less than the specified limits for all considered dead-time uncertainties. Methods to compute the margins are presented in the paper. The work gave insight into how dead-time uncertainties change the Nyquist curve and that the Nyquist diagram can be separated into permissible and impermissible areas that depend on frequency.

During the work of Paper II, the author of the thesis had several discussions on PID controller and measurement filter design regarding noise sensitivity with the author of [Garpinger, 2009]. This was interesting from the PPI controller point of view, as the noise sensitivity of the predictor was to be analyzed. An iterative design method for discrete time PI and PID controllers and measurement filters was presented in [Garpinger, 2009]. Robustness was considered by constraining the peak values of the sensitivity functions, while noise sensitivity was considered

by constraining the transfer function from measurement noise to control signal as $\|CFS\|_2 \leq \eta_1$. However, it was pointed out that the resulting feedbacks were suboptimal. The author of the thesis, inspired by the work in [Garpinger, 2009], constructed a framework to pose and solve the joint optimization problem of PI/PID controllers and measurement filters, resulting in optimal feedbacks. Robustness and noise sensitivity were considered as in [Garpinger, 2009]. The framework has been used in both Paper I and III and is thus a significant contribution even though not explicitly stated in the papers. It was constructed in MATLAB® using the Control System Toolbox™, Optimization Toolbox™, and Simulink®, see [The MathWorks, Inc, 2010a, The MathWorks, Inc, 2010b, The MathWorks, Inc, 2010c].

A main issue with the constraint $\|CFS\|_2 \leq \eta_1$, is that rapid variations in the control signal are treated in the same manner as slow variations. However, rapid variations cause in general more wear on actuators than slow variations. This inspired to the first part of the work in Paper I, presenting a constraint on the inter-sample behavior of the control signal due to measurement noise as $\|\Delta_z CFS\|_2 \leq \eta_2$, where Δ_z is the difference operator. A guideline on how to set η_2 is given in the paper. The second part of Paper I considers the measurement filter order for PI and PID controllers. Controllers and measurement filters with different orders were designed for a batch of processes with the constraints above. In papers published on PID control, the most common measurement filter is the first order filter that only acts on the derivative part, yielding a limited high-frequency gain but no roll-off in the feedback. However, the results in Paper I show the importance of roll-off when considering noise sensitivity constraints. Comparisons with optimal high-order controllers designed via Youla parametrization were made. When considering processes with lag-dominated dynamics, the comparisons show that the optimal high-order controller emphasizes the same frequency regions as a PID controller with a second order measurement filter with low damping. To the best knowledge of the authors, the co-design of PI/PID controllers and measurement filters with the considered constraints, has not been considered elsewhere.

The constructed framework for optimization was extended to also include the PPI controller and the robustness margins presented in Paper II. Hence, comparisons between the two prediction types of the PID and the PPI controller using both robustness and noise sensitivity constraints, could be performed. The result of the work is presented in Paper III. In general, the differences between the two prediction methods are that the PPI predictor is able to give larger phase advance and higher gain peak over a narrower frequency interval than what the derivative part of a PID controller can, while the derivative part is able to give phase advance and gain increase over a wider frequency interval than what the PPI predic-

tor can. For the selected constraint parameters in Paper III, the performances of the two prediction methods are similar for the majority of the considered processes, reflecting processes found in an industrial setting. However, for processes and constraints that allow the frequency interval for phase advance and gain increase in the feedback to be significantly wider than what the PPI controller is able to use, the PID controller is significantly better. To the best knowledge of the authors, optimization of the PPI controller with associated measurement filter, regarding both robustness and noise sensitivity, has not been considered elsewhere.

1.8 Future Work

This section provides some interesting areas for future work, and is preferably read after the papers I–III have been read.

The upper amplitude limits on the sensitivity functions and the extended sensitivity functions presented in Paper II may be frequency dependent. However, for simplicity, the limits were frequency independent in Paper I and III. Frequency dependent limits could be found via e.g., parameter uncertainties in the process model. Implications of using these limits, compared to commonly used values of frequency independent limits, would give further insight on how robustness specifications affect the design of low-level controllers.

The noise sensitivity constraint presented in Paper I, and used both in Paper I and III when designing low-level controllers with measurement filters, are based on white measurement noise. However, measurement noise in practice does very rarely contain low-frequency components. An interesting path to take for the optimization formulation is to use simple models to describe the noise characteristics and include them the in constraints.

Academic papers on design of low-level controllers focus in general on a performance criteria and robustness towards process uncertainties regarding instability. Lately, designs considering the noise sensitivity of the control signal have also occurred. However, it is also of interest how the performance is changed due to process variations, which is very rarely discussed. Performing an analysis of the optimal low-level controllers and measurement filters in Paper I and III regarding robust performance would be interesting. Especially an analysis of the predictive PI controller would be interesting as it gives phase advance and increased gain over only a narrow frequency interval. An analysis regarding parameter changes in a first-order system with dead-time was provided in [Ingimundarson and Hägglund, 2002] for PI and PID controllers as well as a PI controller with Smith predictor structure. A more unified approach

than the presented one would however be desirable.

Working with low-level controllers and filters, and the requirements pointed out in Section 1.1, an important aspect of future work is to focus on keeping things as simple as possible, making the results useful in industry.

References

Åström, K. J. and T. Hägglund (2006): *Advanced PID Control*. ISA - The Instrumentation, Systems, and Automation Society, Research Triangle Park, NC 27709.

Šekara, T. and M. Mataušek (2009): "Optimization of PID Controller Based on Maximization of the Proportional Gain Under Constraints on Robustness and Sensitivity to Measurement Noise." *IEEE Transactions of Automatic Control*, **54:1**, pp. 184–189.

Dahlin, E. (1968): "Designing and Tuning Digital Controllers." *Instruments and Control Systems*, **42**, June, pp. 77–83.

Garpinger, O. (2009): "Design of Robust PID Controllers with Constrained Control Signal Activity." Licentiate Thesis. Department of Automatic Control, Lund University, Sweden.

Higham, J. (1968): "'Single-term' control of first- and second-order processes with dead time." *Control*, Feb, pp. 2–6.

Hägglund, T. (1996): "An industrial dead-time compensating PI controller." *Control Engineering Practice*, **4:6**, pp. 749–756.

Ingimundarson, A. and T. Hägglund (2002): "Performance comparison between PID and dead-time compensating controllers." *Journal of Process Control*, **12**, pp. 887–895.

Isaksson, A. and S. Graebe (2002): "Derivative filter is an integral part of PID design." *Control Theory and Applications, IEE Proceedings*, **149:1**, pp. 41–45.

Kristiansson, B. and B. Lennartson (2006a): "Evaluation and simple tuning of PID controllers with high-frequency robustness." *Journal of Process Control*, **16:2**, pp. 91–103.

Kristiansson, B. and B. Lennartson (2006b): "Robust tuning of PI and PID controllers: Using derivative action despite sensor noise." *IEEE Control Systems Magazine*, **26:1**, pp. 55–69.

Normey-Rico, J., C. Bordons, and E. Camacho (1997): "Improving the robustness of dead-time compensating PI controllers." *Control Engineering Practice*, **5:6**, pp. 801–810.

O'Dwyer, A. (2009): *Handbook of PI and PID controller tuning rules*, 3rd edition. Imperial College Press.

Palmor, Z. (1980): "Stability properties of Smith dead-time compensator controllers." *International Journal of Control*, **32:6**, pp. 937–949.

Rivera, D., M. Morari, and S. Skogestad (1986): "Internal Model Control. 4. PID Controller Design." *Industrial & Engineering Chemistry Process Design and Development*, **25:1**, pp. 252–265.

Shinskey, F. G. (1994): *Feedback Controllers for the Process Industries*. McGraw-Hill.

Shinskey, F. G. (2001): "PID-deadtime control of distributed processes." *Control Engineering Practice*, **9:11**, pp. 1177–1183.

Skogestad, S. (2003): "Simple analytic rules for model reduction and PID controller tuning." *Journal of Process Control*, **13:4**, pp. 291–309.

Skogestad, S. (2006): "Tuning for smooth PID control with acceptable disturbance rejection." *Industrial & Engineering Chemistry Research*, **45:23**, pp. 7817–7822.

Smith, O. J. M. (1957): "Closed control of loops with dead time." *Chemical Engineering Progress*, **53**, pp. 217–219.

The MathWorks, Inc (2010a): *Control System Toolbox™ User's Guide, Version 9*. The MathWorks, Inc, 3 Apple Hill Drive, Natick, MA 01760-2098.

The MathWorks, Inc (2010b): *Optimization Toolbox™ User's Guide, Version 5*. The MathWorks, Inc, 3 Apple Hill Drive, Natick, MA 01760-2098.

The MathWorks, Inc (2010c): *Simulink® User's Guide, Version 7*. The MathWorks, Inc, 3 Apple Hill Drive, Natick, MA 01760-2098.

Ziegler, J. and N. Nichols (1942): "Optimum settings for automatic controllers." *Trans. ASME*, **64**, pp. 759–768.

2

Optimization of High-Level Polymer Grade Changes

2.1 Problem Formulation

Why Grade Changes?

Polymer, such as polyethylene, comes in different grades, i.e., has different properties such as color, texture, odor, and mechanical properties. The different grades are usually composed of the same raw materials, but they are produced at different reactor operating conditions such as raw material concentration ratios, pressures and temperatures. Today, more than 100 million tons of polymers are produced per year with a wide variety of grades and prices, see [Dünnebier *et al.*, 2005] and [Kadam *et al.*, 2007], and the use of polymer has increased in several areas such as automotive, electronics, and food during the last decades. Specific polymer properties are desired for each area and application by the customer and the diversification has steadily been increasing.

For the polymer producers to increase their profitability, the above has made it imperative to have flexible operation of production, see [Backx *et al.*, 1998], and to make specific tailoring of the produced polymer. However, it is prohibitively expensive to invest in process equipments such that each grade may be produced continuously. Instead, reactors capable of producing a multitude of grades are used. Adaptation to the highly demand driven market, raw material pricing and sell prices of polymers, is achieved by grade changes, i.e., changing production from one grade to another, utilizing the same process equipment, see Figure 2.1 for an illustration. This results in product campaigns that run between a couple of days up to weeks before change of product. During the grade transfers,

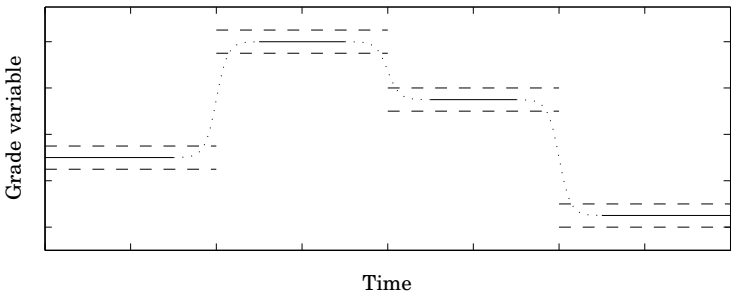

Figure 2.1 Example of grade changes. Solid lines (–) represent stationary production, while dotted lines (··) represent transitions, i.e., non-stationary production. Dashed lines (--) show polymer grade variable intervals specifying on-grade polymer.

the produced polymer is in most cases considered to be off-grade, meaning that it does not fulfill the properties of neither start nor end grade. Such polymer must be sold at a lower price than premium polymer, and often to a lower price than the production cost. The schedule of products, made at a supervisory level, aim to minimize the losses during transitions.

Grade Change Requirements

During a grade change, reactor operating conditions change continuously and for a grade change strategy to be useful in practice it should satisfy four properties as pointed out in e.g. [McAuley and MacGregor, 1992, Flores-Tlacuahuac *et al.*, 2006, Chatzidoukas *et al.*, 2003],

- the reactors should during the transition be operated with obeyed safety requirements on e.g., pressures, concentrations, temperatures, inflows and production rates.
- the transition should be made during continuous production.
- transfer product properties from start grade to end grade, minimizing or maximizing some pre-determined quantity, e.g., production of off-specification polymer, transition time, or total profit during the transition.
- the transition should not adversely affect the quality or consistency of the on-grade polymer in the reactor at the end of the transition period.

The first point is obvious, while the second one considers economy. Even though a grade change is faster when performing stop-and-start of the reactor compared to performing it during continuous production, it is not

economically recommended due to the large losses in raw material [Chatzidoukas *et al.*, 2003].

What quantity to minimize or maximize during transition may depend on market conditions, see [Takeda and Ray, 1999]. This thesis considers mainly the problem of maximizing total profit during the transition, i.e., the difference between revenues and costs.

The last point above considers the measures used when defining a grade. Newly produced polymer has instantaneous values of polymer quality variables, reflecting the reactor condition at the time it was produced. This polymer is mixed with polymer in the reactor bed, yielding the bed average polymer quality variables, which are often used when defining a polymer grade. As the bed average measures are to be changed at transition, rapid transitions may be performed by over- and undershooting the instantaneous variables considerably. Thus, even though the transition polymer has correct bed average values, it may be composed of polymer with considerably different instantaneous properties, see [McAuley and MacGregor, 1992]. Such transitions should therefore be avoided.

Grade Change Challenges

Changing operating conditions in polymerization reactors comes with a set of challenges, and several different authors have used a multitude of solution approaches, see Paper VI for an overview. The polymerization process is inherently non-linear since e.g., the reaction rates depend on concentrations of monomer, co-monomer and hydrogen in a non-linear fashion. In addition, the exothermic reaction depends on the catalyst properties and also on the reactor temperature, making reactor runaway possible during a grade change if the reactor temperature is not properly controlled.

Operating conditions, both during steady state operation and grade changes, are limited to known safe regions, which must be respected when formulating an optimization problem for finding optimal grade change trajectories. Measurements of operating conditions such as pressures, temperatures and concentrations during grade changes are available on-line, while measurements of polymer grade variables are found via product sampling and examination in laboratory settings associated with long delays, see [Embiruçu *et al.*, 1996].

For rapid grade transitions, the reactor inflows of raw material and diluents are required to change not only quickly and often with over- or undershoots, but also simultaneously. The effect on the reactor state from each inflow is complicated and to handle these interactions, advanced, multivariable, control strategies are imperative [Takeda and Ray, 1999]. Flows of raw material, diluents, and also off-gas flows, are limited by minimum and maximum values. Additionally, their rates of change are also limited, which must be considered at transition optimization.

The main polymer production plant considered in this thesis incorporates three cascaded reactors, and they affect each other in the forward direction, not only by raw material components and diluents, but also via catalyst and polymer properties. Additionally, the reactors also partly affect each other in the reverse direction. This is because unreacted raw material and diluents are sent for purification to a recycle area, consisting of three distillation columns, and are subsequently used as inflows to the reactors.

The recycle area contributes to a significantly better economy of the plant. However, when considering grade changes with hydrogen mass decreases in the reactors, the recycle area yields longer transition times, as also noted in [McAuley and MacGregor, 1992]. This is because hydrogen has a very low reaction rate, yielding that significant parts of the total hydrogen inflows to the reactors come from the recycle area. Thus, to remove hydrogen fast from the reactors, closing hydrogen fresh inflows may in some cases not give fast enough transitions, and economically undesirable off-gases on the recycle distillation columns must be used.

Thus, with the above in consideration, formulating an optimization problem for transferring the operating point of a polymer plant from stationary production of one grade to another, is a great challenge.

2.2 The PIC-LU Project

Process Industrial Center – Lund University (PIC-LU) is a collaboration between the departments Automatic Control and Chemical Engineering at Lund University and several companies, one of which is Borealis AB. The core of the center is close collaboration between academia and industry on process industrial problems. The aim is that the solutions could be generalized and applied outside the scope of the original problem. The PIC-LU project started in July 2008.

PIC-LU and Borealis AB

Parts of this thesis, Paper IV and VI, are results from close collaboration with Borealis AB, who originally formulated the research project in PIC-LU, acknowledging the need of grade change optimization in industry. Borealis AB has actively participated in the project and their contributions have been, among others,

- mathematical models of their Borstar® reactors
- measurement data from the plant PE3 at Borealis AB, Stenungsund, Sweden

- significant feedback on the results regarding relevance and applicability
- personnel resources
- several meetings at Borealis AB and telephone conferences

The above has provided a great insight into their work, plant operation and needs regarding grade transitions. Additionally, the Ph.D. students involved in the project have been at a one week internship in the process control room of PE3 at Borealis AB, getting familiar with operators' work and the plant during grade changes.

Lund University has contributed with the work of two full time Ph.D. students, P. Larsson and N. Andersson, constructing a Modelica library for the plant, solving grade change optimization problems and performing model calibrations in various settings. Also, a part time Assistant Professor, J. Åkesson, has been involved, developing the used Modelica based optimization tool JModelica.org.

PE3 at Borealis AB

Borealis is one of the worlds largest polymer producers and one of their sites are located in Stenungsund, Sweden, where the polyethylene plant PE3, considered in this thesis, is found. PE3 is a Borstar® plant developed by Borealis and consists of two slurry reactors and one fluidized bed gas-phase reactor in cascade and a recycle area constituted of three distillation columns for recovery of unreacted components and diluents, see Figure 2.2. Additionally, an area for further processing of the polymer, such as pelleting, blending, baggaging and storing, is a part of the plant. This part will however not be covered in this thesis.

The Borstar® process was primarily developed to produce bi-modal polyethylene and at PE3, high-density polyethylene (HDPE) is produced. The main raw material is ethylene, which together with Borealis' proprietary Ziegler-Natta catalyst control the plant production rate. Hydrogen and butene are used for control of melt index and density. Propane is used as diluent in the slurry reactors, while also nitrogen is used in the gas-phase reactor (GPR).

In the pre-polymerization reactor, see Figure 2.2, which is comparatively small and has inflows of catalyst, ethylene, hydrogen and propane, the catalyst is coated with polymer, preventing it to break later in the process. The polymer produced is conveyed into the subsequent loop reactor, and the low molecular weight part of the bi-modal polyethylene is produced under super-critical conditions. The raw materials ethylene and hydrogen and the diluent propane are fed continuously to the reactor, producing approximately half of all polymer at the plant. The polymer slurry

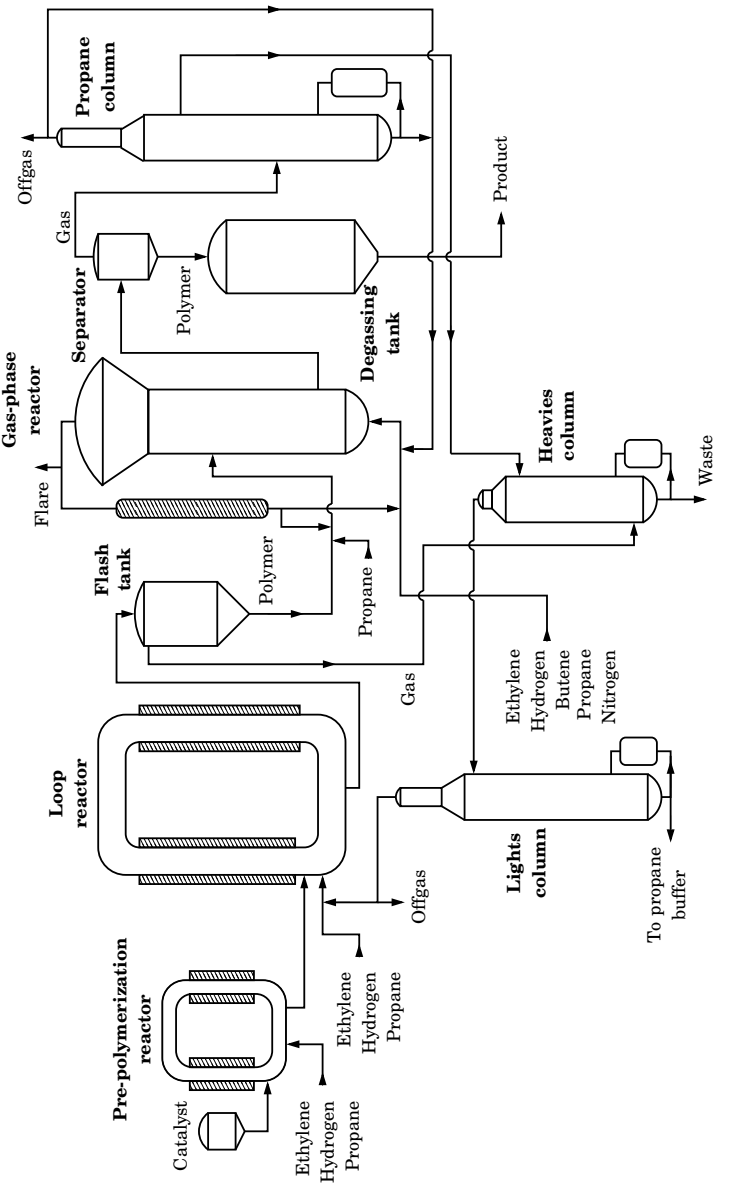

Figure 2.2 Overview of the plant PE3 at Borealis AB including three Borealis Borstar® reactors and a recovery area with three distillation columns.

is transported from the loop reactor to a flash tank, separating polymer and gases. Unreacted raw material and diluent is sent for purification to the heavies distillation column and further to the lights distillation column, from which the top flow is subsequently used as inflow to the loop reactor and the bottom flow, mainly propane, is stored in a propane buffer. The polymer is conveyed into the GPR by using a part of the recycle flow of the GPR, and a propane purge flow assure that no leakage of GPR gas mixture to the flash tank is present. With a lower concentration of hydrogen in the GPR compared to the loop reactor, high molecular weight polymer is produced, which broadens the molecular weight distribution and yields the bi-modal end polymer. Co-monomer butene is added for control of the end product density. Approximately, the second half of the total polymer production at the plant is in the GPR. The conversion per pass through in the GPR is low and the gas reaching the reactor top section is cooled and fed back into the reactor together with the fresh feeds. Polymer, together with gas, is continuously withdrawn at the reactor bottom and fed to a separator, from which the gas is sent to the propane distillation column. The polymer is sent to a degassing tank and then further to pelleting. Top and bottom flow of the propane column are fed back into the GPR, while the side draw, mainly propane, is sent to the heavies column and then further to the lights column, and thus, subsequently to either the loop reactor or the propane buffer.

Current Grade Change Practice at PE3

At PE3, a non-linear model predictive controller (NMPC) is used for plant operation, see [Andersen *et al.*, 2000]. The NMPC utilizes a non-linear physical model, updated recursively using plant measurements and uses a thermodynamic package for calculation of e.g., fluid densities and instantaneous production rates. These are parts of the Advanced Process Control (APC) used on the Borealis Borstar® reactors.

During grade changes, the NMPC is disconnected from the plant, and some inflows and inflow ratios are set in manual mode and controlled by the operators, as experienced during [Internship, PE3 Borealis AB, 2009]. This is because the operators find the NMPC lacking aggressiveness and they have their own ideas of how certain steps in the grade transitions should be performed. At a grade transition, the operators of the reactors follow a recipe which is a combination of a time schedule and a task and action list, based on the experience of former transitions made between the two considered grades. This list may have the conceptual look of,

1. Approximately 20 h before transition, start decreasing polymer mass in the loop reactor to X tons and ethylene inflow to Y kg/h.

2. Decrease production rate in the loop reactor to Z tons/h, 2 h prior transition time.
3. Increase the butene inflow to the gas-phase reactor with W kg/15 min and make a slight overshoot over the target value.
4. Increase the hydrogen inflow to the loop reactor with Q g/30 min. Observe the hydrogen-ethylene molar ratio; it may increase too fast since the ethylene is decreased.
5. During the transition, at all times, keep the bed level and the bulk density in the gas-phase reactor under close watch.
6. ...

As the new grade is reached, the NMPC is again connected to the plant and controls it towards steady state.

After each transition, the recipe is updated by an experienced process engineer based on how successful the grade change was. This procedure is also followed elsewhere, see [Takeda and Ray, 1999, Tousain, 2002].

Even if a recipe is followed by the operators, two transitions between the same polymer grades will never be the same for several reasons, and some of them are, as explained in [Internship, PE3 Borealis AB, 2009] and noted in [Kadam *et al.*, 2007],

- initial points are never exactly the same
- disturbances act on the reactors and distillation columns during the transitions
- two different operators may perform the same task in two different ways

Additionally, the operators work in shifts and they also take turn in what reactor to control. It may thus take several months before an operator performs the same grade change again on the same reactor, and thus acquire experience.

The recipes developed iteratively by experience work well. This does not mean they are optimal grade change procedures and there is a clear need for operator support and process engineer tools and advisory systems for finding, according to some criteria, optimal trajectories for the transitions. The optimal trajectories may also be used at a grade scheduling level.

PIC-LU Project Aims

The PIC-LU project aims at developing prototypes of tools and methods for off-line grade change optimization and analysis, that can be generalized to processes other than polymer plants. It is a feasibility study of a platform

that should be used by and support process and planning engineers to find feasible transition paths between grades that have low safety risks and are economically tenable. The project may be divided into four different parts,

1. Construct a Modelica model library containing components corresponding to units at the PE3 plant, such as reactors and distillation columns. The library should contain models and templates for simulation, parameter estimation, optimization, as well as models for verification of optimization results.

2. Perform parameter sensitivity analysis of the model constructed from the model library and develop methods for model calibration based on plant measurement data from stationary production and grade transitions.

3. Perform a feasibility study of grade change optimization using models from the constructed model library, aiming at maximizing the profit during transition under plant constraints.

4. Design an engineering support system with a graphical user interface where calibration and grade change optimization problems are formulated, solved and presented in a user-friendly manner.

The resulting Modelica library is described in Supplement A. Calibration using stationary plant data together with the Modelica models has been performed in [Andersson *et al.*, 2011], while parameter sensitivity analysis and calibration using dynamic data is work in progress. Grade change optimization results based on the Modelica library are presented in Paper IV and VI and in [Larsson *et al.*, 2010]. In Paper V, a reactor previously published by other authors is considered for optimization. The design of an engineering support system that is linked to the measurement and product database at Borealis AB was performed as a M.Sc. thesis project supervised by P. Larsson, see [Stenmark, 2011].

2.3 Modelica

The Modelica language for modeling of complex systems is becoming widely used in industry, see [The Modelica Association, 2011]. Applications include robotics, automotive and power plants, and models are almost exclusively used for simulation. The most important features of the Modelica language are [Fritzson, 2004],

- Modelica is based on equations instead of assignment statements and acausal modeling may therefore be performed. The equations can be stated by mixing differential, algebraic and discrete equations and there is no need for the modeler to solve for certain variables as e.g., derivatives.
- Modelica supports multi-domain modeling, i.e., models from different domains such as electrical, mechanical, thermodynamic, hydraulic, biological and control applications can be used together.
- Modelica is an object-oriented language providing structuring features such as classes, components, and inheritance, which gives the modeler means to build reusable model libraries.
- Modelica has strong support for building models using components, connections between components, and defining interfaces, making it easy for the modeler to structure the model in a hierarchical manner.

Most of the above features were extensively used in papers IV–VI. Libraries were constructed and included, amongst others, reactor and distillation column models, models for stationary and dynamic optimization, models for verification of optimization results and templates defining different plant configurations. The model library used in Paper IV and VI is described in Supplement A and is one of the main contributions of the PIC-LU project. The modeling and optimization methodology used in papers IV–VI will be described by an example, based on the Hicks-Ray continuously stirred tank reactor (CSTR) system, see [Hicks and Ray, 1971].

Example 2.1—Modeling of a CSTR reactor.
The Hicks-Ray continuously stirred tank reactor (CSTR) model was originally presented in [Hicks and Ray, 1971]. It describes an exothermic reaction with temperature dependence and the model has two states, the concentration C and the temperature T, and one algebraic variable, the reaction rate R_r. The reactor is cooled by a jacket that has a coolant flow with temperature T_c, which is the control input. The CSTR model is

$$V\dot{C} = F_0(C_0 - C) - VR_r \tag{2.1}$$

$$V\dot{T} = F_0(T_0 - T) - \frac{dHV}{\rho C_p} R_r + \frac{2UV}{r\rho C_p}(T_c - T) \tag{2.2}$$

$$R_r = Ck_0 \exp\left(-\frac{E}{RT}\right), \tag{2.3}$$

where the first two equations describe the component and energy balance, respectively, and the third describes the reaction rate. The model contains

```
model CSTR
  //Input
  input Real Tc(nominal=Tc_0);

  //States
  Modelica.SIunits.Concentration C(start=C_init,fixed=true,nominal=C_0);
  Modelica.SIunits.Temp_K T(start=T_init,fixed=true,nominal=T_0);

  //Algebraic variable
  Real R_r(start=R_r_init,nominal=R_r_0,final unit="mol/(s.m3)");

  //Nominal values
  parameter Modelica.SIunits.Concentration C_0 = 1000;
  parameter Modelica.SIunits.Temp_K T_0 = 350;
  parameter Modelica.SIunits.Temp_K Tc_0 = 300;
  parameter Real R_r_0(final unit="mol/(s.m3)") = C_0*k0*exp(-EdivR/T_0);

  //Initial values
  parameter Modelica.SIunits.Concentration C_init = 1;
  parameter Modelica.SIunits.Temp_K T_init = 1;
  parameter Real R_r_init(final unit="mol/(s.m3)") = C_init*k0*exp(-EdivR/T_init);

  //Model parameters
  parameter Modelica.SIunits.VolumeFlowRate F_0 = 1/600;
  parameter Modelica.SIunits.Length r = 0.219;
  parameter Modelica.SIunits.Volume V = 100;
  parameter Modelica.SIunits.Temp_K EdivR = 8750;
  parameter Modelica.SIunits.Density rho = 1000;
  parameter Modelica.SIunits.SpecificHeatCapacity Cp = 0.239*1000;
  parameter Modelica.SIunits.DensityOfHeatFlowRate U = 915.6;
  parameter Real k0(final unit="1/s") = 7.2e10/60;
  parameter Real dH(final unit="J/mol") = -5e4;

equation
  V*der(C) = F_0*(C_0-C) - V*R_r;
  V*der(T) = F_0*(T_0-T) - dH*V*R_r/(rho*Cp) + 2*U*V/(r*rho*Cp)*(Tc-T);
  R_r = C*k0*exp(-EdivR/T);
end CSTR;
```

Listing 2.1 Modelica model `CSTR` in Example 2.1.

simplifications such as constant volumetric hold-up and equal density and heat capacity of feed and product streams. More elaborate models can be found in [Luyben, 2007].

The above model will be used both for simulation, finding stationary points, dynamic optimization and verification of the optimal solution. In Listing 2.1, it is encoded in the Modelica model `CSTR`. The Modelica code is divided into two sections, one with all variables and parameters and one with the equations describing the system. At the top, the input T_c is found together with the states C and T and reaction rate R_r. Each of these is given correct unit either by using the standard Modelica library or using the `unit` attribute directly. They are also given nominal values which are used as scaling factors when solving an optimization problem. Setting correct units in the model is advantageous since available simulation tools for Modelica models may notify the user if different terms in the equations are incompatible. The initial state is set by parameters and

when the model is used for e.g., simulation or optimization, the desired initial state is set by changing the parameter values. For now, they are both set equal to 1. The initial values may either be fixed or free, i.e., specified to certain values or only used as initial guesses when solving an initialization problem. Below the initial value parameters are the model parameters. The model equations are in the second section, indicated by `equation`, and written in a form identical to Eqs. (2.1)–(2.3). With proper initial values, the model may now be simulated using an appropriate tool. □

2.4 Dynamic Optimization Methods

Over the last decades, dynamic optimization has received significant attention in academia and the application of dynamic optimization has increased in industry. It is used both for on-line tasks such as model predictive control (MPC) and state-estimation, and off-line tasks such as trajectory optimization and model parameter optimization. The optimization problem on the time interval $[t_0,\ t_f]$ may in general be formulated as

$$\begin{aligned} &\min_{u(t)} J(x(t_f)) \\ &\text{s.t. } F(\dot{x}(t), x(t), w(t), u(t)) = 0 \\ &\quad F_0(\dot{x}(t_0), x(t_0), w(t_0), u(t_0)) = 0 \\ &\quad C_{\text{ineq}}(\dot{x}(t), x(t), w(t), u(t)) \leq 0 \\ &\quad C_{\text{end}}(\dot{x}(t_f), x(t_f), w(t_f), u(t_f)) \leq 0 \\ &\quad x(t_0) = x_0, \end{aligned} \tag{2.4}$$

where x, w and u are states, algebraic variables and control variables, respectively, and x_0 is the initial state. The cost function J to be minimized is scalar, F is the differential-algebraic equation (DAE) representing the dynamics of the system to be optimized, F_0 represent the DAE augmented with additional initial conditions and C_{ineq} and C_{end} are path and end point inequality constraints, respectively. Several different approaches for solving the optimization problem in Eq. (2.4) exist and they may be divided into indirect and direct methods, see [Biegler, 2010, Betts, 2009]

The indirect, or variational approach, is based on the solution of the first order necessary conditions for optimality obtained from Pontryagin's Maximum Principle, see [Pontryagin *et al.*, 1962]. If no inequality constraints are present in the problem, the conditions may be written as a set of DAEs and several approaches to solve these exist. However, if inequality constraints are present, the activation sequence must be known

a priori and it may also be difficult to find initial guesses for adjoint variables. These drawbacks make the variational methods hard to apply to large-scale systems.

In direct methods, the basic idea is to transform the infinite dimensional optimization problem in Eq. (2.4) to a finite dimensional non-linear programming problem (NLP), see [Binder *et al.*, 2001]. The size of the finite dimensional problem depends on what type of transformation is used, and there are two main branches of direct methods; sequential and simultaneous methods. In the context of polymer grade changes, it is mainly sequential methods and collocation methods, which is a subgroup of simultaneous methods, that have received the most attention. Since collocation is used in papers IV–VI, it will be the main focus in this section. However, short overviews of other direct methods will be given as well, together with a comparison of the solution methods.

Sequential Methods

In sequential methods, the control variables are parametrized by a finite number of parameters p, for instance by piecewise polynomials [Vassiliadis, 1993]. Given initial condition of the DAE, and initial values of the parameters p, the system may be integrated and the result used for evaluating the cost function in the optimization problem in Eq. (2.4). Thus, the cost function depends only on the parameters p, i.e., $J(x(t_f)) = \tilde{J}(p)$. An NLP solver updates the parameters and the system is integrated again, repeating the procedure, as illustrated in Figure 2.3. When the optimization procedure terminates it returns the parameters describing the optimal control profile. Gradients of the cost function with respect to the control signal parameters p are obtained either by sensitivity functions of the DAE system or by integration of the adjoint equations. Path constraints can be approximated by introducing a penalty term in the cost function or by evaluating the constraint function on a fine time grid where the constraints are enforced, see [Binder *et al.*, 2001].

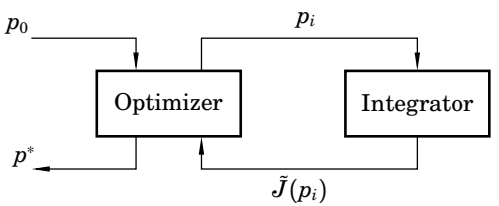

Figure 2.3 Illustration of a sequential method for solving a dynamic optimization problem where p_0 is the initial value of the control parameters, p_i the control parameters updated by the optimizer, $\tilde{J}(p_i)$ the cost function value given when integrating the system, and p^* is the optimal value of the control parameters.

Simultaneous Methods

The simultaneous methods include mainly two different approaches, multiple shooting and collocation.

Multiple Shooting A step towards fully discretizing the problem is made in the multiple shooting method where the optimization interval is divided into a number of segments and in each segment the DAE is integrated separately with initial values that are optimization variables. Continuity of the state profiles are enforced by equality constraints of the state profile end and state profile initial value of two contiguous segments. The control variables are parametrized as in the sequential methods. Sensitivities are obtained for both control parameters and initial conditions for the states in each segment. This approach, compared to sequential methods, adds the possibility to enforce path constraints in each grid point, but they may not be satisfied in between the grid points.

Collocation In the collocation method, the optimization problem is fully discretized by approximating both states, algebraic variables and control variables by polynomials, resulting in one large NLP. The collocation scheme briefly presented below is the one used in the JModelica.org platform, see [Åkesson *et al.*, 2010], which subsequently is used in papers IV–VI for formulating and solving optimization problems.

The optimization interval $[t_0,\ t_f]$ is divided into N_e elements, each with a normalized length $h_0, \ldots, h_{N_e-1}$ with the property that

$$\sum_{i=0}^{N_e-1} h_i = 1. \tag{2.5}$$

The element junction points t_i may thus be written as

$$t_i = t_0 + (t_f - t_0) \sum_{k=0}^{i-1} h_k, \quad i = 1, \ldots, N_e - 1. \tag{2.6}$$

In each element, N_c Radau based collocation points $\tau_j \in (0,\ 1]$, $j \in \{1, \ldots, N_c\}$ are introduced, which gives the collocation time points

$$t_{i,j} = t_0 + (t_f - t_0) \left(\sum_{k=0}^{i-1} h_k + \tau_j h_i, \right),\ i = 0, \ldots, N_e - 1,\ j = 1, \ldots, N_c, \tag{2.7}$$

where the indices i and j correspond to element i and collocation point j in the element, respectively. The state, algebraic variable, and control

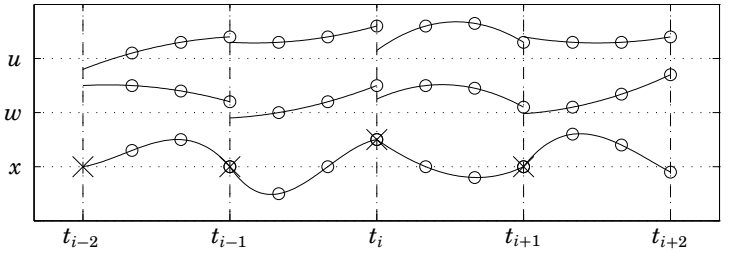

Figure 2.4 Example of approximations of control, algebraic and state variable profiles in a collocation method with $N_c = 3$. The circles ($\circ$) represent collocation points and crosses ($\times$) represent the extra interpolation points used when enforcing continuous state variable profiles.

profiles are approximated by Lagrange polynomials based on the Radau collocation points τ_j. A Lagrange polynomial of order $N_c - 1$ is defined by

$$L_j^{N_c}(\tau) = \begin{cases} 1, & \text{if } N_c = 1 \\ \prod_{k=1, k\neq j}^{N_c} \dfrac{\tau - \tau_k}{\tau_j - \tau_k}, & \text{if } N_c \geq 2, \end{cases} \tag{2.8}$$

and thus at collocation point τ_k

$$L_j^{N_c}(\tau_k) = \begin{cases} 1, & \text{if } j = k \\ 0, & \text{if } j \neq k. \end{cases} \tag{2.9}$$

The state variables are approximated by Lagrange polynomials of order N_c, where the extra point $\tau_0 = 0$ is used, while algebraic variables and control profiles are approximated by Lagrange polynomials of order $N_c - 1$, in each element, see Figure 2.4 for an example. The approximated profiles on the time interval $[t_i,\ t_{i+1}]$ are written as

$$x(t) = \sum_{k=0}^{N_c} x_{i,k} L_k^{N_c+1}\left(\frac{t - t_i}{h_i(t_f - t_0)}\right), \quad t \in [t_i, t_{i+1}] \tag{2.10}$$

$$w(t) = \sum_{k=1}^{N_c} w_{i,k} L_k^{N_c}\left(\frac{t - t_i}{h_i(t_f - t_0)}\right), \quad t \in [t_i, t_{i+1}] \tag{2.11}$$

$$u(t) = \sum_{k=1}^{N_c} u_{i,k} L_k^{N_c}\left(\frac{t - t_i}{h_i(t_f - t_0)}\right), \quad t \in [t_i, t_{i+1}], \tag{2.12}$$

and with the properties of the Lagrange polynomials it follows that

$$x(t_{i,j}) = \sum_{k=0}^{N_c} x_{i,k} L_k^{N_c+1}(\tau_j) = x_{i,j} \quad i = 0,\ldots,N_e-1,\ j = 0,\ldots,N_c \quad (2.13)$$

$$w(t_{i,j}) = \sum_{k=1}^{N_c} w_{i,k} L_k^{N_c}(\tau_j) = w_{i,j} \quad i = 0,\ldots,N_e-1,\ j = 1,\ldots,N_c \quad (2.14)$$

$$u(t_{i,j}) = \sum_{k=1}^{N_c} u_{i,k} L_k^{N_c}(\tau_j) = u_{i,j}, \quad i = 0,\ldots,N_e-1,\ j = 1,\ldots,N_c, \quad (2.15)$$

where $x_{i,j}$, $w_{i,j}$ and $u_{i,j}$ now represent the discretized profiles. As Radau points are used, the last collocation point is $\tau_{N_c} = 1$ and with the extra interpolation point for the state variables at $\tau_0 = 0$, continuity over the element borders are ensured by enforcing the relation

$$x_{i,N_c} - x_{i+1,0} = 0, \quad i = 0,\ldots,N_e-1. \quad (2.16)$$

The state derivatives are approximated on the time interval $[t_i,\ t_{i+1}]$ by the derivative of Eq. (2.10) as

$$\dot{x}(t) = \frac{1}{h_i(t_f - t_0)} \sum_{k=0}^{N_c} x_{i,k} \dot{L}_k^{N_c+1}\left(\frac{t - t_i}{h_i(t_f - t_0)}\right), \quad t \in [t_i,\ t_{i+1}], \quad (2.17)$$

which thus gives

$$\dot{x}(t_{i,j}) = \frac{1}{h_i(t_f - t_0)} \sum_{k=0}^{N_c} x_{i,k} \dot{L}_k^{N_c+1}(\tau_j) = \dot{x}_{i,j}, \quad \begin{matrix} i = 0,\ldots,N_e-1 \\ j = 1,\ldots,N_c, \end{matrix} \quad (2.18)$$

where $\dot{x}_{i,j}$ now represent the discretized state derivative trajectory.

For the initial value problem, i.e., F_0 in Eq. (2.4), introduce the variables $\dot{x}_{0,0}$, $w_{0,0}$ and $u_{0,0}$. To provide an equation for $u_{0,0}$, it may for instance be chosen equal to $u_{0,1}$, or as in JModelica.org, by interpolation using the Lagrange polynomials as

$$u_{0,0} = \sum_{k=1}^{N_c} u_{0,k} L_k^{N_c}(0). \quad (2.19)$$

The variables representing the trajectories may now be summarized as

- at the initial point t_0: $\dot{x}_{0,0}, x_{0,0}, w_{0,0}, u_{0,0}$.

- at the collocation points $t_{i,j}$: $\dot{x}_{i,j}, x_{i,j}, w_{i,j}, u_{i,j}$, $i = 0, \ldots, N_e - 1$, $j = 1, \ldots, N_c$.
- at the element junction points t_i: $x_{i,0}$, $i = 1, \ldots, N_e$.

Considering the original optimization problem in Eq. (2.4), the constraints are transformed into only being valid at the collocation points, the initial point and end point as

$$F(\dot{x}_{i,j}, x_{i,j}, w_{i,j}, u_{i,j}) = 0, \qquad i = 0, \ldots, N_e - 1,\ j = 1, \ldots, N_c \tag{2.20}$$

$$F_0(\dot{x}_{0,0}, x_{0,0}, w_{0,0}, u_{0,0}) = 0 \tag{2.21}$$

$$C_{\text{ineq}}(\dot{x}_{i,j}, x_{i,j}, w_{i,j}, u_{i,j}) \leq 0, \qquad i = 0, \ldots, N_e - 1,\ j = 0, \ldots, N_c \tag{2.22}$$

$$C_{\text{end}}(\dot{x}_{N_e-1,N_c}, x_{N_e-1,N_c}, w_{N_e-1,N_c}, u_{N_e-1,N_c}) \leq 0. \tag{2.23}$$

If all variables defining the trajectories are collected in a vector $\overline{x}$, the equality equations in Eq. (2.16) and Eqs. (2.18)–(2.21) are collected in $h(\overline{x}) = 0$, and the inequality conditions in Eqs. (2.22)–(2.23) are collected in $g(\overline{x}) \leq 0$, then the dynamic optimization problem is transformed into an NLP defined as

$$\begin{aligned} \min_{\overline{x}} \ & f(\overline{x}) \\ \text{s.t.} \ & h(\overline{x}) = 0 \\ & g(\overline{x}) \leq 0, \end{aligned} \tag{2.24}$$

where $f(\overline{x}) = J(x_{N_e-1,N_c})$. This NLP may be solved directly and simultaneously for all state, algebraic and control variables representing the approximated trajectories and thus, no simulation, i.e., use of a DAE solver, is involved.

Comparison of Direct Methods

Choosing optimization method when solving the optimal control problem in Eq. (2.4) requires some considerations as the individual methods both have advantages and disadvantages, see [Binder *et al.*, 2001]. Several papers on grade change optimization have been written, and they are clearly dominated by sequential and collocation methods.

The sequential methods have the advantage of being conceptually very simple and intuitive for the user, giving confidence in the methods. The methods can be applied using standard NLP solvers, as the NLP to solve is in general small compared to the one at collocation methods. It may also take advantage of developments of state of the art DAE integrators. A disadvantage with the sequential methods is the computational burden, since a DAE is integrated in every iteration. In particular, this is true if

also considering sensitivity or adjoint equations. However, this approach also yields the dynamic constraints of the model equations to be fulfilled in each step. A premature stop of the algorithm produces a control vector yielding in general better trajectories than the initial guess. Path constraints and unstable systems, which are common in grade transitions for polymer reactors, are difficult to manage with sequential methods.

Collocation methods do not rely on DAE integrators as the optimization problem is fully discretized. However, the resulting NLP in Eq. (2.24) is in general very large. To solve it efficiently, the sparsity structure of the constraint Jacobian and Hessian must be exploited. Such NLP solvers exist and have been developed significantly during the last two decades, see [Biegler *et al.*, 2002]. Even with state of the art NLP solvers, such as [Wächter and Biegler, 2006], the NLP is sensitive to scaling of the variables. If the problem is ill-conditioned, convergence may be slow or even lost. Initial values for all variables are also essential for good convergence, i.e., trajectory values at all collocation points are desirable. In papers IV–VI, scaling and initial values of all variables have been imperative for good convergence and in some cases also to have convergence at all.

After successful termination by the NLP solver, and only then, are the dynamic constraints of the DAE fulfilled within tolerances. Thus, a premature stop of the algorithm yields unusable trajectories. Compared to the sequential methods, introducing path constraints at the collocation time points are straight forward as seen in Section 2.4, and the discretization also renders the method better suited for unstable systems.

The multiple shooting method, which is not commonly used in literature of polymer grade change optimizations, inherits properties both from sequential and collocation methods. Path constraints can only be considered at segment junctions and may thus be violated inside the segments, which is similar to the collocation method where the constraints may be violated between the collocation points. The numerical stability properties are improved compared to sequential methods when many segments are used. The computational burden is still large, as a DAE is integrated in each segment, and the number of variables to solve for in the NLP requires tailored NLP solvers. Initial values should be supplied for all segment junctions and the dynamics are only fulfilled at successful termination.

As previously stated, the collocation method was chosen when solving the grade transition optimization problems in papers IV–VI. This was with the background of its direct capability of handling constraints on all included variables, which is important in grade transitions. Also, an implementation of a collocation method was available in the JModelica.org platform, c.f. Section 2.5, which includes the Optimica extension that bridges the gap between Modelica models and formulating an optimization prob-

lem. This platform had been used successfully in [Haugwitz, 2007], where optimization of start-ups of a plate reactor was considered. In parallel to the work in papers IV–VI, several other applications have been considered using JModelica.org, such as power plants, post-combustion adsorption units, robotics and pendulum systems, see [Casella *et al.*, 2011, Åkesson *et al.*, 2011, Olofsson *et al.*, 2011, Hast *et al.*, 2009, Giselsson *et al.*, 2009].

2.5 JModelica.org

The Modelica language has been developed with the aim of simulation and simulation tools have become very sophisticated during the last decades. Now, focus is also directed towards using the models for optimization. Support has started to emerge in various forms, e.g., model integration tools that interface several design tools for analysis, simulation and optimization, modeling tools with limited optimization add-ons, and numerical optimization packages, see [Åkesson *et al.*, 2010].

Using state of the art numerical solvers is not straight forward as numerical packages often require high level of model details, including derivatives and sparsity structures. Additionally, users are often required to be skilled since the original optimization problem often has to be transcribed in some way.

Dynamic optimization is often an iterative process. To try different solution methods, it is beneficial if the optimization problem is stated in a high-level fashion, directly associated with the mathematical formulation in Eq. (2.4), with the option of selecting the solution approach. From the perspective of the PIC-LU project, where prototype software for grade change optimization is developed and aimed towards process engineers, the methodology of solving the optimization problems should be as automated as possible. The process engineer is not expected to be highly conversant with optimization methods, nor numerical optimization algorithms. From the software developer's side, it should be straight forward to interface with different types of optimization algorithms.

One software package that supports the above is JModelica.org, an open-source platform that is well integrated with Modelica models and that uses Optimica for formulation of dynamic optimization problems. An optimization class and optimization attributes are introduced in Optimica, making it possible to encode the optimization problem in a high-level fashion similar to the formulation in Eq. (2.4) and structured as a Modelica model, see [Åkesson, 2008] for further details. JModelica.org bridges the gap between simulation models expressed in a high-level language and state of the art optimization algorithms.

The JModelica.org platform includes a compiler for Modelica and Optimica models, generating C code that contains the model equations and XML output that holds model meta data such as variable specifications, names and attributes. A run-time library provides a C interface for the generated code, having, amongst others, functions to set parameters in the compiled model. The interface can be divided into four different parts: an ODE interface, a DAE interface, a DAE initialization interface and an optimization interface. The two first provide evaluation of the ODE derivative function and residual function of the DAE, respectively, while the latter two provide functions for solving the DAE initialization problem and evaluation of the cost function and the constraints. In addition, for all interfaces, Jacobians and sparsity patterns can be obtained for all the functions by the utilization of CppAD, a package for symbolic differentiation [Bell, 2011].

Two different optimization algorithms for solving dynamic optimization problems are implemented in JModelica.org. One is a collocation based method, as presented in Section 2.4, that is implemented in C. It is interfaced with the state of the art NLP solver IPOPT, that is developed particularly for solving problems arising when discretizing a dynamic optimization problem with collocation, see [Wächter and Biegler, 2006]. The other algorithm is a multiple shooting method implemented in Python, relying on the integrator SUNDIALS, see [Bock and Plitt, 1984] and [Hindmarsh *et al.*, 2005]. The implementations of the optimization algorithms serve as examples of how the C interface is used such that users may contribute with other optimization algorithms.

For scripting and automating the optimization procedures, JModelica.org contains a Python package. It provide means for managing the compilers and file input/output for simulation and optimization, and is also used for calling the functions in the run-time library interface. Python is a free open-source language, supporting for instance scientific computing, see [Python Software Foundation, 2011]. It has packages for e.g., plotting and creating GUIs, highly suitable for the aims of the PIC-LU project, i.e., developing prototype versions of software for process engineers. See [Åkesson *et al.*, 2010] for a more in-depth review of JModelica.org.

As JModelica.org has been used in papers IV–VI for grade change optimization using the presented collocation method, the optimization methodology will be shown by an example using the CSTR reactor in Example 2.1. Dynamic optimizations and verifications of optimal solutions in the papers are performed as in the example. For finding stationary points of a system, the method in the example is similar to the one used in Paper IV, while the stationary points in Paper V and VI were found via optimization with regards to economy.

Example 2.2—Optimal Change of Operating Point for a CSTR.
The reactor presented in Example 2.1 has non-linear dynamics and the rate of the exothermic reaction increases rapidly with increasing temperature. Two different stationary points, A and B, for the reactor will be computed, where A corresponds to a cold reactor with low reaction rate and B corresponds to a higher temperature and a higher reaction rate. The difficulty of changing operating point from A to B is to increase the reaction rate with a controlled reactor temperature increase.

The two operating points are defined by coolant flows with temperatures $T_c^{\mathrm{A}} = 250$ K and $T_c^{\mathrm{B}} = 280$ K, respectively, and to solve for the two points, an initialization model `CSTR_init` is constructed, see Listing 2.2. It contains the component `CSTR`, as defined in Example 2.1, a parameter that sets the coolant temperature in the `equation` section with a value that may be modified from Python, and initial equations that hold at initial time $t = 0$. As seen in the `initial equation` section in the model, the derivatives of the reactor states are set to 0 at initial time, thus specifying stationary conditions. The variables to solve for are $C(0)$, $T(0)$, $R_r(0)$, $\dot{C}(0)$ and $\dot{T}(0)$, and with the five equations at initial time, i.e., model and initial equations, the initial equation system is well defined. By setting the coolant flow to any of the two operating point values, the system is solved by invoking the DAE initialization algorithm in JModelica.org. The resulting two stationary operating points are reported in Table 2.1.

The change of operating point will be optimized by formulating a quadratic cost function. The temperature in the reactor is constrained to be lower than 350 K and the coolant flow has lower and upper limits of 230 K and 370 K, respectively, and rate constraints of ±20 K/s. Using the coolant temperature derivative as decision variable allows to easily set

```
model CSTR_init
   CSTR cstr(C(fixed=false),T(fixed=false));
   parameter Modelica.SIunits.Temp_K Tc_init = 1;
equation
  cstr.Tc = Tc_init;
initial equation
  der(cstr.C) = 0;
  der(cstr.T) = 0;
end CSTR_init;
```

Listing 2.2 Modelica model `CSTR_init` for finding stationary points in Example 2.2.

Table 2.1 Stationary operating points for the CSTR in Example 2.2.

Operating point i	C^i [mol/m^3]	T^i [K]	R_r^i [mol/m^{3}s]	T_c^i [K]
A	956.3	250.1	0.0007288	250
B	338.8	280.1	0.01102	280

its constraints. The dynamic optimization problem on the time interval $t \in [0,\ 160]$ for transferring the reactor operating point from A to B, may be formulated as

$$\begin{aligned}
&\min_{\dot{T}_c} \int_0^{160} \left(q_C(C^{\mathrm{B}} - C)^2 + q_T(T^{\mathrm{B}} - T)^2 + q_{T_c}(T_c^{\mathrm{B}} - T_c)^2 + q_{\dot{T}_c}\dot{T}_c^2\right) dt \\
&\text{s.t. Eqs. } (2.1) - (2.3) \\
&\qquad T_c = \int_0^t \dot{T}_c \, d\tau \\
&\qquad T \leq 350 \\
&\qquad 230 \leq T_c \leq 370 \\
&\qquad -20 \leq \dot{T}_c \leq 20 \\
&\qquad C(0) = C^{\mathrm{A}},\ T(0) = T^{\mathrm{A}},\ T_c(0) = T_c^{\mathrm{A}},
\end{aligned} \tag{2.25}$$

where q_j, $j \in \{C,\ T,\ T_c,\ \dot{T}_c\}$ are weights and C^i, T^i, T_c^i, $i \in \{\mathrm{A},\ \mathrm{B}\}$ are stationary points corresponding to the two operating points in Table 2.1. A term penalizing $\dot{T}_c$ is added to influence the smoothness of T_c. Using the Optimica extension, an optimization model `CSTR_opt` is constructed that expresses the optimization problem, see Listing 2.3. The class attributes `startTime` and `finalTime` are used for setting the optimization interval, while `objective` defines the cost function. The first section of the optimization model contains an input, i.e., the derivative of T_c, a CSTR component and the cost variable. Additionally, nominal values for the input and cost are set, and reference values and cost function weights, that may be set from Python, are declared. In the `equation` section, the input is connected to the derivative of the CSTR input and the cost function is constructed, expressed as in the original optimization problem, see Eq. (2.25). In the third section, beginning with `constraint` and specific for Optimica, are the constraints expressed directly on the model variables.

The optimization problem is to be solved by collocation, and as pointed out in Section 2.4, providing initial values for all variables at the collocation points are advantageous for good convergence. For this reason, the simulation model `CSTR_trajGen`, providing such values, is constructed, see Listing 2.4. It contains the same variables as the optimization model does and is simulated in JModelica.org by initializing the model from Python to operating point A and then holding the coolant flow temperature constant, i.e., the reactor is operated in steady state during the simulation of 160 s. The reference values in the cost function are set to operating point B, yielding an increasing cost function during the simulation. The simulation result is saved and used as initial guess for the optimization.

```
optimization CSTR_opt(objective=cost(finalTime),startTime=0.0,finalTime=160)
  input Modelica.SIunits.TemperatureSlope Tc_der(start=0,fixed=false,nominal=Tc_der_0);

  CSTR cstr(Tc(start=Tc_A,fixed=true));
  Real cost(start=0,fixed=true,nominal=cost_0);

  //Nominal values
  parameter Modelica.SIunits.TemperatureSlope Tc_der_0 = 20;
  parameter Real cost_0 = 100;

  //Initial value for Tc
  parameter Modelica.SIunits.Temp_K Tc_A = 1;

  //Reference values
  parameter Modelica.SIunits.Concentration C_B = 1;
  parameter Modelica.SIunits.Temp_K T_B = 1;
  parameter Modelica.SIunits.Temp_K Tc_B = 1;

  //Cost function weights
  parameter Real q_C(final unit="m6/(mol2.s)") = 1;
  parameter Real q_T(final unit="1/(K2.s)") = 1;
  parameter Real q_Tc(final unit="1/(K2.s)") = 1;
  parameter Real q_Tc_der(final unit="s/K2") = 1;

equation
  der(cstr.Tc) = Tc_der;
  der(cost) = q_C*(C_B-cstr.C)^2 + q_T*(T_B-cstr.T)^2
            + q_Tc*(Tc_B-cstr.Tc)^2 + q_Tc_der*Tc_der^2;

constraint
  cstr.T <= 350;
  cstr.Tc >= 230;
  cstr.Tc <= 370;
  Tc_der <= 20;
  Tc_der >= -20;
end CSTR_opt;
```

Listing 2.3 Optimica model `CSTR_opt` for formulating the optimization problem in Example 2.2.

An element length of 1 s is used in the collocation method with 3 collocation points in each element. The decision variable, i.e., the derivative of the coolant temperature, is constant in each element. The optimization is invoked from Python, resulting in an NLP with approximately 5000 variables which is solved in less than 20 s by IPOPT. Using numerical methods, the solution is always an approximation. To verify the solution, $\dot{T}_c$ is used as input to a verification model, see Listing 2.5, which is initialized to operating point A and then simulated 160 s. The optimization and verification results are found in Figure 2.5, and are practically identical. The used collocation method corresponds to a fixed step size Radau solver, while the solver used in the verification simulation was IDA from the SUNDIALS suite, see [Hindmarsh *et al.*, 2005], which is a variable step size backward differentiation formula (BDF) solver with error control. Thus, it is most likely that the solution found fulfills the model equations, at least to specified tolerances.

```
model CSTR_trajGen
  CSTR cstr(Tc(start=Tc_A,fixed=true));
  Real cost(start=0,fixed=true);

  Modelica.SIunits.TemperatureSlope Tc_der = Tc_der_init;

  //Parameters for temperature trajectory
  parameter Modelica.SIunits.Temp_K Tc_A = 1;
  parameter Modelica.SIunits.TemperatureSlope Tc_der_init = 1;

  //Reference values
  parameter Modelica.SIunits.Concentration C_B = 1;
  parameter Modelica.SIunits.Temp_K T_B = 1;
  parameter Modelica.SIunits.Temp_K Tc_B = 1;

  //Cost function weights
  parameter Real q_C(final unit="m6/(mol2.s)") = 1;
  parameter Real q_T(final unit="1/(K2.s)") = 1;
  parameter Real q_Tc(final unit="1/(K2.s)") = 1;
  parameter Real q_Tc_der(final unit="s/K2") = 1;

equation
  der(cstr.Tc) = Tc_der;
  der(cost) = q_C*(C_B - cstr.C)^2 + q_T*(T_B - cstr.T)^2
            + q_Tc*(Tc_B - cstr.Tc)^2 + q_Tc_der*Tc_der^2;
end CSTR_trajGen;
```

Listing 2.4 Modelica model `CSTR_trajGen` for generating initial trajectories for optimization problem in Example 2.2.

```
model CSTR_sim
  input Modelica.SIunits.TemperatureSlope Tc_der;
  CSTR cstr(Tc(start=Tc_A,fixed=true));
  parameter Modelica.SIunits.Temp_K Tc_A = 1;
equation
  der(cstr.Tc) = Tc_der;
end CSTR_sim;
```

Listing 2.5 Modelica model `CSTR_sim` for simulation and verification of optimal solution in Example 2.2.

The change of operating point is performed by increasing the reactor temperature as fast as possible in the beginning, the constraint on $\dot{T}_c$ is active until T_c reaches its maximum value. At approximately $t = 30$ s, the increase in temperature T gives a drastic increase in reaction rate R_r. The coolant flow temperature is decreased as rapidly as possible with the constraint on $\dot{T}_c$ active, holding the reactor temperature at its constraint. As the concentration approaches its reference value, the reactor is cooled with T_c at its lower constraint, yielding the reactor temperature and reaction rate to reach their operating point B values. □

A User's Perspective on JModelica.org and Collocation

At the start of PIC-LU, the JModelica.org project was already initiated. However, it has evolved and matured during the PIC-LU project. Evalu-

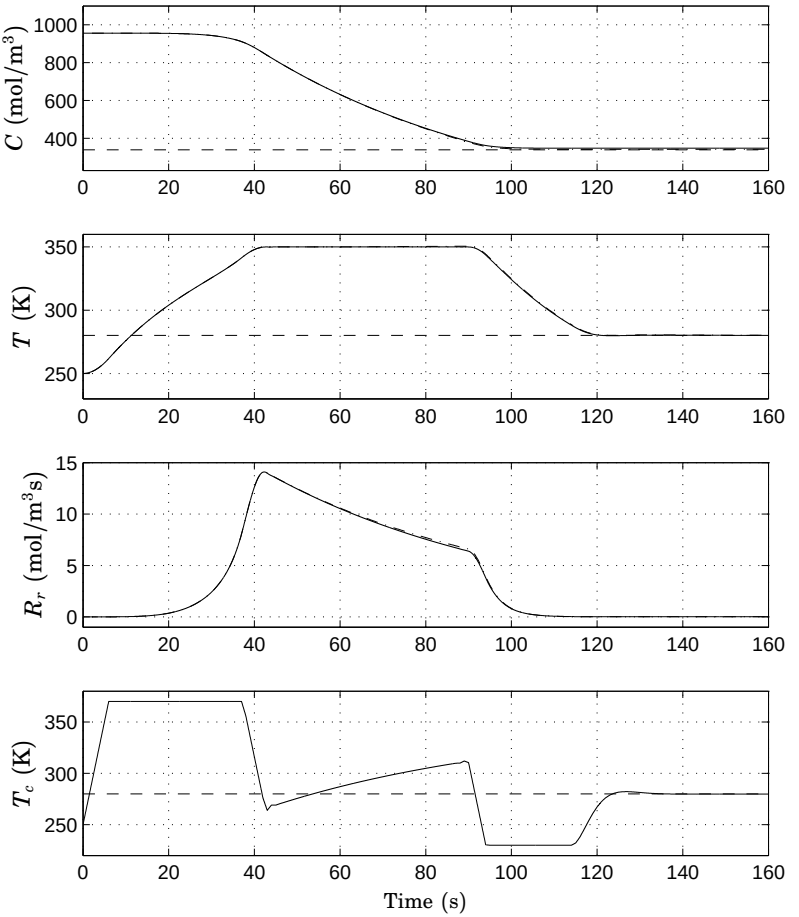

Figure 2.5 Optimal change of operating point for the CSTR in Example 2.2. Collocation based trajectories (–), simulated trajectories (- - -) and reference values (--), i.e., desired stationary end point.

ating a tool such as JModelica.org, it must be taken into account that it is mostly focused on research, algorithm development and education. The perspective given here will be in the light of using the collocation method for solving dynamic optimization problems.

The main advantages of JModelica.org for a user is the simplicity of formulating optimization problems at a high level, following the Modelica-way of modeling, and not having to discretize the model and optimization problem manually when interfacing state of the art optimization algo-

rithms. However, for the use of numerical solvers, some precautions must be taken that are obstacles in the solving methodology, partly distracting the user from the optimization results.

As noted in Section 2.4 and seen in Example 2.2, states, algebraic variables and inputs are given nominal values for scaling in the optimization problem. This requires the modeler and the optimization algorithm user to know approximately in what ranges the different variables are. This may not be a problem as the system can be simulated near the considered operating points used at dynamic optimization, yielding approximate values. However, these values are only indications since the optimal solution may require large changes in states, algebraic variables and inputs. The optimal solution is only known after scaling has been performed, but to reach the optimal solution, scaling must be performed correctly. This has shown to be a major task requiring iteration, both in small optimization examples, as Example 2.2, and in large-scale problems, such as papers IV–VI, and especially if considering control derivatives as decision variables. When Paper IV was written, scaling with `nominal` was not supported in JModelica.org, manual scaling of variables was instead performed by P. Larsson.

In the collocation method, the problem is solved simultaneously for states, algebraic variables, inputs, but also state derivatives, and as the scaling is set by the `nominal` attribute in the models, there is no direct way of setting the scaling factors of the state derivatives. The solution to this in JModelica.org is that the state derivative inherits the scale factor from the state. This can cause an unsuitable scale factor to be used for the derivatives, considering for instance a state with large value but with small changes during optimization, or vice versa. Additionally, a scaling factor must be provided for the objective function, and thus the optimal value must approximately be known prior to performing optimization.

The scaling problems are somewhat relieved by using automatic scaling in the NLP solver IPOPT, but it has turned out to be one of the major obstacles in the solution methodology. An automatic scaling procedure in JModelica.org is highly desirable and a prerequisite if the tool should be used by non-advanced users.

Simulation of Modelica models is not as sensitive to how the equations are written as optimization has turned out to be. Changing an equation, by for instance multiplication with a constant on both sides, changes the Jacobian. Means for equation scaling, similar to the variable scaling using `nominal`, are desirable, but lacking in JModelica.org. An automatic scaling procedure would be preferred, as this will allow the modeler to write the equations in the most intuitive manner, as was the aim of the Modelica language. And also, the platform would not have to rely on scaling of the Jacobians in the NLP solver.

If problems occur in solving the resulting NLP from collocation, such as slow or lack of convergence, it is difficult for an user to see what remedies to take. It may be a variable that causes problems, by for instance non-suitable scaling, but it can also be some part of the cost function yielding too small or large derivatives making step sizes in the NLP solver too large or small. An analysis of the results from a premature stop can yield some answers, but as the DAE is not fulfilled, the system cannot be simulated with resulting trajectories to find a solution to the problems. However, this property is inherent to the collocation method.

2.6 Contributions Overview

The main aims of the PIC-LU project considered in this thesis are construction of a Modelica library for the plant PE3 at Borealis AB and to perform dynamic optimizations of grade changes. The library is described in Supplement A and has been used in Paper IV and VI. It contains connectors, reactor and distillation column models, models for optimization and verification of optimization results, and different templates defining plant configurations. Dynamic optimization of grade changes are considered in papers IV–VI and in [Larsson *et al.*, 2010]. The papers give a good overview of the project progression over time and Paper VI has the highest value of contribution. The work has evolved together with the development of the Modelica library, but also with JModelica.org.

Using a simple quadratic cost function and only the pre-polymerization reactor, the work in [Larsson *et al.*, 2010] was an introduction for the thesis' author to polymerization reactor operation and the use of JModelica.org. It was also the initiation of the Modelica library. The library has undergone several changes since then and the description in [Larsson *et al.*, 2010] is out of date. The choice of quadratic cost function is motivated by its simplicity, it is well known from other optimization problems and yields often rapid convergence. Additionally, it had been used before by several other authors for optimization of grade changes.

In step towards using the whole plant model, the loop reactor and the gas-phase reactor were added to the structure, increasing model complexity. Again, a quadratic optimization criterion was set up, resulting in Paper IV. This was a performance measure of the tools and optimization methodology, showing that they are capable to solve such large-scale problems. The optimizations in both [Larsson *et al.*, 2010] and Paper IV were performed with manually scaled variables, implemented by P. Larsson, since the scaling feature with nominal variables values was not available in JModelica.org at that time. This procedure was cumbersome, but gave insight into the numerical optimization methods.

Quadratic cost functions are advantageous in many aspects, but they may be difficult to design such that they resemble the economical cost of grade changes. As one aim of the PIC-LU project was to consider the economy during a grade change, a cost function expressed in terms of prices of raw material and diluents and product sell prices was therefore constructed and applied to a smaller model of a gas-phase reactor in Paper V. This model has been used by several other authors, and the model equations as well as the model parameters are openly available, which is rare in the community due to e.g., model sizes, limited article lengths, but also confidentiality reasons. The cost function also took into concern the quality variable intervals used when defining on-grade polymer and economical incentives were added to produce on-target polymer, which has not been, to the best knowledge of the paper's authors, considered elsewhere. Also, active use of the reactor bleed stream as a decision variable and a preparatory time interval prior transition time, are both uncommon in the articles published in the community, but shown to be very useful. Due to the severe non-linearities in the economic cost function, the optimization is much more difficult compared to a quadratic cost function. Performing initial optimizations and analysis on a smaller, previously published model, compared to using the full confidential Borstar® model directly, was critical for cost function design choices. This yielded also the results reproducible by the community.

The main paper concerning grade changes in this thesis is Paper VI, where the Borstar® reactors are complemented with a recycle area, i.e., a model of the plant PE3 at Borealis AB is used. This required design of simple models of the distillation columns in the recycle area by using measurement data, and the resulting models are incorporated in the Modelica library of the plant. The cost function regarding economy developed in Paper V were used, including prices of raw materials and diluents and polymer sell prices, quality variable intervals and economical incentives to produce on-target polymer. Adding the recycle area to the three Borstar® reactors changed the overall system dynamics considerably compared to Paper IV, as the outflows of the reactors essentially are additional inflows to the reactors. This yields for instance longer time constants and difficulties in removing hydrogen from the reactors. The solutions from grade change optimizations take into consideration the recycled components and how they are affected by the fresh inflows and reactor states. The flare flow of the GPR is used as a decision variable, and so are the off-gas flows on two of the three recycle distillation columns. To the best knowledge of the authors of the paper, using off-gases in a recycle area of a plant as decision variables, has not been studied in previous work in the community, and proved to be useful when removing hydrogen from the reactor. A great majority of the papers published in the field of polymer grade

transitions utilizes a quadratic cost function, either on grade variables, controls or states, or a combination. From the results in Paper VI, it is not clear how a quadratic cost function should be designed to approximate the behavior of the solution. For instance, the resulting off-gas flows on the distillation columns have high peaks during short time intervals, which may be difficult to select weights for in a quadratic optimization criteria.

At Borealis AB, the work in the PIC-LU project has generated several questions on how they operate the PE3 plant today during grade changes, how different costs relate to each other and how an optimization problem concerning PE3 should be formulated. Plans of changing from recipe based transitions to an on-line transition management system exist. Niclas Carlsson, Asset Development Expert at Borealis AB, expressed that a tool similar to the prototype outcome of the PIC-LU project would be very useful for optimizing input trajectories to such a system.

2.7 Future Work

The papers presented in this thesis are part of a feasibility study. Several different interesting paths may be taken to improve the work and some of them will be mentioned briefly here. This section is preferably read after the papers IV–VI have been read.

Solutions Analysis

Sensitivity analysis with respect to model and parameter errors of the solutions from the optimizations may be performed. This may be done either in open loop or in closed loop with e.g., an (N)MPC with feedforward trajectories from the optimization. This is interesting both from a model perspective, i.e., to see what parameters are important to have good estimates of, and also from an application point of view if the trajectories should be used on the physical plant.

Modeling

Models of the production of inerts, such as ethane, in the reactors should be added. The inert content in the overall system is an important aspect of the off-gas flow control in the recycle area as the enrichment of inerts is undesirable and can be suppressed by the off-gas flows. More detailed models of the polymer, using e.g. molecular weight distributions, is another interesting path to take. Models of the recycle area components can be improved significantly, as the current models are only simple filters with split factors, and also, additional components such as e.g., flash and degassing tanks may be included in the model. Developing models has not been a main focus in PIC-LU, as the reactor models were provided by Borealis AB.

Solution Method

In papers IV–VI, the collocation method was used for solving the optimization problems. A comparison with sequential methods, and perhaps also multiple shooting, in terms of e.g., convergence rate, effort of scaling and constraints handling, would be very interesting. Handling of the discrete non-approximated non-linear economic cost function using e.g., mixed integer dynamic optimization may also be used in the comparison.

Cost Function

Terms considering, for instance, costs of cooling, heating, electricity, steam flows and other major operating costs are natural extension of the cost function that regards economy. In the same cost function, set-point handling of operation variables may be troublesome if the number of operation variables is increased compared to the numbers in the presented papers. Other strategies such as e.g., quadratic penalties or more elaborate methods can be tried. In any case, the penalty for deviating from set-points will always be compared to the increase in difference between revenues and costs, yielding tuning difficult.

It would be interesting to try different approximations of the on-grade function, trying to improve convergence rate. Especially, approximations where the on-grade function derivatives with respect to the quality variables not tend to 0 outside the on-grade interval. This would perhaps push quality variable trajectories toward on-grade more than the considered approximation, and also affect the off-grade price, introducing a trade-off between profit accuracy and convergence rate.

Not explicitly part of the cost function, but affecting it, are minimum and maximum values of different variables. These limits may not be the same during steady state operation and during dynamic grade transition. For example, if the minimum values of the off-gas flows are lower during transition than during stationary production, then the dynamic optimization with regards to economy will try to reach a stationary production point with lower off-gas flows than what the stationary optimization is capable of. This may yield undesirable transients in the beginning of the optimization interval and just prior constant control flows.

Finally, reverse engineering of the weights in a quadratic cost function using the economically optimal trajectories would be interesting. This would give an indication of how close one may get to the economical optimum when using quadratic cost functions.

References

Åkesson, J. (2008): "Optimica—An Extension of Modelica Supporting Dynamic Optimization." In *6th International Modelica Conference 2008*. Modelica Association.

Åkesson, J., K.-E. Årzén, M. Gäfvert, T. Bergdahl, and H. Tummescheit (2010): "Modeling and Optimization with Optimica and JModelica.org — Languages and Tools for Solving Large-Scale Dynamic Optimization Problem." *Computers & Chemical Engineering*, **34:11**, pp. 1737–1749.

Åkesson, J., R. Faber, C. Laird, K. Prölss, H. Tummescheit, S. Velut, and Y. Zhu (2011): "Models of a post-combustion absorption unit for simulation, optimization and non-linear model predictive control schemes." In *8th International Modelica Conference*.

Andersen, K., M. Hillestad, and T. Koskelainen (2000): "Predictive Control for a BORSTAR Polyethylene Process." In *Proc. 1st European Conference on the Reaction Engineering of Polyolefins*. Lyon, France.

Andersson, N., P. Larsson, J. Åkesson, S. Haugwitz, and B. Nilsson (2011): "Calibration of a polyethylene plant for grade change optimizations." In *Proceedings of the 21st European Symposium on Computer-Aided Process Engineering*. Chalkidiki, Greece.

Backx, T., O. Bosgra, and W. Marquardt (1998): "Towards intentional dynamics in supply chain conscious process operations." In *Proc. Foundations of Computer-Aided Process Operations '98*. Snowbird, Utah, USA.

Bell, B. (2011): "CppAD, A Package for Differentiation of C++ Algorithms." `http://www.coin-or.org/CppAD/`.

Betts, J. (2009): *Practical Methods for Optimal Control and Estimation Using Nonlinear Programming*. Society for Industrial Mathematics.

Biegler, L. (2010): *Nonlinear Programming: Concepts, Algorithms, and Applications to Chemical Processes*. Society for Industrial Mathematics.

Biegler, L., A. Cervantes, and A. Wächter (2002): "Advances in simultaneous strategies for dynamic optimization." *Chemical Engineering Science*, **57**, pp. 575–593.

Binder, T., L. Blank, H. G. Bock, R. Bulitsch, W. Dahmen, M. Diehl, T. Kronseder, W. Marquardt, S. J., and O. von Stryk (2001): *Introduction to model based optimization of chemical processes on moving horizon*, chapter Online optimization of large scale systems. Springer.

Bock, H. G. and K. J. Plitt (1984): "A multiple shooting algorithm for direct solution of optimal control problems." In *Proceedings 9th IFAC World Congress, Budapest, Hungary*, pp. 243–247. Pergamon Press.

Casella, F., F. Donida, J. Åkesson, and F. Donida (2011): "Object-oriented modeling and optimal control: A case study in power plant start-up." In *18th IFAC World Congress, Milano, Italy*.

Chatzidoukas, C., J. Perkins, E. Pistikopoulos, and C. Kiparissides (2003): "Optimal grade transition and selection of closed-loop controllers in a gas-phase olefin polymerization fluidized bed reactor." *Chemical Engineering Science*, **58:16**, pp. 3643 – 3658.

Dünnebier, G., D. van Hessem, J. Kadam, K.-U. Klatt, and M. Schlegel (2005): "Optimization and control of polymerization processes." *Chemical Engineering & Technology*, **28:5**, pp. 575–580.

Embiruçu, M., E. Lima, and J. Pinto (1996): "A survey of advanced control of polymerization reactors." *Polymer Engineering & Science*, **36:4**, pp. 433–447.

Flores-Tlacuahuac, A., A. Biegler, and E. Saldívar-Guerra (2006): "Optimal grade transitions in the high-impact polystyrene polymerization process." *Industrial & Engineering Chemistry Research*, **45:18**, pp. 6175–6189.

Fritzson, P. (2004): *Principles of Object-Oriented Modeling and Simulation with Modelica 2.1*. IEEE Press, Wiley Interscience.

Giselsson, P., J. Åkesson, and A. Robertsson (2009): "Optimization of a Pendulum System using Optimica and Modelica." In *Proceedings of the 7th International Modelica Conference 2009*. Modelica Association, Como, Italy.

Hast, M., J. Åkesson, and A. Robertsson (2009): "Optimal Robot Control using Modelica and Optimica." In *Proceedings of the 7th International Modelica Conference 2009*. Modelica Association, Como, Italy.

Haugwitz, S. (2007): *Modeling, Control and Optimization of a Plate Reactor*. PhD thesis ISRN LUTFD2/TFRT--1080--SE, Department of Automatic Control, Lund University, Sweden.

Hicks, G. A. and W. H. Ray (1971): "Approximation methods for optimal control synthesis." *The Canadian Journal of Chemical Engineering*, **49:4**, pp. 522–528.

Hindmarsh, A., P. Brown, K. Grant, S. Lee, R. Serban, D. Shumaker, and C. Woodward (2005): "Sundials: Suite of nonlinear and differential/algebraic equation solvers." *ACM Trans. Math. Softw.*, **31**, September, pp. 363–396.

Internship, PE3 Borealis AB (2009): "Personal communication with operators of the plant PE3 at Borealis AB, Stenungsund, Sweden, during one week of internship."

Kadam, J. V., W. Marquardt, B. Srinivasan, and D. Bonvin (2007): "Optimal grade transition in industrial polymerization processes via NCO tracking." *AIChE Journal*, **53:3**, pp. 627–639.

Larsson, P., N. Andersson, J. Åkesson, and S. Haugwitz (2010): "Modelica Based Grade Change Optimization for a Polyethylene Reactor." In *Proceedings of the 9th International Symposium on Dynamics and Control of Process Systems*. Leuven, Belgium.

Luyben, W. (2007): *Chemical Reactor Design and Control*. John Wiley & Sons.

McAuley, K. B. and J. F. MacGregor (1992): "Optimal grade transitions in a gas phase polyethylene reactor." *AIChE Journal*, **38:10**, pp. 1564–1576.

Olofsson, B., H. Nilsson, A. Robertsson, and J. Åkesson (2011): "Optimal tracking and identification of paths for industrial robots." In *Proc. 18th World Congress of the International Federation of Automatic Control (IFAC)*. Milano, Italy.

Pontryagin, L. S., V. G. Boltyanskii, R. V. Gamkrelidze, and E. F. Mischenko (1962): *The Mathematical Theory of Optimal Processes*. John Wiley & Sons Inc.

Python Software Foundation (2011): "Python Programming Language - Official Website." `http://www.python.org`.

Stenmark, M. (2011): "A graphical user interface for polyethylene production grade changes.". Master's thesis, Department of Automatic Control, Lund University, Sweden. In preparation.

Takeda, M. and W. Ray (1999): "Optimal-grade transition strategies for multistage polyolefin reactors." *AIChE Journal*, **45:8**, pp. 1776–1793.

The Modelica Association (2011): "The Modelica Association Home Page." `http://www.modelica.org`.

Tousain, R. (2002): *Dynamic optimization in business-wide process control*. PhD thesis, Delft University of Technology.

Vassiliadis, V. (1993): *Computational Solution of dynamic optimization problems with general differential algebraic constraints*. PhD thesis, University of London, London, UK.

Wächter, A. and L. T. Biegler (2006): "On the implementation of an interior-point filter line-search algorithm for large-scale nonlinear programming." *Mathematical Programming*, **106:1**, pp. 25–58.

Paper I

Control Signal Constraints and Filter Order Selection for PI and PID Controllers

Per-Ola Larsson and Tore Hägglund

Abstract

Large control signal derivatives or inter-sample differences may harm actuators. An optimization constraint limiting such variations, related to measurement noise, is derived. Using the constraint, optimal PI, PID and measurement filters with different orders are designed for several processes and compared to the optimal linear controller of high order found via Youla parametrization. Simulations of load disturbance rejections and measurement noise sensitivities are shown and conclusions on filter order selection for PI and PID controllers are drawn.

1. Introduction

Proportional-Integral (PI) and Proportional-Integral-Derivative (PID) controllers have been used for decades and are still today the most commonly used controllers in for instance process industry, see [Desbourough and Miller, 2002]. Several tuning methods exist and during the recent years a considerable research effort has been made for improvements, both in robustness and disturbance rejection. However, in practice, as noted in [Isaksson and Graebe, 2002], PI controllers are often chosen over PID controllers even though a considerable improvement can be made by adding a derivative part. One reason mentioned is the noise sensitivity introduced by the derivative part. This may give undesirable control signal variations, leading to expensive wear of actuators. Controller de-tuning is one remedy, used in e.g., λ-tuning and internal model control, see [Åström and Hägglund, 2006] and [Skogestad, 2004], while another is to set controller parameter bounds, see [Skogestad, 2006].

For PID, derivative filters of order one is commercial standard, where the time constant has a preset relation to derivative time [O'Dwyer, 2009]. However, as shown in [Isaksson and Graebe, 2002], the filter cut-off frequency may have a significant impact on both performance and noise sensitivity and should thus be part of the design procedure of the controller. Recently, four-parameter tunings have emerged. In [Kristiansson and Lennartson, 2006] and [Šekara and Mataušek, 2009] an upper bound on the $\mathcal{H}_\infty$-norm of the transfer function from measurement noise to control signal is used while tuning PID controllers with first order filters. The $\mathcal{H}_2$-norm of the transfer function is used in [Garpinger, 2009] together with PI and PID controllers with order one roll-off by using appropriate filters. In [Fransson and Lennartson, 2003], PID is used with a second order filter together with $\mathcal{H}_\infty$-norm constraints on the transfer functions from noise to control signal and its derivative.

Light filtering of measured signal implies ability to react fast to load disturbances but gives often undesirable variations in control signal due to noise, while substantial filtering yields the opposite if the same controller settings are used. There is hence a trade-off and a need for quantifying performance gains and noise rejection abilities for different filter orders when constraints are set on control signal behaviour.

In this paper, such a behaviour constraint is presented, involving the closed loop transfer function from noise to control signal, that is related to measurement noise and practical considerations. Optimal PI(D) controllers and noise filters with different orders together with optimal linear high order controllers will be designed. Simulations of load disturbances and noise rejection abilities will be shown for the different control structures.

2. Specifications on Control Signal

2.1 Control Signal Inter-Sample Amplitude Difference

The control structure considered can be found in Figure 1 with process P and controller C with the measurement filter F such that CF is at least proper. Controlled process output is denoted f and measured output y, while the control signal, measurement noise and load disturbance are denoted u, n and d, respectively. As mentioned in Section 1, a highly varying control signal is undesirable due to e.g., wear of actuators. It is important to emphasize that in most cases it is not the size of the control signal amplitude, assuming it is in actuator range, that may be harmful. It is rapid fluctuations in the control signal that may cause most damage.

Fluctuations in the control signal can be seen by e.g. large derivatives or large inter-sample differences. Since the control signal is in discrete time with constant value between sampling instants, the approximation of the derivative, i.e., $\Delta u/h$, where Δu is the inter-sample amplitude difference and h is the sampling period, will be used. Assuming that the measurement noise is white with zero mean and standard deviation σ_n, then the discrete time derivative of the control signal will be zero mean with standard deviation

$$\frac{\sigma_{\Delta u}}{h} = \left\| \frac{z-1}{zh} \frac{CF}{1+PCF} \right\|_2 \sigma_n, \tag{1}$$

where $\sigma_{\Delta u}$ is the standard deviation of Δu.

The above measure may be used to constrain control signal movement, and two different view points may be taken,

1. Considering control signal derivative, as used in velocity limiters, see [Shinskey, 1994].
2. Considering inter-sample differences associated with e.g., full control signal range.

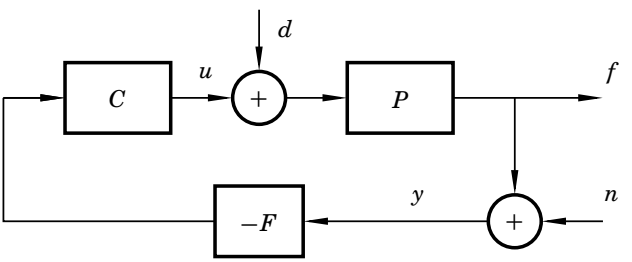

Figure 1. Process P, controller C, and measurement filter F.

The two view points are application and user dependent and differ only in a scaling factor of h^{-1} in Eq. (1), and are thus identical. In the sequel, the inter-sample difference view point will be used, removing h^{-1} from both sides.

Since Δu is a stochastic process, a measure of the control signal activity is how large part of the distribution of Δu is outside a certain limit, $\pm\Delta u_{\text{limit}}$. Assuming that α percent of the control activity is allowed outside the limit and using that Δu is normal, leads to the relation

$$\Delta u_{\text{limit}} = \sigma_{\Delta u}\lambda_{\alpha/2}, \tag{2}$$

where $\lambda_{\alpha/2}$ is a quantile for a normal distribution, giving

$$\left\| \frac{z-1}{z}\,\frac{CF}{1+PCF} \right\|_2 = \frac{\Delta u_{\text{limit}}}{\sigma_n} \cdot \frac{1}{\lambda_{\alpha/2}}.$$

Since equality does not have to be fulfilled at controller design, the constraint becomes

$$\left\| \frac{z-1}{z}\,\frac{CF}{1+PCF} \right\|_2 \leq \frac{\Delta u_{\text{limit}}}{\sigma_n} \cdot \frac{1}{\lambda_{\alpha/2}}.$$

This constraint relates directly to measurement signal quality, i.e., measurement noise, and allowed control signal movement. When used at feedback system design, it can specify how active the control signal may be.

Constraint Properties Some properties of the constraint may be remarked,

- smaller α, i.e., less accepted activity outside the limits, yields larger $\lambda_{\alpha/2}$ and a tighter constraint.
- more noise, i.e., larger σ_n, yields tighter constraint.
- larger inter-sample difference acceptance, i.e., larger Δu_{limit}, yields softer constraint.

Specifying Constraint Limit The noise variance σ_n may be estimated using standard techniques on measurement data, see e.g., [Shinskey, 1994], while the inter-sample amplitude limit may be related to control signal range and actuator properties. Selecting α will then determine the constraint. However, these specifications may be scaled in relation to each other yielding the same upper limit. For simplicity, Δu_{limit} and σ_n are set equal, and all specifications are collected in α, leading to the simplified constraint

$$\left\| \Delta_z \frac{CF}{1+PCF} \right\|_2 \leq \frac{1}{\lambda_{\alpha/2}}, \tag{3}$$

where $\Delta_z = (z-1)/z$ has been introduced.

2.2 Control Signal Energy

The constraint in Section 2.1 limits rapid variations in the control signal. However, also control signal energy and low frequency variations due to measurement noise should be considered. As in [Garpinger, 2009], the variance of the control signal amplitude due to noise is used, i.e.,

$$\frac{\sigma_u^2}{\sigma_n^2} = \left\| \frac{CF}{1+PCF} \right\|_2^2 \leq \eta^2.$$

The limit η is application dependent, and for simplicity chosen to 1 when investigating the constraint in Section 2.1, yielding no energy amplification of the noise.

3. Feedback Structures

3.1 PID and Measurement Filter

The considered PI(D) controllers are on parallel form, i.e.,

$$C(s) = K_C \left(1 + \frac{1}{T_i s} + T_d s\right),$$

where the integral and derivative parts are discretized using forward and backward differences, respectively, with sampling period h. For comparison, three different measurement filters will be used such that the controllers have roll-offs of orders 0–2 in continuous time, i.e., a PI without filter will also be compared. Using roll-off less than 2 would not be possible if continuous time was considered, using that Δ_z/h corresponds to s, since the transfer function in Eq. (3), with a proper process, must be strict proper in this case. The filters are restricted to have at most two tuning parameters, yielding few optimization variables. A natural choice is the damping ζ and time constant T_f of the filters, and thus the three different filters are chosen as

$$\begin{aligned} F_1(s) &= \frac{1}{sT_f + 1}, \qquad F_2(s) = \frac{1}{s^2 T_f^2 + 2\zeta T_f s + 1}, \\ F_3(s) &= F_1(s)F_2(s), \end{aligned} \tag{4}$$

and sampled using zero-order hold technique. Note that the third order filter does not have full degree of freedom when choosing poles since only two parameters may be specified.

3.2 Youla Parametrization

For evaluation of designed PI(D) controllers and measurement filters, the optimal linear controller of high order, i.e., the Youla parametrization, also known as Q-parametrization, will be used. Additionally, this controller will give a performance bound. Consider the generalized process in Figure 2,

$$G = \begin{bmatrix} G_{\mathbf{zw}} & G_{\mathbf{z}u} \\ G_{y\mathbf{w}} & G_{yu} \end{bmatrix},$$

where $\mathbf{z}$ is controlled outputs, y measured output, u controlled input and $\mathbf{w}$ exogenous inputs, with negative SISO feedback K. Closing the loop yields

$$\begin{aligned} H_{\mathbf{zw}} &= G_{\mathbf{zw}} - G_{\mathbf{z}u} K \left(I + G_{yu} K\right)^{-1} G_{y\mathbf{w}} \\ &= G_{\mathbf{zw}} - G_{\mathbf{z}u} Q G_{y\mathbf{w}}, \end{aligned}$$

where $Q = K \left(I + G_{yu} K\right)^{-1}$. If G is stable, then $H_{\mathbf{zw}}$ is stable for all stable transfer functions Q.

Choosing G properly, many convex control costs and specifications, including those used in this paper, may be set on the individual elements of $H_{\mathbf{zw}}$. They are convex in Q due to the affine relationship between $H_{\mathbf{zw}}$ and Q. However, since Q may be any stable transfer function, the search space when optimizing over Q is infinite dimensional. For numerical computations, Q is parametrized as a FIR filter,

$$Q(z) = \sum_{i=0}^{N-1} q_i z^{-i},$$

where N is the length and the convexity properties are found in the q_i coefficients. This methodology is found in e.g., [Boyd *et al.*, 1990] and [Wernrud, 2008a], and implemented in the toolbox QTOOL, see [Wernrud, 2008b], which is used when solving the optimization problem to be stated.

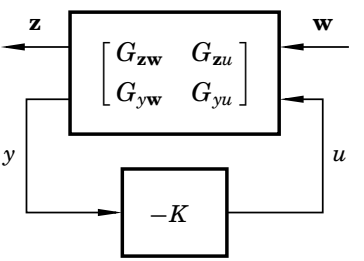

Figure 2. Set-up with generalized process G, SISO negative feedback controller K, exogenous inputs $\mathbf{w}$, control input u, controlled outputs $\mathbf{z}$ and measured output y.

Finding K from Q is a direct calculation as the mapping is unique. Compared to PI(D) control, no additional measurement filter will be designed, it is incorporated in K directly. Choosing N large, then K, and thus $H_{\mathbf{zw}}$, may be shaped almost arbitrarily as long as the constraints are respected.

4. Optimization Problem

4.1 Optimization Problem Formulation

The integrated absolute error (IAE) at a load disturbance step is used as objective function to minimize, see e.g., [Åström and Hägglund, 2006]. Robustness towards multiplicative and inverse multiplicative uncertainties, see [Zhou and Doyle, 1998], may be achieved by constraining the $\mathcal{H}_\infty$-norm of the sensitivity functions,

$$S = \frac{1}{1+KP}, \qquad T = \frac{KP}{1+KP}$$

where K is the feedback transfer function, e.g., controller and measurement filter. Frequency independent upper limits M_S and M_T as in e.g., [Åström and Hägglund, 2006], hold the number of optimization parameters to select reasonably small.

With a load disturbance step applied at process input at initial time when the system is in steady state, the optimization problem may be stated as

$$\begin{aligned}
\underset{\mathcal{K}}{\text{minimize}} \quad & h\sum_{k=0}^{\infty}|f(k)| && \text{(5a)}\\
\text{subject to} \quad & \|S\|_\infty \le M_S && \text{(5b)}\\
& \|T\|_\infty \le M_T && \text{(5c)}\\
& \|KS\|_2 \le \eta && \text{(5d)}\\
& \|\Delta_z KS\|_2 \le 1/\lambda_{\alpha/2}, && \text{(5e)}
\end{aligned}$$

where $\mathcal{K}$ contains PI(D) and measurement filter parameters or FIR coefficients at Youla parametrization. In the case of PI(D) control, K is factorized as $K = CF$ as in Section 2.

4.2 Additional Constraints on PI(D) Measurement Filters

Two constraints on the filter parameters are set. They will restrain the PI(D) and measurement filter from being a richer structure compared to how they are normally used.

Damping ζ In [Kristiansson and Lennartson, 2006], a ζ around 0.4 is used as a rule of thumb for a second order filter. However, a small ζ may give oscillations in the control signal due to the amplitude peak and in general, a measurement filter may only perform attenuation of the measured signal. The filters defined in Eq. (4) have static gain 1 and if the damping coefficient is restricted to be greater than $1/\sqrt{2}$, this is fulfilled. Additionally, to have only one break point of the filter, defined by T_f, an upper limit of 1 is set on ζ, giving the following constraint in the optimization problem,

$$\zeta \in \left[1/\sqrt{2},\ 1\right].$$

Time Constant T_f The time constant of the measurement filter must be smaller than the inverse of the largest modulus of the controller zeros. That is, filtering is only present at higher frequencies than e.g., the derivative action start frequency of a PID controller. Since the system is sampled, the filter cut-off frequency must be lower than the Nyquist frequency. Thus, the filter time constant is restrained to be in the interval

$$T_f \in \left[\frac{h}{\pi},\ T_i\right], \text{ or} \tag{6a}$$

$$T_f \in \left[\frac{h}{\pi},\ \left|\frac{1}{2T_d} + \sqrt{\frac{1}{4T_d^2} - \frac{1}{T_i T_d}}\right|^{-1}\right], \tag{6b}$$

for PI and PID, respectively. The upper limits are derived from continuous time controllers and hold approximately for discrete time versions if high enough sampling rate.

4.3 General Process for Youla Parametrization

The considered process P in Figure 1, with control signal u and load disturbance d, process output f, and measured output y, may be written in state-space form as

$$\begin{aligned}\mathbf{x}_{k+1} &= \mathbf{A}\mathbf{x}_k + \mathbf{B}u_k + \mathbf{B}d_k\\ f_k &= \mathbf{C}\mathbf{x}_k + \mathbf{D}u_k + \mathbf{D}d_k\\ y_k &= f_k + n_k.\end{aligned}$$

Letting $u_k^d = u_k + d_k$, we can define the general signals

– Control input: u_k

- Exogenous inputs: $\mathbf{w}_k = [\, d_k \quad n_k \,]^T$
- Controlled outputs: $\mathbf{z}_k = [\, f_k \quad u_k^d \quad \Delta u_k \,]^T$
- Measured output: y_k

which gives the following generalized process G, using the state vector $\mathbf{x}_{k+1}^e = [\, \mathbf{x}_{k+1}^T \quad u_k \,]^T$,

$$\mathbf{x}_{k+1}^e = \begin{bmatrix} \mathbf{A} & \mathbf{0} \\ \mathbf{0} & 0 \end{bmatrix} \mathbf{x}_k^e + \begin{bmatrix} \mathbf{B} & \mathbf{0} & \mathbf{B} \\ 0 & 0 & 1 \end{bmatrix} \begin{bmatrix} d_k \\ n_k \\ u_k \end{bmatrix}$$

$$\begin{bmatrix} \mathbf{z_k} \\ y_k \end{bmatrix} = \begin{bmatrix} \mathbf{C} & 0 \\ \mathbf{0} & 0 \\ \mathbf{0} & -1 \\ \mathbf{C} & 0 \end{bmatrix} \mathbf{x}_k^e + \begin{bmatrix} \mathbf{D} & 0 & \mathbf{D} \\ 1 & 0 & 1 \\ 0 & 0 & 1 \\ \mathbf{D} & 1 & \mathbf{D} \end{bmatrix} \begin{bmatrix} d_k \\ n_k \\ u_k \end{bmatrix}.$$

The closed loop transfer function from $\mathbf{w}_k$ to $\mathbf{z}_k$ is then

$$H_{\mathbf{zw}} = \begin{bmatrix} PS & -T \\ S & -KS \\ -\Delta_z T & -\Delta_z KS \end{bmatrix},$$

containing all relevant transfer functions for stability analysis and to solve the optimization problem in Eq. (5). $H_{\mathbf{zw}}$ may be used directly in QTool, see [Wernrud, 2008b], by associating the objective cost in time domain and constraints in frequency domain with the corresponding matrix elements. The resulting optimization problem is solved using Yalmip [Löfberg, 2004] and SeDuMi [Sturm, 1999] with built-in functions in QTool [Wernrud, 2008b].

5. Process Batch

As pointed out in [Åström and Hägglund, 2006], PI(D) control is not suitable for all processes. An appropriate process batch was given with process dynamics ranging from first to eighth order, with or without time delays. The batch includes integrating, non-oscillative, and oscillative processes as well as processes with non-minimum phase zeros. A subset of the batch has been used in e.g., [Kristiansson and Lennartson, 2006] and [Šekara and Mataušek, 2009] to evaluate four parameter designs for PID. The optimization problem posed in Section 4.1 has been solved for the batch for PI and PID control with different filter orders and for Youla parametrized controllers.

6. Performance Comparison

The optimization problem for PI(D) and measurement filter is solved using the Optimization Toolbox™, Control System Toolbox™ and Simulink® in MATLAB®, see [The MathWorks, Inc, 2010b, The MathWorks, Inc, 2010a, The MathWorks, Inc, 2010c]. Two processes from the batch serve as examples, using sampling time $h = 0.02$ and the constraints

$$M_S = M_T = 1.4,\ \eta = 1,$$
$$\alpha = 15\% \ \text{ yielding } \ 1/\lambda_{\alpha/2} = 0.97.$$

With load steps of amplitude 1 and measurement noise with standard deviation of 0.025, the performances of the different feedback designs will be shown.

6.1 Example I: $P_1(s) = 1/((s+1)(0.5s+1))$

Optimization results for P_1, i.e., IAE, constraint function values and controller parameters, can be found in Table 1 and Figure 3 shows load disturbance and noise responses.

Table 1. Optimal controllers for $P_1(s) = 1/\left((s+1)(0.5s+1)\right)$.

$\text{Type}_{\text{order}}$	IAE	$\|S\|_\infty$	$\|T\|_\infty$	$\|KS\|_2$	$\|\Delta_z KS\|_2$
PI_0	1.15	1.40	1.10	0.70	0.97
PI_1	0.77	1.40	1.04	0.91	0.97
PI_2	0.76	1.40	1.05	1.00	0.97
PID_1	0.77	1.40	1.04	0.91	0.97
PID_2	0.55	1.40	1.13	1.00	0.38
PID_3	0.59	1.40	1.12	1.00	0.30
Youla	0.47	1.40	1.17	1.00	0.43
	K_C	T_i	T_d	T_f	ζ
PI_0	0.69	0.65	–	–	–
PI_1	1.38	1.07	–	0.022	–
PI_2	1.39	1.05	–	0.012	0.71
PID_1	1.38	1.07	0	0.022	–
PID_2	2.11	1.06	0.27	0.150	0.71
PID_3	2.06	1.11	0.29	0.087	0.98

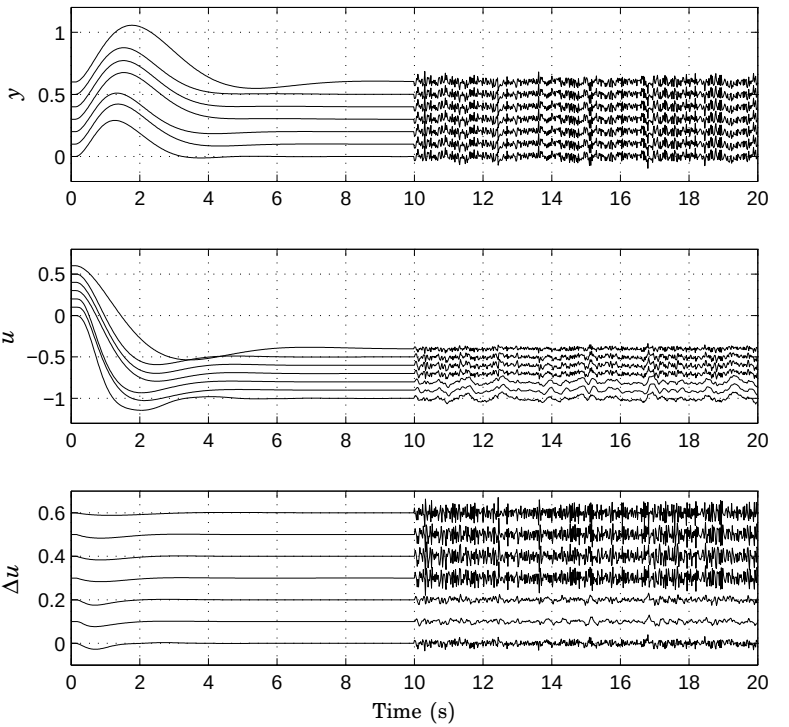

Figure 3. Top to bottom, responses for (indices denote filter order): PI_0, PI_1, PI_2, PID_1 (PI_1), PID_2, PID_3, and Youla param. controller at step load disturbance and measurement noise for $P_1(s)$. Upper: Output y. Middle: Control signal u. Lower: Inter-sample control signal differences Δu. Biases with steps of 0.1 have been added for separation.

For low order processes such as P_1, a PI controller is often considered sufficient. With no filter action, K_C is the high frequency gain, yielding it sensitive to the constraint in Eq. (5e). However, adding filter action of order 1, the inverse of the integral gain, i.e., T_i/K_C, a good estimate of IAE for closed loop systems with essentially monotone load step response, may be decreased. This effect is also seen in Figure 4, showing the feedback transfer functions, where the small filter time constant makes the amplitude curve drop at high frequencies. The phase tends to $-180°$ due to the filter sampling. Increasing noise filter order to 2 has small effect on the responses, see figures 3 and 4. The optimal second order filter has damping $\zeta = 1/\sqrt{2}$, i.e., as low as possible, which has a more distinct cut-off than a first order filter. Due to the increased roll-off, the filter time constant may be halved compared to first order filter, still fulfilling the high

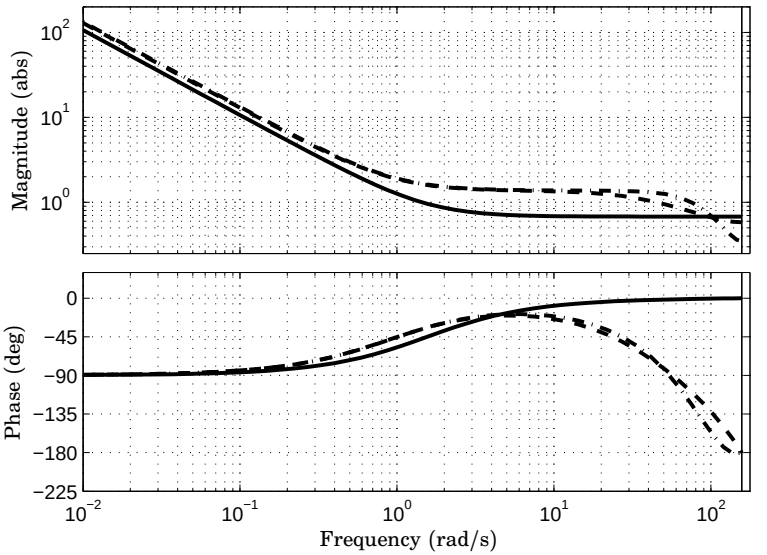

Figure 4. Optimal PI controllers and measurement filters (indices denote filter order), PI_0 (–), PI_1 (- -) and PI_2 (-·-) for $P_1(s)$.

frequency emphasizing constraint in Eq. (5e). However, this increases the constraint function in Eq. (5d), see Table 1.

For PID control, with a first order filter, i.e., no roll-off, and a $T_d > 0$, T_i/K_C has to be increased a considerable amount compared to a PI with first order filter to fulfill the control signal constraints. This is due to the additional constraint in Eq. (6b), yielding that with T_d close to 0 and first order filter, the feedback will essentially be a PI without any filter action. For a first order filter, it is thus optimal to choose $T_d = 0$, recovering a PI controller while using the constraint in Eq. (6a) instead. However, increasing filter order, i.e., roll-off in the feedback, derivative action may be allowed, increasing performance significantly, see Table 1 and Figure 3. The optimal second order filter has $\zeta = 1/\sqrt{2}$, thus trying to save as much of the phase and gain at mid-frequencies as possible. However, the increased mid-frequency gain requires larger filter time constant, $T_f = 0.150$, such that enough attenuation is given at high frequencies to hold the control signal constraints. This implies that control effort is shifted towards lower frequencies, i.e., the control signal energy constraint is active instead of the control signal inter-sample difference, see Table 1 and responses in Figure 3. This decreases e.g., wear on actuators. Third order filter decreases the inter-sample differences further, but to the cost of increased

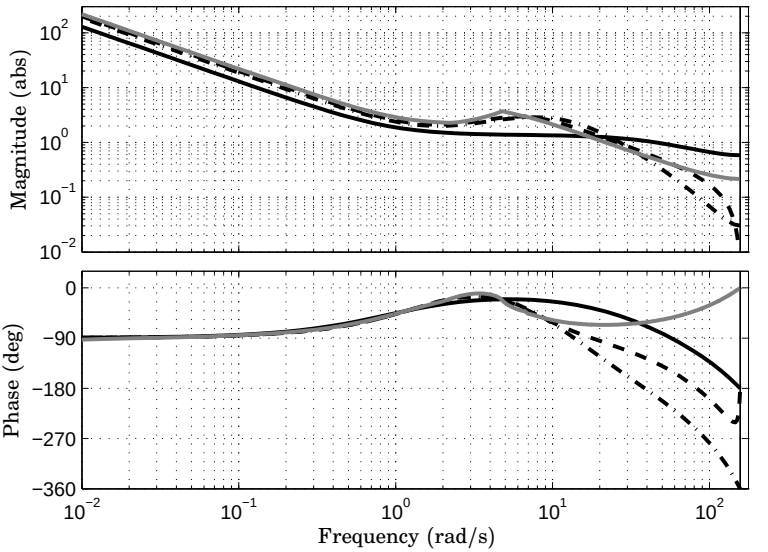

Figure 5. Optimal PID controllers and measurement filters (indices denote filter order), PID_1 (–) (PI_1), PID_2 (- -), and PID_3 (-·-) and Youla parametrized controller (grey) for $P_1(s)$.

IAE. The damping of the optimal third order filter is large and a smaller filter time constant is possible due to the higher roll-off.

To evaluate PI(D) control performance, a Youla parametrized controller with $N = 1000$, corresponding to a 20 s. long FIR filter, was designed. Performance results can be found in Table 1 and Figure 3 and controller transfer function is shown in Figure 5. There are strong similarities between PID control with filter order higher than 1 and the Youla controller. The same constraints are active and the magnitude of the feedback transfer function has the same characteristics. Due to the high order, the Youla controller is able to give a higher peak and phase advance at mid-frequencies and also phase advance at high frequencies. This contributes to the only 15% better IAE value than the optimal PID with second order filter, showing that PID is close to optimal for this process when control signal and robustness constraints are set.

6.2 Example II: $P_2(s) = 1/(s+1)^4$

Increased complexity of the process, comparing P_1 and P_2, often requires increased complexity of the controller for good performance. PI and PID controllers and a Youla parametrized controller were designed for P_2 and

Table 2. Optimal controllers for $P_2(s) = 1/(s+1)^4$.

$\text{Type}_{\text{order}}$	IAE	$\|S\|_\infty$	$\|T\|_\infty$	$\|KS\|_2$	$\|\Delta_z KS\|_2$
$\text{PI}_{0,1,2}$	5.24	1.40	1.00	0.43	0.61
PID_1	4.45	1.40	1.00	0.68	0.97
PID_2	3.05	1.40	1.04	1.00	0.37
PID_3	3.13	1.40	1.04	1.00	0.21
Youla	2.34	1.40	1.04	1.00	0.31
	K_C	T_i	T_d	T_f	ζ
$\text{PI}_{0,1,2}$	0.43	2.26	–	–	–
PID_1	0.80	3.41	1.16	1.37	–
PID_2	0.95	2.44	1.19	0.21	0.71
PID_3	0.93	2.46	1.20	0.14	0.71

the results are found in Table 2 while step and noise responses are seen in Figure 6.

Pure PI control is not able to be sufficiently aggressive for the control signal constraints to be active and hence, adding a measurement filter will not increase performance. However, adding derivative gain and a first order filter and thus increasing controller complexity, decreases IAE but at the same time increases noise sensitivity seen by the active constraint of inter-sample control signal amplitude. Compared to P_1, it is however possible to have PID control with a first order measurement filter, although the derivative gain is small since the filter cancels much of the gain, see Figure 7 for the feedback transfer functions. The phase of the feedback at high frequencies tend to $-180°$ due to sampling effects. The upper limit on T_f from Eq. (6b) is approximately 2, which the optimal value is close to. With orders 2 and 3 of the filter, a larger derivative action may be used since the filters are able to decrease feedback gain at high frequencies. The optimal filters have low damping, $\zeta = 1/\sqrt{2}$ and significantly smaller T_f, 0.21 and 0.14, respectively. This yields as much as possible of the derivative phase advance and gain can be used to increase performance, as seen in Table 2, which also shows that control action is shifted to lower frequencies compared to a first order filter. This effect is also seen in figures 6 and 7.

The Youla parametrized controller with $N = 1200$ has again the same magnitude characteristics as a PID with higher order filter, see Fig-

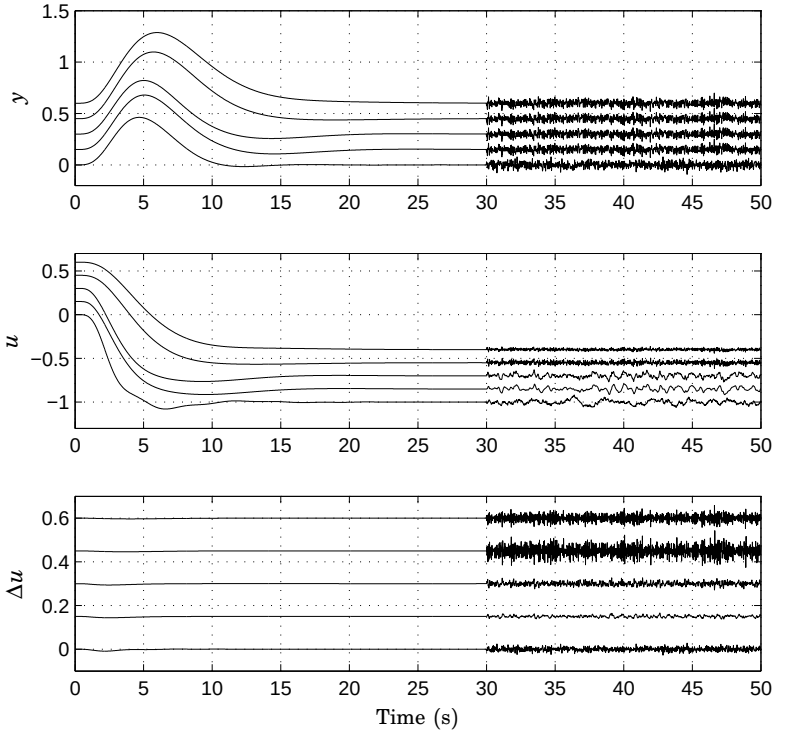

Figure 6. Top to bottom, responses for (indices denote filter order): $PI_{0,1,2}$, PID_1, PID_2, PID_3, and Youla parametrized controller at step load disturbance and measurement noise for $P_2(s)$. Upper: Output y. Middle: Control signal u. Lower: Inter-sample control signal differences Δu. Biases with steps of 0.15 have been added for separation.

ure 7. It is able to give larger amplification and phase advance at mid-frequencies than a derivative part due to its high order, which yields a 23% better performance than the optimal PID controller. Optimizations without the lower bound on ζ have been performed, yielding the resulting measurement filter to give a peak to the feedback similar to the Youla parametrized controller and results in [Fransson and Lennartson, 2003]. However, in this case, the filter is more than a noise attenuating filter.

7. General Results and Conclusions

For low order simple processes, e.g., first and well damped second order dynamics, PI control is sufficiently aggressive for at least one of the

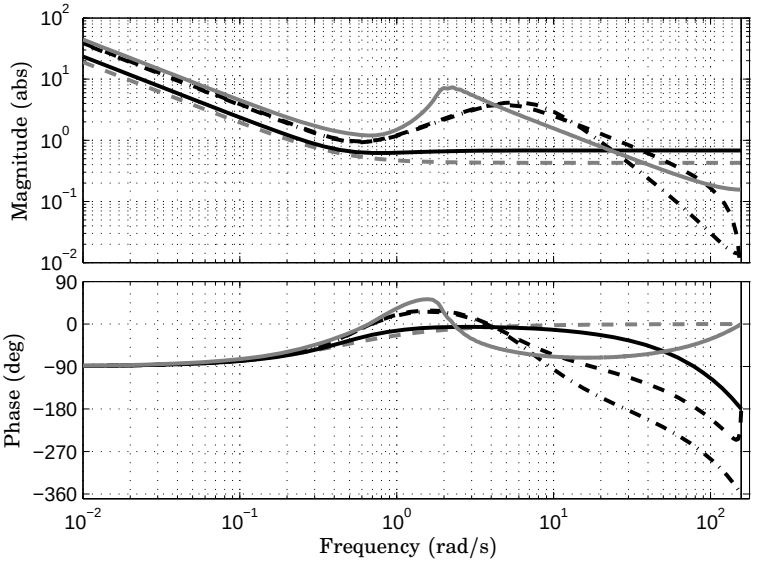

Figure 7. Optimal PI(D) controllers and measurement filters (indices denote filter order), $PI_{0,1,2}$ (gray - -), PID_1 (–), PID_2 (- -) and PID_3 (-·-) and Youla parametrized controller (grey –) for $P_2(s)$.

control signal constraints to be active. It has also been noted that, in general, if no filter is used, the control signal inter-sample constraint is active while control signal amplitude constraint is far from active. Adding a filter increases performance significantly and yields more control signal energy in mid-frequencies, increasing the control signal amplitude constraint function, as was seen for P_1. However, for higher order and oscillative processes, PI control will in general not give active control signal constraints if not set very hard. It has also been noted that the performance difference between no filter and first order filter for PI control is significant when control signal constraints are active, while the difference between first and second order filter is small, which was seen for P_1.

PID control, with its derivative action, is for the process batch in general able to have at least one of the control signal constraints active due to the derivative action. A PID controller with a first order filter often have very small or no derivative action since the filter cancels it to hold the control signal constraints. When using second or third order filters, which in general has as low damping as possible to save phase advance and gain, performance is increased. Due to the roll-off, smaller filter time constants may be used, noise sensitivity is decreased, and control signal energy is shifted to mid-frequencies where it is less harmful for actuators.

The difference between second and third order filters is however slight. This filter effect was seen in both examples.

Youla parametrized controllers, that due to high orders have the ability to choose the most important frequencies in the feedback, emphasizes the importance of increased gain and phase advance at mid frequencies with a strong peak and roll-off in the feedback, as shown in the examples. For the constraints set in Section 4.1 and considered processes without large time delays, the magnitude of the Youla parametrized controller is very similar to a PID controller with roll-off apart from having a slightly more defined peak at mid-frequencies, compare to [Fransson and Lennartson, 2003]. However, this is not realizable by the PI(D) controllers due to the constraint on ζ. Processes with large time delays yield the Youla parametrized controllers to give feedback similar to dead-time compensating control.

Numerical values of α and η are application dependent and the values set in this paper may be used as starting point. As seen from the simulations, the control signal inter-sample amplitude constraint will limit e.g., wear on actuators, and together with the characteristics of Youla parametrized controllers, it is concluded that measurement filters should be chosen such that roll-off is present in the feedback.

References

Åström, K. and T. Hägglund (2006): *Advanced PID Control*. ISA - The Instrumentation, Systems, and Automation Society, Research Triangle Park, NC 27709.

Boyd, S., N. Khraishi, C. Barratt, S. Norman, V. Balakrishnan, and D. Meyer (1990): *QDES – version 1.5*. Information Systems Laboratory, Electrical Engineering Department, Stanford University.

Šekara, T. and M. Mataušek (2009): "Optimization of PID Controller Based on Maximization of the Proportional Gain Under Constraints on Robustness and Sensitivity to Measurement Noise." *IEEE Transactions of Automatic Control*, **54:1**, pp. 184–189.

Desbourough, L. and R. Miller (2002): "Increasing customer value of industrial control performance monitoring—Honeywell's experience." In *AIChe Symposium Series*, vol. 98.

Fransson, C. and B. Lennartson (2003): "Low order multicriteria $\mathcal{H}_\infty$ design via bilinear matrix inequalities." In *Proceedings of 42nd IEEE Conference on Decision and Control*, vol. 5, pp. 5161–5167.

Garpinger, O. (2009): "Design of Robust PID Controllers with Constrained Control Signal Activity." Licentiate Thesis. Department of Automatic Control, Lund University, Sweden.

Isaksson, A. and S. Graebe (2002): "Derivative filter is an integral part of PID design." *Control Theory and Applications, IEE Proceedings*, **149:1**, pp. 41–45.

Kristiansson, B. and B. Lennartson (2006): "Robust tuning of PI and PID controllers: Using derivative action despite sensor noise." *IEEE Control Systems Magazine*, **26:1**, pp. 55–69.

Löfberg, J. (2004): "Yalmip: A toolbox for modeling and optimization in MATLAB." In *Proceedings of the CACSD Conference*. Taiwan.

O'Dwyer, A. (2009): *Handbook of PI and PID controller tuning rules*, 3rd edition. Imperial College Press.

Shinskey, F. (1994): *Feedback Controllers for the Process Industries*. McGraw-Hill.

Skogestad, S. (2004): "Simple analytic rules for model reduction and PID controller tuning." *Modeling, Identification and Control*, **25:2**, pp. 85–120.

Skogestad, S. (2006): "Tuning for Smooth PID Control with Acceptable Disturbance Rejection." *Industrial and Engineering Chemistry Research*, **45:23**, pp. 7817–7822.

Sturm, J. F. (1999): "Using SeDuMi 1.02, a MATLAB toolbox for optimization over symmetric cones." *Optimization Methods and Software*, **11–12**, pp. 625–653.

The MathWorks, Inc (2010a): *Control System Toolbox™ User's Guide, Version 9*. The MathWorks Inc, 3 Apple Hill Drive, Natick, MA 01760-2098.

The MathWorks, Inc (2010b): *Optimization Toolbox™ User's Guide, Version 5*. The MathWorks, Inc, 3 Apple Hill Drive, Natick, MA 01760-2098.

The MathWorks, Inc (2010c): *Simulink® User's Guide, Version 7*. The MathWorks, Inc, 3 Apple Hill Drive, Natick, MA 01760-2098.

Wernrud, A. (2008a): *Approximate Dynamic Programming with Applications*. PhD thesis ISRN LUTFD2/TFRT--1082--SE, Dept. of Automatic Control, Lund University, Sweden.

Wernrud, A. (2008b): *QTool 0.1 – Reference Manual*. Department of Automatic Control, Lund University.

Zhou, K. and J. Doyle (1998): *Essentials of Robust Control*. Prentice Hall, Inc, Upper Saddle River, New Jersey 07458, USA.

Paper II

Robustness Margins Separating Process Dynamics Uncertainties

Per-Ola Larsson and Tore Hägglund

Abstract

In controller design, not only set-point tracking and disturbance rejection can be considered, also robustness towards process uncertainties is a key issue. In this paper, new robustness measures that divide uncertainties into dead time and non-dead time uncertainties, are presented. It is shown, to the contrary of classic measures such as phase/gain/dead time margins, to guarantee stability towards simultaneous process changes, but at the same time being more flexible and less conservative than the robust control framework. The measures depend on extended sensitivity functions and are well illustrated in a Nyquist diagram giving valuable insight. Procedures to calculate the robustness margins are presented and examples are given.

Errata

Page	Location	Correction
106	Text line 29	Remove “[Åström and Hägglund, 2006]”
115	Text line 37	“1/1.4” should read “1/2.9”
117	First eq. on page	Remove “Re$CP(i\omega_k) =$”
117	Figure 5	Remove “Re$CP(i\omega_k)$”

1. Introduction

In the design of a controller, one is often focused on achieving good set point and load responses by tuning controller parameters. Nevertheless, one of a control systems most important tasks is preserving closed loop stability even though process parameters such as time constants, gains, and dead time, change simultaneously within certain limits. A system achieving this is known as a robust system, or a system with robustness margins. Often, the more robust a system is, the more conservative is the tuning of responses, which gives a clear trade-off, see e.g., [Shinskey, 1994, Skogestad and Postlethwaite, 2005]. It is hence desirable to model process uncertainties as accurately as possible when designing the controller and that the robustness measures used can handle the detailed description.

Many robustness measures exist today, and the most common ones used on a regular basis are described in Section 2. However, they have some shortcomings as will be seen in the same section. In this paper, we will instead present new robustness margins in Sections 3 and 4 that give constraints on extended versions of the sensitivity functions and that are able to separate between delay and delay free uncertainties. It will be seen that the margins, computed as in Sections 5 and 6, contain the existing robustness measures as special cases. Also, they have a clear, illustrative interpretation in a Nyquist diagram giving insight into how different uncertainties influence closed loop robustness.

2. Existing Robustness Measures

2.1 Classic Measures

The robustness measures below, commonly used in industrial settings, do not require extensive uncertainty modeling.

Phase and Gain Margin Most common are the phase and gain margin, denoted ϕ_m and g_m, respectively. They give robustness towards phase and gain increases up to ϕ_m and g_m in the process, although, not at the same time. Note that ϕ_m is defined at the lowest frequency where the amplitude of the open loop is 1 and g_m at the lowest frequency where the open loop phase is $-180°$.

Dead Time Margin The traditional way of defining a dead time margin, is by finding the smallest additional delay in the open loop at the frequency of ϕ_m giving an unstable closed loop system. That is, if the phase margin is ϕ_m at the frequency ω_ϕ, then the dead time margin is $\Delta L_{\max} = \phi_m/\omega_\phi > 0$. Note that the dead time margin is not defined for negative delay errors.

2.2 Model Uncertainty Based Methods

If a model of the process is derived, there are often uncertainty bounds on e.g., gains, time constants, and dead times. By combining these intervals an uncertainty region for the process transfer function is found. The shape of this region often has a complex description and is hard to handle at a systematic controller design, see for instance [Morari and Zafiriou, 1989]. The most commonly used systematic approach is therefore to bound this region by a disk with certain radius, i.e., norm bound uncertainty. In a Nyquist diagram this can be illustrated as an uncertainty circle at every frequency. This leads to the design possibility of setting constraints on the sensitivity and complementary sensitivity function

$$S(s) = \frac{1}{1 + P(s)C(s)}, \qquad T(s) = \frac{P(s)C(s)}{1 + P(s)C(s)},$$

where $P(s)$ and $C(s)$ are the process and controller transfer function, respectively. The constraints are often expressed as

$$\|S(s)W_S(s)\|_\infty < 1, \qquad \|T(s)W_T(s)\|_\infty < 1,$$

that is, by the infinity norm, see [Morari and Zafiriou, 1989, Åström and Hägglund, 2006, Zhou and Doyle, 1998, Skogestad and Postlethwaite, 2005]. This is known as robust stability in the framework of robust control and the weights $W_S(s)$ and $W_T(s)$ are design parameters. If the uncertainty regions are hard to model, the weights can be chosen as constants and the constraints are expressed as $\|S(s)\|_\infty < M_S$ and $\|T(s)\|_\infty < M_T$. The constraints can then be illustrated as frequency independent circles in a Nyquist diagram and are commonly used in process control due to its simplicity, see e.g. [Åström and Hägglund, 2006].

One of the main problems with the above approach is the possibility of conservatism. The region covered by a circle might not in reality have a shape resembling a circle and thus, the process model can contain practically infeasible processes.

2.3 Motivating Example

Consider the first order process with dead time

$$P(s) = \frac{1}{s+1}\, e^{-s}.$$

We design a PI controller using the method described in e.g., [Åström and Hägglund, 2006, Garpinger and Hägglund, 2008], i.e., minimizing

the Integrated Absolute Error (IAE) at a load disturbance step with the constraints $\|S(s)\|_\infty < 1.4$ and $\|T(s)\|_\infty < 1.4$. The resulting controller is

$$C(s) = 0.36\left(1 + \frac{1}{0.98s}\right)$$

and the classic robustness margins for the system are

$$g_m = 4.25, \quad \phi_m = 68^\circ, \quad \Delta L_{\max} = 3.2 \text{ s},$$

which are considered almost too conservative. A gain margin as small as 2 is considered standard in practice.

The robustness margins in Section 2.1 consider separate process variations, that is, either in the dead time or time constants/gains alone. This is not a realistic viewpoint since a process most often has simultaneous changes. Consider a delay change of 50% of the delay margin and a gain increase of 40% of the gain margin in the above system. This would give an unstable closed loop system even though we are well below the robustness specifications.

Instead, in the framework of robust control, we can guarantee stability if we model the uncertainties properly. Consider the above process again, but we have an uncertainty of the dead time, $\Delta L \in [-1, 1]$. The systematic way of modeling this uncertainty is by the weight

$$W_T(i\omega) = \begin{cases} |e^{-i\omega} - 1| & \omega < \pi \\ 2 & \omega \geq \pi. \end{cases}$$

If we design a PI controller by minimizing IAE with the above weight on the complementary sensitivity function, we achieve an IAE of 1.77 and a delay margin of 1.74 s. This can be compared to the case when we only consider the delay margin at an optimization. Then we have an IAE of 1.52 and a delay margin of 1.06 s. Note that it is not optimal for the delay margin constraint to be active. We can see that disk approximation of the dead time uncertainty gives large conservatism. This is due to an error in dead time gives only rotation of the Nyquist curve and is badly approximated by a circle.

The above two, rather simple, examples show that there is a need for a robustness measure that simultaneously considers time delay, phase, and gain changes, and nonlinearities, and at the same time being flexible enough such that conservatism is as small as possible.

The above process example with a PI controller will be revisited in the following sections.

3. Complementary Sensitivity Function Based Robustness

As noted in the introduction, one of the key features of feedback is to attain good performance even though the process changes. In this section, we will derive a measure, using the complementary sensitivity function, of how large process variations the closed loop system can tolerate.

3.1 Extended Complementary Sensitivity Function

Assume a nominal model $P(s) = P_o(s)e^{-sL}$ where $P_o(s)$ is delay free. We will now consider variations in process dynamics. Assume that we have a dead time error in the process, ΔL, which is in the interval $[\Delta L_{\min},\ \Delta L_{\max}]$. Assume further that uncertainties in time constants and gains can be modeled with a stable additive transfer function, $\Delta P(s)$, which corresponds to a multiplicative relative uncertainty. The process model including uncertainties is then

$$P_o(s)\left(1+\frac{\Delta P(s)}{P_o(s)}\right)e^{-s(L+\Delta L)}$$

which is assumed to be norm bounded. Denote the controller by $C(s)$ and consider Figure 1 where the nominal open loop $CP(i\omega)$, assumed stable, is drawn in a Nyquist diagram. With the delay uncertainty ΔL, point A will be rotated with phase $-\omega\Delta L$ and then be shifted by $|C\Delta P(i\omega)e^{-i\omega(L+\Delta L)}| = |C\Delta P(i\omega)|$ in any direction. That is, A will stay inside a circle with radius $\|C\Delta P(s)\|_\infty$ and center $CP(i\omega)e^{-i\omega\Delta L}$. The distance from $CP(i\omega)e^{-i\omega\Delta L}$ to the critical point -1 is

$$|1+CP(i\omega)e^{-i\omega\Delta L}|.$$

This means that the perturbation $C\Delta P(i\omega)e^{-i\omega(L+\Delta L)}$ will not give sufficient shift to induce instability provided that

$$|C\Delta Pe^{-i\omega(L+\Delta L)}| = |C\Delta P| < |1+CPe^{-i\omega\Delta L}|.$$

This should hold for all ω, ΔP, and ΔL, and dividing by CP_o and using that $|e^{-i\omega(L+\Delta L)}| = 1$, we can write it as

$$\left|\frac{\Delta P(i\omega)}{P_o(i\omega)}\right| < \left|\frac{1+CP(i\omega)e^{-i\omega\Delta L}}{CP(i\omega)e^{-i\omega\Delta L}}\right|.$$

Introducing the extended complementary sensitivity function

$$T(s,\Delta L) = \frac{CP(s)e^{-s\Delta L}}{1+CP(s)e^{-s\Delta L}}$$

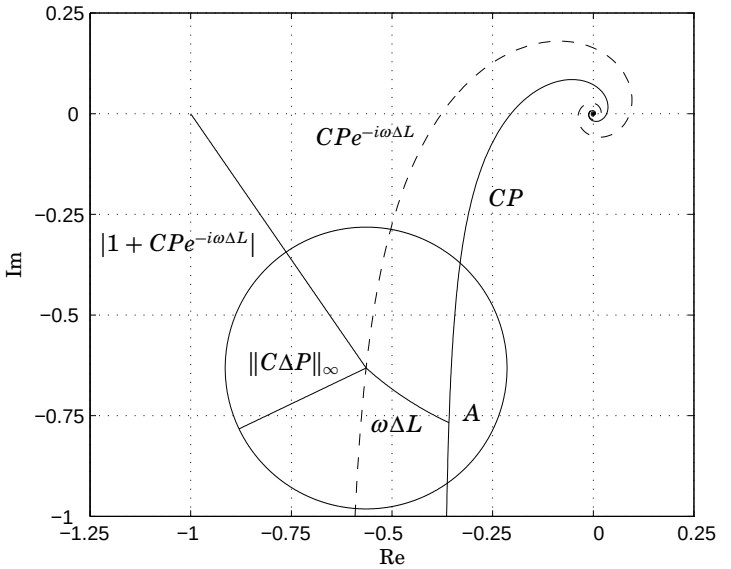

Figure 1. Nyquist diagram of nominal loop transfer function and its uncertainty due to process variations in delay free part and time delay, ΔP and ΔL, respectively.

we thus have the following condition for robust stability,

$$\left\| \frac{\Delta P(s)}{P_o(s)} T(s, \Delta L) \right\|_\infty < 1, \quad \Delta L \in [\Delta L_{\min},\ \Delta L_{\max}].$$

3.2 Nyquist Interpretation

The robustness criterion can easily be illustrated graphically in a Nyquist diagram. Consider a certain frequency ω and introduce the notations

$$\begin{aligned} CP(i\omega) &= \mathrm{Re}CP(i\omega) + i\mathrm{Im}CP(i\omega) = x + iy \\ \phi_\Delta &= \omega\Delta L. \end{aligned}$$

We can then write

$$\begin{aligned} CP(i\omega)e^{-i\omega\Delta L} &= (x + iy)(\cos\phi_\Delta - i\sin\phi_\Delta) \\ &= (x\cos\phi_\Delta + y\sin\phi_\Delta) + i(y\cos\phi_\Delta - x\sin\phi_\Delta). \end{aligned}$$

The magnitude of $T(i\omega, \Delta L)$ at ω is then given by

$$|T(i\omega, \Delta L)| = \sqrt{\frac{x^2 + y^2}{1 + 2x\cos\phi_\Delta + 2y\sin\phi_\Delta + y^2 + x^2}},$$

and is constant for x, y and ϕ_Δ satisfying

$$x^2 + y^2 = M_{T_\omega}^2 (1 + 2x\cos\phi_\Delta + 2y\sin\phi_\Delta + y^2 + x^2),$$

where $M_{T_w} = |T(i\omega, \Delta L)|$ has been introduced for convenience. This can be written as

$$\left(x + \left(\frac{M_{T_\omega}^2}{M_{T_\omega}^2 - 1}\right)\cos\phi_\Delta\right)^2 + \left(y + \left(\frac{M_{T_\omega}^2}{M_{T_\omega}^2 - 1}\right)\sin\phi_\Delta\right)^2 - \frac{M_{T_\omega}^2}{\left(M_{T_\omega}^2 - 1\right)^2} = 0,$$

which is a circle with center and radius

$$-\left(\frac{M_{T_\omega}^2}{M_{T_\omega}^2 - 1}\right)(\cos\phi_\Delta, \sin\phi_\Delta), \quad \frac{M_{T_\omega}}{M_{T_\omega}^2 - 1},$$

respectively. Hence, if $T(i\omega, \Delta L)$ should be smaller than some value M_{T_ω} as defined by the robust stability condition, the Nyquist curve at a certain frequency ω must be strictly outside the defined frequency dependent circle if $M_{T_\omega} > 1$, otherwise inside the circle.

Since it is assumed that only the interval of the delay uncertainty is know, i.e., $[\Delta L_{\min},\ \Delta L_{\max}]$, the above condition at a certain frequency ω must hold for all ΔL. It is easily seen that a prohibited area then is given in the Nyquist diagram which can be used in assessing robustness of the system.

Note that $\Delta L_{\min}$ and $\Delta L_{\max}$ will give the fastest movement clockwise and counter clockwise, respectively, of the center as $\omega : 0 \to \infty$. Analogously, if $\Delta L = 0$ no movement of the circle centers will take place and we recover the ordinary robust stability notation.

3.3 Specification Choices

To use the above defined robust stability condition, the uncertainty interval for ΔL and additive frequency dependent error ΔP for the delay free part needs to be specified. Hence, we have the flexibility to treat delay uncertainties as a special case leading to reduced conservatism.

Considering only ΔP we can relate to the usual setting of weights in robust control, the only difference is that the inequality should hold for all ΔL. A simple, and now less conservative choice, is to define

$$M_{T_\Delta} = \max_{\Delta L \in [\Delta L_{\min}, \Delta L_{\max}]} \|T(s, \Delta L)\|_\infty,$$

which can be calculated in the controller design. With this specification, a relative uncertainty of the delay free part of less than $1/M_{T_\Delta}$ guarantees

a stable system even in the presence of delay uncertainties. This correspond to the simplified condition of M_T, see Section 2.1, and the radii of the circles are in this case constant. Note that it is not certain that the maximum is achieved at the ends of the interval. The robustness condition can easily be evaluated using the Nyquist diagram and the prohibited areas.

If we in the specification set $\Delta L = 0$, we get in return the ordinary condition for robust stability. On the contrary, letting $M_{T_\Delta} \to \infty$, i.e., $\Delta P \to 0$, the centers of the circles tend to $(-\cos \omega \Delta L, -\sin \omega \Delta L)$ with the radii tending to 0. Hence, the area will be an arc. This implies that we have recovered the ordinary definition of dead time margin except now all frequencies are accounted for. Thus, in the example in Section 2.3, using the above robustness criteria, we would have found the PI controller with lowest IAE.

The newly defined robustness criteria can be considered to be in between ordinary robust control and classic robustness margins, since it is less conservative than ordinary robust stability but at the same time guarantees stability to simultaneous process uncertainties.

3.4 Motivating Example Revisited

Consider again the example in Section 2.3. The specification using M_T is intended to give robustness towards delay and gain/time constants changes. Instead, using the definition of M_{T_Δ} we can split the robustness into two parts. Consider the case when $M_{T_\Delta} = 1.4$ is desired, as in the example. Using the definition in Section 3.1 we have that $\Delta L \in [-1, 1.06]$. This interval is much smaller than what the traditional delay margin indicates, since we now have simultaneous robustness towards process uncertainties. The optimization problem to calculate this interval is presented and solved in Section 5.

According to the definition of M_{T_Δ} it is not possible to have a delay margin of 3.2 s as in the original example since then we must have $M_{T_\Delta} \to \infty$. For example, if we let the delay uncertainty be in the interval $[-1, 1.6]$ we have $M_{T_\Delta} = 2.1$. In Figure 2 the prohibited area is shown for $\omega = 0.475$ and 1.5 rad/s. Note that for $\omega = 0.475$ rad/s the Nyquist curve touches the prohibited area. The optimization problem for this result is posed and solved in Section 6.

4. Sensitivity Function Based Robustness

In this section we will consider a measure related to the sensitivity function and how it is associated with process uncertainties and disturbance responses.

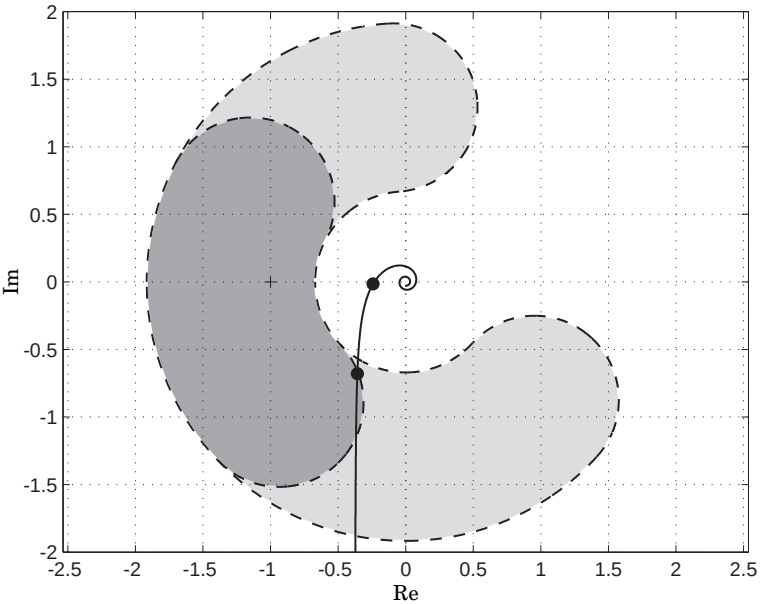

Figure 2. Illustration of prohibited areas for the Nyquist curve in the example, Section 3.4. We have $\Delta L \in [-1, 1.6]$ and $M_{T_\Delta} = 2.1$ and areas are shown for $\omega = 0.475$ and 1.5 rad/s, dark and light grey, respectively. Note that the Nyquist curve touches the prohibited area for $\omega = 0.475$ rad/s.

4.1 Extended Sensitivity Function

In the case of the complementary sensitivity function we considered multiplicative uncertainties of the delay free part of the process. Consider now on the contrary an inverse multiplicative uncertainty, i.e., we have a process model as

$$P_o(s)\left(1+\frac{\Delta P(s)}{P_o(s)}\right)^{-1} e^{-s(L+\Delta L)}.$$

Assuming the open loop with uncertainties is stable and norm bounded, the condition for robust stability is, see [Skogestad and Postlethwaite, 2005],

$$\left|1+CP_o(i\omega)\left(1+\frac{\Delta P(i\omega)}{P_o(i\omega)}\right)^{-1} e^{-i\omega(L+\Delta L)}\right| > 0 \Leftrightarrow$$
$$\left|1+\frac{\Delta P(i\omega)}{P_o(i\omega)}+CP_o e^{-i\omega(L+\Delta L)}\right| > 0,$$

for all $\Delta L \in [\Delta L_{\min},\ \Delta L_{\max}]$, $\Delta P(i\omega)$, and ω. Since $\Delta P(i\omega)$ can have any direction in the complex plane we can express the condition as

$$\left|1 + CP_o e^{-i\omega(L+\Delta L)}\right| - \left|\frac{\Delta P(i\omega)}{P_o(i\omega)}\right| > 0.$$

Introducing the extended sensitivity function

$$S(s, \Delta L) = \frac{1}{1 + CPe^{-s\Delta L}}$$

the robust stability condition is

$$\left\| \frac{\Delta P(s)}{P_o(s)} S(s, \Delta L) \right\|_\infty < 1, \quad \Delta L \in [\Delta L_{\min},\ \Delta L_{\max}].$$

The extended sensitivity function also measures the closed loop sensitivity. This can be illustrated as follows. Consider a closed loop system

$$G(s) = \frac{CP_o(s)e^{-sL}}{1 + CP_o(s)e^{-sL}},$$

where $P_o(s)$ is delay free and L is the delay. It is easily derived, by taking the derivative of $G(s)$ with respect to $P_o(s)$, that

$$\frac{dG(s)}{G(s)} = \frac{1}{1 + CP(s)} \frac{dP_o(s)}{P_o(s)},$$

and hence with a delay uncertainty in the process we have

$$\frac{dG(s)}{G(s)} = S(s, \Delta L) \frac{dP_o(s)}{P_o(s)}.$$

We see that the extended sensitivity function gives an estimate of how sensitive the closed loop system is towards changes in the delay free part of the process.

Consider instead an open loop and a closed loop system with outputs $Y_{ol}(s)$ and $Y_{cl}(s)$, and the delay uncertainty ΔL. We then have the relationship

$$\frac{Y_{cl}(s)}{Y_{ol}(s)} = \frac{1}{1 + CP(s)e^{-s\Delta L}} = S(s, \Delta L).$$

With $S(s, \Delta L)$ it is hence easy to see what frequencies of the disturbances that will be attenuated or amplified, respectively.

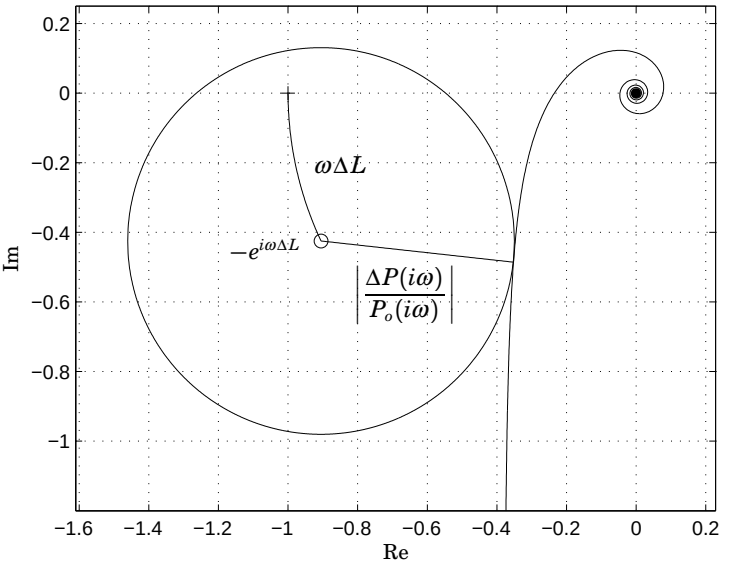

Figure 3. Nyquist curve of a nominal transfer function and illustration of robust stability inequality based on inverse multiplicative uncertainty.

4.2 Nyquist Interpretation

As with $T(s,\Delta L)$, we can illustrate the conditions on $S(s,\Delta L)$ in a Nyquist diagram. If we have $P(i\omega) = P_o(i\omega)e^{-i\omega L}$, the complex quantity $1 + CP(i\omega)e^{-i\omega\Delta L}$ for a certain frequency ω can be interpreted as the distance from the Nyquist curve $CP(i\omega)$ multiplied with the delay uncertainty, i.e., $CP(i\omega)e^{-i\omega\Delta L}$, to the point -1. That is, $1/S(i\omega,\Delta L)$ is the distance from -1 to the rotated Nyquist curve. For a certain weight $\Delta P(s)/P_o(s)$ we have the robust stability inequality

$$|1 + CP(i\omega)e^{-i\omega\Delta L}| = |e^{i\omega\Delta L} + CP(i\omega)| > \left|\frac{\Delta P(i\omega)}{P_o(i\omega)}\right|.$$

Thus, at a certain frequency ω we see that the Nyquist curve must be outside a circle with center $-e^{i\omega\Delta L}$ and radius $|\Delta P(i\omega)/P_o(i\omega)|$, see Figure 3. Since, again, we only know the interval of ΔL, i.e., $\Delta L \in [\Delta L_{\min}, \Delta L_{\max}]$, the Nyquist curve at ω must be outside an area defined by the circles for all ΔL in this set.

4.3 Specification Choices

As for the specification of $T(s,\Delta L)$, we need to specify ΔP and ΔL for $S(s,\Delta L)$ which again gives the flexibility to separate the different uncer-

tainties. The radii of the frequency dependent circles is defined by ΔP while the movement of the centers is given by ΔL. For simplicity, assume a frequency independent uncertainty in the delay free part. Analogous to M_{T_Δ}, we can then introduce

$$M_{S_\Delta} = \max_{\Delta L \in [\Delta L_{\min}, \Delta L_{\max}]} \|S(s, \Delta L)\|_\infty,$$

as a measure, corresponding to constant radii of $1/M_{S_\Delta}$. This will not only guarantee robustness towards inverse multiplicative uncertainties of magnitude $1/M_{S_\Delta}$ when a delay uncertainty is present, but also bound sensitivity of the closed loop system and worst case amplification of disturbances. Note that the maximum might not be achieved at the boundaries of ΔL. The choice of interval for ΔL depends, naturally, on the real process and model fidelity. In the design phase, the robustness criterion above can easily be assessed in a Nyquist plot.

Note that, analogous to the constraint on $T(s, \Delta L)$, the constraint on $S(s, \Delta L)$ degenerates to the ordinary robust stability notion if no dead time uncertainty is modelled, and to a dead time margin over all frequencies if no uncertainty in the delay free part P_o is present.

4.4 Motivating Example Revisited

Consider again the example in Section 2.3 where a first order system with dead time was controlled by a PI-controller. We can now determine the systems robustness and sensitivity using the separate measures of M_{S_Δ} and ΔL.

If M_{S_Δ} is chosen as M_S in the example, we see that by the definition of M_{S_Δ} the system is not robust toward any positive dead time error since the Nyquist curve touches the M_S-circle. This interpretation emphasized the fact that process uncertainties are now considered simultaneously instead of separate since by the old definition of delay margin, the system is robust towards an error up to 3.2 s. To have a delay margin, we must hence accept a higher sensitivity by increasing M_{S_Δ}, that is, decreasing the circles radii. Using for example $M_{S_\Delta} = 1.8$, the uncertainty interval of ΔL we can accept is then $[-1, 0.67]$.

In the opposite case, consider the dead time interval $[-1, 1.6]$ as in Section 3.4. For this system, we must accept a sensitivity and robustness towards delay free errors of $M_{S_\Delta} = 2.9$, which is more than twice as large as the sensitivity defined by the ordinary M_S-circle. Again, this is due to the simultaneous process changes. The prohibited areas for the Nyquist curve for this case are shown in Figure 4. Note that both areas stem from circles with same radii, i.e, $1/1.4$.

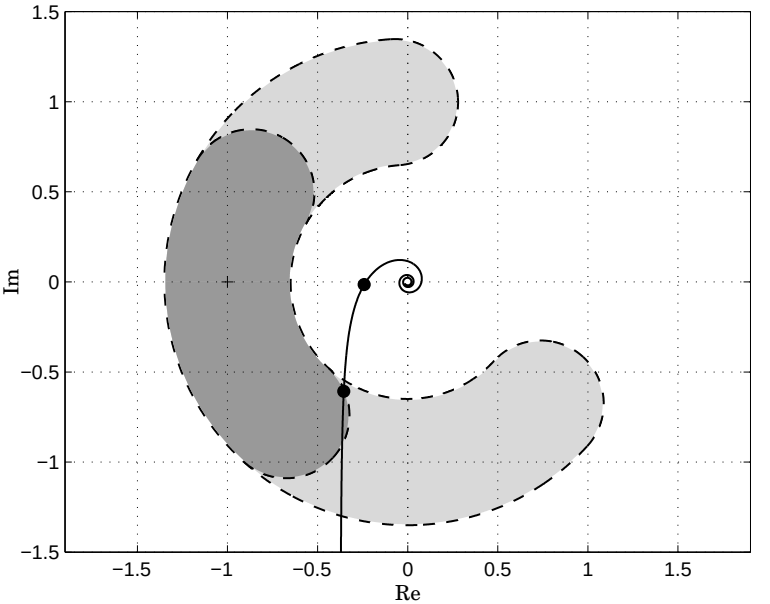

Figure 4. Illustration of prohibited areas for the Nyquist curve in the example, Section 4.4. We have $\Delta L \in [-1, 1.6]$ and $M_{s_\Delta} = 2.9$ and areas are shown for $\omega = 0.52$ and 1.5 rad/s, dark and light grey, respectively. Note that the Nyquist curve touches the prohibited area for $\omega = 0.52$ rad/s.

5. Delay Margin Calculation

In this section, we will consider the case when we have specified the weights on the extended sensitivity functions, i.e., ΔP, and the largest delay margin interval is to be calculated. For clarity, we will do this for constant weights, but the calculations are straightforward to extend to frequency dependent weights. The below outlined optimization was used in the examples in Sections 3.4 and 4.4.

Assume that we have the constraints

$$\|T(s, \Delta L)\|_\infty < M_{T_\Delta}, \qquad \|S(s, \Delta L)\|_\infty < M_{S_\Delta},$$

where it is assumed that $M_{T_\Delta} > 1$. The constraint can then be illustrated as circles with radii $r = M_{T_\Delta}/(M_{T_\Delta}^2 - 1)$ and $1/M_{S_\Delta}$, respectively, and center of the form $c \cdot (\cos \omega \Delta L,\ \sin \omega \Delta L)$, where $c = -M_{T_\Delta}^2/(M_{T_\Delta}^2 - 1)$ or -1. Hence, the center angle relative the origin is determined by $\omega \Delta L$, which will be used in the following. Consider Figure 5, where two circles are drawn in the complex plane. The leftmost has center at c and radius r,

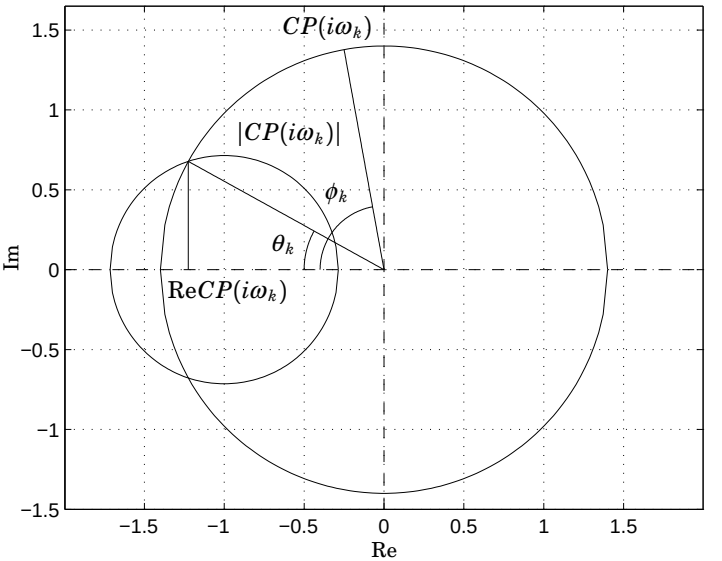

Figure 5. Definition of θ_k and ϕ_k used in the time delay margin calculation.

corresponding to one of the constraints above. Assume that we have a frequency vector ω with indexation k and a Nyquist curve $CP(i\omega)$ of a stable closed system. The rightmost circle has center at the origin and radius $|CP(\omega_k)|$, where $C(s)$ and $P(s)$ is the controller and process transfer function, respectively. The index k is chosen such that the two circles intersect, that is, the Nyquist curve at frequency ω_k is able to rotate inside the constraint circle if a ΔL is present. The real part of the intersection points is

$$\mathrm{Re}CP(i\omega_k) = \frac{|CP(i\omega_k)|^2 + c^2 - r^2}{2c},$$

and the angle θ_k, see Figure 5, can be determined as follows,

$$\theta_k = \arccos\left(-\frac{|CP(i\omega_k)|^2 + c^2 - r^2}{2c|CP(i\omega_k)|}\right).$$

Now consider point $CP(i\omega_k)$ on the Nyquist curve. Then we can define the angle $\phi_k = \pi - \arg CP(i\omega_k)$ in Figure 5. Since a negative ΔL gives a counter clockwise rotation of the Nyquist curve, i.e., $e^{-i\omega_k(L+\Delta L)}$, we can, for the frequency ω_k, define the largest negative ΔL such that the upper half of the constraint circle is reached, as

$$\Delta L_-(k) = -\frac{\phi_k - \theta_k}{\omega_k} \leq 0.$$

Similarly we have for a positive ΔL

$$\Delta L_+(k) = \frac{2\pi - \phi_k - \theta_k}{\omega_k} \geq 0,$$

which rotates the Nyquist curve such that it reaches the lower half of the constraint circle. Now define the set

$$\mathcal{K} = \{k \mid |CP(i\omega_k)| \in [c-r, c+r]\},$$

that is, $\mathcal{K}$ is the set of indices of frequencies where it is possible for the Nyquist curve to rotate into the constraint circle. Thus, using $\Delta L_-(k)$ and $\Delta L_+(k)$ for all k in the above set, the delay margin interval can be calculated as

$$\Delta L_{\min} = \max_{k\in\mathcal{K}} \Delta L_-(k), \qquad \Delta L_{\max} = \min_{k\in\mathcal{K}} \Delta L_+(k),$$

when using one of the constraint circles. If both M_{S_Δ} and M_{T_Δ} are used, the minimization/maximization is performed for both circles. Note that in the calculation of $\Delta L_{\min}$ it is possible that the result fulfills $L + \Delta L_{\min} < 0$. Obviously, in this case we have $\Delta L_{\min} = -L$. The calculation is straightforward to extend for frequency dependent weights by using frequency dependent r and c.

6. Delay Free Uncertainty and Sensitivity Calculation

The opposite case of Section 5, i.e., when the time delay uncertainty is specified and the sensitivity and robustness towards delay free errors are calculated, is presented in this section. The calculations in Section 5 of the dead time margin will be used and for simplicity constant weights are assumed. The procedure below was used in the examples in Sections 3.4 and 4.4.

Large robustness in sense of M_j, i.e., either M_{S_Δ} or M_{T_Δ}, is equivalent to small values and hence a large radius on the corresponding circle. Considering a Nyquist diagram of a stable system, it is clear that the larger the radius is the smaller must the uncertainty in dead time be, hence $\Delta L_{\min}$ and $\Delta L_{\max}$ is an increasing and decreasing function, respectively, of circle radius. The choice of M_j is therefore equivalent to decreasing M_j until the specified limit of time delay uncertainty becomes active. Hence,

we can formulate it as a simple optimization problem,

$$\begin{aligned} \min_{M_j > M_j^{\min}} \quad & M_j \\ \text{s.t. } & \Delta L_{\min}(M_j) < \Delta L_{\min} \\ & \Delta L_{\max}(M_j) > \Delta L_{\max}, \end{aligned}$$

where $\Delta L_{\min}(M_j)$ and $\Delta L_{\max}(M_j)$ are the dead time margins as function of M_j as calculated in Section 5. The constraints $\Delta L_{\min}$ and $\Delta L_{\max}$ are the limits in the predefined time delay uncertainty interval. The optimization variable constraint $M_j > M_j^{\min}$ is either $M_{T_\Delta} > 1$ or $M_{S_\Delta} > 0$.

If both M_{S_Δ} and M_{T_Δ} are specified, the minimization is performed for each of them.

7. Summary

In this note we have described new robustness measures. Simultaneous process changes are considered and the measures are therefore more suitable to use than classic measures such as gain, phase, and dead time margins. The new measures separate dead time and other process uncertainties, and are hence more flexible and less conservative than robust stability in the robust control framework. The new robustness constraints on the sensitivity functions can be illustrated in a Nyquist diagram yielding understanding of the inherent problem of dead time. It has also been shown that the aforementioned known measures are found as special cases. Procedures to calculate the new measures have been presented and exemplified.

References

Åström, K. J. and T. Hägglund (2006): *Advanced PID Control*. ISA - The Instrumentation, Systems, and Automation Society, Research Triangle Park, NC 27709.

Garpinger, O. and T. Hägglund (2008): "A Software Tool for Robust PID Design." In *Proc. 17th IFAC World Congress, Seoul, Korea*.

Morari, M. and E. Zafiriou (1989): *Robust Process Control*. Prentice Hall, Englewood Cliffs, NJ 07632.

Shinskey, F. (1994): *Feedback Controllers for the Process Industries*. McGraw-Hill.

Skogestad, S. and I. Postlethwaite (2005): *Multivariable Feedback Control: Analysis and Design*, 2nd edition. John Wiley & Sons Ltd, Chichester, West Sussex PO19 8SQ, England.

Zhou, K. and J. C. Doyle (1998): *Essentials of Robust Control*. Prentice Hall, Inc, Upper Saddle River, New Jersey 07458, USA.

Paper III

Comparison Between Robust PID and Predictive PI Controllers with Constrained Control Signal Activity

Per-Ola Larsson and Tore Hägglund

Abstract

A performance comparison between PID and predictive PI (PPI) controllers, i.e., two different prediction methods, is presented. Optimization of controller and measurement filter parameters, considering load disturbance rejection, robustness and noise sensitivity, is performed for a batch of industrially representative processes. For a majority of the processes and the constraints chosen, results show that the performances of the controllers are similar. However, the PID controller yield better performance for processes where increased phase and gain may be achieved over a wider frequency interval than what is possible by the PPI controller.

Submitted to the *2012 IFAC Conference on Advances in PID*, Brescia, Italy.

1. Introduction

Low-level controllers in the process industry are required to have few tuning parameters, be easy to tune manually, and the parameters should affect the control loop in an intuitive manner. The most common control structure in process industry is the PID structure, and most often is the derivative action turned off, resulting in a PI controller. This is due to the introduction of noise sensitivity by the derivative part, but also because it requires tuning and additional filtering. Adding derivative action may increase performance significantly and joint design of PID controller and measurement filter for load rejection, where limitations on noise sensitivity may be set, have recently emerged, see for instance [Kristiansson and Lennartson, 2006, Garpinger, 2009, Larsson and Hägglund, 2011].

Adding derivative action to a PI controller yields phase advance, i.e., prediction capability. Another type of prediction is given by a Smith predictor, see [Smith, 1957]. The Smith predictor structure contains a model of the process without dead-time, which is used for simulation internally with the control signal as input. If the model is accurate, its output is a prediction of the process output with the prediction horizon equal to the process dead-time. However, adding a predictor structure increases the number of controller parameters significantly and adds to the operational complexity. A simplified form of the Smith predictor structure with a PI controller, denoted PI_τ or predictive PI (PPI), has the same number of parameters as the PID controller and can be tuned manually in an analogous manner, see [Shinskey, 1994] and [Hägglund, 1996].

Performance comparisons between the PID and the PI controller with a Smith predictor structure, regarding load disturbances, have been made in e.g., [Kristiansson and Lennartson, 2001] and [Ingimundarson and Hägglund, 2002]. In this paper, comparison between the performance of the PID and the PPI controller will be considered. The differences to the beforementioned references are that the compared control structures have the same number of tuning parameters and the comparison is performed in a discrete time setting. Additionally, both robustness towards process uncertainty and control signal noise sensitivity are considered using other types of measures.

2. Feedback and Controller Structures

The closed loop considered in the comparison is shown in Figure 1, where P, C and F are the process, controller and measurement filter, respectively. The sensor signal Y, giving information about the process output X, is corrupted by measurement noise N. The load disturbance D is as-

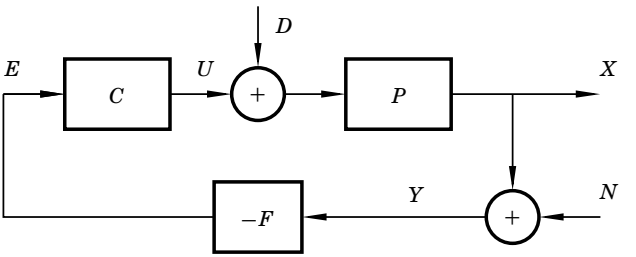

Figure 1. Closed loop control structure with process P, controller C and measurement filter F.

sumed to enter on the process input together with the control signal U, which is calculated by the controller from the control error E.

The considered PID controller is on parallel form with the input-output relation

$$U = K\left(1 + \frac{1}{sT_i} + sT_d\right)E,$$

where K, T_i and T_d are proportional gain, integral time and derivative time, respectively. The comparison will be made in a discrete time setting and the integral and derivative parts are discretized using forward and backward differences, respectively, with sampling period h.

The input-output relation of the PPI controller is

$$\begin{aligned} U &= K\left(1 + \frac{1}{sT_i}\right)\left(E - \frac{K^{-1}}{sT_i + 1}\left(1 - e^{-sL}\right)U\right) \\ &= K\left(1 + \frac{1}{sT_i}\right)E - \frac{1}{sT_i}\left(1 - e^{-sL}\right)U, \end{aligned}$$

where K, T_i and L are the proportional gain, integral time and controller dead-time, respectively. Compared to a PI controller with Smith predictor, the process model in the PPI controller is parametrized with gain K^{-1}, time constant T_i and dead-time L. Thus, only for certain values of the parameters is the PPI controller equal to a PI controller with a Smith predictor using a first order model with dead-time, i.e., model matching. The PPI controller is not limited to model matching and its performance can in general be improved if model matching is not considered, see [Shinskey, 2001]. Due to the model parametrization, the PPI controller handles integrating processes, no additional filters are required as for the Smith predictor structure.

The input-output relation of the PPI controller shows that an ordinary PI controller acts on the control error E and the prediction, due to the process model parametrization, is performed by low-pass filtering the control

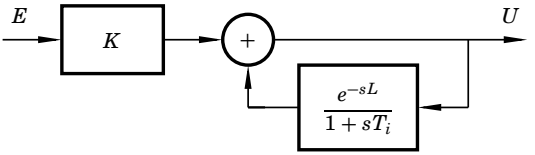

Figure 2. Implementation of the predictive PI controller.

signal U. The transfer function of the PPI controller can be factorized as $C_0 C_{\text{pred}}$, where C_0 is a PI controller and C_{pred} is a predictor structure as

$$C_0 = K\left(1 + \frac{1}{sT_i}\right), \quad C_{\text{pred}} = \frac{1}{1 + \frac{1}{sT_i}\left(1 - e^{-sL}\right)}.$$

The predictor behavior is essentially determined by the ratio L/T_i and its gain tends to 1 at high frequencies. Thus, the PPI controller gain tends to K.

The PPI controller may be implemented by introducing the dead-time L in the positive feedback in a PI controller implementation, see Figure 2. Discretization is made by zero-order hold of the positive feedback transfer function.

To achieve desired noise sensitivity level of the feedback, measurement filters should be designed together with the controllers, see [Isaksson and Graebe, 2002]. In [Larsson and Hägglund, 2011], it was shown that a second order filter with damping $1/\sqrt{2}$ is preferable to a first order filter for a PID. To achieve the same roll-off in the feedback when using a PPI controller, a first order filter will be used together with the PPI. The filters are parametrized by the time constant T_f as

$$F_{\text{PPI}} = \frac{1}{sT_f + 1}, \quad F_{\text{PID}} = \frac{1}{s^2 T_f^2 + \sqrt{2} T_f s + 1},$$

and are discretized using zero-order hold. Thus, both the design of a PID controller and a PPI controller, with their associated measurement filters, will have four parameters to determine.

3. Comparison of Prediction Methods

The two controllers presented in the previous section perform prediction in two different ways. A Taylor series expansion of the time-domain control error $e(t + T_d)$ is

$$e(t + T_d) \approx e(t) + T_d \frac{de(t)}{dt} + \ldots$$

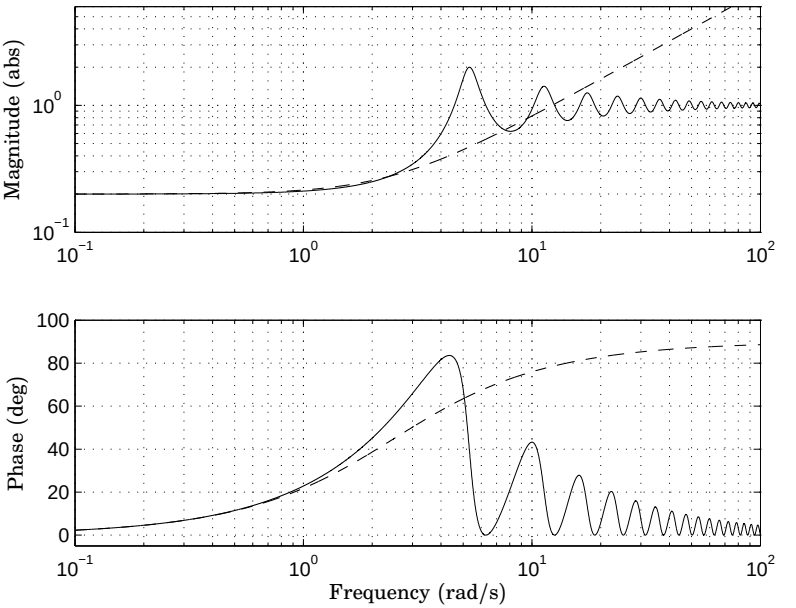

Figure 3. The predictor C_{pred} in the PPI controller (–) and a PD controller (--).

The two first terms is the linear prediction performed jointly by the proportional and derivative part of the PID controller. The prediction in the PPI controller is performed by C_{pred}, which has the following Taylor series expansion for small s, see [Åström and Hägglund, 2006],

$$C_{\text{pred}} = \frac{1}{1 + L/T_i}\left(1 + \frac{1}{2}\frac{(L/T_i)^2}{1 + L/T_i}T_i s + \ldots\right).$$

In Figure 3, the transfer function C_{pred}, with $T_i = 0.25$ and $L = 1$, is shown together with a PD controller with K and T_d set using the Taylor series expansion of C_{pred} as

$$K = \frac{1}{1 + L/T_i}, \quad T_d = \frac{1}{2}\frac{(L/T_i)^2}{1 + L/T_i}T_i.$$

The predictor C_{pred} has a distinct phase advance peak, associated with a peak in the gain. The phase advance falls rapidly after the peak. The PD controller has an increasing phase over a wider frequency interval, associated with a steadily increasing gain. As noted in the previous section, the gain of C_{pred} tends to 1 at high frequencies, while the gain of the PD

controller tends to infinity, hence the orders of F_{PPI} and F_{PID}. Adding the measurement filters to the predictors, the phase advances will be smaller and gains lower, but the differences in characteristics remain.

4. Robustness and Noise Sensitivity

Robustness towards process uncertainties is imperative to consider at controller design. The Smith predictor structure, and thus also the PPI controller, is sensitive towards modeling errors in the process dead-time, see [Palmor, 1980]. A method to reduce the sensitivity, presented in [Normey-Rico *et al.*, 1997], is to add a low-pass filter in the feedback structure. This approach requires at least one parameter in the added filter to be set, yielding undesirable increase in design complexity. Another method was presented in [Kristiansson and Lennartson, 2001], where an upper gain limit on the open-loop transfer function is set after the phase crossover frequency. In [Ingimundarson and Hägglund, 2002], the open-loop gain was instead limited to be strictly less than 1 after the gain crossover frequency. The last two methods may be conservative as they imply that any reduction in process dead-time will never yield instability, even though bounds on the dead-time uncertainty may be known.

The robustness measures for process uncertainties to be used in this paper were presented in [Larsson and Hägglund, 2009] for continuous time systems and can be used for discrete time systems with negligible approximation errors if an appropriate sample period is used, see Appendix A. The measures consider upper amplitude limits on S_Δ and T_Δ, which are the closed loop sensitivity and complementary sensitivity functions extended to depend on the process dead-time uncertainty ΔL. Constraints may be set as

$$\|S_\Delta(\Delta L)\|_\infty \leq M_S \tag{1}$$
$$\|T_\Delta(\Delta L)\|_\infty \leq M_T, \tag{2}$$

which should hold for all considered ΔL in an interval $\Delta \underline{L} \leq \Delta L \leq \Delta \overline{L}$, where $\Delta \underline{L}$ and $\Delta \overline{L}$ and lower and upper bounds on the dead-time uncertainty. Thus, the constraints guarantee that the maximum gains of the sensitivity functions S and T are less than or equal to M_S and M_T, respectively, when the process dead-time is changed within the interval. The parameters M_S and M_T may be specified to set desired robustness towards process gain and time constant uncertainties. See [Larsson and Hägglund, 2009] for a method to calculate the largest interval, which includes 0, for ΔL in Eqs. (1)–(2) when a nominal Nyquist curve and M_S and M_T are given.

Measurement noise may yield undesirable activity of the control signal. Assuming the noise is white with zero mean and with variance, i.e., energy, σ_n^2, then the constraint

$$\|CFS\|_2 \leq \eta_u,$$

where S is the sensitivity function, limits the control signal energy due to measurement noise to $\sigma_u^2 \leq \eta_u^2 \sigma_n^2$. Rapid variations in the control signal are also undesirable from an actuator point of view. In [Larsson and Hägglund, 2011], a measure was presented that considers the inter-sample amplitude of the control signal, i.e., derivative, due to measurement noise. It may be expressed as

$$\|\Delta_z CFS\|_2 \leq \eta_{\Delta u},$$

where Δ_z is the difference operator, i.e., $\Delta_z = (z-1)/z$. Both the above constraints on noise sensitivity of the control signal will be used in the design of controllers and measurement filters.

5. Optimization Formulation

The controllers and measurement filters will be compared using the integrated absolute error (IAE) at a load disturbance step as performance measure. The design optimization problem, with the constraints in the previous section, may be stated as follows,

$$\begin{aligned}
\underset{\mathcal{K}}{\text{minimize}} \quad & h\sum_{k=0}^{\infty}|x(k)| \\
\text{subject to} \quad & \|S_\Delta(\Delta L)\|_\infty \leq M_S, \quad \Delta\underline{L} \leq \Delta L \leq \Delta\overline{L} \\
& \|T_\Delta(\Delta L)\|_\infty \leq M_T, \quad \Delta\underline{L} \leq \Delta L \leq \Delta\overline{L} \\
& \|CFS\|_2 \leq \eta_u \\
& \|\Delta_z CFS\|_2 \leq \eta_{\Delta u} \\
& \underline{T}_f \leq T_f \leq \overline{T}_f,
\end{aligned} \tag{3}$$

where $\mathcal{K}$ contains controller and measurement filter parameters, $x(k)$ is the process output when a load disturbance step is applied at initial time, and h is the sample period. The constraints on the extended sensitivity functions are required to hold for all dead-time uncertainties ΔL that are in the interval defined by $\Delta\underline{L}$ and $\Delta\overline{L}$. The lower limit on T_f is set to $\underline{T}_f = h/\pi$ due to sampling. The upper limit $\overline{T}_f$ is set such that the filter break point is at a higher frequency than the frequency where derivative

action or prediction by C_{pred} is begun. That is, the filter may not be used for loop-shaping at low- and mid-frequencies, only for attenuation at high frequencies, i.e., as a measurement filter. For the PPI controller, the inverse of the lowest frequency where the controller amplitude curve has a positive derivative, denoted ω_f, is taken as an upper limit and may be calculated numerically in the optimization. For PID control, the limit is taken as the inverse of the largest modulus of the controller zeros of the continuous time transfer function. Thus, for F_{PPI} and F_{PID}, respectively, the upper limits are

$$\overline{T}_f = \frac{1}{\omega_f}, \quad \text{and} \quad \overline{T}_f = \left| \frac{1}{2T_d} + \sqrt{\frac{1}{4T_d^2} - \frac{1}{T_i T_d}} \right|^{-1}.$$

6. Process Batch and Design Parameters

Controllers and filters have been optimized for the following batch of 82 industrially representative processes,

$$P_1 = \frac{e^{-s}}{sT+1}, \; T = 0.1, 0.2, 0.3, 0.5, 1, 1.5, 4, 10, 50$$

$$P_2 = \frac{e^{-s}}{(sT+1)^2}, \; T = 0.1, 0.2, 0.3, 0.5, 1, 2, 6, 10, 50$$

$$P_3 = \frac{1}{(s+1)(sT+1)^2}, \; T = 0.05, 0.1, 0.2, 0.5, 2, 5, 10$$

$$P_4 = \frac{1}{(s+1)^n}, \quad n = 3, 4, 5, 6, 7, 8$$

$$P_5 = \frac{1}{\Pi_{k=0}^{3}(\alpha^k s+1)}, \quad \alpha = 0.4, 0.5, \ldots, 0.9$$

$$P_6 = \frac{e^{-sL_1}}{s(sT_1+1)}, \quad P_7 = \frac{e^{-sL_1}}{(sT+1)(sT_1+1)}, \quad T = 1, 10$$

$$L_1 = 0.02, 0.05, 0.1, 0.3, 0.5, 0.7, 0.9, 1, \; L_1 + T_1 = 1$$

$$P_8 = \frac{1-\alpha s}{(s+1)^3}, \quad \alpha = 0.1, 0.2, \ldots, 1.1$$

$$P_9 = \frac{1}{(s+1)((sT)^2 + 1.4sT + 1)}, \quad T = 0.1, 0.2, \ldots, 1.$$

The batch includes both lag-dominated, delay-dominated, oscillative and integrating processes as well as processes with inverse step responses. All processes are sampled using zero-order hold with sample period $h = 0.02$

at optimization. In all designs, $M_S = M_T = 1.4$, which is a common value when considering upper limits on the sensitivity functions, see [Åström and Hägglund, 2006]. The noise sensitivity constraints are set to $\eta_u = \eta_{\Delta u} = 1$, see [Larsson and Hägglund, 2011] for design choices. For simplicity, if the considered process has a dead-time L, then $\Delta\underline{L} = -L/10$ and $\Delta\overline{L} = L/10$. If the process is modeled without dead-time, only an additive dead-time uncertainty is considered by $\Delta\underline{L} = 0$ and $\Delta\overline{L} = \tilde{L}/10$, where $\tilde{L}$ is the apparent dead-time of the process.

The optimization problems are solved in MATLAB® using the Control System Toolbox™, Optimization Toolbox™, and Simulink®.

7. Batch Results

Ratios between the resulting IAE for the PPI and PID structures are found in Figure 4 as functions of the normalized process dead-time τ. For a majority of the processes, the performances of the two prediction methods are similar, yielding ratios within 0.9–1.1. Comments on the specific processes are given below.

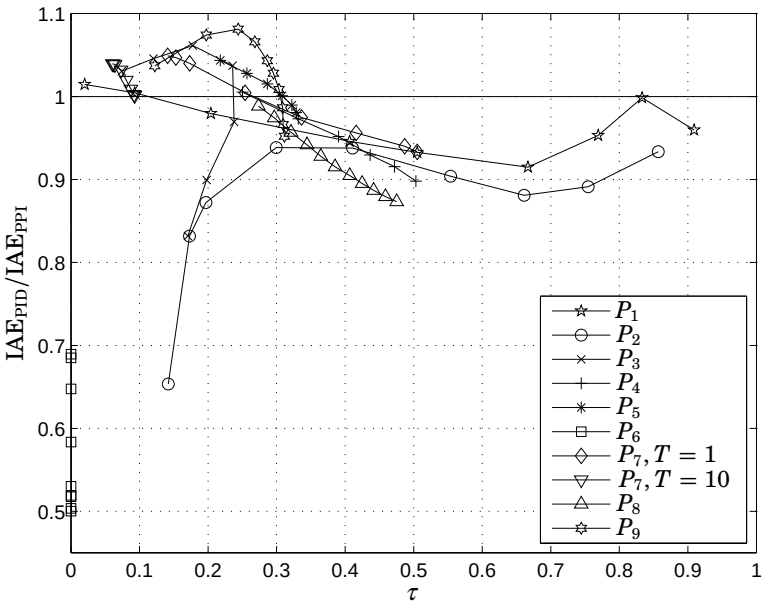

Figure 4. Ratios between IAE for PID and PPI feedback structures as a function of normalized dead-time τ for the processes in the batch.

For the PPI structure and P_1 and P_2 with $\tau > 0.5$, it is only the constraint on $\|S_\Delta\|_\infty$ that is active, limiting the peak gains. For the PID structure, the corresponding limit is $\tau > 0.8$. For these processes, a derivative part may give gain increase and phase advance over a wider frequency interval than the PPI predictor, which yields a better performance for the PID structure. See Example I in Section 8, where the designs for P_1 with $T = 0.3$ are shown in detail.

At τ close to 0, P_1 is essentially a first-order process, requiring no phase advance in the feedback for high low-frequency gain and thus low IAE. Resulting feedbacks are basically PI controllers with measurement filters and the constraints on $\|CFS\|_2$ and $\|S_\Delta\|_\infty$ are active.

For higher order processes, phase advance in the feedback may increase performance significantly. For P_2 and P_3 with large time constants, i.e., $T \geq 10$, and thus small τ, phase advance should be made at low frequencies for high performance. As the constraint functions $\|CFS\|_2$ and $\|\Delta_z CFS\|_2$ are calculated over all frequencies and essentially only over high frequencies, respectively, significant gain increase in the open-loop can be given in desired frequency interval as the measurement filter can decrease the gain sufficiently at high frequencies. This benefits the PID structure, which can have phase advance and gain increase over a wider frequency interval than the PPI structure, and has therefore significantly better performance for these processes. Both control structures have the constraints on $\|S_\Delta\|_\infty$ and $\|CFS\|_2$ active. However, the PID controller has higher gain than the PPI controller at low frequencies, and the PPI controller has higher gain than the PID controller at high frequencies.

In comparison with P_2 and P_3 with $T \geq 10$, the other non-integrating processes with $0 < \tau < 0.5$, except for P_1, have essentially smaller time constants. Thus, the phase advance should be at higher frequencies. Here, the phase advance and gain of the derivative part may not be used over a significantly wider frequency interval than the interval with phase advance and gain given by the PPI predictor, resulting in similar performances of the two controller structures. In general, both structures have the constraint on $\|S_\Delta\|_\infty$ active for the considered processes. The PID structure has always $\|CFS\|_2$ on the constraint, but never $\|\Delta_z CFS\|_2$. The PPI structure has in general a smaller T_f than the PID structure, resulting in a higher high-frequency gain and either $\|CFS\|_2$ or $\|\Delta_z CFS\|_2$ active. This will be seen in Example II below, where P_9 with $T = 0.3$ is considered.

The open-loop transfer function for the integrating processes P_6 has an initial phase of $-\pi$ rad/s , requiring phase advance to rotate the Nyquist curve away from the robustness constraints. This can be made over a wider frequency interval by the PID structure than by the PPI structure, resulting in a significantly better performance for the PID structure. Both control structures have $\|S_\Delta\|_\infty = \|T_\Delta\|_\infty = 1.4$, while the PID structure

has $\|CFS\|_2$ active for all values of L and the PPI structure has $\|\Delta_z CFS\|_2$ active only for $L < 0.3$. Thus, the PPI structure cannot give enough phase advance for $L \geq 0.3$ over a wide frequency interval such that the gain can be increased and yield the control signal constraints active.

8. Design Examples

Table 1 shows the resulting IAE, parameter and constraint function values for Example I and II below. Nyquist diagrams, Bode diagrams of the feedbacks and load disturbance step responses are shown in figures 5–7 for Example I and in figures 8–10 for Example II. In the load disturbance response simulations, the measurement signal is in the second half corrupted with zero mean white noise with a standard deviation of 0.025.

8.1 Example I: $P_1,\ T = 0.3$

The optimal PPI controller with measurement filter for P_1 with $T = 0.3$ was not able to give sufficient gain for the noise sensitivity constraints to be active, yielding the filter time constant to be at its lower bound. The presented result for the PPI controller is therefore from an optimization without measurement filter. To yield phase advance, the PPI controller

Table 1. IAE, feedback parameter and constraint function values in Example I and II.

Process	Controller	IAE	K	T_i	T_d	L	T_f
$P_1,\ T = 0.3$	PPI	2.17	0.60	0.17	-	1.1	-
	PID	2.10	0.29	0.61	0.30	-	0.034
$P_9,\ T = 0.3$	PPI	0.825	2.0	0.46	-	0.98	0.042
	PID	0.892	1.1	0.77	0.32	-	0.096

Process	Controller	$\|S_\Delta\|_\infty$	$\|T_\Delta\|_\infty$	$\|CFS\|_2$	$\|\Delta_z CFS\|_2$
$P_1,\ T = 0.3$	PPI	1.40	1.00	0.61	0.84
	PID	1.40	1.00	1.0	0.89
$P_9,\ T = 0.3$	PPI	1.40	1.08	1.0	0.84
	PID	1.40	1.13	1.0	0.52

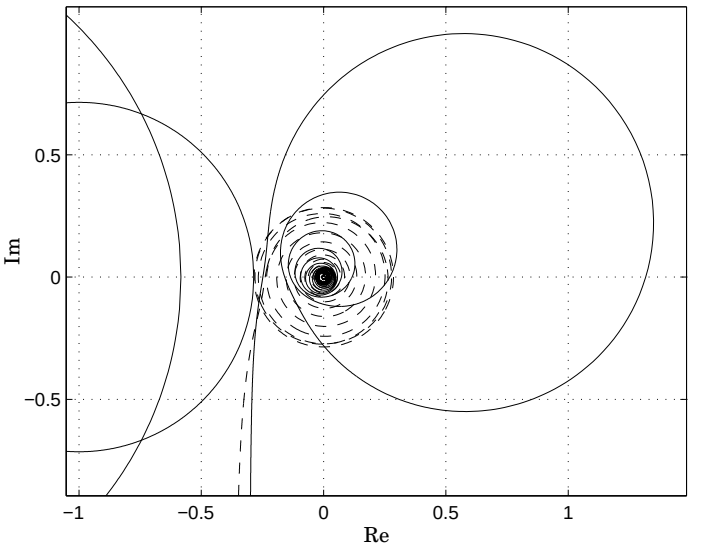

Figure 5. Nyquist curves in Example I with PPI (–) and PID (--). Circles correspond to $\|S\|_\infty = \|T\|_\infty = 1.4$.

makes gain peaks, resulting in loops in the Nyquist diagram. Prior the phase cross-over frequency, $\Delta L = \Delta\overline{L}$ yields $\|S_\Delta\|_\infty = M_S$, while the two first gain peaks yield $\|S_\Delta\|_\infty = M_S$ for $\Delta L = \Delta\underline{L}$. Hence, the robustness constraint limits the loop gain to be even larger, and hence also the phase advance of the predictor. After the two first peaks, the open loop tends to 0 as the gain of the predictor tends to 1. The PPI controller is not able to increase its gain at higher frequencies, and the noise sensitivity constraints are not active. The optimal controller parameters are not equal to model-matched design.

The PID controller follows the initial phase advance of the PPI controller, but the gain does not have, nor is able to have, a distinct peak at mid frequencies. Prior the phase cross-over frequency, $\Delta L = \Delta\overline{L}$ yields $\|S_\Delta\|_\infty = M_S$. After the phase cross-over frequency, the PID controller can increase its gain, yielding phase advance over a wide frequency interval. As the process gain decreases with frequency, the PID gain increases, making the Nyquist curve to be almost circular and $\|S_\Delta\|_\infty = M_S$ at the negative real axis. At higher frequencies, the measurement filter yields roll-off such that the noise sensitivity constraints are met. The control signal from the PID controller, compared to the PPI controller, reacts faster when the load disturbance is seen in the measurement signal and is also more sensitive to measurement noise.

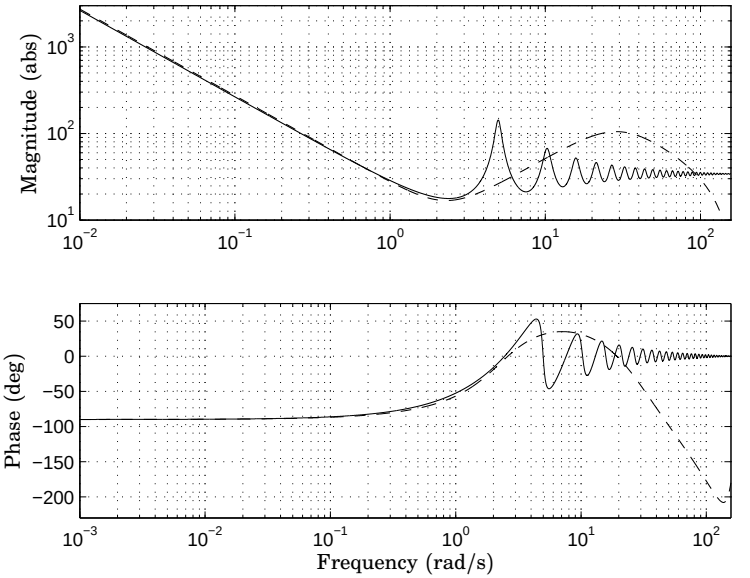

Figure 6. Bode diagram of feedbacks in Example I with PPI (–) and PID (--).

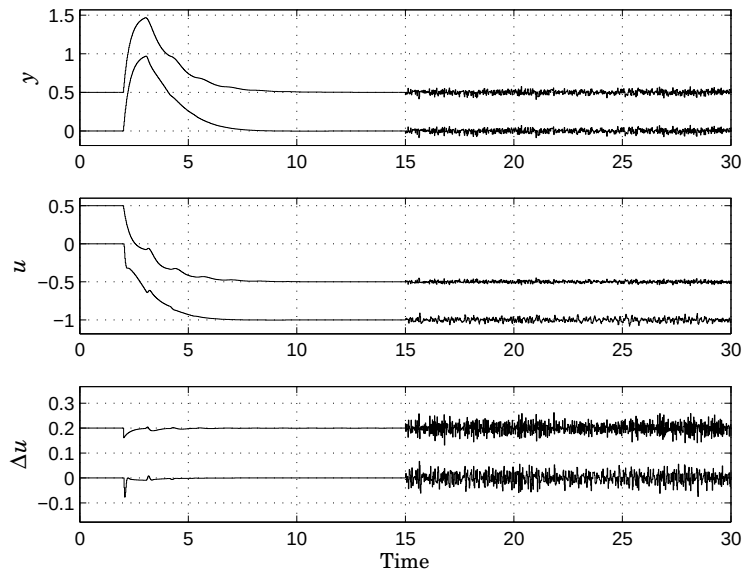

Figure 7. Load disturbance responses in Example I with PPI (upper curves) and PID (lower curves). *Top*: Measurement signal. *Middle*: Control signal. *Bottom*: Inter-sample difference of control signal. Biases of 0.5 and 0.2 are added for separation.

The maximum phase advance and associated gain are higher for the PPI structure than for the PID structure. However, for this example, phase advance and gain increase over a wider frequency interval are better than over a narrow interval. This results in a 5% lower IAE for the PID structure compared to the PPI structure.

8.2 Example II: $P_9,\ T = 0.3$

The optimal PPI controller with measurement filter for the process P_9 with $T = 0.3$, have the robustness constraint $\|S_\Delta\|_\infty \leq M_S$ active prior the phase cross-over frequency when $\Delta L = \Delta\overline{L}$. Phase advance is given by the predictor, but is limited together with the gain as $\|S_\Delta\|_\infty = M_S$ at the negative real axis in the Nyquist diagram. The highest gain of the predictor is at the first peak. Since the process is of third order and the measurement filter time constant yields roll-off such that the noise sensitivity constraints are fulfilled, the Nyquist curve tends to 0 rapidly after the first predictor peak. The process may be approximated by a first order system with dead-time with static gain, time constant and dead-time approximately equal to 1, 1 and 0.35, respectively. From the controller parameters, it is seen that the design of the optimal PPI controller does not resemble model-matched design.

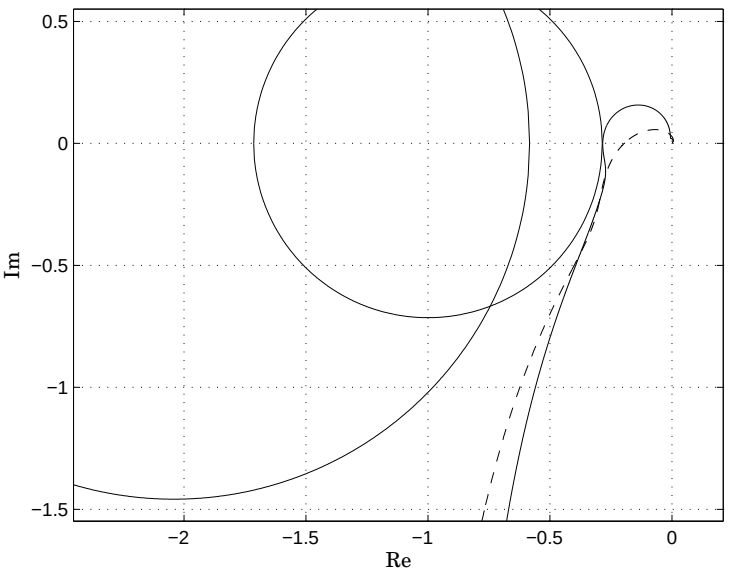

Figure 8. Nyquist curves in Example II with PPI (–) and PID (--). Circles correspond to $\|S\|_\infty = \|T\|_\infty = 1.4$.

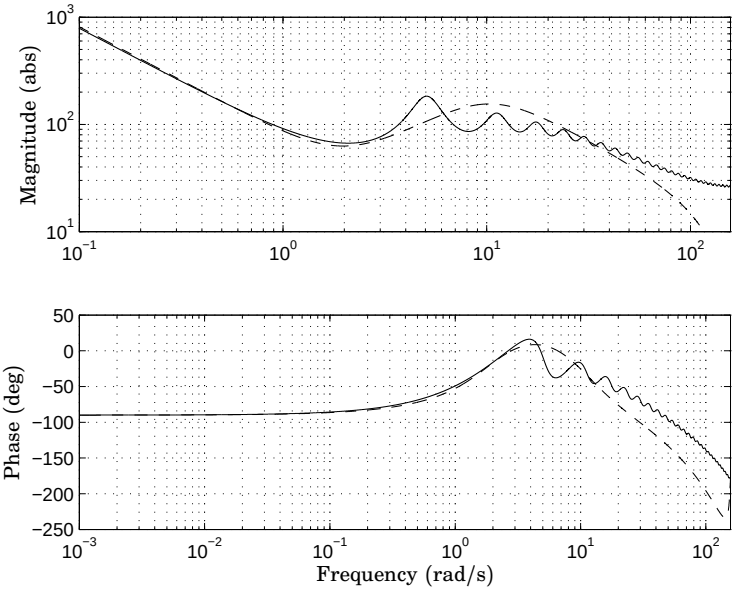

Figure 9. Bode diagram of feedbacks in Example II with PPI (–) and PID (--).

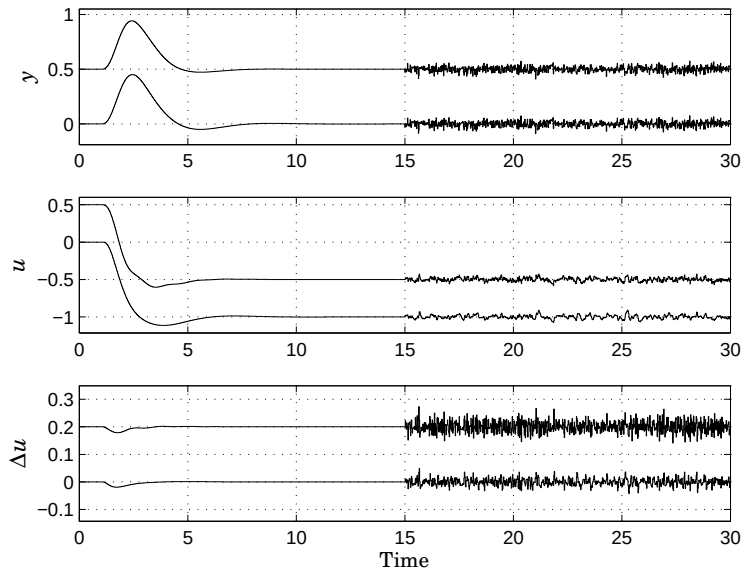

Figure 10. Load disturbance responses in Example II with PPI (upper curves) and PID (lower curves). *Top*: Measurement signal. *Middle*: Control signal. *Bottom*: Inter-sample difference of control signal. Biases of 0.5 and 0.2 are added for separation.

The PID controller follows the phase advance of the PPI controller and has $\|S_\Delta\|_\infty = M_S$ for $\Delta L = \Delta\overline{L}$ prior the phase cross-over frequency. Compared to Example I, the PID controller may not increase its gain and phase over such a wide frequency interval above the phase cross-over frequency due to the noise sensitivity constraints. The differences in increased gain and phase given by the two prediction methods are not as large as in Example I.

The optimal PPI structure yields a slightly higher gain cross-over frequency compared to the PID structure. It also has significantly higher gain at high frequencies. This yields the inter-sample sensitivity of the control signal due to noise to be larger, as seen in the load disturbance responses, but gives also a more rapid response to load disturbances. The PPI structure gives approximately 7.5% lower IAE than the PID structure. Hence, in this example, it is advantageous to use a feedback structure that may yield significant gain and phase advance peaks over a narrow frequency interval.

9. Summary

This paper presented a comparison between PID and PPI controllers with associated measurement filters, considering load disturbance rejection, robustness towards process uncertainties and noise sensitivity of the control signal. For the optimization parameters chosen and the majority of the processes in the batch, the performances of the two different structures, and hence the different prediction methods, are similar. However, for some processes with comparatively large time constants, the derivative part is allowed by the noise sensitivity constraints to yield phase advance and increased gain over a frequency interval wider than what is possible by the PPI predictor. This yields better performance by the PID structure than by the PPI structure.

References

Åström, K. and T. Hägglund (2006): *Advanced PID Control*. ISA - The Instrumentation, Systems, and Automation Society, Research Triangle Park, NC 27709.

Garpinger, O. (2009): "Design of Robust PID Controllers with Constrained Control Signal Activity." Licentiate Thesis. Department of Automatic Control, Lund University, Sweden.

Hägglund, T. (1996): "An industrial dead-time compensating PI controller." *Control Engineering Practice*, **4**, pp. 749–756.

Ingimundarson, A. and T. Hägglund (2002): "Performance comparison between PID and dead-time compensating controllers." *Journal of Process Control*, **12**, pp. 887–895.

Isaksson, A. and S. Graebe (2002): "Derivative filter is an integral part of PID design." *Control Theory and Applications, IEE Proceedings*, **149:1**, pp. 41–45.

Kristiansson, B. and B. Lennartson (2001): "Robust PI and PID controllers including Smith predictor structure." In *Proceedings of the 2001 American Control Conference*, vol. 3, pp. 2197–2202.

Kristiansson, B. and B. Lennartson (2006): "Robust tuning of PI and PID controllers: Using derivative action despite sensor noise." *IEEE Control Systems Magazine*, **26:1**, pp. 55–69.

Larsson, P. and T. Hägglund (2009): "Robustness Margins Separating Process Dynamics Uncertainties." In *Proceedings of the 2009 European Control Conference*.

Larsson, P. and T. Hägglund (2011): "Control Signal Constraints and Filter Order Selection for PI and PID Controllers." In *Proceedings of the 2011 American Control Conference*.

Normey-Rico, J., C. Bordons, and E. Camacho (1997): "Improving the robustness of dead-time compensating PI controllers." *Control Engineering Practice*, **5:6**, pp. 801–810.

Palmor, Z. (1980): "Stability properties of Smith dead-time compensator controllers." *International Journal of Control*, **32:6**, pp. 937–949.

Shinskey, F. (1994): *Feedback Controllers for the Process Industries*. McGraw-Hill.

Shinskey, F. (2001): "PID-deadtime control of distributed processes." *Control Engineering Practice*, **9:11**, pp. 1177–1183.

Smith, O. (1957): "Closed Control of Loops with Dead Time." *Chemical Engineering Progress*, **53**, May, pp. 217–219.

Appendix A. Robustness Calculation

The robustness calculation method presented in [Larsson and Hägglund, 2009] is based on the open loop transfer function $C(s)F(s)G(s)$, where $C(s)$ is the controller, $F(s)$ is the measurement filter and $G(s) = G_0(s)e^{-sL}$ is the nominal process. The method considers a rotation of the Nyquist curve such that a point on the curve with amplitude close to 1 is rotated a certain angle. From the rotation, the corresponding change ΔL in dead-time can be calculated. When $G(s)$ is discretized using zero-order hold (ZOH), then

$$G_0(s)e^{-sL} \xrightarrow{\text{ZOH}} P_0(z)z^{-n},$$

where $n = \lceil L/h \rceil$, h is the sampling period, and $\lceil \cdot \rceil$ is the ceiling function. Adding ΔL to the time delay does not change $G_0(s)$, however, it may change $P_0(z)$ as

$$G_0(s)e^{-s(L+\Delta L)} \xrightarrow{\text{ZOH}} \tilde{P}_0(z)z^{-m},$$

where $m = \lceil (L + \Delta L)/h \rceil$. For the case $\Delta L = kh$, i.e., ΔL is an integer number of sample intervals, $\tilde{P}_o(z) = P_o(z)$ and $m = n + k$. However, for the case $\Delta L \neq kh$, $\tilde{P}_o(z)$ and $P_o(z)$ have minor differences in both phase and amplitude affecting the Nyquist curve. The differences are mainly at high frequencies close to the Nyquist frequency and if an appropriate sampling period is selected, the differences are negligible in the frequency interval wherein ΔL is computed. Hence, the method to calculate ΔL in [Larsson and Hägglund, 2009] may be used, yielding negligible errors. This is confirmed when analyzing the designed controllers and filters for the considered process batch.

Paper IV

Modeling and Optimization of a Grade Change for Multistage Polyethylene Reactors

Per-Ola Larsson, Johan Åkesson, Staffan Haugwitz and Niklas Andersson

Abstract

Grade changes in polyethylene reactors, i.e., changes of operating conditions, are performed on a regular basis to adapt to market demands. In this paper, a dynamic optimization procedure is presented built upon the Modelica language extended with Optimica constructs for formulation of optimization problems. A Modelica library for the Borstar® multistage polyethylene reactors at Borealis AB, consisting of two slurry and one gas phase reactor, has been constructed. Using JModelica.org, a framework to translate dynamic optimization problems to NLP problems, optimal grade transitions between grades currently used at Borealis AB, can be calculated. Optimal inflows and grade key variables are shown.

Errata and Clarifying Notes

Page	Text line	Correction
150	20	"$\mathbf{x}_B$" should read "$\mathbf{y}_B$"
151	10	"$\mathbf{y}$" should read "$\mathbf{w}$"

- Correction of the discussion in Section 3 regarding outtake of polymer slurry from the pre-polymerization reactor: The polymer slurry is transferred by transfer legs, yielding the outflow and reactor contents to have equal concentrations. This is modeled as in Paper VI.
- Clarification of the grade definition in Section 5.1 and the DAE initialization problem in Section 5.2: The polymer grade is defined by bed average concentrations and concentration ratios $\overline{X}_{e1}$, $\overline{X}_{he1}$, $\overline{X}_{e2}$, $\overline{X}_{he2}$, $\overline{X}_{p3}$, $\overline{X}_{e3}$, $\overline{X}_{he3}$ and $\overline{X}_{be3}$, polymer production rates Q_1 and Q_2, split factor S, and pressure P_3 in the gas-phase reactor. These variables are contained in the output $\mathbf{y}$ of the model and their specifications for a grade are set in $\mathbf{y}_{\text{spec.}}$. Table 2 in the paper should be as Table 2 below.

  Specifying $\overline{X}_{e1}$ and $\overline{X}_{he1}$ implicitly specifies $\overline{X}_{h1}$ and thus also $\overline{X}_{p1}$ as the sum of the molar concentrations is normalized to 1, see Paper VI.

Table 2. Normalized grade definitions.

Grade	A	B	Grade	A	B
$\overline{X}_{e1}$	1	1.000	$\overline{X}_{p3}$	1	1.009
$\overline{X}_{he1}$	1	0.37	$\overline{X}_{e3}$	1	0.8828
Q_1	1	1.064	$\overline{X}_{he3}$	1	1.846
$\overline{X}_{e2}$	1	1.160	$\overline{X}_{be3}$	1	1.279
$\overline{X}_{he2}$	1	2.371	S	1	0.9167
Q_2	1	1.134	P_3	1	1.000

- The following constraints should be added to the dynamic optimization problem in Eq. (12):

$$\mathbf{u} = \int_{t_1}^{t} \dot{\mathbf{u}}\, d\tau, \quad \mathbf{x}(t_1) = \mathbf{x}_A, \quad \mathbf{u}(t_1) = \mathbf{u}_A.$$

1. Introduction

Polyethylene reactors are able to produce different grades by manipulating inflows of raw material. It is imperative for polyethylene manufacturers to change product grades to increase profitability as market demands change, but also due to market competition and raw material pricing. The result is product campaigns, varying in length between a few days up to weeks. During grade transitions it is therefore of importance that production of off-specification material, i.e., material that does not fulfill specification of any grade, is minimized. On the other hand, there is also a cost in raw material and time that has to be taken into account when performing a grade change, see e.g., [van Brempt *et al.*, 2004].

The grade transition problem has been the subject of several papers. For gas phase reactors, [McAuley and MacGregor, 1992] uses the control variable parametrization method (CVP) with control profiles approximated by series of ramps, while in [Gisnas *et al.*, 2003] optimization results in bang-bang type solutions. A series of two slurry reactors has been considered by [Takeda and Ray, 1999], also using the method of CVP, and in [Prata *et al.*, 2008] a grade change for a series of a slurry and a gas phase reactor was performed with a discretization scheme based on direct single and multiple shooting.

This paper presents an optimization procedure for a grade change of a Borstar® polyethylene plant including three polyethylene reactors in series, two slurry and one gas phase reactor, and is an extension of [Larsson *et al.*, 2010] where one reactor was considered. The developed plant model is encoded in the Modelica language and a simultaneous optimization method based on collocation is applied using the optimization extension Optimica and the framework of JModelica.org.

2. Borstar® Polyethylene Plant

The Borstar® polyethylene plant incorporates in total three polyethylene reactors, two slurry and one gas phase reactor (GPR), see Figure 1. It is a bimodal plant and can thus produce polymer with a two-peaked molecular weight distribution. The pre-polymerization slurry reactors main function is to induce the polymerization in a pre-specified composition and has a negligable production compared to the two other reactors. It has catalyst, monomer ethylene and the chain transfer agent hydrogen along with the diluent propane as inflows. Using the second reactor, i.e., the loop slurry reactor, polymer with low molecular weight is shaped. The loop reactor has the same material inflow as the pre-polymerization reactor except that no catalyst is added. Temperature and pressure is high resulting in

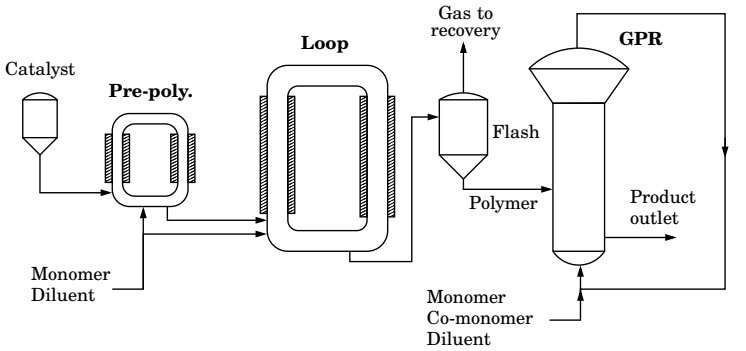

Figure 1. Reactor chain of a Borstar® process: pre-polymerization, loop, and gas phase reactor.

a super-critical state of the polyethylene slurry. The slurry stream from loop reactor is fed to a flash tank where gases are separated from polymer, which are transported to recovery area and the GPR, respectively. To the subsequent fluidized bed GPR, apart from the same type of raw material added to the loop reactor, also the co-monomer butene is added together with nitrogen. This gives the high molecular weight polymer resulting in the bimodal polymer product.

3. Plant Model

Several assumptions are made when modeling, keeping model complexity resonable and usable for grade change optimization. The two loop reactors are assumed to have perfect temperature and pressure control, while control systems for reactor content volumes are in regulatory mode and incorporated in the model. Both loop reactors have high volumetric circulation rates compared to outflow rates. This results in recycle ratios well above 30, yielding no considerable gradients of molecular species nor temperatures exists along the reactors, see [Zacca and Ray, 1993]. The latter is also supported with measurements along the reactor. Thus, the loop reactors can be considered well-mixed. The outtakes of polymer from the loop reactors are settling legs, making the outflow have higher concentration of polymer than the reactor contents, see [Reginato *et al.*, 2003]. Hence, the approach of non-ideal CSTR for the loop reactors is suitable, see [Reginato *et al.*, 2003] and [Touloupides *et al.*, 2010], where the settling legs are modelled using discharge factors.

The temperature in the GPR is assumed to be controlled to a constant value and the regulatory system for bed level is incorporated in the model, using the outflow as control variable. The content in the GPR is assumed

Table 1. Components summary and abbrev.

Component	i	Component	i
Catalyst	c	Propane	p
Ethylene	e	Nitrogen	n
Hydrogen	h	Polyethylene	pe
Butene	b	Incorp. butene	pb

well mixed and conversion per pass through is low, making the gas composition approximately uniform in the bed, see e.g., [Xie *et al.*, 1994] and [McAuley and MacGregor, 1992].

The model, derived by Borealis AB and used today in a non-linear model predictive controller of the plant, includes both first principles, semi-empirical, and empirical relations. The main inflows are, as described in Section 2, the raw materials, diluents and catalyst which gives a total of 12 control inputs available for optimization at a grade change. If the reactors are numbered from left to right with index j, i.e., $j \in \{1, 2, 3\}$, then for every component i in Table 1 that is a fluid, gas or catalyst, the mass balance read

$$\dot{m}_{ij} = q_{i,j-1} + u_{ij} - q_{ij} - r_{ij}, \tag{1}$$

where q_{ij} and r_{ij} is the outflow and reaction rate of component i, respectively, in reactor j and u_{ij} is the controlled inflow of component i. Note that q_{ij}, r_{ij} or u_{ij} might be zero depending on which reactor or component that is considered.

For the polymer, i.e., polyethylene and incorporated butene, it is important to indicate in what reactor it has been formed due to the process bi-modality, and therefore an extra index, $k \in \{1, 2, 3\}$, is supplied. For a solid component in a reactor it is formed in, i.e., $j = k$, the mass balance is

$$\dot{m}_{ijk} = h_{ij} - q_{ijk}, \tag{2}$$

where h_{ij} is the production rate of the polymer component i in reactor j and is a function of the reaction rates of the raw materials in Eq. (1). For a polymer component in a reactor it has not been formed in, i.e., $j \neq k$, it reads

$$\dot{m}_{ijk} = q_{i,j-1,k} - q_{ijk}, \tag{3}$$

which is a pure transportation of the component through the reactor. For every fluid or gas component, the instantaneous molar concentration X_{ij}

may be calculated. Molar concentrations and all component masses for reactor j are collected in vectors $\mathbf{X}_j$ and $\mathbf{m}_j$.

The reaction rates used above are calculated using extended Arrhenius expressions of the form

$$r_{ij} = R_{ij}(\mathbf{c}_j, P_j, \mathbf{m}_j, \mathbf{X}_j) \exp\left(\frac{k_{ij1}}{T_j} + k_{ij2}\right), \tag{4}$$

where R_{ij} is a non-linear function of the catalyst properties $\mathbf{c}_j$, reactor pressure P_j and the component masses and concentrations. The reaction rate is inversely proportional to the temperature T_j in the exponent with two empirical constant k_{ij1} and k_{ij2} for each component i and reactor j. Analogously, reaction rates are collected in the vector $\mathbf{r}_j$.

The states of the Ziegler-Natta catalyst in reactor j, such as mean activity and deactivated sites, have the non-linear dynamics of a function C_j,

$$\dot{\mathbf{c}}_j = C_j(\mathbf{c}_j, \mathbf{r}_j, \mathbf{m}_j, q_{c,j-1}, u_{c1}), \tag{5}$$

where the two last variables are the inflow of catalyst from previous reactor and controlled input of catalyst to pre-polymerization reactor, respectively.

By using reactor geometry, knowledge of the reactor content properties and empirical relations for a super-critical state, the densities for fluids and solids in each reactor may be calculated. In general, densities have dependencies as

$$\boldsymbol{\rho}_j = \varrho_j(\mathbf{X}_j, P_j, T_j), \tag{6}$$

with the non-linear function ϱ_j, where $\boldsymbol{\rho}_j$ is a vector containing densities for fluids and solids in reactor j.

Pressure in the GPR is given by reactor content properties and temperature through the non-linear function P_3

$$P_3 = \mathrm{P}_3(\mathbf{X}_3, \mathbf{m}_3, \boldsymbol{\rho}_3, T_3). \tag{7}$$

The resulting polymer properties depends on the ratios between monomer, co-monomer and hydrogen, see e.g. [McAuley and MacGregor, 1991], and the model therefore also includes the following ratios,

$$\begin{aligned} X_{he1} &= X_{h1}/X_{e1}, \qquad X_{he2} = X_{h2}/X_{e2} \\ X_{he3} &= X_{h3}/X_{e3}, \qquad X_{be3} = X_{b3}/X_{e3}. \end{aligned} \tag{8}$$

Note that there is no butene-ethylene ratio in the pre-polymerization and loop reactors since co-monomer is only added in the GPR.

Due to the residence time in each reactor, also the bed average of the concentrations and concentration ratios defined above, emphasized with a bar, e.g., $\overline{X}_{ij}$, are considered. These indicate during what conditions, in average, the polymer has been formed and are calculated by filtering the instantaneous values using the ratio between mass of solids and outflow of solids for considered reactor as time constant.

The bi-modality of the polyethylene molecular weight distribution is formed by producing polymers with different molecular weight in loop reactor and GPR. A measure of the bi-modality is the split factor, calculated using masses of polyethylene produced in the different reactors as

$$S = \frac{m_{pb33} + m_{pe33}}{m_{pb33} + m_{pe33} + m_{pe32} + m_{pe31}}, \tag{9}$$

i.e., as the ratio of polymer mass in the GPR formed in the GPR to the total mass of polymer in the GPR.

For economical reasons, the production rate of solids in each reactor is considered when optimizing a transition, which is defined as the sum of production rate of polyethylene and incorporated butene in each reactor, i.e.,

$$Q_j = h_{pe,j} + h_{pb,j}. \tag{10}$$

The model contains, apart from Eqs. (1)–(10) also additional algebraic equations. If the inputs and outputs of the model are denoted $\mathbf{u}$ and $\mathbf{y}$, respectively, and the states and algebraic variables are denoted $\mathbf{x}$ and $\mathbf{w}$, the model can be written in the general non-linear index 1 differential algebraic equation (DAE) form

$$\begin{aligned} \mathbf{0} &= \mathbf{F}(\dot{\mathbf{x}}, \mathbf{x}, \mathbf{w}, \mathbf{u}) \\ \mathbf{y} &= \mathbf{g}(\mathbf{x}, \mathbf{w}, \mathbf{u}). \end{aligned} \tag{11}$$

The model has n_y outputs, used for defining a grade with correct production rate, and $n_u = 12$ inputs and $n_x = 55$ states, $n_w = 180$ algebraic variables and 225 equations, disregarding $\mathbf{g}(\cdot)$, and has been subjected for calibration using plant measurement data in [Andersson *et al.*, 2011].

4. Modeling and Optimization Environment

Modelica, a high level language for encoding of complex physical systems aimed at simulation and supporting object oriented concept is used for plant modeling. Main features of the language are that text-book style declarative differential and algebraic equations may be used and mixed,

but it lacks language constructs for formulating dynamic optimization problems. Notations such as cost functions, constraints and mechanism to select input and parameters to optimize has been proposed in the Optimica extension, see [Åkesson, 2008], enabling the user to construct such problems based on Modelica models.

Numerical solver interfaces are typically written in C or FORTRAN and the translation of Modelica models and optimization problems are performed in the framework JModelica.org, an open source project targeted at dynamic optimization, see [Åkesson *et al.*, 2010]. It features compilers supporting code generation of Modelica/Optimica models to C, a C API for evaluating model equations and their derivatives, optimization algorithms and supports the Optimica extension.

The JModelica.org platform contains an implementation of a simultaneous optimization method based on collocation on finite elements, [Biegler *et al.*, 2002]. In this method, states, inputs and algebraic variables, are parametrized by Lagrange polynomials based on Radau points of order three, two and two, respectively. This corresponds to a fully implicit Runge-Kutta method, and possesses well known and strong stability properties. The dynamic optimization problem is thus translated into a nonlinear program (NLP), which may be very large. To efficiently solve the NLP, derivative information together with sparsity patterns of the constraint Jacobians need to be provided to the numerical solver. In JModelica.org, the simultaneous optimization algorithm is interfaced with the large-scale NLP solver IPOPT, see [Wächter and Biegler, 2006], particularly developed to solve NLP problems arising in simultaneous dynamic optimization. Simultaneous methods handle non-linear systems well, and also, constraints on state, input and algebraic variables are easily incorporated, and is thus well suited for the optimization of a grade transition treated in this paper.

Using the Modelica language, a library of necessary entities was constructed, see [Larsson *et al.*, 2010]. The library contains models both for simulation, experiments as well as optimization models with Optimica constructs.

5. Optimal Grade Transition

5.1 Grade Definition

Many measures may to be used when defining a grade, such as densities, molecular weight, molecular distribution, melt flow indices and raw material concentrations, which are controlled by polymerization conditions. Commercial practice is to give grade specifications by melt index and

density due to convenience in industrial settings, see [Xie *et al.*, 1994]. Melt flow indices are measures of the molecular weight distribution and may be used to calculate the flow ratio, yeilding a polydispersity measure. However, as indicated in [Xie *et al.*, 1994], these measures only give relative properties and not detailed information about polymer structure, which if desired, requires detailed models not suitable for over all plant optimization as considered in this paper.

In [McAuley and MacGregor, 1991], relations between melt index, density and reactor concentration ratios, both monomer and co-monomer, was presented based on reaction kinetics. Only a limited number of products is produced, and thus only a few steady state operation points exists where melt index may give measurement data. Thus, using this operation data, which is taken with a two hour interval, will give models with large uncertaintes. Therefore, the concentration ratios, verified with process data, will be used when defining a grade. The concentration ratio data are calculated from chromatography measurements, i.e., component concentration measurements, with a sampling interval of 1 minute.

Except from the concentrations above also the split factor is used when defining a grade. Additionally, also the GPR pressure and the production rates are considered, although not effecting polymer properties directly. Table 2 lists variable values from a grade transition performed at Borealis AB, normalized by grade A. The reactant concentrations are specified from polymer properties while inert gases are given specifications from e.g., desired partial pressures, heat removal from exothermic reaction and other operating conditions. Note that e.g., specifying X_{e1} and X_{he1} implicitly also specifies X_{h1}, and thus also the remaining gas, i.e., X_{p1}, since reactor content volume is constant at stationarity. Similar argument holds for X_{p2} and X_{n3}. The split factor is set to give correct bi-modality of the polymer. This, together with specifications of Q_1 and Q_2 implicitly defines production rate in GPR, and thus also total production rate. GPR pressure is set to nominal reactor value.

5.2 DAE Initialization

A grade transition changes production from one steady state to another, both representing on-specification production. The DAE initialization and stationarity problem for a specific grade requires the output $\mathbf{y}$, containing all variables defining a grade from the previous section, and derivatives $\dot{\mathbf{x}}$ to be specified. The variables to solve for are $\mathbf{x}$, $\mathbf{u}$, and $\mathbf{w}$. Here, $\mathbf{u}$ is now an algebraic variable instead of input and its size determines how many grade specifications may be used, i.e., size of $\mathbf{y}$, if the non-linear equation system should have zero degrees of freedom. For full flexibility, as used here, all variables in $\mathbf{u}$ will be free. If constructing the extended algebraic

Table 2. Normalized grade definitions.

Grade	A	B	Grade	A	B
X_{e1}	1	1.000	X_{p3}	1	1.009
X_{he1}	1	0.37	X_{e3}	1	0.8828
Q_1	1	1.064	X_{he3}	1	1.846
X_{e2}	1	1.160	X_{be3}	1	1.279
X_{he2}	1	2.371	S	1	0.9167
Q_2	1	1.134	P_3	1	1.000

variable vector $\mathbf{z} = [\,\mathbf{w},\quad \mathbf{u}\,]$, the problem may be formulated as

$$\begin{aligned} 0 &= \tilde{\mathbf{F}}(\dot{\mathbf{x}}, \mathbf{x}, \mathbf{z}) \\ 0 &= \dot{\mathbf{x}} \\ 0 &= \tilde{\mathbf{g}}(\mathbf{x}, \mathbf{z}) - \mathbf{y}_{\text{spec.}}, \end{aligned}$$

where $\tilde{\mathbf{F}}$ and $\tilde{\mathbf{g}}$ corresponds to $\mathbf{F}$ and $\mathbf{g}$ without input $\mathbf{u}$, and $\mathbf{y}_{\text{spec.}}$ contains the grade definitions in Table 2. The first equation has, as the DAE in Eq. (11), $n_x + n_w$ equations, and the second and third has n_x and n_u, respectively, and thus, there is equally many equations as variables to solve for, yielding zero degrees of freedom.

The problem is encoded with JModelica.org using the Modelica models. Initial guesses may be set for all variables to solve for and upper and lower limits helps the solver. The solution time for each grade is less than 10 seconds.

For the two grades, inputs $\mathbf{u}_\text{A}$ and $\mathbf{u}_\text{B}$ can be defined, giving stationary production. Analogously, define the outputs $\mathbf{y_A}$ and $\mathbf{y}_\text{B}$, state vectors $\mathbf{x}_\text{A}$ and $\mathbf{x}_\text{B}$, and algebraic vectors $\mathbf{w}_\text{A}$ and $\mathbf{w}_\text{B}$.

5.3 Dynamic Optimization of Grade Transition

The dynamic optimization problem solves for optimal trajectories between the two grades A and B, satisfying dynamics and constraints on states, algebraic variables, inflows and outputs.

Initial conditions of the plant is the solution from DAE initialization for grade A, i.e., $\mathbf{x}_\text{A}$, $\mathbf{w}_\text{A}$, and $\mathbf{u}_\text{A}$, and a quadratic cost function that includes deviations from grade B specifications in form of $\mathbf{x}_\text{B}$, $\mathbf{w}_\text{B}$ and $\mathbf{u}_\text{B}$ is used. Introducing the deviation vectors

$$\Delta\mathbf{y} = \mathbf{y} - \mathbf{y}_\text{B}, \quad \Delta\mathbf{u} = \mathbf{u} - \mathbf{u}_\text{B}, \quad \Delta\mathbf{w} = \mathbf{w} - \mathbf{w}_\text{B},$$

the dynamic grade transition optimization problem can be formulated as

$$\min_{\dot{\mathbf{u}}} \int_{t_1}^{t_2} \begin{bmatrix} \Delta\mathbf{y} \\ \Delta\mathbf{u} \\ \Delta\mathbf{w} \\ \dot{\mathbf{u}} \end{bmatrix}^T \begin{bmatrix} \mathbf{Q}_{\Delta\mathbf{y}} & 0 & 0 & 0 \\ 0 & \mathbf{Q}_{\Delta\mathbf{u}} & 0 & 0 \\ 0 & 0 & \mathbf{Q}_{\Delta\mathbf{w}} & 0 \\ 0 & 0 & 0 & \mathbf{Q}_{\dot{\mathbf{u}}} \end{bmatrix} \begin{bmatrix} \Delta\mathbf{y} \\ \Delta\mathbf{u} \\ \Delta\mathbf{w} \\ \dot{\mathbf{u}} \end{bmatrix} dt \tag{12}$$

$$\begin{aligned} \text{subj. to } & \mathbf{0} = \mathbf{F}(\dot{\mathbf{x}}, \mathbf{x}, \mathbf{w}, \mathbf{u}), \quad \mathbf{y} = \mathbf{g}(\mathbf{x}, \mathbf{w}, \mathbf{u}), \\ & \mathbf{y}_{\min} \leq \mathbf{y} \leq \mathbf{y}_{\max}, \quad \mathbf{u}_{\min} \leq \mathbf{u} \leq \mathbf{u}_{\max}, \\ & \mathbf{w}_{\min} \leq \mathbf{w} \leq \mathbf{w}_{\max}, \quad \dot{\mathbf{u}}_{\min} \leq \dot{\mathbf{u}} \leq \dot{\mathbf{u}}_{\max}, \\ & \mathbf{x}_{\min} \leq \mathbf{x} \leq \mathbf{x}_{\max}, \end{aligned}$$

The weight $\mathbf{Q}_{\Delta\mathbf{y}}$ may be used to emphasize importance of the different grade defining variables, while $\mathbf{Q}_{\Delta\mathbf{w}}$ and $\mathbf{Q}_{\Delta\mathbf{u}}$ is used to remove too large over- and undershoots of algebraic variables and inflows. The optimization variables are the inflow derivatives $\dot{\mathbf{u}}$, which gives possibility to directly include them in the cost function using $\mathbf{Q}_{\dot{\mathbf{u}}}$ to control inflow smoothness, and also in the constraints, without any additional filtering of the inflows $\mathbf{u}$. All weights are chosen diagonal for simplicity.

Over- and undershoots are accepted up to a certain limit for the instantaneous concentrations and ratios, i.e, X_{ij}, set as constraints on $\mathbf{y}$. However, for the bed average concentrations and ratios, i.e., $\overline{X}_{ij}$, and the split S, no over- or undershoots are accepted in the grade change. The constraints on the algebraic variables $\mathbf{w}$ and states $\mathbf{x}$ are for instance limits on volumes, pressures, reaction rates, component masses and catalyst properties, while constraints on inflows, both magnitudes and rates of changes, concern physical limits such as e.g., pump capacities.

5.4 Optimal Grade Transition Trajectories

For non-convex optimization it is advantageous to have good initial values. Since a simultaneous method is used, all variables at all discretization points are solved for at the same time, hence, initial trajectories should be supplied. Since the stationary points are known, i.e., solved for in DAE initialization problem, one can generate initial trajectories by ramping inflows from $\mathbf{u}_{\mathrm{A}}$ to $\mathbf{u}_{\mathrm{B}}$ and simulate the response. This can be performed in JModelica.org where simulation is available through SUNDIALS, see [Hindmarsh *et al.*, 2005].

The transition time is normalized to 1 time unit (t.u.) and the dynamic optimization problem have been solved several times for different element lengths approximately in the range 0.015-0.075 t.u. with 3 collocation points in each element. Resulting optimal inflows have been used

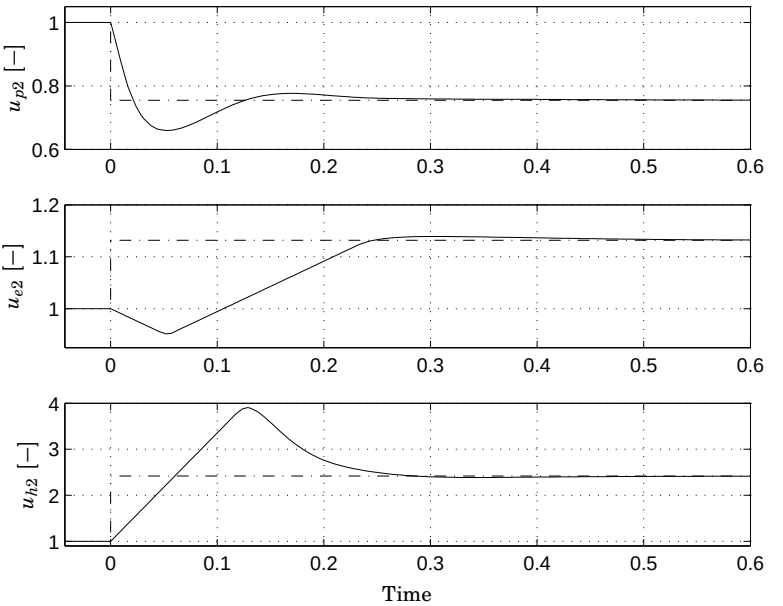

Figure 2. Optimal inflows to loop reactor (−) and values for grade A and B at stationarity (---).

as inputs in simulations, showing that the discretization is fine enough, i.e., the difference between simulated response and discretized response from optimization is negligable. After discretization, the NLP problem contains approximately 20.000-200.000 variables depending on number of elements. Using an Intel® Core™2 Duo CPU@3.00GHz, a solution is obtained in approximately 5-90 minutes depending on number of variables and initial values.

Figures 2-3 show the resulting optimal inflows to the loop reactor, key grade variables, and mass of polymer in loop reactor, respectively, while figures 4-6 shows the corresponding for GPR. Note the scaling, i.e., the transition is 1 time unit (t.u.) and all variables have initial value 1.

Since the production rate Q_2 is higher in grade B than in grade A, the inflow of ethylene is increased in total and at the same time inflow of the diluent propane is decreased, making room for more ethylene and hydrogen, as shown in Figure 2. This results in a larger mass of polymer in the loop, see Figure 3. Both X_{e2} and X_{h2} are higher in grade B than in grade A and to meet the hydrogen specification, the inflow of hydrogen is increased. To reach the specification of the hydrogen-ethylene ratio X_{he2} rapidly, the inflow of ethylene is initially decrased and hydrogen overshot. Note that both the inflow of ethylene and hydrogen have their deriva-

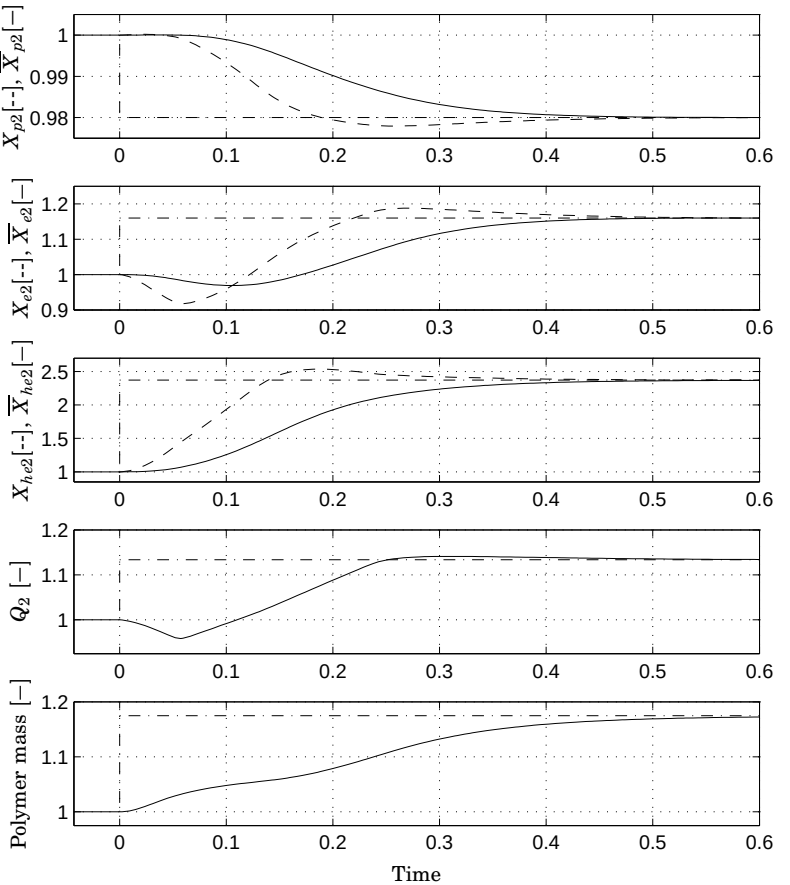

Figure 3. Instantanous (--) and bed average conc. and ratios, production rate and polymer mass (–) for loop and values for grade A and B at stationarity (---).

tive constraints active in the beginning, seen by the linear decrease and increase, performing the transition of X_{he2} as fast as possible.

From Figure 3 it is seen that the under- or overshoot constraints on the averaged concentrations and ratios are followed and the instantaneous measures have over- or undershoots. The transition in loop reactor is completed after 0.5 t.u.

The split S, see Figure 5, which indirectly depends on the production rates, is decreased by increasing the production rate Q_2 but also lowering production rate Q_3. This is performed by decreasing the ethylene inflow u_{e3}, see Figure 4, and thus also the ethylene concentration X_{e3}. The ethy-

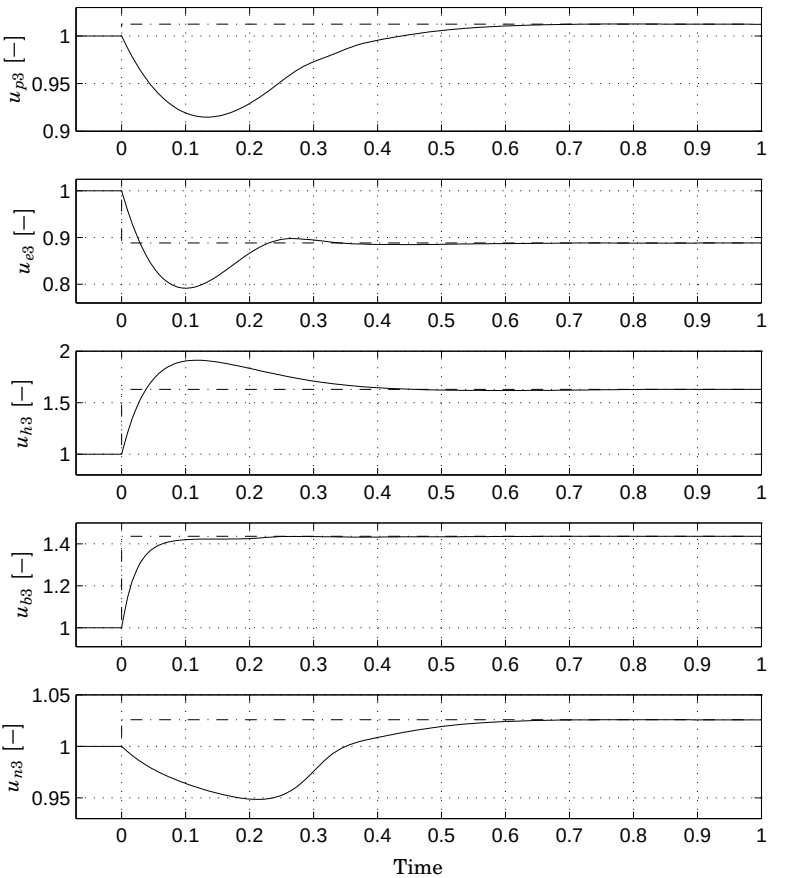

Figure 4. Optimal inflows to GPR (–) and values for grade A and B at stationarity (-·-).

lene inflow has an undershoot giving a more rapid decrease of production rate. The change in u_{e3} is not enough for the specification on X_{be3} to be fulfilled and an increase of butene inflow, u_{b3}, is required, see figures 4 and 6. Analogously, inflow of hydrogen is increased. Propane and nitrogen are changed such that e.g., reactor pressure P_3 is inside desired limits, specified to ±1% from nominal pressure, see Figure 5.

All averaged concentrations and ratios in the GPR, and also in the prepolymerization reactor although not shown here, together with the split, follow constraints of no under- or overshoot. Corresponding instantaneous values do have under- and overshoots, yielding faster transition.

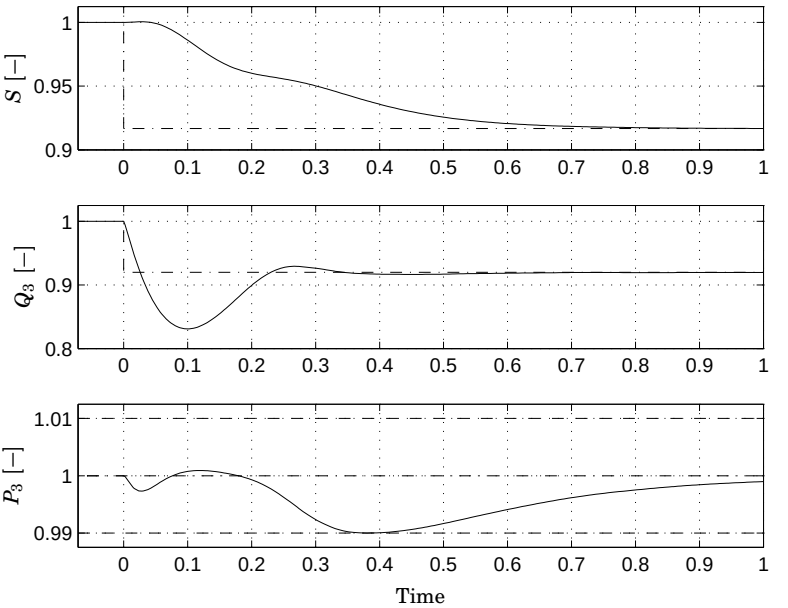

Figure 5. Split, production rate and pressure for GPR (−) and values for grade A and B at stationarity (---), and pressure limits (--).

6. Summary and Future Work

In this paper, modeling of multistage polyethylene reactors has been performed in the high level language Modelica. Optimal trajectories for transition between grades currently used at Borealis AB have been found by formulating an optimization problem using Optimica constructs and solved in the framework of JModelica.org.

Future work includes modeling of additional polymer specifications such as melt indices and densities and also economic objectives in the optimization formulation.

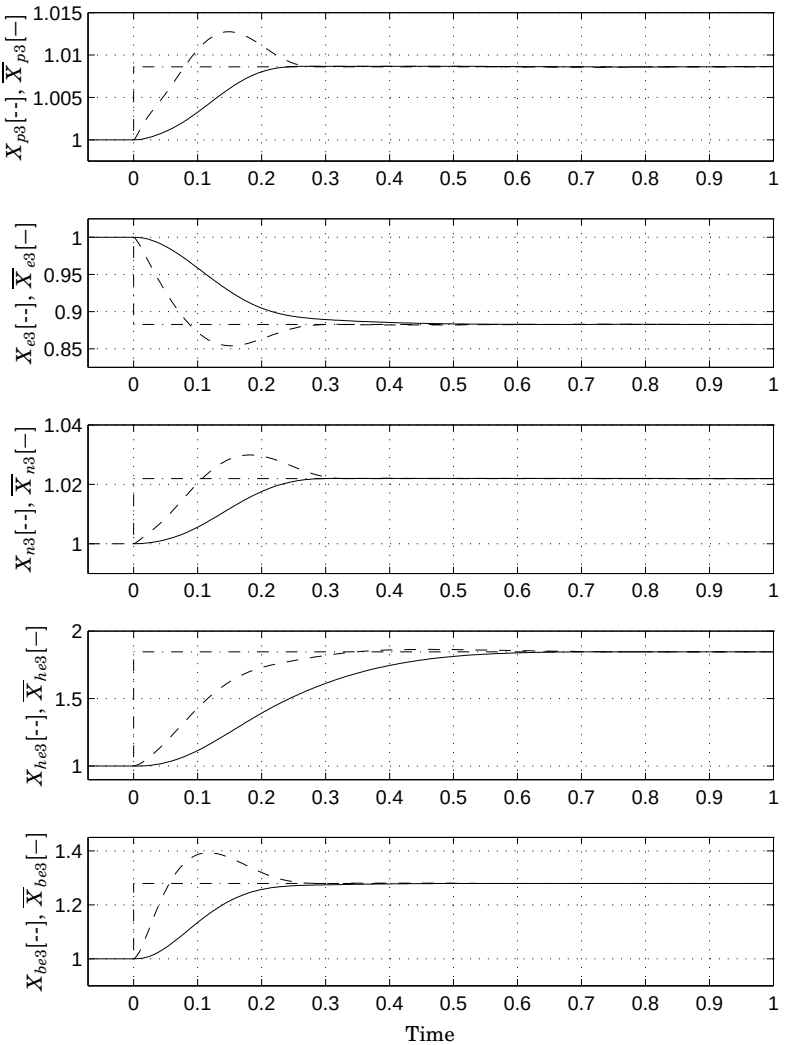

Figure 6. Instantanous (--) and bed average concentrations and ratios (–) for GPR and values for grade A and B at stationarity (---).

References

Åkesson, J. (2008): "Optimica—An Extension of Modelica Supporting Dynamic Optimization." In *6th Int. Modelica Conference 2008*. Modelica Association.

Åkesson, J., K.-E. Årzén, M. Gäfvert, T. Bergdahl, and H. Tummescheit (2010): "Modeling and Optimization with Optimica and JModelica.org — Languages and Tools for Solving Large-Scale Dynamic Optimization Problem." *Computers & Chemical Engineering*, **34:11**, pp. 1737–1749.

Andersson, N., P. Larsson, J. Åkesson, S. Haugwitz, and B. Nilsson (2011): "Calibration of a polyethylene plant for grade change optimizations." In *Proceedings of the 21st European Symposium on Computer-Aided Process Engineering*. Chalkidiki, Greece.

Biegler, L., A. Cervantes, and A. Wächter (2002): "Advances in simultaneous strategies for dynamic optimization." *Chemical Engineering Science*, **57**, pp. 575–593.

Gisnas, A., B. Srinivasan, and D. Bonvin (2003): "Optimal grade transitions for polyethylene reactors." In *Process Systems Engineering*, pp. 463–468. Kunming, China.

Hindmarsh, A., P. Brown, K. Grant, S. Lee, R. Serban, D. Shumaker, and C. Woodward (2005): "Sundials: Suite of nonlinear and differential/algebraic equation solvers." *ACM Trans. Math. Softw.*, **31**, September, pp. 363–396.

Larsson, P., N. Andersson, J. Åkesson, and S. Haugwitz (2010): "Modelica Based Grade Change Optimization for a Polyethylene Reactor." In *Proceedings of the 9th International Symposium on Dynamics and Control of Process Systems*. Leuven, Belgium.

McAuley, K. and J. MacGregor (1991): "On-line inference of polymer properties in an industrial polyethylene reactor." *AIChE Journal*, **37:6**, pp. 825–835.

McAuley, K. and J. MacGregor (1992): "Optimal grade transitions in a gas phase polyethylene reactor." *AIChE Journal*, **38:10**, pp. 1564–1576.

Prata, A., J. Oldenburg, and A. Kroll (2008): "Integrated scheduling and dynamic optimization of grade transitions for a continuous polymerization reactor." *Computers & Chemical Engineering*, **32:3**, pp. 463–477.

Reginato, A., J. Zacca, and A. Secchi (2003): "Modeling and simulation of propylene polymerization in nonideal loop reactors." *AIChE Journal*, **49:10**, pp. 2642–2654.

Takeda, M. and W. Ray (1999): "Optimal grade transition strategies for multistage polyolefin reactors." *AIChE Journal*, **45:8**, pp. 1776–1793.

Touloupides, V., V. Kanellopoulos, P. Pladis, C. Kiparissides, D. Mignon, and P. Van-Grambezen (2010): "Modeling and simulation of an industrial slurry-phase catalytic olefin polymerization reactor series." *Chemical Engineering Science*, **65:10**, pp. 3208–3222.

van Brempt, W., P. van Overschee, T. Backx, and O. Moen (2004): "Plantwide economical dynamic optimization: Application on a Borealis Borstar process model." In *ADCHEM2003*. Hong Kong.

Wächter, A. and L. T. Biegler (2006): "On the implementation of an interior-point filter line-search algorithm for large-scale nonlinear programming." *Mathematical Programming*, **106:1**, pp. 25–58.

Xie, T., K. McAuley, C. Hsu, and D. Bacon (1994): "Gas phase ethylene polymerization: Production processes, polymer properties, and reactor modeling." *Ind. and Eng. Chemistry Research*, **33:3**, pp. 449–479.

Zacca, J. and W. Ray (1993): "Modelling of the liquid phase polymerization of olefins in loop reactors." *Chemical Engineering Science*, **48:22**, pp. 3743–3765.

Paper V

Cost Function Design for Economically Optimal Grade Changes for a Polyethylene Gas-Phase Reactor

Per-Ola Larsson, Johan Åkesson and Niklas Andersson

Abstract

This paper considers optimization of stationary production and dynamic grade changes for a gas phase polyethylene reactor. The designed cost function considers costs of inflows and revenues from produced polymer. At dynamic optimization, the cost function uses grade variable intervals for defining on-grade polymer and includes economical incentives to produce on-target polymer. Additionally, it also considers a preparatory time interval prior defined transition time, used for economical preparation of reactor state. A previously published model of a gas phase reactor is used and several grade changes are optimized, showing the effects of an economical cost function.

 To appear in *Proceedings of the 50th IEEE Conference on Decision and Control and European Control Conference*, Orlando, USA, 2011.

1. Introduction

Polyethylene gas phase reactors (GPR) are today able to produce several different grades defined by industrial standard quality variables. Production is a continuous process and polyethylene properties are altered by manipulating the inflows of fresh raw material. This is valuable for producers since they can adapt to market conditions, both in terms of raw material pricing, product price and market demands. This has led to product campaigns varying in length between a few days up to weeks. During grade transition, i.e., the transferring of production from one product to another, there is in general production of polymer that is not acceptable as neither start nor end grade and must be sold at a lower price. This, together with inflow costs, must be taken into account when performing economic optimization of grade changes.

The grade change problem has been formulated and solved in several different ways. Quadratic criteria penalizing deviation from end grade multiplied by production rate, yielding less off-grade polymer, was used in [McAuley and MacGregor, 1992] together with a sequential method. With a similar method, quality variable intervals defining polymer grades was used in [Takeda and Ray, 1999] by having different quadratic functions inside and outside the intervals. Collocation based optimization of grade changes, using quadratic critera has been considered in e.g., [Flores-Tlacuahuac *et al.*, 2006]. However, translating economics into weights in a quadratic criteria is a difficult task. Economics was considered to an extent in [Gisnas *et al.*, 2003], comparing minimization of total transition time and minimization of off-grade polymer production. A more direct approach was considered in [Tousain, 2002], where maximization of profit during the transition was performed using quality variable intervals and a sequential method. However, the optimization procedure did not enforce quality variables to be on-target, only inside acceptable intervals, and thus not considering product consistency towards market and raw material and product price changes. The contributions of this paper are the development of a continuously differentiable cost function that considers plant economy and that uses quality variable intervals. The cost function also adds incentives to produce a polymer that is on-target. Additionally, the optimization includes a time interval prior defined transition time, used for economical preparation of reactor state. A model of a GPR previously published in [McAuley *et al.*, 1995] is used for demonstrating the cost function and its implications by maximizing profit during several different transitions.

2. Process Description

2.1 Process Overview

The process consists of the reactor and a cooling system with a compressor and heat exchanger, see the schematic diagram in Figure 1 and also [McAuley *et al.*, 1995]. The gas phase, providing the fluidization in the reactor, consists of the monomer ethylene, co-monomer butene and hydrogen and also inert nitrogen, while the solid phase is polyethylene and a heterogeneous Ziegler-Natta catalyst. Ethylene is the main raw material, while butene and hydrogen are added for density and melt index control, respectively. Nitrogen is used as carrier for added catalyst and heat removal from the exothermic reaction [McAuley *et al.*, 1995]. The unreacted gas at the top of the reactor may either be bled off in the bleed stream used for pressure and impurity control of the reactor or it is recycled through the cooling system. The recycled part is added to the fresh gas feed and since the single pass conversion is as low as 2–5%, the recycle stream is much larger than the fresh feed [McAuley *et al.*, 1995]. The produced polyethylene is withdrawn at the bottom of the reactor.

2.2 Modeling Assumptions

A first-principles model, capturing the main dynamics of the process, is presented in [McAuley *et al.*, 1995]. Several assumptions are made and motivated, keeping model complexity low, yielding it advantageous for grade transition optimization and evaluation of cost function design. Gas and solid phases in the reactor are assumed well mixed, the temperature

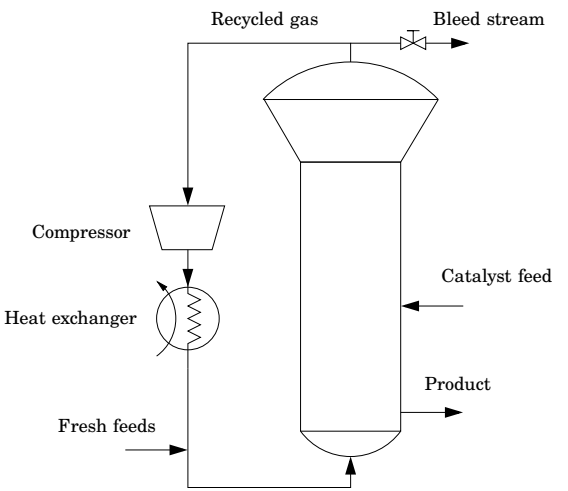

Figure 1. Schematic diagram of a gas phase reactor with recycle system.

in the reactor is uniform and perfectly controlled, and a constant bed level is achieved by a perfect bed level controller. Variable bed level has been considered in e.g., [Gisnas *et al.*, 2003] but this is often not used in practice due to the risk of polymer sticking to reactor walls, creating hot spots. Further, the time-delay associated with the recycle flow through compressor and heat exchanger is negligible compared to reactor dynamics and the gas exiting with the product outflow is captured directly and recycled.

2.3 Mathematical Model

The process model, described in [McAuley *et al.*, 1995], is a macro scale model suited for grade transition optimization and control [Xie *et al.*, 1994]. Based on the assumptions in 2.2, the following mass balances are written for the gas phase components,

$$V_g \frac{dx_e}{dt} = u_e/M_e - b_e - r_e \tag{1}$$

$$V_g \frac{dx_b}{dt} = u_b/M_b - b_b - r_b \tag{2}$$

$$V_g \frac{dx_h}{dt} = u_h/M_h - b_h - r_h \tag{3}$$

$$V_g \frac{dx_n}{dt} = u_n/M_n - b_n, \tag{4}$$

where x_i, $i \in \{e, b, h, n\}$, are molar concentrations of ethylene, butene, hydrogen and nitrogen, respectively. The concentrations are increased by fresh inflows of the gases, i.e., u_i, and decreased by bleed flows b_i and reaction rates r_j, $j \in \{e, b, h\}$, for the reactive components. The inflows together with the total bleed u_B are control variables and the component bleeds may be calculated from respective mole fraction and total bleed [McAuley *et al.*, 1995]. M_i are the molar weights and V_g is the gas volume in the reactor and is assumed constant.

The Ziegler-Natta catalyst is assumed to have one active site, as in [Gisnas *et al.*, 2003], and the number of moles of active catalyst sites in the bed, Y, may be modeled as [McAuley *et al.*, 1995]

$$\frac{dY}{dt} = u_Y a_Y - Y\frac{r}{B_w} - k_d Y - k_f Y x_h + k_h N x_e \tag{5}$$

$$N = \frac{Y k_f x_h}{k_h x_e + r/B_w}, \tag{6}$$

where N is the number of moles of sites deactivated by hydrogen, modeled using the stationary hypothesis. The bed weight B_w is assumed constant

Table 1. Parameter and constant values in process model.

Param.	Value	Unit	Param.	Value	Unit
P_v	17.225	bar	k_{ph}	0.036	$m^3/(molh)$
T	360	K	k_h	3.6	$m^3/(molh)$
M_e	28.05	g/mol	k_f	0.3168	$m^3/(molh)$
M_h	2.016	g/mol	k_d	0.36	1/h
M_b	56.11	g/mol	k_1	0.100	$(g/10min)^{1/3.5}$
M_n	28.0	g/mol	k_2	0.400	$(g/10min)^{1/3.5}$
R	$8.314 \cdot 10^{-5}$	$m^3bar/(molK)$	k_3	0.700	$(g/10\ min)^{1/3.5}$
V_g	150	m^3	p_1	989	kg/m^3
B_w	35 000	kg	p_2	10.3	$kg/m^3/\ln(g/10min)$
a_Y	0.548	mol/kg	p_3	-38.0	kg/m^3
k_{pe}	306	$m^3/(molh)$	p_4	0.300	–
k_{pb}	10.8	$m^3/(molh)$			

motivated by only minor variations in the gas mixture and polymer density. The first term on the right hand side of Eq. (5) is inflow of active sites where u_Y is a control flow and a_Y is a catalyst constant, while the second term is outflow of catalyst. Next, two terms of deactivation of catalyst are found, and the last term considers reactivation. The constants k_d, k_f, and k_h are rate constants for deactivation, site deactivation by hydrogen, and reactivation reaction with ethylene, respectively. Parameter values for the model are found in Table 1.

Reactor pressure P, with a reference value of P_v, is calculated using the gas components as,

$$P_i = x_i RT, \quad i \in \{e, b, h, n\} \tag{7}$$

$$P = P_e + P_b + P_h + P_n, \tag{8}$$

where R and T are the ideal gas constant and reactor temperature, respectively, and P_i is the partial pressure of component i. Due to the bed level assumption, the production rate r is equal to the total reaction rate, and found directly from the reaction rates and molar weights M_i as,

$$r = M_e r_e + M_b r_b + M_h r_h \tag{9}$$

$$r_i = Y k_{pi} x_i, \quad i \in \{e, b, h\}, \tag{10}$$

where k_{pi} are pseudo-propagation rate constants. Compared to [McAuley *et al.*, 1995], a small rate constant is added for hydrogen.

The two most frequently used quality variables for polyethylene are melt index MI, an indirect measure of the molecular weight, and density ρ, see e.g., [Xie *et al.*, 1994]. Polymer produced at a certain time instant has in general different quality variables values than the mixture of polymer in the reactor, i.e., the cumulative values of the bed. This is because the polymerization reaction is much faster than the dynamics of the gas and solids phase in the reactor [McAuley and MacGregor, 1991]. Instantaneous values for MI and ρ in this study are calculated as

$$MI = \left(k_1 + k_2 x_h / x_e + k_3 x_b / x_e\right)^{3.5} \tag{11}$$

$$\rho = p_1 + p_2 \ln MI + p_3 \left(x_b / x_e\right)^{p_4}, \tag{12}$$

while the cumulative values are found as

$$\frac{d}{dt} MI_c^{-\frac{1}{3.5}} = \frac{1}{B_w / r} \left(MI^{-\frac{1}{3.5}} - MI_c^{-\frac{1}{3.5}} \right) \tag{13}$$

$$\frac{d}{dt} \left(\frac{1}{\rho_c} \right) = \frac{1}{B_w / r} \left(\frac{1}{\rho} - \frac{1}{\rho_c} \right). \tag{14}$$

The four equations above have the same structure as derived in [McAuley and MacGregor, 1991]. The parameter values used in this paper can be found in Table 1.

The reactor states, algebraic variables and control flows in the model are collected in $\mathbf{x}$, $\mathbf{w}$ and $\mathbf{u}$, respectively.

3. Grade Definition and Prices

The two cumulative quality variables MI_c and ρ_c in the previous section define a polyethylene grade and are also center values for the intervals that define acceptable values for premium priced product. Added to the list of quality variables is the reactor pressure with a target value of P_v, see Table 1. The pressure has not a direct effect on product properties in the model, but can instead be seen as a reactor operations quality variable affecting long term production. The quality variable values and intervals for all grades A–E considered in this paper can be found in Table 2.

The polymer sell price (\$/kg) depends on the polymer properties. Premium sell price for grade j, denoted S_j, $j \in \{\mathrm{A}, \ldots, \mathrm{E}\}$, is assumed to be given only if all quality variables are inside their defined intervals, otherwise the off-grade price S_{off} (\$/kg) is given. However, for e.g., consistency reasons to the market, the quality variables should be as close to target values as possible. Table 2 gives the premium prices S_j, and Table 3 gives the inflow costs C_i (\$/kg), $i \in \{e, b, h, n, Y\}$, and off-grade polymer sell price S_{off} .

Table 2. Grade definitions with intervals, polymer sell prices and instantaneous profits.

Grade j	MI_j	ρ_j	P_j	x_h/x_e	x_b/x_e	S_j	R_j
A	0.35	944.0	P_v	0.40	0.70	10.35	21544
B	0.35	948.5	P_v	0.84	0.44	10.35	21847
C	0.90	952.0	P_v	0.75	0.83	10.64	25063
D	0.50	952.0	P_v	1.03	0.45	9.45	9575
E	0.25	942.0	P_v	0.38	0.61	11.25	33882
Interval	± 0.025	± 1	± 0.15	-	-	-	-

Table 3. Costs of inflows and off-grade polymer sell price.

C_e	C_b	C_h	C_n	C_Y	S_{off}
8	10	60	0.03	750	6.75

4. Modeling and Optimization Framework

The process is modeled using the Modelica language, which is a high level language for complex physical models, where the user may mix differential and algebraic equations. For optimization, the open source platform JModelica.org is used [Åkesson *et al.*, 2010]. This platform has been successfully used on significantly larger reactor models, see [Larsson *et al.*, 2011].

JModelica.org contains an implementation of a simultaneous optimization method based on collocation on finite elements [Biegler *et al.*, 2002]. State and algebraic variables are parametrized by Lagrange polynomials of order three and two, respectively, based on Radau points, while the inputs are constant during each finite element. This yields a non-linear program (NLP) with structure, which is exploited by the solver IPOPT [Wächter and Biegler, 2006].

5. Optimization Formulation

5.1 General Process Constraints

Specifications of MI_c and ρ_c sets the ratios of the reactants, but not the production level. If the product sell price is greater than the inflow costs,

the production level will in general be as high as possible, limited by, for instance, safety, post-processing capacity, lump formation due to too high ethylene partial pressure or catalyst amount and insufficient heat removal. This sets limits on e.g., ethylene concentration, and subsequently, limits on the other reactant concentrations may be set. For the reactor pressure to be on its target value, nitrogen is added, which also should be able to remove enough heat. In addition, to handle impurities, a non-zero bleed is preferred in industry, see [McAuley and MacGregor, 1992] and [Gisnas *et al.*, 2003], which sets a lower limit on the bleed. The behavior of the inflows, both in terms of range and rate of change, is limited due to e.g., pump capacities and safety.

5.2 Stationary Optimization

During stationary production, the quality variables should be on targets, while the reactor is operated in an economically beneficial way, respecting process safety and constraints. The instantaneous production profit for grade j, denoted R_j, is the difference between revenue from sold polymer and inflow costs as

$$R_j = S_j r - \sum_{i \in \{e,b,h,n,Y\}} C_i u_i.$$

The profit may be maximized during stationary production by solving the following optimization problem,

$$\begin{aligned} \min_{\dot{\mathbf{x}},\mathbf{x},\mathbf{w},\mathbf{u}} \quad & -R_j \\ \text{s.t. Eqs. (1)–(14)} \quad & \\ & \mathbf{x}_{\min} \leq \mathbf{x} \leq \mathbf{x}_{\max} \\ & \mathbf{w}_{\min} \leq \mathbf{w} \leq \mathbf{w}_{\max} \\ & \mathbf{u}_{\min} \leq \mathbf{u} \leq \mathbf{u}_{\max} \\ & \dot{\mathbf{x}} = \mathbf{0} \\ & MI_c = MI_j,\ \rho_c = \rho_j,\ P = P_j, \end{aligned} \tag{15}$$

The inequality constraints are related to the limitations in the previous section and the three last equality constraints yield production corresponding to grade j in Table 2.

5.3 Dynamic Optimization

Upon performing a transition it is important not to only focus on the end grade. Before the actual transition, preparations may be performed in the reactor state such that the transition becomes easier. If a transition time t_{T} is defined, then the grade transition cost function may be divided into

two parts that concentrate on start and end grade, respectively. In each part, the revenue is a function of the quality variables and production rate. In the ideal case, if all quality variables are inside their interval, the sell price is S_j, while if at least one is outside, the product sell price is S_{off}. Considering the first part, i.e., time before t_{T}, the instantaneous profit for start grade j is,

$$R_j = ((S_j - S_{\text{off}})\theta_j(\boldsymbol{Q}) + S_{\text{off}})\, r - \sum_{i \in \{e,b,h,n,Y\}} C_i u_i,$$

where the effective sell price is $(S_j - S_{\text{off}})\theta_j(\boldsymbol{Q}) + S_{\text{off}}$. $\boldsymbol{Q}$ contains the quality variables, i.e., $\boldsymbol{Q} = [\,MI_c,\ \rho_c,\ P\,]$, and $\theta_j(\boldsymbol{Q}) = 1$ if all quality variables are inside their intervals defined by grade j, else $\theta_j(\boldsymbol{Q}) = 0$. R_j is non-linear and discrete due to $\theta_j(\boldsymbol{Q})$ and must be made continuously differentiable for efficient optimization. One approximation is

$$\tilde{\theta}_j(\boldsymbol{Q}) = \left(\sum_{i=1}^{n_Q} \left(2\, \frac{q_i - q_{ji}}{w_{ji}} \right)^{n_i} + 1 \right)^{-1},$$

where n_Q is the length of $\boldsymbol{Q}$, q_i is the ith quality variable in $\boldsymbol{Q}$, q_{ji} and w_{ji} are q_i's target value and interval width, respectively, specified by grade j, and n_i is a sufficiently large even integer giving satisfying approximation error. An alternative would be to use e.g., trigonometric functions [Tousain, 2002].

An incentive to be on-target is that premium sell price S_j is only given when all quality variables are on-target, i.e., a reward for product consistency towards the market. This can be formulated by giving a large percentage of S_j when on-grade but off-target, and then add the small remainder depending on how close the quality variables are their target values. This is an approximation of the relation between price and quality variables in Section 3. However, the small remainder should only be greater than the cost of change of inflows required to move the quality variables from the interval boundary to the target. This cost is in general very small in comparison to the cost of the fresh feeds. Thus, $\tilde{\theta}_j$ may be given an extension fulfilling these properties as,

$$\Pi_j(\boldsymbol{Q}) = \tilde{\theta}_j(\boldsymbol{Q}) \left(p + \frac{1-p}{n_Q} \sum_{i=1}^{n_Q} \left(\left(2\, \frac{q_i - q_{ji}}{h_{ji}} \right)^2 + 1 \right)^{-1} \right),$$

where $p \in [0, 1]$ determines the percentage of the difference $S_j - S_{\text{off}}$ that at least is given additionally when on-grade compared to off-grade, q_i is the ith quality variable in $\boldsymbol{Q}$, q_{ji} is q_i's target value for grade j and h_{ji}

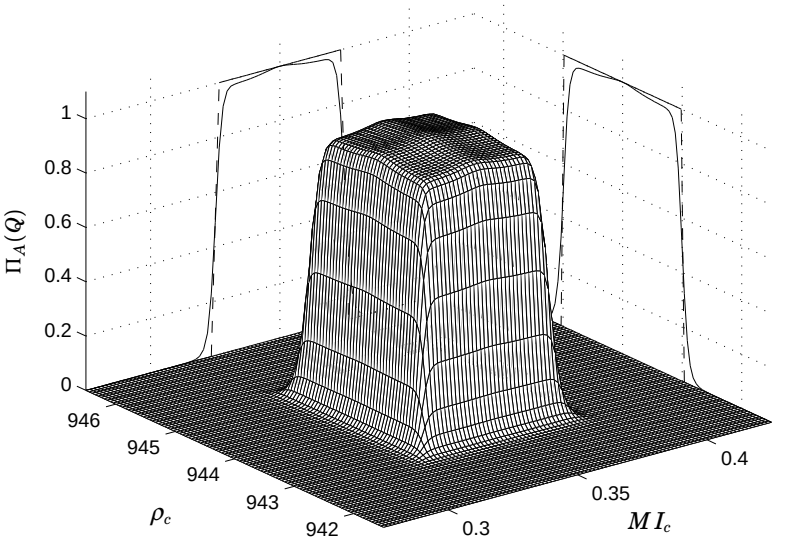

Figure 2. Example of $\Pi_A(Q)$ with only MI_c and ρ_c, i.e., $n_Q = 2$, with parameters $n_i = 20$, $p = 0.95$, $h_{Ai} = w_{Ai}/6$. Projections of $\Pi_A(Q)$ (–) and $\theta_A(Q)$ (--) are also shown for comparison.

defines the width of the effective sell price peak at target value for quality variable q_i and grade j. Thus, for every quality variable being on-target, a $(1-p)/n_Q$-part of $S_j - S_{\text{off}}$ is added to the effective sell price. An example of $\Pi_A(Q)$ with only MI_c and ρ_c can be found in Figure 2.

The start grade j and the end grade k at a transition have different on-grade functions, i.e., Π_j and Π_k. To calculate the approximated total profit during a transition, a switch between Π_j and Π_k, defined by t_{T}, is included in the instantaneous profit R during a grade change as

$$R = (S_j - S_{\text{off}})\Pi_j(Q)T(t_{\text{T}})r + (S_k - S_{\text{off}})\Pi_k(Q)\left(1 - T(t_{\text{T}})\right)r + S_{\text{off}}\,r - \sum_{i\in\{e,b,h,n,Y\}} C_i u_i,$$

The switch may be well approximated by

$$T(t_{\text{T}}) = 1/2 - \arctan\left(\gamma(t - t_{\text{T}})\right)/\pi,$$

with a large γ. In this study, $\gamma = 500$ has been used, which gave a sufficiently small approximation error compared to an ideal step function.

The dynamic optimization problem on the time interval $t_{\text{start}} \leq t_{\text{T}} \leq t_{\text{end}}$ of transferring production from grade j to grade k may be stated using the above R, as

$$\begin{aligned}
&\min_{\dot{\mathbf{u}}} \int_{t_{\text{start}}}^{t_{\text{end}}} \left(-R + \dot{\mathbf{u}}^T \mathcal{U}_d \dot{\mathbf{u}}\right) dt \\
&\text{s.t. Eqs. (1)–(14)}, \quad \mathbf{u} = \int_{t_{\text{start}}}^{t} \dot{\mathbf{u}}\, d\tau \\
&\quad \mathbf{x}_{\min} \leq \mathbf{x} \leq \mathbf{x}_{\max}, \quad \mathbf{w}_{\min} \leq \mathbf{w} \leq \mathbf{w}_{\max} \\
&\quad \mathbf{u}_{\min} \leq \mathbf{u} \leq \mathbf{u}_{\max} \quad \dot{\mathbf{u}}_{\min} \leq \dot{\mathbf{u}} \leq \dot{\mathbf{u}}_{\max} \\
&\quad \mathbf{x}(t_{\text{start}}) = \mathbf{x}_j, \ \mathbf{u}(t_{\text{start}}) = \mathbf{u}_j \\
&\quad \mathbf{u} = \mathbf{u}_k, \ t \geq t_{\text{end}} - T_c
\end{aligned} \tag{16}$$

where $\mathbf{x}_j$ and $\mathbf{u}_j$ are state and control flows from stationary optimization of grade j and $\mathbf{u}_k$ is from stationary optimization of grade k.

In order to penalize highly varying inflows, the control flow derivatives $\dot{\mathbf{u}}$ are used as optimization variables and a quadratic term with the diagonal matrix $\mathcal{U}_d$ is introduced.

The control signal constraint of holding $\mathbf{u}$ constant to end grade specified values during a time interval of T_c at the end of the optimization interval is due to the finite optimization horizon. If the constraint is not included, it would be economically beneficial to close all inflows just prior t_{end} since this will not effect production until after t_{end} due to reactor dynamics. Thus, in this case, the instantaneous profit would be greater at t_{end} than found at stationary optimization, but the end point is not stationary and impossible to retain. T_c should be chosen large enough such that the system essentially is in stationarity at t_{end}, independently of the control flow movement prior $t_{\text{end}} - T_c$

Inequality constraints on MI and ρ are set for preventing excessive under- and overshoots since this may give a product with a mixture of polymers that have significantly different MI and ρ. Even though the cumulative values are on-target, the transition polymer may in these cases differ considerably from on-target polymer produced at stationarity, see [McAuley and MacGregor, 1992] for a further discussion.

6. Optimization Results

As all grades cost less than sell price to produce, the stationary optimization aims to maximize production, which has limits as pointed out in Section 5.1. Assuming the limit of raw material is high, it is the ethylene partial pressure, catalyst, and down-stream capacity that sets the

Table 4. Variable limits at optimization.

Variable	Lower limit	Upper limit
r	5000	13500
P_e	1	6
u_B	5000	10000
MI	$\min(MI_j, MI_k) - 2w_{j1}$	$\max(MI_j, MI_k) + 2w_{j1}$
ρ	$\min(\rho_j, \rho_k) - 2w_{j2}$	$\max(\rho_j, \rho_k) + 2w_{j2}$
P	$P_v - 0.3$	$P_v + 0.3$

limits. To minimize the amount of expensive catalyst used, the ethylene partial pressure should be as high as possible. Table 4 shows the most important limits used at all optimizations, both static and dynamic. At all economically optimal stationary solutions, both ethylene partial pressure and production rate are on their upper bounds, and amount of catalyst is well inside limits. Additionally, the bleed flow is at its minimum, yielding minimum waste of raw materials and diluent. In Table 2, the resulting instantaneous profits R_j are reported together with the ratios x_h/x_e and x_b/x_e. It is mainly the sell price S_j that contribute to the differences in profits as the inflow costs are similar for all grades, dominated by ethylene.

From the stationary optimization, initial and end values are given to the dynamic optimization which is specified to be 36 h long and divided into three parts,

- 12 h before transition time t_T.
- 12 h after transition time t_T.
- 12 h with control flows equal to stationary optimization result of end grade, i.e., $T_c = 12$ h.

This does not specify the transition time, only upper limits on preparation and completion times are defined.

The on-grade functions Π_j in the optimizations utilizes MI_c, ρ_c and P as quality variables with the intervals in Table 2. For simplicity, all quality variables are treated equally by setting the function parameters as in the example in Figure 2. The under- and overshoot limits on MI and ρ are given by using start and end grade values and intervals, see Table 4. These limits are process and user specific and are trade-offs between fast change of cumulative values and the range of instantaneous polymer properties in the end product. Hard limits are also set on the

reactor pressure due to e.g., safety reasons. The cost of highly varying inflows is set by $\mathcal{U}_d$, yielding smooth control flows.

Four consecutive grade changes, A to E, have been optimized, and quality variables, control flows, on-grade functions, production and economics are found in figures 3–5. The element length in the discretization is chosen to 10 min. and the figures show only the first 24 hours of optimization, since stationarity is reached at this time for all optimizations.

Considering the first grade change, A–B, only an increase of density requires changes in both hydrogen and butene concentrations. To prepare a fast transition, inflows of hydrogen and butene do small changes that first decrease the instantaneous value ρ. Then, by making fast changes in the inflows, the rate of change of ρ_c during the off-grade time is greater than if the preparation not had been performed. This is since ρ was given time to accelerate to a greater rate of change before leaving start grade specification. Preparative operations like this are found in all considered grade changes. They are the preparation equivalents of making under- and overshoots in the instantaneous values after the start grade has been left, which is also performed at the transitions. Additionally, the inflows are synchronized such that the polymer is on-grade during only a short time interval, even though the inflows change over a significantly longer time period. In this first grade change, the overshoot of ρ reaches the constraint set in Table 4. During the transition, inflow of nitrogen is closed, making room for the hydrogen overshoot and an increase of catalyst holds production high even with the undershoot of butene inflow, yielding time constants for MI_c and ρ_c as small as possible. Only a small increase of bleed is used, minimizing waste, and the transition is performed in approximately 1 h as can be seen from the on-grade functions in Figure 5.

At the second grade change, B–C, starting at $t = 24$ h, both MI and ρ are to be increased. Rapid increase of u_b and decrease of u_e and a small increase in u_h causes MI to be on overshoot limit, thus giving as fast rise of the cumulative value as possible. However, u_e may not be decreased too much since this will decrease the production and hence increase the time constant for MI_c and ρ_c. The overshoot constraint of MI is kept active while decreasing u_h and increasing u_e and u_b such that ρ is as large as possible. To make room for more butene in the reactor without too much bleed, u_n is completely closed and reactor pressure is at its upper limit. The transition is performed in approximately 6 h.

A decrease of only MI_c, as in the change C–D, is performed by decreasing u_b and increasing u_h. More nitrogen is added to the reactor to keep pressure at target due to the loss of butene. Production rate is kept high with increased u_e and u_Y, making time constants for MI_c and ρ_c small. As quality variables come close to grade D specifications, the nitrogen is turned off and the reactor is filled with correct concentrations of hydro-

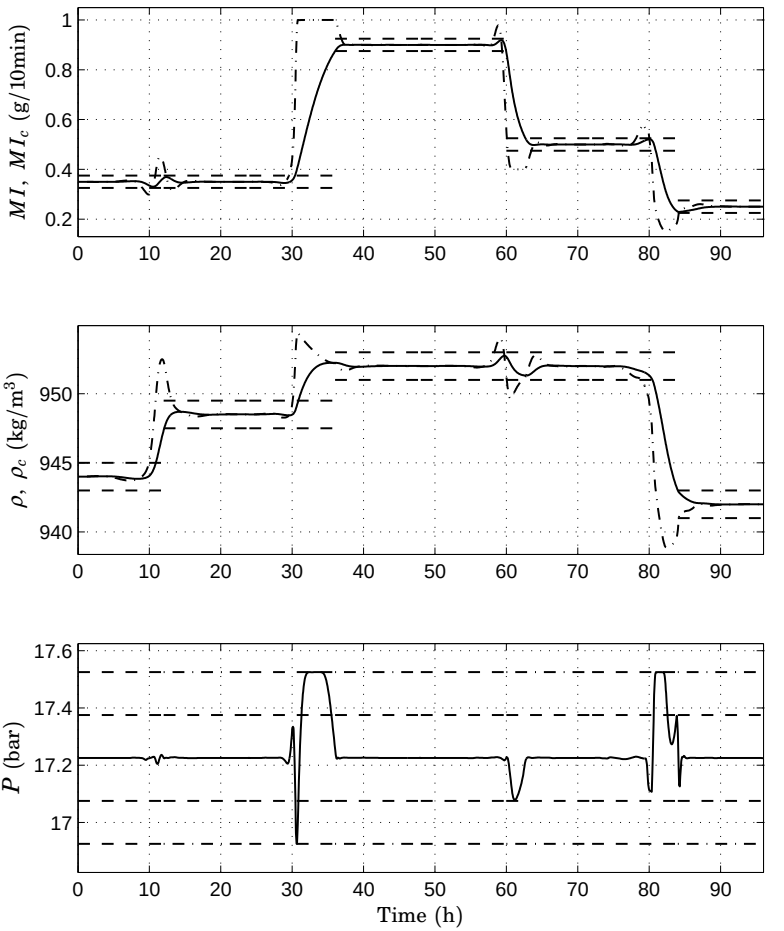

Figure 3. *Upper* and *middle*: Instantaneous MI and ρ (- · -), cumulative MI_c and ρ_c (—) and quality variable intervals (--). *Bottom*: P (—) with quality interval (--) and limits (- · -).

gen and butene. The transition takes 2.5 h and hold both ρ_c and P inside quality variable intervals.

Grade changes with large decreases in hydrogen concentration are considered hard, see e.g. [McAuley and MacGregor, 1992], due to the slow hydrogen dynamics in the reactor. This is seen in the last transition, D–E. To lower the hydrogen concentration as fast as possible, u_h is completely closed and the bleed is at maximum. To minimize raw material waste,

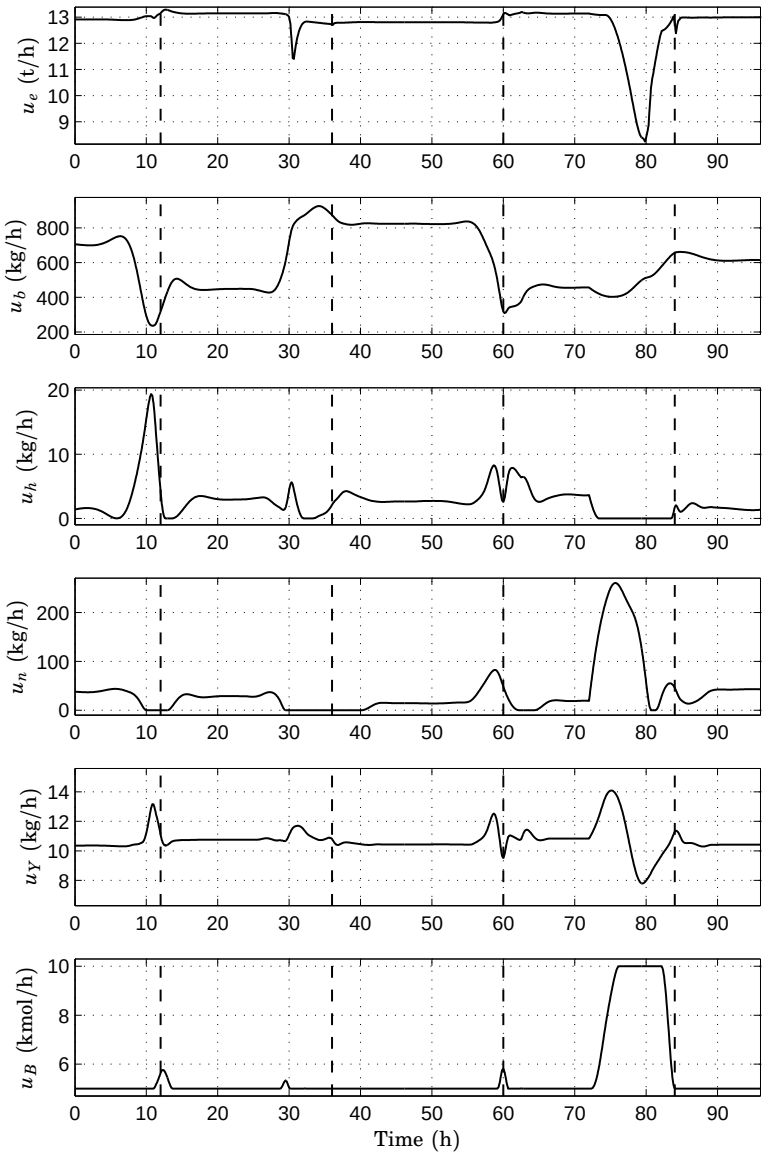

Figure 4. Control flows at transitions. Vertical lines (--) indicate transition times defined by t_T.

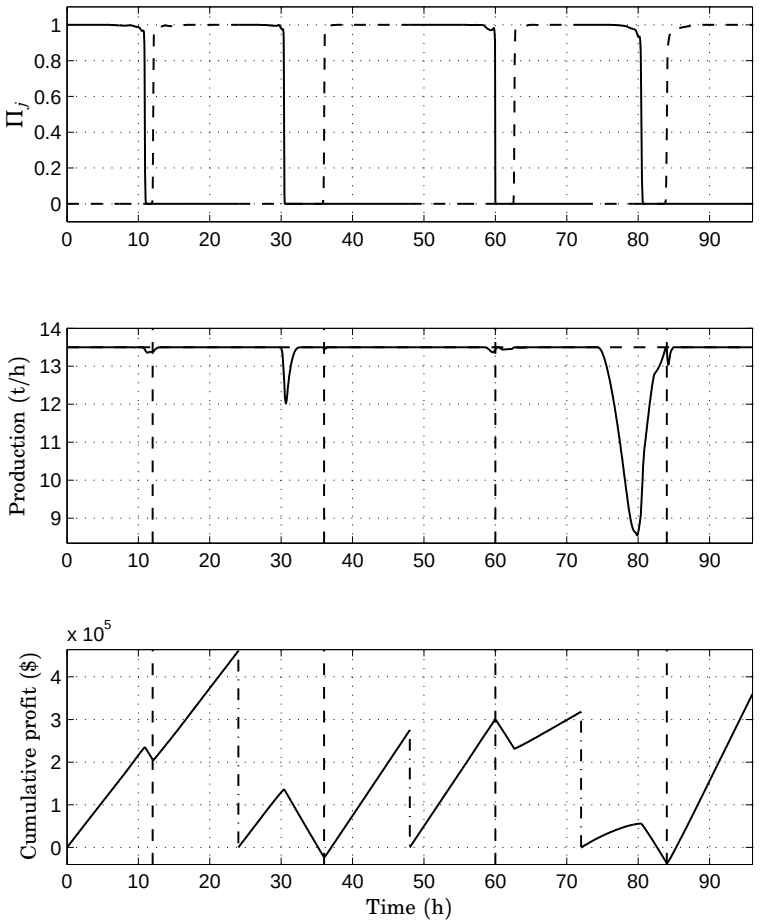

Figure 5. *Upper*: On-grade functions Π_j (– and --). *Middle*: Production rate. *Bottom*: Cumulative profit, set to 0 at optimization start. Vertical lines (--) indicate transition times defined by t_T.

u_e is decreased substantially, and the amount of catalyst in the reactor is increased such that the production rate is not decreased too much. A large amount of inexpensive nitrogen is instead inserted into the reactor to keep pressure and to bleed off until enough hydrogen is removed. Close to transition time, u_e and u_n are again increased and decreased, respectively, making time constants for MI_c and ρ_c small again, yielding fast transfer. A small overshoot of u_b and small corrective actions in u_h

give fast settling of MI_c and ρ_c and the transition takes approximately 4 h. This transfer shows that a bleed stream is effective for hydrogen decreases.

For all transitions, the grade change is made such that the grade with highest instantaneous profit is produced as for a long time as possible, as seen in Figure 5. This is due to the maximization of cumulative profit.

7. Summary

An economic cost function, with a preparatory time interval prior grade change, utilizing quality variable intervals and giving incentives to produce on-target polymer, has been presented and used for several transitions. The main effects of the cost function are

- the grade with highest profit of the two transition grades is produced for as long time as possible.
- control flows are synchronized to yield short off-grade periods and are actively changed over larger time intervals than the off-grade periods.
- hydrogen and butene inflows make preparations of instantaneous variables before defined transition time, and the transitions are performed with significant under- or overshoots. This yields the cumulative values, defining the grade, to move fast through the off-grade interval.
- production rate is often as high as possible, set mainly by ethylene and catalyst inflows, yielding a small time constant for cumulative quality variables.

References

Åkesson, J., K.-E. Årzén, M. Gäfvert, T. Bergdahl, and H. Tummescheit (2010): "Modeling and Optimization with Optimica and JModelica.org — Languages and Tools for Solving Large-Scale Dynamic Optimization Problem." *Computers & Chemical Engineering*, **34:11**, pp. 1737–1749.

Biegler, L., A. Cervantes, and A. Wächter (2002): "Advances in simultaneous strategies for dynamic optimization." *Chemical Engineering Science*, **57**, pp. 575–593.

Flores-Tlacuahuac, A., A. Biegler, and E. Saldívar-Guerra (2006): "Optimal grade transitions in the high-impact polystyrene polymerization process." *Industrial & Engineering Chemistry Research*, **45:18**, pp. 6175–6189.

Gisnas, A., B. Srinivasan, and D. Bonvin (2003): "Optimal grade transitions for polyethylene reactors." In *Process Systems Engineering*, pp. 463–468. Kunming, China.

Larsson, P., J. Åkesson, S. Haugwitz, and N. Andersson (2011): "Modeling and Optimization of Grade Changes for Multistage Polyethylene Reactors." In *Proceedings of the 18th IFAC World Congress*. Milano, Italy.

McAuley, K., D. Macdonald, and P. McLellan (1995): "Effects of operating conditions on stability of gas-phase polyethylene reactors." *AIChE Journal*, **4:41**, pp. 868–879.

McAuley, K. and J. MacGregor (1991): "On-line inference of polymer properties in an industrial polyethylene reactor." *AIChE Journal*, **37:6**, pp. 825–835.

McAuley, K. and J. MacGregor (1992): "Optimal grade transitions in a gas phase polyethylene reactor." *AIChE Journal*, **38:10**, pp. 1564–1576.

Takeda, M. and W. H. Ray (1999): "Optimal grade transition strategies for multistage polyolefin reactors." *AIChE Journal*, **45:8**, pp. 1776–1793.

Tousain, R. (2002): *Dynamic optimization in business-wide process control*. PhD thesis, Delft University of Technology.

Wächter, A. and L. T. Biegler (2006): "On the implementation of an interior-point filter line-search algorithm for large-scale nonlinear programming." *Mathematical Programming*, **106:1**, pp. 25–58.

Xie, T., K. McAuley, C. Hsu, and D. Bacon (1994): "Gas phase ethylene polymerization: Production processes, polymer properties, and reactor modeling." *Industrial and Engineering Chemistry Research*, **33**, pp. 449–479.

Paper VI

Model-Based Optimization of Economical Grade Changes for the Borealis Borstar® Polyethylene Plant

Per-Ola Larsson, Johan Åkesson, Niclas Carlsson and Niklas Andersson

Abstract

In this paper, economical grade changes are considered for a Borealis Borstar® polyethylene plant model, incorporating two slurry-phase reactors, one gas-phase reactor and a recycle area with three distillation columns. The model is constructed in the Modelica language and the JModelica.org platform is used for optimization. The designed cost function expresses the economical profit during a grade change and is formulated using on-grade intervals for seven polymer quality variables such as melt index, density and reactor split factors reflecting polymer bi-modality. Additionally, incentives to produce polymer with quality variables on grade target values, not only inside grade intervals, are added together with a preparatory time interval prior defined transition time. In total, twelve inflows and three purge flows are used at optimization. Two optimal grade changes are thoroughly reviewed, showing the effect of using a cost function that regards plant economy. The resulting trajectories can be divided into three phases with distinguishing features, and the synchronization of inflows and usage of recycle area off-gas flows are important in the optimized grade changes.

Submitted to *Computers & Chemical Engineering*.

1. Introduction

Today, polymers are widely used in many different production areas and applications such as car parts, electronics and foods, and the polymer production is over 100 million tons per year, see [Dünnebier *et al.*, 2005] and [Kadam *et al.*, 2007]. The different areas require different grades of polymer, produced with the same type of raw material but at different polymerization conditions. To increase profitability, the polymer producers have to follow the changing market, both considering polymer sell prices and grade demands, but also raw material pricing, see [Backx *et al.*, 1998]. To have several production lines that each produce one specific grade is not economically tenable, instead grade transitions are considered at generic production lines. The result is product campaigns, lasting from a couple of days up to weeks of continuous production. During the transition, as it is performed during polymer production, off-grade polymer is produced, which must be sold at a much lower price than premium polymer. Thus, there is an enormous economical incentive to perform the grade transitions as advantageous as possible as shown in [Flores-Tlacuahuac *et al.*, 2006], where it is estimated that several hundred thousand dollars are lost in non-optimized transitions for a medium sized plant.

The grade transition problem has been considered by several authors previously, and one of the earliest was [Debling *et al.*, 1994], considering polyolefin production and heuristic transition rules applied to their dynamic simulator POLYRED. Model-based optimization of transitions emerged during the same time period, using different kinds of cost functions and solution methods.

There are two main methods that have been used for solving dynamic grade transition optimization problems, namely, sequential and collocation methods, see [Binder *et al.*, 2001], and they both result in nonlinear programs (NLP). In sequential methods, the control trajectories are parametrized with a small number of parameters and the model is simulated to evaluate e.g., cost function and gradients, and an NLP solver updates the parameters iteratively. In collocation, all state, algebraic variable and control trajectories are discretized, resulting in a large NLP, requiring specialized solvers that explore the problem structure.

Early ground-breaking work on model-based optimization was performed by [McAuley and MacGregor, 1992] on a gas-phase reactor using a sequential method with inflows parametrized with ramps. The cost function considered deviations of melt index and density, weighted with production rate, rewarding production of polymer close to specified grade. [Takeda and Ray, 1999] continued with the model-based approach using POLYRED, considering multistage polyolefin reactors and using piecewise constant control flows. They acknowledge that a polymer is considered

on-grade if the polymer quality variables are sufficiently close to grade defined values. Therefore, they used a quadratic cost function of density and average molar weight, with weights depending on density and average molar weight values. They also weighted with time to penalize long term deviation from target. Both easy and hard transitions, i.e., optimizing a few inflows and all inflows, respectively, were considered. A year after, [Wang *et al.*, 2000] also used time weighted quadratic penalties with a sequential method, with the addition of also having switching times of the control profiles as decision variables and ramps between the constant parts. Four different optimal profiles for the considered slurry reactor were tracked using a model predictive controller (MPC) utilizing the nonlinear model by linearization along the trajectories. Closed loop simulations with model mismatches and successful results were shown. Selection of closed loop controllers were incorporated with trajectory optimization in [Chatzidoukas *et al.*, 2003], while considering a gas-phase reactor with quadratic penalty on quality variables, resulting in a mixed-integer dynamic optimization problem. Recently, a model- and measurement-based approach was introduced by [Bonvin *et al.*, 2005] with subsequent work in [Kadam *et al.*, 2007]. Using optimized trajectories from a sequential method, a solution model is constructed where the control variables are described by arcs and switching times, related to necessary conditions of optimality. The control variables are then adapted on-line by measurements during transition, trying to track the necessary conditions of optimality. The optimization is based on minimization of the transition time. However, it does not consider stationary production at the optimization interval end, only that correct grade is reached.

An approach to grade changes regarding plant economy, trying to maximize the profit during a grade change, has been considered by, for instance, [van der Schot *et al.*, 1999, van Brempt *et al.*, 2001, van Brempt *et al.*, 2002, van Brempt *et al.*, 2004] with sequential methods using intervals for quality variables to defined on-grade production. The cost function was based on raw material and polymer prices and was designed such that the added value by polymer production was maximized. In [Tousain, 2002], a framework for optimization regarding inflow costs and production revenues was constructed where on- and off-grade intervals also were used. It was built upon a sequential method and applied to, among others, a gas-phase polyethylene reactor.

In [Larsson *et al.*, 2011a], orthogonal collocation was used together with a cost function for maximization of the profit during grade change while considering intervals for grade variables to define on-grade polymer production. Additionally, economical incentives to be on grade targets, not only inside on-grade intervals, were added. Collocation was also used by [Flores-Tlacuahuac *et al.*, 2006], considering a polystyrene polymerization

process using a quadratic cost function of states and control variables. [Cervantes *et al.*, 2002] used a model of a polyethylene plant. However, the cost function used at transition optimization only considered concentration of butene.

In this paper, a model of the Borealis Borstar® polyethylene plant PE3 at Borealis AB in Stenungsund, Sweden, is considered. Both optimization of stationary economical production and dynamic economical transitions between grades are performed. The transitions are optimized using orthogonal collocation of the model, which is an extension of the model used in [Larsson *et al.*, 2010] and [Larsson *et al.*, 2011b] for grade change optimization with quadratic criterias and in [Andersson *et al.*, 2011] for plant data-based calibration. A cost function, previously considered on a small gas-phase reactor model and published in [Larsson *et al.*, 2011a], is extended and used. It expresses the economical profit during transition using quality variable intervals and rewards production on grade target values. Additionally, it incorporates a preparatory time interval prior the defined transition time, making economical preparations possible.

The first contribution of this paper is the application of the considered cost function on a significantly larger model compared to the model in [Larsson *et al.*, 2011a], showing the applicability of the cost function, and also the solution method, to large-scale systems. Secondly, it is seen that the economically optimal grade transitions can be divided into three phases with distinguishing features and synchronized control flows. Thirdly, active use of the off-gases on the distillation columns at the recycle area of the plant is a significant contribution, as they are seen to be very useful during a transition with hydrogen decreases. Fourthly, using the Modelica language, a Modelica library containing components corresponding to the plant units was constructed and used when formulating and solving optimization problems using the Modelica extension Optimica together with the platform JModelica.org.

2. Overview of the Plant PE3 at Borealis AB

The plant PE3 at Borealis AB incorporates three reactors in cascade and three distillation columns for recycling of unused raw material and diluents, see Figure 1. The reactors are of Borealis Borstar® technology, developed by Borealis mainly to produce high-strength, bi-modal type polyethylene. The two first reactors are of slurry type while the third is a fluidized bed gas-phase reactor. The distillation columns are of packed, adsorption and stripper type. Table 1 summarizes the notations used in the sequel for the different components and subsystems.

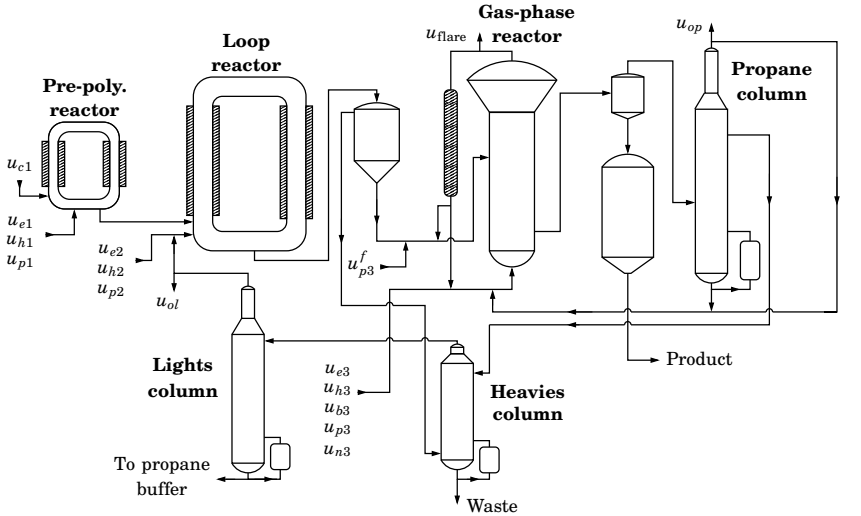

Figure 1. Schematic diagram of the plant PE3 at Borealis AB with the three cascaded Borealis Borstar® reactors and a recycle area with three distillation columns.

Table 1. Component, reactor and distillation column notations.

Component	Subscript	Subsystem	Subscript
Ethylene	e	Pre-poly. reactor	1
Hydrogen	h	Loop reactor	2
Butene	b	Gas-phase reactor	3
Propane	p	Propane column	4
Nitrogen	n	Heavies column	5
Polyethylene	pe	Lights column	6
Incorp. butene	pb		
Catalyst	c		

The pre-polymerization reactor, that has the main function of inducing polymerization in a pre-specified composition, has inflows of the raw materials ethylene and hydrogen, diluent propane and catalyst, denoted u_{e1}, u_{h1}, u_{p1} and u_{c1}, respectively. Compared to the two other reactors, the polymer production in the pre-polymerization reactor is very low.

The polymer slurry is transferred out from the pre-polymerization reactor using transfer legs to the loop slurry reactor that has the same inflow components as the pre-polymerization reactor except for catalyst,

denoted u_{e2}, u_{h2} and u_{p2}. Polymer with low molecular weight is produced, i.e., one of the peaks in the bi-modal molecular weight distribution. With high temperature and pressure, the polyethylene slurry is in a super-critical state in the loop reactor, and the polymer has low solubility in the diluent, thus decreasing the risk of fouling. Approximately half of the total polyethylene production is produced in the loop reactor. The polymer slurry is withdrawn from the loop reactor via settling legs and continuous outtake and transferred to a flash tank where polymer and gases are separated. The gas mixture is sent to the heavies column at the recycle area, see Figure 1, while the polymer is transported to the gas-phase reactor (GPR) using a part of the recycle gas of the GPR. A fixed propane purge flow u_{p3}^{f} assure that no leakage of GPR recycle gas to the flash tank is present. Fresh inflows to the GPR are, apart from the same type of components as to the loop reactor, also inert nitrogen for pressure control and the co-monomer butene used for controlling the polymer density. The inflows to the GPR are denoted u_{e3}, u_{h3}, u_{b3}, u_{p3} and u_{n3}. In the GPR, due to the low concentration of hydrogen, high molecular weight polymer is produced, yielding the second peak in the molecular weight distribution and thus the bi-modal end product. When the gases reach the expanded top section of the reactor, they are led through a cooler and again inserted into the reactor together with the fresh feeds at the reactor bottom. The polymer and gas mixture may be withdrawn continuously or using a batch system at the reactor bottom, and are transferred to a separator from which the gases go to the propane column in the recycle area and the finished product is transferred to pelleting via a degassing tank.

The recycle area consist of three distillation columns, i.e., propane, heavies, and lights column, see Figure 1. The propane column is a packed column and its main task is to remove propane from the gas mixture from the GPR, and send the remaining gas back to the GPR via top and bottom outtakes. Prior to the column is a pre-condenser, used for removing some of the light components, which decreases the load on the column. The removed components are added to the top flow of the column and led back to the GPR. The side flow, mainly propane, is led to the heavies column together with the gas mixture from the flash tank, while the bottom flow composed of heavy components are recycled directly back to the GPR.

The heavies column is an adsorption column, i.e., the components that are to be removed are accumulated at the column bottom. The components to be removed are heavier components than propane together with oligomers formed in the loop reactor during polymerization as a bi-product. The top flow of the heavies column are led to the lights stripper column, where light components and a small amount of propane are dis-

tilled to the top and recycled directly into the loop reactor together with the fresh feeds. The bottom flow from the lights column may be considered to be pure propane and is stored in a propane buffer to be used as fresh inflows.

Except for the inflows to the reactors above, two off-gas flows and one flare flow flows may be used for control. Off-gases on propane and lights columns denoted u_{op} and u_{ol}, respectively, are sent to other parts of the industrial area, and the flare flow u_{flare} on the gas-phase reactor is sent directly to be burnt.

3. Modeling and Optimization Environment

Models of reactors and distillation columns are encoded in the Modelica language. Modelica is a high level language, designed for modeling of complex physical systems. Some of its main features are, see [The Modelica Association, 2011] and [Fritzson, 2004],

- the possibility to express the model equations in a text-book declarative style, i.e., there is no need to solve for certain variables when implementing the model.
- differential and algebraic equations may be mixed.
- it is an object oriented language with classes, components and inheritance.
- it supports component-based modeling with the possibility of interconnecting the components.

These features were utilized when a model library for the plant was constructed. The library, which is an extension of the library presented in [Larsson *et al.*, 2010], contains reactor and distillation column models, optimization models for stationary and dynamic optimization, and simulation and validation models.

Simulation of Modelica models is a well established technology. However, optimization utilizing Modelica models is not yet advanced since the language lacks support for formulating such problems. In [Åkesson, 2008], the extension Optimica was proposed and includes notations for cost function and constraints as well as means to select optimization variables. Recently, the open-source platform JModelica.org was presented, which includes the Optimica compiler, see [Åkesson *et al.*, 2010]. JModelica.org can generate C code containing the model equations and XML code containing variables names and parameter values from the Modelica/Optimica models. It also includes an Application Programming Interface (API)

for evaluating the compiled Modelica model equations and optimization notions such as cost function and constraints specified in the Optimica code. Additionally, automatic differentiation is used for evaluation of Jacobians and sparsity patterns. The API also includes an algorithm for discretization of a dynamic optimization problem, such as the grade transition problem, by direct collocation on finite elements, see [Biegler *et al.*, 2002]. In the implemented method, state and algebraic variables are approximated by Lagrange polynomials based on Radau points of order three and two, respectively. The inputs may be discretized similarly to the algebraic variables or specified to be constant over each finite element. In the work presented in this paper, constant inputs over the finite elements are used. The discretization, which corresponds to a fully implicit Runge-Kutta method and thus has the same strong stability properties, results in a large NLP. This problem is efficiently solved by the large-scale NLP solver IPOPT, see [Wächter and Biegler, 2006], by providing it with derivatives and sparsity patterns of constraint Jacobians computed in the API. The collocation method incorporates constraints on states, algebraic variables and inputs directly and handles non-linear systems well and is thus suited for optimization of grade transitions based on the plant model in this paper.

4. Quality Variables

The main quality variables used today at Borealis AB are polymer melt index and density and reactor split factors. Both density and melt index may easily be measured in an industrial setting and are associated with end-use characteristics, see [Xie *et al.*, 1994, Richards and Congalidis, 2006]. The models that are used for describing density and melt index produced at a certain time instant are correlation models based on the work in [McAuley and MacGregor, 1991]. They use the power law relationship between melt index and weight average molecular weight, and relates the quality variables to raw material concentrations in the reactors.

The polymer in the reactors is composed of polymers that may have been produced during different reactor conditions. It is therefore important to separate between instantaneous properties, describing the polymer produced at a certain time instant, and bed average properties, describing the mean value of the polymer properties throughout the polymer mass in the reactor. The bed average melt index and density are found by mixing rules as proposed in [McAuley and MacGregor, 1991].

The cascaded reactors in the Borstar® process has the ability to produce a tri-modal polymer, i.e., the molecular weight distribution of the finished polymer has three peaks. However, as the production rate in the

pre-polymerization reactor is significantly smaller than in the loop reactor and the GPR, and the polymerization conditions are very similar in the pre-polymerization and the loop reactor, the polymer can be considered bi-modal. The model used in the optimizations does not contain such detailed information as molecular weight distribution. Instead, as a measure of the bi-modality, split factors between zero and one are used, providing information about how much of the finished polymer has been produced in each reactor. The split factor for the pre-polymerization reactor is close to zero, while for the loop reactor and the GPR, the split factors are close to 0.5. To provide a bed average measure of the bi-modality, bed average values of the split factors are used.

5. Plant Model

Modeling of a polymer reactor may be performed in different levels of detail and assumptions, see e.g., [Xie *et al.*, 1994], and the chosen level depend on model usage. The same holds for distillation columns, and as the considered plant incorporates three reactors and three distillation columns and the model should be used for optimization, macro-scale modeling is used. This means, no finer level of polymer modeling than e.g., mass balances and reaction rates are considered, which is appropriate for grade transition optimization as noted in [Xie *et al.*, 1994]. Also, simple dynamics with split factors for the distillation columns are used.

5.1 Reactor Models

The two loop reactors are both assumed to have perfect temperature control, constant pressures and well mixed contents. Control systems in regulatory mode are incorporated in the models for holding reactor content volumes constant using outflows as control variables. As the polymer slurry is taken out from the pre-polymerization reactor using transfer legs, the outflow has the same concentrations as the reactor content and the reactor may be modeled as an ideal continuously stirred tank reactor (CSTR). However, since the loop reactor uses both continuous outtake and settling legs, the outflow has a higher concentration of polymer than the reactor content, see [Reginato *et al.*, 2003]. Therefore, using a modeling approach of a non-ideal CSTR where the settling legs are modeled using a discharge factor is thus suitable, see [Reginato *et al.*, 2003, Touloupides *et al.*, 2010]. The subsequent flash tank is assumed to have negligible hold-up time compared to the reactors and recycle area and is excluded from the model.

The temperature in the GPR is assumed to be controlled to a constant value and the regulatory system for the bed volume is incorporated in

the model using the outflow as control variable. The polymer and gas in the bed are assumed well mixed and the conversion per pass-through is low. The gas composition in and above the bed is therefore assumed equal and uniform, see [McAuley and MacGregor, 1992, Xie *et al.*, 1994]. It is also assumed that the time delay associated with gas recycling through the cooler is negligible. With these assumptions, the GPR may be modeled with outflow and reactor bed concentrations equal. The subsequent separator between the GPR and the propane column has negligible hold-up time for the gas mixture and is excluded from the model together with the degassing tank.

The reactor models, derived by Borealis and used today in an on-line non-linear model predictive controller (NMPC) of the plant, include both first principles, semi-empirical, and empirical relations. For optimization, there are 12 control inflows of raw material, diluents and catalyst to the reactors and one flare flow from the GPR, as given in Section 2.

Pre-Polymerization Reactor For the pre-polymerization reactor, which has no direct inflows from the recycle area, the mass balances for fluids, polymer and catalyst are

$$\dot{m}_{e1} = u_{e1} - w_{e1} - r_{e1} \tag{1}$$
$$\dot{m}_{h1} = u_{h1} - w_{h1} - r_{h1} \tag{2}$$
$$\dot{m}_{p1} = u_{p1} - w_{p1} \tag{3}$$
$$\dot{m}_{pe1} = r_{pe1} - w_{pe11} \tag{4}$$
$$\dot{m}_{c1} = u_{c1} - w_{c1} \tag{5}$$
$$m_{f1} = m_{e1} + m_{h1} + m_{p1} \tag{6}$$
$$m_{s1} = m_{pe1} + m_{c1}, \tag{7}$$

where $w_{i1(1)}$ and r_{i1} are outflows and reaction rates, respectively, and m_{f1} and m_{s1} are total masses of fluids and solids. The reaction rates are extended non-linear Arrhenius expressions with pre-factors $R_{i1}(\cdot)$ depending on reactor condition, i.e.,

$$r_{e1} = R_{e1}(m_{c1}, a_1, X_{e1}, X_{h1}, P_1) \exp\left(\frac{k_{e11}}{T_1} + k_{e12}\right) \tag{8}$$
$$r_{h1} = R_{h1}(m_{c1}, a_1, X_{h1}, P_1) \exp\left(\frac{k_{h11}}{T_1} + k_{h12}\right) \tag{9}$$
$$r_{pe1} = r_{e1} + r_{h1}, \tag{10}$$

where P_1 and T_1 are the reactor pressure and temperature, respectively, k_{e11}, k_{e12}, k_{h11} and k_{h12} are reaction kinetics parameters and r_{pe1} is the

total reaction rate in the pre-polymerization reactor. The molar concentrations X_{i1} of the fluids are defined as

$$X_{i1} = \frac{m_{i1}/M_i}{\sum_{j\in\{e,h,p\}} m_{j1}/M_j}, \qquad i \in \{e,h,p\}, \tag{11}$$

where M_i and M_j are the molar weights of the different components.

The plant model use a Ziegler-Natta catalyst activity profile along the cascaded reactors, modeled with mean activity and deactivated sites. For the pre-polymerization reactor, the catalyst states are

$$\dot{a}_1 = f_{a1}(u_{c1}, m_{c1}, a_1, d_1, a_0, d_0, r_{pe1}) \tag{12}$$

$$\dot{d}_1 = f_{d1}(u_{c1}, m_{c1}, a_1, d_1, a_0, d_0), \tag{13}$$

where $f_{a1}(\cdot)$ and $f_{d1}(\cdot)$ are non-linear functions and a_0 and d_0 are initial values of mean activity and deactivated sites for unused catalyst.

Polymer properties such as melt index and density will be used for defining a polymer grade in the loop reactor and the GPR. However, reliable models of these quantities could not be found for the pre-polymerization reactor due to lack of data. Since production in the prepolymerization reactor compared to in the loop reactor and in the GPR is small and that it has similar reactor conditions as the loop reactor, its end effect on the product quality variables is negligible. Instead, for further calculations, polymer density is set to an average value ρ_{s1} of prepolymerization reactor polymer produced at the plant for different grades, while melt index is not calculated. To define the polymer grade in the prepolymerization reactor, the bed average of the molar ratio of hydrogen and ethylene will be used, which is calculated from the instantaneous ratio defined as

$$X_{he1} = \frac{X_{h1}}{X_{e1}}. \tag{14}$$

Using the solid-phase residence time, which is the ratio between mass of solids m_{s1} and solids outflow w_{s1}, the bed average ratio is found as

$$\dot{\overline{X}}_{he1}\frac{m_{s1}}{w_{s1}} = -\overline{X}_{he1} + X_{he1}. \tag{15}$$

Fluid density ρ_{f1} in the pre-polymerization reactor is calculated using an empirical relation depending on pressure, temperature and fluid molar concentrations, utilized when calculating reactor content volume V_1 as,

$$\rho_{f1} = \varrho_1(P_1, T_1, X_{e1}, X_{h1}, X_{p1}) \tag{16}$$

$$V_1 = \frac{m_{f1}}{\rho_{f1}} + \frac{m_{s1}}{\rho_{s1}}. \tag{17}$$

Assuming the reactor is always full of fluids and solids and that the fluid is incompressible, the total volumetric outflow q_1 is set by

$$q_1 = \frac{u_{p1} + u_{e1} + u_{h1}}{\rho_{f1}} + \frac{u_{c1}}{\rho_c} - r_{pe1}\left(\frac{1}{\rho_{f1}} - \frac{1}{\rho_{s1}}\right) + K_1\left(V_1 - V_1^{\text{ref}}\right), \quad (18)$$

where ρ_c is the catalyst density. The two first terms are the total inflow to the pre-polymerization reactor, while the third term compensate for volume contraction due to polymerization. At stationarity, due to the incompressibility assumptions on the fluids and the mass balances, the volumetric flow constituted of the three first terms is equal to the volumetric outflow. An additional volumetric outflow is added to obtain correct volume of reactor content at stationarity, i.e., a proportional controller with gain K_1 and set-point V_1^{ref}. At stationarity, the contribution of this terms is zero and there will be no stationary error of V_1.

The volumetric outflow from the pre-polymerization reactor is the sum of solid and fluid volumetric outflows, i.e.,

$$q_1 = \frac{w_{s1}}{\rho_{s1}} + \frac{w_{f1}}{\rho_{f1}}. \quad (19)$$

Since transfer legs are used, the ratio of solid and fluid outflows and the ratio of solid and fluid masses in the reactor are equal. Using this relation and solving for the two mass flows yields,

$$w_{s1} = \frac{m_{s1}}{\frac{m_{s1}}{\rho_{s1}} + \frac{m_{f1}}{\rho_{f1}}}\, q_1 \quad (20)$$

$$w_{f1} = \frac{m_{f1}}{\frac{m_{s1}}{\rho_{s1}} + \frac{m_{f1}}{\rho_{f1}}}\, q_1. \quad (21)$$

The component-wise fluid and solid outflows are found using mass fractions as

$$w_{i1} = \frac{m_{i1}}{m_{f1}}\, w_{f1}, \qquad i \in \{e, h, p\} \quad (22)$$

$$w_{j1} = \frac{m_{j1}}{m_{s1}}\, w_{s1}, \qquad j \in \{pe, c\}. \quad (23)$$

Loop Reactor The loop reactor has the same model structure as the pre-polymerization reactor. However, it has both fresh inflows, inflows from recycle area, and also inflows from the pre-polymerization reactor.

The mass balances for fluids, polymer and catalyst and the total mass of fluids and solids are written as,

$$\dot{m}_{e2} = u_{e2} + w_{e2}^{\text{rec}} + w_{e1} - w_{e2} - r_{e2} \tag{24}$$
$$\dot{m}_{h2} = u_{h2} + w_{h2}^{\text{rec}} + w_{h1} - w_{h2} - r_{h2} \tag{25}$$
$$\dot{m}_{p2} = u_{p2} + w_{p2}^{\text{rec}} + w_{p1} - w_{p2} \tag{26}$$
$$\dot{m}_{pe21} = w_{pe11} - w_{pe21} \tag{27}$$
$$\dot{m}_{pe2} = r_{pe2} - w_{pe22} \tag{28}$$
$$\dot{m}_{c2} = w_{c1} - w_{c2} \tag{29}$$
$$m_{f2} = m_{e2} + m_{h2} + m_{p2} \tag{30}$$
$$m_{s2} = m_{pe21} + m_{pe2} + m_{c2}, \tag{31}$$

where superscript rec indicates that a flow is coming from the recycle area. The outflows are controlled by a volume controller and a settling factor models the settling leg effect. To be able to calculate the grade defining split factors, the polymer mass in the loop reactor is divided into two states. First, m_{pe21} is the mass of polyethylene formed in the pre-polymerization reactor and second, m_{pe2} is the mass polyethylene formed in the loop reactor.

Similar to the pre-polymerization reactor, the reaction rates are extended non-linear Arrhenius expressions as

$$r_{e2} = R_{e2}(m_{c2}, a_2, X_{e2}, X_{h2}, P_2) \exp\left(\frac{k_{e21}}{T_2} + k_{e22}\right) \tag{32}$$
$$r_{h2} = R_{h2}(m_{c2}, a_2, X_{h2}, P_2) \exp\left(\frac{k_{h21}}{T_2} + k_{h22}\right) \tag{33}$$
$$r_{pe2} = r_{e2} + r_{h2}, \tag{34}$$

where P_2 and T_2 are the reactor pressure and temperature, respectively, k_{e21}, k_{e22}, k_{h21} and k_{h22} are reaction kinetics parameters and r_{pe2} is the total reaction rate in the loop reactor. The molar concentrations X_{i2} of fluids are found as,

$$X_{i2} = \frac{m_{i2}/M_i}{\sum\limits_{j\in\{e,h,p\}} m_{j2}/M_j}, \qquad i \in \{e,h,p\}, \tag{35}$$

where M_i and M_j are the molar weights of the different components.

The catalyst properties have non-linear dependencies on catalyst inflow and mass and total reaction rate, similar to the catalyst property

models in the pre-polymerization reactor model, i.e.,

$$\dot{a}_2 = f_{a2}(w_{c1}, m_{c2}, a_2, d_2, a_1, d_1, r_{pe2}) \tag{36}$$

$$\dot{d}_2 = f_{d2}(w_{c1}, m_{c2}, a_2, d_2, a_1, d_1). \tag{37}$$

Modeling of the polymer density in the loop reactor could not be performed reliably due to lack of plant data. Therefore, the density was set to an average value ρ_{s2} of the loop polymer produced at the plant for different grades, yielding the instantaneous and bed average densities equal. As the polymer in the loop reactor is produced without any co-monomer, no branching of the polymer is present which results in a polymer density with only minor variations due to raw material concentrations. Thus, a constant value is justified. Fluid density may, as in the previous reactor, be calculated using an empirical relation and is used when calculating reactor content volume V_2 as

$$\rho_{f2} = \varrho_2(P_2, T_2, X_{e2}, X_{h2}, X_{p2}) \tag{38}$$

$$V_2 = \frac{m_{f2}}{\rho_{f2}} + \frac{m_{s2}}{\rho_{s2}}, \tag{39}$$

where m_{f2} and m_{s2} are total masses of fluids and solids, respectively.

As for the pre-polymerization reactor, the volumetric outflow is set by the total volumetric inflow, a volume contraction term due to polymerization, and a proportional controller with gain K_2 and set-point V_2^{ref} for obtaining correct stationary volume, i.e.,

$$\begin{aligned} q_2 = {} & \frac{u_{p2} + u_{e2} + u_{h2}}{\rho_{f2}} + \frac{w_{p2}^{\text{rec}} + w_{e2}^{\text{rec}} + w_{h2}^{\text{rec}}}{\rho_{f2}} \\ & + \frac{w_{s1}}{\rho_{s2}} + \frac{w_{f1}}{\rho_{f2}} - r_{pe2}\left(\frac{1}{\rho_{f2}} - \frac{1}{\rho_{s2}}\right) + K_2\left(V_2 - V_2^{\text{ref}}\right). \end{aligned} \tag{40}$$

The volumetric outflow is composed of solid and fluid flows as

$$q_2 = \frac{w_{s2}}{\rho_{s2}} + \frac{w_{f2}}{\rho_{f2}}. \tag{41}$$

As the loop reactor uses settling legs, the concentration of solids is higher in the outflow than in the reactor. The ratio of solid and fluid outflows is not equal to the ratio of solid and fluid masses in the reactor and is instead modeled using a settling factor $s_2 > 1$ and the mass fraction z_{s2} of solids in the reactor as,

$$w_{f2} = w_{s2} g_2 \tag{42}$$

$$g_2 = \frac{1 - s_2 z_{s2}}{s_2 z_{s2}}, \tag{43}$$

where the mass fraction of solids is

$$z_{s2} = \frac{m_{s2}}{m_{s2} + m_{f2}}. \tag{44}$$

Solving for solid and fluid flows in Eq. (41) and using Eq. (42) yields

$$w_{s2} = \frac{1}{\frac{1}{\rho_{s2}} + \frac{g_2}{\rho_{f2}}} q_2 \tag{45}$$

$$w_{f2} = \frac{g_2}{\frac{1}{\rho_{s2}} + \frac{g_2}{\rho_{f2}}} q_2. \tag{46}$$

For a settling factor $s_2 = 1$, no settling of the polymer is present and the above equations degenerate to equations similar to the pre-polymerization reactor case. However, for the loop reactor, a settling factor of $s_2 > 1$ is used due to the settling legs.

The component-wise fluid and solid outflows used in the mass balances are found by the mass ratios of the reactor content and the fluid and solid outflows, i.e.,

$$w_{i2} = \frac{m_{i2}}{m_{f2}} w_{f2}, \qquad i \in \{e, h, p\} \tag{47}$$

$$w_{j2} = \frac{m_{j2}}{m_{s2}} w_{s2}, \qquad j \in \{pe, c\} \tag{48}$$

$$w_{pe21} = \frac{m_{pe21}}{m_{s2}} w_{s2}. \tag{49}$$

A model for the instantaneous melt index MI_2 of the loop reactor produced polymer, based on the work in [McAuley and MacGregor, 1991], is used. The model has the structure

$$\ln MI_2 = l_{21} + \beta \ln \left(l_{22} + l_{23} \frac{X_{h2}}{X_{e2}} \right), \tag{50}$$

where X_{h2} and X_{e2} are molar concentrations of hydrogen and ethylene, respectively, β is a constant approximately equal to 3.5, see [Vinodograd and Malkin, 1980] and l_{21}, l_{22} and l_{23} are model parameters. Following [McAuley and MacGregor, 1991], the dynamics of the bed average melt index is found by mixing the current bed average with the melt index of the currently produced polymer as

$$\frac{d}{dt} \left(\overline{MI}_2^{-\frac{1}{\beta}} \right) \frac{m_{s2}}{w_{s2}} = -\overline{MI}_2^{-\frac{1}{\beta}} + MI_2^{-\frac{1}{\beta}}, \tag{51}$$

where the quotient m_{s2}/w_{s2} is the solid-phase residence time of the loop reactor.

Note that there is no modeling of the mixing of pre-polymerization reactor polymer and loop reactor polymer with regards to quality variables, motivated by the low production of polymer in the pre-polymerization reactor and similar reactor conditions. It is thus assumed that the polymer transferred out from the loop reactor have density and melt index equal to the density and melt index of the polymer produced in the loop reactor.

Gas-Phase Reactor Except for the fluid components in the two previous reactors, the co-monomer butene and the diluent nitrogen are used in the GPR. The mass balances for the gases, polymer produced in either pre-polymerization reactor, loop reactor or GPR and catalyst and total masses of gas and polymer are given by

$$\dot{m}_{e3} = u_{e3} + w_{e3}^{\text{rec}} - w_{e3}^{\text{flare}} - w_{e3} - r_{e3} \tag{52}$$
$$\dot{m}_{h3} = u_{h3} + w_{h3}^{\text{rec}} - w_{h3}^{\text{flare}} - w_{h3} - r_{h3} \tag{53}$$
$$\dot{m}_{b3} = u_{b3} + w_{b3}^{\text{rec}} - w_{b3}^{\text{flare}} - w_{b3} - r_{b3} \tag{54}$$
$$\dot{m}_{p3} = u_{p3} + w_{p3}^{\text{rec}} - w_{p3}^{\text{flare}} - w_{p3} + u_{p3}^{f} \tag{55}$$
$$\dot{m}_{n3} = u_{n3} + w_{n3}^{\text{rec}} - w_{n3}^{\text{flare}} - w_{n3} \tag{56}$$
$$\dot{m}_{pe31} = w_{pe21} - w_{pe31} \tag{57}$$
$$\dot{m}_{pe32} = w_{pe22} - w_{pe32} \tag{58}$$
$$\dot{m}_{pe3} = r_{pe3} - w_{pe33} \tag{59}$$
$$\dot{m}_{pb3} = r_{pb3} - w_{pb33} \tag{60}$$
$$\dot{m}_{c3} = w_{c2} - w_{c3} \tag{61}$$
$$m_{f3} = m_{e3} + m_{h3} + m_{b3} + m_{p3} + m_{n3} \tag{62}$$
$$m_{s3} = m_{pe31} + m_{pe32} + m_{pe3} + m_{pb3} + m_{c3}, \tag{63}$$

where w_{i3}^{flare} is the flare flow of component i, u_{p3}^{f} is the fixed propane purge flow assuring no leakage of GPR gas mixture to the flash tank and m_{pb3} is the mass of polyethylene with incorporated butene. The total solids outflow from the GPR is the production rate of the plant, i.e.,

$$w_{s3} = w_{pe31} + w_{pe32} + w_{pe33} + w_{pb33} + w_{c3}. \tag{64}$$

The reaction rates are analogous to the reaction rates in the two pre-

vious reactors, i.e.,

$$r_{e3} = R_{e3}(m_{c3}, a_3, X_{e3}, X_{h3}, X_{b3}, P_3) \exp\left(\frac{k_{e31}}{T_3} + k_{e32}\right) \tag{65}$$

$$r_{h3} = R_{h3}(m_{c3}, a_3, X_{h3}, P_3) \exp\left(\frac{k_{h31}}{T_3} + k_{h32}\right) \tag{66}$$

$$r_{b3} = R_{b3}(m_{c3}, a_3, X_{b3}, P_3) \exp\left(\frac{k_{b31}}{T_3} + k_{b32}\right) \tag{67}$$

$$r_{pe3} = r_{e3} + r_{h3} \tag{68}$$

$$r_3 = r_{pe3} + r_{b3}, \tag{69}$$

where P_3 and T_3 are the pressure and temperature, respectively, k_{e31}, k_{e32}, k_{h31}, k_{h32}, k_{b31} and k_{b32} are reaction kinetics parameters and r_3 is the total reaction rate in the GPR. The reaction rate of hydrogen is several magnitudes smaller than for ethylene and butene and it is assumed that all reacted hydrogen gives polyethylene without incorporated butene.

The catalyst property models are similar to the analogous in the prepolymerization and loop reactor models, i.e.,

$$\dot{a}_3 = f_{a3}(w_{c2}, m_{c3}, a_3, d_3, a_2, d_2, r_3) \tag{70}$$

$$\dot{d}_3 = f_{d3}(w_{c2}, m_{c3}, a_3, d_3, a_2, d_2), \tag{71}$$

and so is also the fluid molar concentrations X_{i3},

$$X_{i3} = \frac{m_{i3}/M_i}{\sum\limits_{j\in\{e,h,b,p,n\}} m_{j3}/M_j}, \qquad i \in \{e,h,b,p,n\}, \tag{72}$$

where M_i and M_j are molar weights of the different components.

The instantaneous split factors for the polymer in the GPR may be calculated directly from the different polymer masses as

$$S_1 = \frac{m_{pe31}}{m_{pe31} + m_{pe32} + m_{pe3} + m_{pb3}} \tag{73}$$

$$S_2 = \frac{m_{pe32}}{m_{pe31} + m_{pe32} + m_{pe3} + m_{pb3}} \tag{74}$$

$$S_3 = \frac{m_{pe3} + m_{pb3}}{m_{pe31} + m_{pe32} + m_{pe3} + m_{pb3}}, \tag{75}$$

and using the GPR solids residence time m_{s3}/w_{s3}, the bed average bi-

modality measures are given by

$$\dot{\overline{S}}_1 \frac{m_{s3}}{w_{s3}} = -\overline{S}_1 + S_1 \tag{76}$$

$$\dot{\overline{S}}_2 \frac{m_{s3}}{w_{s3}} = -\overline{S}_2 + S_2 \tag{77}$$

$$\dot{\overline{S}}_3 \frac{m_{s3}}{w_{s3}} = -\overline{S}_3 + S_3. \tag{78}$$

The polymer in the GPR is essentially a mixture of loop produced polymer and polymer being produced in the GPR. Several mixing rules for polymers with different melt indices and densities exist and the most commonly used in literature are presented in [McAuley and MacGregor, 1991] and will also be used here.

The instantaneous melt index of the mixed polymer is calculated from the bed average melt index $\overline{MI}_2$ of the incoming loop reactor polymer and the instantaneous melt index MI_3 of the polymer produced in the GPR as

$$MI_{\text{mix}}^{-\frac{1}{\beta}} = (1 - S_3)\overline{MI}_2^{-\frac{1}{\beta}} + S_3 MI_3^{-\frac{1}{\beta}}. \tag{79}$$

MI_3 is modeled by following the structure in [McAuley and MacGregor, 1991] as

$$\ln MI_3 = l_{31} + \beta \ln \left(l_{32} + l_{33}\frac{X_{h3}}{X_{e3}} + l_{34}\frac{X_{b3}}{X_{e3}} \right), \tag{80}$$

where l_{31}, l_{32}, l_{33} and l_{34} are model parameters. The bed average melt index $\overline{MI}_{\text{mix}}$ of the mixed polymer in the GPR, i.e., the melt index of the final product, is found by mixing bed average melt index and instantaneous melt index of polymer added to the bed as

$$\frac{d}{dt}\left(\overline{MI}_{\text{mix}}^{-\frac{1}{\beta}}\right)\frac{m_{s3}}{w_{s3}} = -\overline{MI}_{\text{mix}}^{-\frac{1}{\beta}} + MI_{\text{mix}}^{-\frac{1}{\beta}}. \tag{81}$$

The instantaneous density ρ_{mix} of the mixed polymer in the GPR is calculated as

$$\frac{1}{\rho_{\text{mix}}} = \frac{1 - S_3}{\rho_{s2}} + \frac{S_3}{\rho_{s3}}, \tag{82}$$

where ρ_{s2} is the density of the polymer from the loop reactor and ρ_{s3} is the instantaneous density of polymer produced in the GPR. Again, using the model structure in [McAuley and MacGregor, 1991], ρ_{s3} may be calculated as

$$\rho_{s3} = p_{31} + p_{32} \ln MI_3 - p_{33}\left(\frac{X_{b3}}{X_{e3}}\right)^{p_{34}}, \tag{83}$$

where p_{31}, p_{32}, p_{33} and p_{34} are model parameters. The bed average density $\overline{\rho}_{\text{mix}}$ of the mixed polymer in the GPR is found from

$$\frac{d}{dt}\left(\frac{1}{\overline{\rho}_{\text{mix}}}\right)\frac{m_{s3}}{w_{s3}} = -\frac{1}{\overline{\rho}_{\text{mix}}} + \frac{1}{\rho_{\text{mix}}}. \tag{84}$$

The gas density ρ_{f3} in the reactor is found by using the total reactor volume V_3 as

$$\rho_{f3} = \frac{m_{f3}}{V_3 - V_{s3}}, \tag{85}$$

where V_{s3} is the solids volume, i.e.,

$$V_{s3} = \frac{m_{s3}}{\overline{\rho}_{\text{mix}}}, \tag{86}$$

and m_{f3} is the total mass of gas in the GPR. The reactor pressure is subsequently given by the ideal gas law as

$$P_3 = \frac{\rho_{f3} R T_3}{\overline{M}_3}, \tag{87}$$

where $\overline{M}_3$ is the mean molar weight of the gases, i.e.,

$$\overline{M}_3 = \frac{\sum_{i\in\{e,h,b,p,n\}} m_{i3}}{\sum_{j\in\{e,h,b,p,n\}} m_{j3}/M_j}, \tag{88}$$

and M_j is the molar weight of component j.

The partial pressures in the reactor are found by the reactor pressure and the molar concentrations as

$$P_{i3} = P_3 X_{i3}, \qquad i \in \{e,h,b,p,n\}. \tag{89}$$

The fluidized bed in the GPR is composed of both polymer and gas and its density depends on the gas velocity through the reactor. As the velocity is close to constant, and both ρ_{f3} and $\overline{\rho}_{\text{mix}}$ only have minor variations, the bed density ρ_{b3} is assumed constant in the model. The total bed volume V_{b3}, used for bed volume control in the model, is the sum of gas volume V_{fb3} in the bed and polymer volume V_{s3}, i.e.,

$$V_{b3} = V_{fb3} + V_{s3}. \tag{90}$$

The total mass of the fluidized bed, i.e., both polymer and gases, is

$$V_{b3}\rho_{b3} = V_{fb3}\rho_{f3} + V_{s3}\overline{\rho}_{\text{mix}} \tag{91}$$

and solving for gas volume in the bed yields

$$V_{fb3} = \frac{\overline{\rho}_{\text{mix}} - \rho_{b3}}{\rho_{b3} - \rho_{f3}} V_{s3}, \tag{92}$$

which may be used when calculating total bed volume.

The outflow from the GPR is at the bottom of the bed, and the ratio of solids and gas in the bed and the ratio of solids and gas in the outflow are thus equal. The volumetric outflow is set by a PI bed volume controller with set-point V_{b3}^{ref}, i.e.,

$$q_3 = K_3\left(V_{b3} - V_{b3}^{\text{ref}}\right) + K_4 \int_{-\infty}^{t} \left(V_{b3} - V_{b3}^{\text{ref}}\right) d\tau, \tag{93}$$

with proportional and integral gain K_3 and K_4, respectively. The mass outflows of solids and gas are found by using the volumetric outflow and the bed density as

$$w_{s3} = \frac{m_{s3}}{m_{s3} + V_{fb3}\rho_{f3}} \rho_{b3} q_3 \tag{94}$$

$$w_{f3} = \frac{V_{fb}\rho_{f3}}{m_{s3} + V_{fb}\rho_{f3}} \rho_{b3} q_3. \tag{95}$$

The component-wise bottom outflows are given by the mass ratios and the gas and solids outflows, i.e.,

$$w_{i3} = \frac{m_{i3}}{m_{f3}} w_{f3}, \qquad i \in \{e, h, b, p, n\} \tag{96}$$

$$w_{j3} = \frac{m_{j3}}{m_{s3}} w_{s3}, \qquad j \in \{pe, pb, c\} \tag{97}$$

$$w_{pe31} = \frac{m_{pe31}}{m_{s3}} w_{s3} \tag{98}$$

$$w_{pe32} = \frac{m_{pe32}}{m_{s3}} w_{s3}. \tag{99}$$

Similarly, the component-wise outflows in the flare flow are

$$w_{i3}^{\text{flare}} = \frac{m_{i3}}{m_{f3}} u_{\text{flare}}, \qquad i \in \{e, h, b, p, n\}. \tag{100}$$

5.2 Distillation Column Models

Modeling of distillation columns may be made very detailed. However, even these detailed models will not describe the recycle area completely since there is also an extensive overlaying control system of the columns and also e.g., pre-condensers and different transport systems for the gas needed to be modeled. The columns also have 3–5 inflow components and the propane column has a side flow, which comprise an even greater modeling task. Additionally, similar to the reactors, a high level of detailed modeling of the distillation columns are not feasible if the models are to be used for optimization.

Two of the most important aspects of recycle area modeling are to estimate how much of the total inflow of components to the reactors are recycle flows and how the recycle flows change when the plant operating point is changed. For instance, approximately half of all hydrogen to the loop reactor is recycled hydrogen and even more for the GPR. Additionally, the recycled part of total butene inflow to the GPR is comparable in size to the fresh feed.

The structure chosen for the recycle area model is similar to the one used in the off-line planning and optimization models currently in use by Borealis AB cracker plant, see [Andersson *et al.*, 2002]. It is assumed that pressures and temperatures in the columns are perfectly controlled, which thus gives constant split factors for the components. Every distillation column together with its control system and supporting components such as pre-condensers, are lumped together to one system where the dominating time constant for each component flow into the system is estimated from measurement data. However, the measurement data could not give a complete mass balance over each system due to lack of sensors and insufficient data quality, and could therefore not support modeling of different time constants for e.g. top, side, and bottom flows of the columns. A crude approximation was made by setting these equal.

Two control flows are present in the recycle area, i.e., the off-gas flows u_{op} and u_{ol} on the propane and lights column, respectively.

Propane Column The overall propane column system is modeled as described above, and each component has an associated time constant T_{i4} as,

$$\dot{w}_{i4} T_{i4} = -w_{i4} + w_{i3}, \quad i \in \{e, h, b, p, n\}, \tag{101}$$

where w_{i3} is the component flow from the GPR. The resulting flows are then divided into the different outtake flows of the system, i.e., top, side

Table 2. Propane and lights column split factors.

	i	e	h	b	p	n
Propane Column	Top, S_{i4}^t	0.88	1	0.13	0.35	1
	Side, S_{i4}^s	0.09	0	0	0.44	0
	Bottom, S_{i4}^b	0.03	0	0.87	0.21	0
Lights Column	Top, S_{i6}^t	1	1	-	0.1	-
	Bottom, S_{i6}^b	0	0	-	0.9	-

and bottom flow, as

$$w_{i4}^t = S_{i4}^t w_{i4} \tag{102}$$
$$w_{i4}^s = S_{i4}^s w_{i4} \tag{103}$$
$$w_{i4}^b = S_{i4}^b w_{i4}, \tag{104}$$

where S_{i4}^t, S_{i4}^s and S_{i4}^b are the component split factors for top, side and bottom, respectively, and are found in Table 2. It is assumed that the light components hydrogen and nitrogen are only present at column top. The heaviest component, i.e., butene, is present at both top and bottom, but not side. Some butene is condensed together with light components in the pre-condenser and added to the top flow back to the GPR, while the column itself is assumed to distill butene only to the bottom. The two remaining components, i.e., propane and ethylene, are present in all outtakes.

The off-gas flow u_{op} is taken from the top flow and may be used for control purposes since this flow has a higher concentration of light components than the gas in the GPR. The component-wise recycle flows back to the GPR, i.e., w_{i3}^{rec}, are thus,

$$w_{i3}^{\text{rec}} = w_{i4}^t + w_{i4}^b - w_{i4}^{op}, \quad i \in \{e,h,b,p,n\}, \tag{105}$$

where the component-wise off-gases are

$$w_{i4}^{op} = \frac{w_{i4}^t}{\sum\limits_{j\in\{e,h,b,p,n\}} w_{j4}^t} u_{op}, \quad i \in \{e,h,b,p,n\}. \tag{106}$$

The side flows w_{i4}^s are led to the heavies column for further processing.

Heavies Column Since the reactor models do not include the production of heavier components such as pentane, hexane, etc., and oligomers, the bottom flow of the heavies column is assumed to be zero, and all inflow components are distilled to the column top. This assumption yields that no split factors are needed for the heavies column and the component flows are

$$\dot{w}_{i5} T_{i5} = -w_{i5} + w_{i2} + w_{i4}^{s}, \quad i \in \{e, h, p\}, \tag{107}$$

where w_{i2} and w_{i4}^{s} are the component flows from the loop reactor and the propane column, respectively, and T_{i5} is the associated time constant of the component. Since it is assumed that all nitrogen and butene in the propane column are recycled directly back to the GPR, the heavies column model incorporates only ethylene, hydrogen and propane.

Lights Column The only inflow to the lights column is from the heavies column and it is therefore only necessary to model ethylene, hydrogen and propane. With measurement data support, it is assumed that the majority of propane is distilled to the column bottom, while all lighter components are distilled to the column top.

The model structure is similar to the propane column model, using an associated time constant and split factors for each component as

$$\dot{w}_{i6} T_{i6} = -w_{i6} + w_{i5} \tag{108}$$

$$w_{i6}^{t} = S_{i6}^{t} w_{i6} \tag{109}$$

$$w_{i6}^{b} = S_{i6}^{b} w_{i6}, \tag{110}$$

where $i \in \{e, h, p\}$. The split factors for the three different components are found in Table 2. The recycle inflow to the loop reactor is the top flow from the lights column except for the off-gas flow u_{ol}, which may be used for control purposes since the light component concentration is high in the recycle flow compared to the concentration in the loop reactor. The component-wise recycle flows are thus

$$w_{i2}^{\mathrm{rec}} = w_{i6}^{t} - w_{i6}^{ol}, \quad i \in \{e, h, p\} \tag{111}$$

with the component-wise off-gas flows

$$w_{i6}^{ol} = \frac{w_{i6}^{t}}{\sum\limits_{j \in \{e,h,p\}} w_{j6}^{t}} u_{ol}, \quad i \in \{e, h, p\}. \tag{112}$$

5.3 Model Form and Size

If a state, algebraic variable and input vector are defined and denoted $\mathbf{x}$, $\mathbf{w}$ and $\mathbf{u}$, respectively, the plant model may be written as a general non-linear index-1 differential-algebraic equation (DAE) as

$$\begin{aligned} \mathbf{0} &= \mathbf{F}\left(\dot{\mathbf{x}}, \mathbf{x}, \mathbf{w}, \mathbf{u}\right) \\ \mathbf{y} &= \mathbf{g}_{\mathbf{y}}\left(\mathbf{x}, \mathbf{w}, \mathbf{u}\right) \\ \mathbf{z} &= \mathbf{g}_{\mathbf{z}}\left(\mathbf{x}, \mathbf{w}, \mathbf{u}\right) \\ \mathbf{x}(t_0) &= \mathbf{x}_0, \end{aligned} \tag{113}$$

where $\mathbf{x}_0$ is the initial state, $\mathbf{y}$ are variables that will be used for defining a polymer grade and $\mathbf{z}$ are additional reactor operation variables with target values that must be considered explicitly. The number of states, algebraic variables and inputs are 46, 167 and 15, respectively, and the number of equations is 213 when disregarding $\mathbf{g}_{\mathbf{y}}$ and $\mathbf{g}_{\mathbf{z}}$.

6. Grade Definition

A polymer grade is defined by the quality variables described in Section 4. As there is no model for melt index in the pre-polymerization reactor, the molar ratio of hydrogen and ethylene is used. The melt index may be modeled dependent only on this ratio and is thus then indirectly determined. For the loop reactor, however, the melt index is specified, which indirectly specifies the raw material molar ratio. For the GPR, both melt index and density are specified, and thus the molar ratio of hydrogen and ethylene and the molar ratio of butene and ethylene are determined. The split factors are specified for the GPR, determining how much of the product is produced in each reactor and hence the bi-modality of the product. Thus, the output vector $\mathbf{y}$, considering polymer quality variables, is

$$\mathbf{y} = [\,\overline{X}_{he1} \quad \overline{MI}_2 \quad \overline{MI}_{\text{mix}} \quad \overline{\rho}_{\text{mix}} \quad \overline{S}_1 \quad \overline{S}_2 \quad \overline{S}_3\,]^T . \tag{114}$$

Two different grades will be considered in the sequel, denoted A and B, and their quality variable values and sell prices E_j, $j \in \{\text{A, B}\}$, are found in Table 3. The quality variables are scaled with grade A values and sell prices are scaled with the ethylene price. These two grades were chosen mainly because all grade variables are different, except for the pre-polymerization reactor split factor which is rarely changed in practice. The transitions between the two grades require increases of hydrogen masses in the reactors, but also decreases, which is significantly harder,

Table 3. Grade defining variables with intervals, product sell prices, and instantaneous profits for grade A and B.

Grade	$\overline{X}_{he1}$	$\overline{MI}_2$	$\overline{MI}_{\text{mix}}$	$\overline{\rho}_{\text{mix}}$	$\overline{S}_1$	$\overline{S}_2$	$\overline{S}_3$	E_j	R_j
A	1.00	1.00	1.00	1.000000	1.000	1.000	1.000	1.24	1.00
B	0.37	6.50	3.51	1.001065	1.000	1.132	0.917	1.46	1.92
±%	±5	±5	±5	±0.1	±0.5	±0.5	±0.5	-	-

Table 4. Target, minimum and maximum values for operation variables for both grade A and B.

Variable	Target	Min	Max
P_3	1	0.99	1.01
P_{p3}	1	0.77	1.08

see [McAuley and MacGregor, 1992]. Additionally, for the same plant production rate, the reaction rates in the loop reactor and the GPR are different for the two grades, and so is the co-monomer content in the polymer, requiring significant changes of both ethylene and butene inflows.

In practice, it is impossible to have the quality variables identical to the defined grade values, i.e., on target values, during long term production. Therefore, the product is considered on-grade if the quality variables are within certain intervals. The sell price E_j of grade j polymer is in practice indifferent to whether the polymer is on target values or only considered on-grade, e.g., a quality variable is only inside specified interval and not on target value. Percentages of the quality variable grade values are used for determining the intervals, see Table 3. However, a product with one or many quality variables on the interval limits is undesirable from a customers point of view, and thus also from the polymer producers', which gives an incentive to be as close as possible to the defined grade values.

Apart from the variables defining a grade, many other variables have targets during operation. Two of these operation variables that will be considered here are the pressure in the GPR and the partial pressure of propane in the GPR, which are included in the output $\mathbf{z}$ in Eq. (113), i.e.,

$$\mathbf{z} = [\, P_3 \quad P_{p3} \,]^T . \tag{115}$$

Normalized target values of the two pressures together with their maximum and minimum values are found in Table 4.

7. Optimization Formulations

This section presents formulations of the stationary optimization problem as well as the grade change optimization problem regarding costs and revenues.

7.1 Plant Constraints

Operating a plant requires several constraints to be respected. Not only are limitations set by operating equipment, but also safety and operating conditions are crucial.

The manipulated inflows have minimum and maximum values set by e.g., minimum cooling by diluents or by maximum pump capacity. The rate of change of the inflows are also constrained due to equipment limitations, but also safety. Changing for instance the inflow of catalyst drastically may have undesirable effects both on raw material concentrations, reaction rates and temperatures in the reactors. The flare flow of the GPR is in practice used for pressure control and may also be used when reactor gas content is to be exchanged rapidly. However, it is desired to have it equal to zero, which is its minimum value set in the model. All minimum and maximum values concerning the control flows are taken from the currently running NMPC.

As seen in Section 6, constraints are set on the GPR pressure, but also on the propane partial pressure and hence the concentration of propane. Such constraints are present on all raw material and diluent molar concentrations in all three reactors. This limits the operating range of the reactors to regions known to be safe. An example is the upper limit on the partial pressure of ethylene in the GPR. As the polymer can be electrostatically charged, it may stick to the reactor walls. A too high ethylene molar concentration can then give high local reaction rate, and since the cooling may not be sufficient, this can lead to lump formation of the polymer.

Minimum and maximum values are also set for both instantaneous and bed average quality variables. During a grade change, a rapid transition of $\mathbf{y}$ from one grade definition to another, requires the instantaneous measures to over- or undershoot. If this is made too aggressively, the polymer outflow from a reactor may be composed of polymers that have widely different instantaneous quality variable values, even though the bed average quality variables are on grade target values, see e.g., [McAuley and MacGregor, 1992].

Component masses in the reactors are constrained by limits of total mass of solids and fluids or gases in the reactors and the molar concentration constraints. The outflow of solids from the reactors, and thus essentially the total reaction rates, have upper limits due to limitations on the systems transferring polymer out from the reactors. Additionally, as

the outflow of solids from the GPR, i.e., the production rate of the plant, is sent downstream for further processing, it must be limited such that subsequent production units are capable of managing the flow.

The recycle part is modeled only with flows and split factors which allows only to set upper and lower limits on the flows. Lower limits on the column off-gases are set in practice to always have bleeds of impurities and undesired inert components, such as ethane, that are produced at polymerization. The plant model does not incorporate these components, but minimum values that are greater than zero are set on the off-gas flows to resemble current practice and are taken from the currently running NMPC.

7.2 Stationary Optimization

At stationary economically optimal production, all quality variables are on grade target values together with the operation variables. Inflows and off-gases are used such that the profit is maximized during production and constraints on both states, algebraic variables and control flows are respected. The considered model has several inflows to be used at optimization and their respective cost, C_i, $i \in \{c, e, h, b, p, n\}$, normalized by the cost of ethylene, can be found in Table 5. Off-gases from the propane and lights columns are sent to other parts of the industrial area and their sell price E_{og} is also found in the table. The flare flow of the GPR however, is burnt directly, and produces no revenue. The instantaneous production profit at on-target production of grade j may be written as

$$R_j = E_j w_{s3} + E_{og} u_{ol} + E_{og} u_{op} + C_p w_{p6}^b - \sum_{i \in \{c,e,h,p\}} C_i u_{i1} - \sum_{i \in \{e,h,p\}} C_i u_{i2} - \sum_{i \in \{e,h,b,p,n\}} C_i u_{i3} - C_p u_{p3}^f. \quad (116)$$

The first term is the revenue due to produced polymer since w_{s3} is the solids outflow from the GPR, i.e., total plant production, while the two next terms are revenues from selling the off-gas flows u_{ol} and u_{op}. The fourth term is the bottom flow of propane from the lights column that is stored in a propane buffer, which is considered to be outside the plant boundaries. The three first negative terms refer to the cost of controlled

Table 5. Costs and sell prices for raw materials, diluents, off-gas and off-grade polymer.

C_c	C_e	C_h	C_b	C_p	C_n	E_{og}	E_{off}
214.6	1.000	8.003	1.419	0.501	0.044	0.266	0.880

fresh inflows to the three reactors, while the last term considers the cost of the fixed purge flow of propane for assuring no leakage of GPR recycle gas to the flash tank.

At economical optimum, the instantaneous profit is maximized, and the desired stationary point is found by solving the following optimization problem,

$$\begin{aligned} \min_{\dot{\mathbf{x}},\mathbf{x},\mathbf{w},\mathbf{u}} \quad & -R_j \\ \text{s.t. } \mathbf{0} &= \mathbf{F}\left(\dot{\mathbf{x}},\mathbf{x},\mathbf{w},\mathbf{u}\right) \\ \mathbf{y}_j &= \mathbf{g}_{\mathbf{y}}\left(\mathbf{x},\mathbf{w},\mathbf{u}\right) \\ \mathbf{z}_j &= \mathbf{g}_{\mathbf{z}}\left(\mathbf{x},\mathbf{w},\mathbf{u}\right) \\ \dot{\mathbf{x}} &= \mathbf{0} \\ \mathbf{x}_{\min} \leq \mathbf{x} &\leq \mathbf{x}_{\max} \\ \mathbf{w}_{\min} \leq \mathbf{w} &\leq \mathbf{w}_{\max} \\ \mathbf{u}_{\min} \leq \mathbf{u} &\leq \mathbf{u}_{\max}, \end{aligned} \tag{117}$$

where R_j is the instantaneous profit for grade j defined in Eq. (116). The vector $\mathbf{y}_j$ contains the grade defined values in Table 3 and thus, the second equality constraint considers on-target production. The third equality constraint considers production target values $\mathbf{z}_j$ found in Table 4 for the operation variables $\mathbf{z}$, and the fourth equality constraint sets stationary production. Inequality constraints are set on states, algebraic variables and control flows according to the discussion in Section 7.1.

7.3 Dynamic Optimization

The economically optimal grade change transfers the plant from stationary production of start grade to stationary production of end grade, with the performance objective of maximizing total profit during transition. The optimization problem posed must thus include the revenue as a function of the quality variables and their specification intervals.

Considering solely product j, the product sell price E_j is only received if all quality variables are inside their intervals specified in Table 3, otherwise, the polymer must be sold at a lower off-grade price denoted E_{off}, see Table 5. Introduce the ideal on-grade function for grade j as

$$\theta_j(\mathbf{y}) = \begin{cases} 1 & \text{if } y_{ji}^{\min} \leq y_i \leq y_{ji}^{\max}, \quad i \in \{1,\ldots,7\} \\ 0 & \text{otherwise,} \end{cases} \tag{118}$$

where $y_{ji}^{\min}$ and $y_{ji}^{\max}$ are the minimum and maximum value of the interval for the ith quality variable in $\mathbf{y}$ for grade j in Table 3. Then Eq. (116)

may be extended to include quality variable intervals for grade j as

$$R_j = ((E_j - E_{\text{off}})\theta_j(\mathbf{y}) + E_{\text{off}})\, w_{s3} + E_{og}u_{ol} + E_{og}u_{op} + C_p w_{p6}^b - \sum_{i\in\{c,e,h,p\}} C_i u_{i1} - \sum_{i\in\{e,h,p\}} C_i u_{i2} - \sum_{i\in\{e,h,b,p,n\}} C_i u_{i3} - C_p u_{p3}^f, \quad (119)$$

where the first term now considers the effective sell price of the polymer depending on quality variable values and the plant production rate. As $\theta_j(\mathbf{y}) = 1$ it equals $E_j w_{s3}$, i.e., revenue from polymer sold as on-grade polymer, while if $\theta_j(\mathbf{y}) = 0$ it equals $E_{\text{off}} w_{s3}$, i.e., revenue from polymer sold as off-grade polymer. The remaining terms consider off-gas and lights column bottom flow revenues and fresh feed costs, as in Eq. (116).

The time when a grade transition is to be carried out is often known several days in advance due to production planning. Therefore, preparations of the reactor contents can be performed prior the specified grade transition time. Considering a transition time t_T and a time interval $t_0 < t_T < t_1$ for an optimization with start grade A and end grade B, then the instantaneous profit is

$$R = \begin{cases} R_{\text{A}}, & t_0 \le t \le t_T \\ R_{\text{B}}, & t_T < t \le t_1. \end{cases} \quad (120)$$

The total profit to be maximized at a grade transition during the considered time interval, i.e., cost function at optimization, is thus

$$V_{\text{eco}} = \int_{t_0}^{t_1} R\, dt. \quad (121)$$

A cost function such as V_{eco} is non-linear, but also discrete due to the on-grade function $\theta_j(\mathbf{y})$. At least two different approaches may be taken. The first one is to consider a mixed-integer non-linear program, which is intrinsically very hard to solve. The second, and chosen approach, is to approximate $\theta_j(\mathbf{y})$ with a continuously differentiable function, resulting in a non-linear program that may be solved by an ordinary NLP solver.

The on-grade function $\theta_j(\mathbf{y})$ is essentially a multivariate rectangle function. Several continuously differentiable approximations exists, such as e.g., trigonometric approximations used in [Tousain, 2002] and rational functions, which will be used here. For a multivariate rectangle function with center and width equal to 0 and 1, respectively, for all variables, a rational function approximation is

$$\text{rect}(\mathbf{x}) \approx \frac{1}{\sum_{k=1}^{n_x} (2x_k)^{n_k} + 1}, \quad (122)$$

where n_x is the length of $\mathbf{x}$ and the even and integer parameters n_k may be used for setting approximation accuracy. Using the grade specific values and intervals for $\mathbf{y}$ in Table 3, $\theta_j(\mathbf{y})$ can thus be approximated by

$$\tilde{\theta}_j(\mathbf{y}) = \left(\sum_{i=1}^{7} \left(2 \frac{y_i - y_{ji}}{y_{ji}^{\max} - y_{ji}^{\min}} \right)^{n_i} + 1 \right)^{-1}, \tag{123}$$

where y_i is the ith quality variable in $\mathbf{y}$, y_{ji} its grade j target value and $y_{ji}^{\max} - y_{ji}^{\min}$ is the interval width.

In Eq. (121), which may now be approximated using $\tilde{\theta}_j(\mathbf{y})$, targets values for neither $\mathbf{y}$ or $\mathbf{z}$ are considered. Depending on raw material pricing and grade produced, it may be economically beneficial to have some or all of the quality variables $\mathbf{y}$ on their interval limits or be at an operating point where $\mathbf{z}$ are off target values. However, from a customers point of view, the quality variables of the product should be the same regardless of e.g., raw material pricing. Thus, an incentive to be on target values should be reflected in the cost function. A formulation of this with regards to economy is to have the effective sell price to peak when all variables are at target values. Thus, for an on-grade polymer, but with quality variables not on target values, the effective sell price used at optimization is much higher than the off-grade price E_{off}, but not as high as the on-grade price E_j. As the quality and operation variables get closer to their target values, the effective sell price in the cost function increases and only when on target values, on-grade sell price E_j is received. The increase in effective sell price as the operation variables get closer to their target values can be seen as a reward for operating the plant under correct conditions.

Many different modeling approaches for this effective sell price dependence on quality and operation variables in the cost function may exist. For simplicity, it is modeled similarly to the on-grade approximation in Eq. (123). Assume that, when the polymer is on-grade, the effective sell price is increased by at least a large percentage p_j of the difference between on-grade and off-grade sell prices, i.e., $E_j - E_{\text{off}}$, compared to the off-grade sell price. Therefore, introduce $\Omega_j(\mathbf{y}, \mathbf{z})$ to model the effective sell price dependence as

$$\begin{aligned} \Omega_j(\mathbf{y}, \mathbf{z}) = p_j &+ \sum_{i=1}^{7} p_{ji} \left(\left(2 \frac{y_i - y_{ji}}{w_{ji}} \right)^2 + 1 \right)^{-1} \\ &+ \sum_{k=1}^{2} l_{jk} \left(\left(2 \frac{z_k - z_{jk}}{h_{jk}} \right)^2 + 1 \right)^{-1}, \end{aligned} \tag{124}$$

where z_k is the kth operation variable in $\mathbf{z}$, y_{ji} and z_{jk} are target values for quality and operation variables, respectively, for grade j found in Table 3

and 4, and the parameters p_j, p_{ij} and l_{jk} fulfills

$$p_j + \sum_{i=1}^{7} p_{ji} + \sum_{k=1}^{2} l_{jk} = 1. \tag{125}$$

The function $\Omega_j(\mathbf{y}, \mathbf{z})$ has a minimum value of p_j, and each quality and operation variable may increase the function value by their respective parameter p_{ji} or l_{jk}, by being on target value. The peak value of $\Omega_j(\mathbf{y}, \mathbf{z})$ is equal to 1 due to the constraints on the parameters p_j, p_{ij} and l_{jk} in Eq. (125), and achieved when all grade and operation variables are on target values. An approximated on-grade function, with small peaks at quality and operation variable target values, may now be defined as

$$\Pi_j(\mathbf{y}, \mathbf{z}) = \tilde{\theta}_j(\mathbf{y})\Omega_j(\mathbf{y}, \mathbf{z}) \tag{126}$$

and the approximated instantaneous profit at production of grade j is

$$\begin{aligned}\tilde{R}_j = ((E_j - E_{\text{off}})\Pi_j(\mathbf{y}, \mathbf{z}) + E_{\text{off}})\, w_{s3} + E_{og}u_{ol} + E_{og}u_{op} + C_p w^b_{p6} \\ - \sum_{i\in\{c,e,h,p\}} C_i u_{i1} - \sum_{i\in\{e,h,p\}} C_i u_{i2} - \sum_{i\in\{e,h,b,p,n\}} C_i u_{i3} - C_p u^f_{p3}.\end{aligned} \tag{127}$$

When any grade variable is outside its grade limits, $\tilde{\theta}_j(\mathbf{y})$ yields $\Pi_j(\mathbf{y}, \mathbf{z})$ close to 0 and the effective polymer sell price close to E_{off}. If all quality and operation variables are at target values, then $\tilde{\theta}_j(\mathbf{y}) = \Omega_j(\mathbf{y}, \mathbf{z}) = 1$ and thus, $\Pi_j(\mathbf{y}, \mathbf{z}) = 1$ and the effective sell price is E_j. If the polymer is on-grade, but not on target values, or any operation variable is not on target value, the effective sell price is in the interval $(p_j E_j + (1 - p_j)E_{\text{off}},\ E_j)$. The tuning parameters for $\Omega_j(\mathbf{y}, \mathbf{z})$ are p_j, p_{ji}, w_{ji}, l_{jk} and h_{jk}, where w_{ji} and h_{jk} determine the peak width in effective sell price given by each variable, while p_{ji} and l_{jk} determine the maximum increase of the effective sell price by each variable. Together they specify the economical incentives for the optimization to yield the quality and operation variables on target values, and thus, have the effective sell price to equal E_j.

Utilizing the approximations above, the approximated total profit during a grade change, when also considering economical incentives to be on target values, is thus

$$\tilde{V}_{\text{eco}} = \int_{t_0}^{t_1} \tilde{R}\, dt, \tag{128}$$

where

$$\tilde{R} = \begin{cases} \tilde{R}_{\text{A}}, & t_0 \le t \le t_T \\ \tilde{R}_{\text{B}}, & t_T < t \le t_1, \end{cases} \tag{129}$$

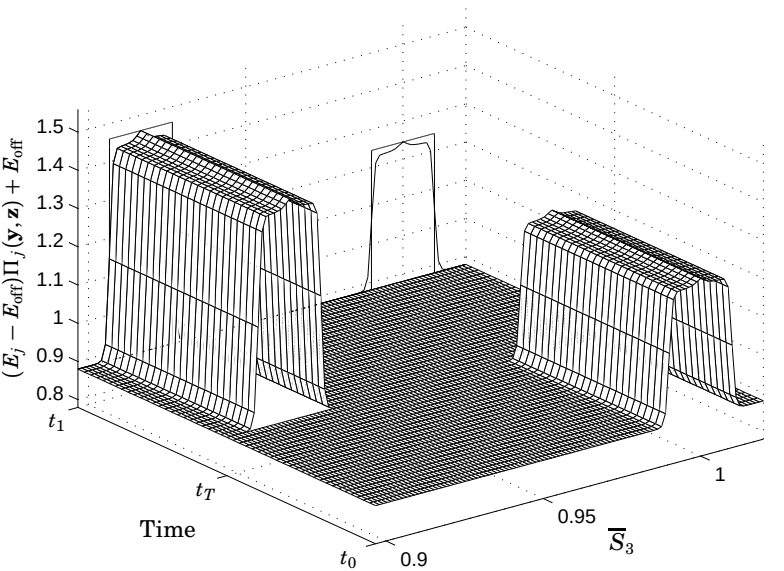

Figure 2. Example of how the effective sell price in $\tilde{R}$ depend on time and on the specifications of $\overline{S}_3$ at transition from grade A to B. The approximated on-grade function parameters are $n_7 = 20$, $p_j = 0.95$, $p_{j7} = 0.05$ and $w_{j7} = (y_{j7}^{\max} - y_{j7}^{\min})/3$. The on-grade interval for $\overline{S}_3$ is for illustrative reasons $2\,(y_{j7}^{\max} - y_{j7}^{\min})$.

if considering a transition from grade A to grade B.

An example of how the effective sell price in $\tilde{R}$ depend on time and specifications during a transition from grade A to B is found in Figure 2, considering only the GPR split factor $\overline{S}_3$. Projections of the effective sell price when using $\theta_j(\mathbf{y})$ and $\Pi_j(\mathbf{y},\mathbf{z})$ are also shown.

If using no end constraints at time t_1, the optimization with the cost function given by Eq. (128) will exploit the slow dynamics of the system by setting all inflows close to zero at t_1. The quality variables $\mathbf{y}$ and operation variables $\mathbf{z}$ will not change considerably at t_1, neither will the total production rate. Thus, at an interval close to t_1, there will effectively be no cost of fresh inflows, since the effect seen after time t_1 of closing all inflows is not taken into account. The end-point at time t_1 from the optimization will thus not be a stationary point, and the economically optimal stationary point of the end grade found in the stationary optimization, will not be reached. One remedy, used in [van Brempt *et al.*, 2001], is to add terms for bookkeeping of plant material hold up at initial and final time. Another method, used here and in e.g., [Tousain, 2002], is to set the control flows equal to economically optimal values for the end

grade during a time interval of length T_c at the end of the optimization interval. The time interval should be long enough such that the system is essentially in stationarity at $t = t_1$, regardless of the control actions taken prior $t = t_1 - T_c$.

As pointed out earlier, constraints are set on the control flow derivatives. The derivatives may be approximated by filtering the control flows with a derivative filter with bounded high frequency gain. Another, more direct approach, is to use the control flow derivatives as decision variables in the optimization, which may then be integrated before being fed to the plant. Thus, the model is extended with the 15 input derivatives

$$\begin{aligned}
&\dot{u}_{i1}, \quad i \in \{c, e, h, p\} \\
&\dot{u}_{j2}, \quad j \in \{e, h, p\} \\
&\dot{u}_{k3}, \quad k \in \{e, h, b, p, n\} \\
&\dot{u}_{ol},\ \dot{u}_{op},\ \dot{u}_{\text{flare}}.
\end{aligned}$$

Apart from setting minimum and maximum values, a quadratic cost on the derivatives is added in order to influence the smoothness of the control flows, i.e.,

$$V_{\dot{u}} = \int_{t_0}^{t_1} \dot{\mathbf{u}}^T \mathbf{U}_d \dot{\mathbf{u}}\, dt, \tag{130}$$

where $\mathbf{U}_d$ is a diagonal matrix and $\dot{\mathbf{u}}$ contains the derivatives. The derivatives are parametrized as piecewise constant over each collocation element, and thus, the control flows are piecewise linear.

The dynamic optimization problem for an economical grade transition over the time interval $t_0 \le t \le t_1$ may now be formulated as

$$\begin{aligned}
\min_{\dot{\mathbf{u}}} \; & -\tilde{V}_{\text{eco}} + V_{\dot{u}} \\
\text{s.t. } & \mathbf{0} = \mathbf{F}(\dot{\mathbf{x}}, \mathbf{x}, \mathbf{w}, \mathbf{u}) \\
& \mathbf{y} = \mathbf{g}_{\mathbf{y}}(\mathbf{x}, \mathbf{w}, \mathbf{u}) \\
& \mathbf{z} = \mathbf{g}_{\mathbf{z}}(\mathbf{x}, \mathbf{w}, \mathbf{u}) \\
& \mathbf{u} = \int_{t_0}^{t} \dot{\mathbf{u}}\, d\tau \\
& \mathbf{x}_{\min} \le \mathbf{x} \le \mathbf{x}_{\max}, \quad \mathbf{w}_{\min} \le \mathbf{w} \le \mathbf{w}_{\max} \\
& \mathbf{u}_{\min} \le \mathbf{u} \le \mathbf{u}_{\max}, \quad \mathbf{y}_{\min} \le \mathbf{y} \le \mathbf{y}_{\max} \\
& \mathbf{z}_{\min} \le \mathbf{z} \le \mathbf{z}_{\max}, \quad \dot{\mathbf{u}}_{\min} \le \dot{\mathbf{u}} \le \dot{\mathbf{u}}_{\max} \\
& \mathbf{x}(t_0) = \mathbf{x}_s, \quad \mathbf{u}(t_0) = \mathbf{u}_s \\
& \mathbf{u} = \mathbf{u}_e, \quad t_1 - T_c \le t \le t_1,
\end{aligned} \tag{131}$$

where the initial values $\mathbf{x}_s$ and $\mathbf{u}_s$ and the control flow end values $\mathbf{u}_e$ are given by the stationary optimizations of start and end grade, respectively. The introduction of control flow derivatives, $\Pi_A(\mathbf{y},\mathbf{z})$, $\Pi_B(\mathbf{y},\mathbf{z})$ and costs function terms $\tilde{V}_{eco}$ and $V_{\dot{u}}$ gives an optimization model with 63 states, 169 algebraic variables, 15 inputs and 232 equations.

7.4 Scaling and Initial Trajectories

The stationary optimization problem and the discretized dynamic optimization problem are both NLP problems that are solved using IPOPT. For good convergence in IPOPT, it is an advantage if all variables are in the same order of magnitude. Therefore, all variables were given a nominal value used for scaling and also the internal scaling in IPOPT was used. Additionally, initial values of all variables are important for convergence rate and for finding a solution at all. For stationary optimization, control flows taken from averaged plant data, corresponding to stationary production of considered grade, were used in simulation of the plant model to find suitable initial values. For the dynamic optimization problem, values of all states, derivatives, algebraic variables and control flows at the collocation points must be supplied. Such trajectories can be found by simulating the model using initial values and constant control flows corresponding to stationary production of start or end grade, found from the stationary optimizations. Both grades have been used for generating initial trajectories with similar convergence results.

8. Examples of Economically Optimal Grade Changes

Transitions between the two grades in Table 3 will be used as examples for the stationary and dynamic optimizations in sections 7.2 and 7.3. The two transitions include changes of all quality variables except for the prepolymerization reactor split factor.

8.1 Stationary Economically Optimal Production

Two stationary economically optimal points are computed, using the grade definition and target values in tables 3 and 4. The resulting instantaneous profits R_j, normalized by R_A, for each product can be seen in Table 3. Since both grades have lower costs than revenues at stationary production, the optimization gives maximum plant production, and thus w_{s3} is at its maximum value. Also, since the costs of the off-gases are higher than what they are sold for, all off-gases and the flare flow are at minimum values. At optimum, the split factors for the reactors are at grade target values, thus essentially setting the relations between the total reaction rates in the reactors.

For a certain set of catalyst properties and catalyst masses in the reactors, the molar concentrations of ethylene in the reactors are essentially determined by the production rate and split factors. The molar ratio X_{he1} and the molar ratios X_{h2}/X_{e2}, X_{h3}/X_{e3} and X_{b3}/X_{e3}, corresponding to specified melt indices and density, subsequently determines the hydrogen and butene molar concentrations. For the GPR, the propane partial pressure sets an equality constraint for the propane molar concentration X_{p3}. Thus, for the three reactors, all molar concentrations are specified if the catalyst properties and masses in the reactors are fixed. However, molar concentrations of the different components do not alone determine the component masses, only ratios, and the optimization may also use the inflow of catalyst to change reactor conditions when finding the economical optimum.

For the GPR, if considering certain values of catalyst properties and mass, maximum solids outflow and polymer production defined by the grade, then the masses of gas and polymer are determined because of the bed volume controller. Using the specifications of the molar concentrations, the component masses in the reactor are also determined. To increase the production in the GPR, either the molar concentrations of raw material must be increased, catalyst properties improved, or the catalyst mass in the GPR increased, and vice versa. Since there is no transfer of fluids from loop reactor to the GPR, the loop only affects the GPR via catalyst properties and polymer flow. In the optimization, the operating conditions in the GPR are thus affected when changing conditions in the first two reactors.

For the pre-polymerization and loop reactor, similarly to the GPR, for certain values of catalyst mass and properties and desired solids outflow and polymer grade, the molar concentrations are defined. However, since the outflows of fluids and solids are controlled by volume controllers, not considering the ratios between masses of fluids and solids, it is at optimization allowed to change these masses. As most of the ethylene is used for polymer production, the outflows of ethylene from the reactors are negligible when compared to the propane outflows. So is also the hydrogen outflow due to the small inflows compared to the propane inflows. The solids outflow from each reactor is essentially determined prior stationary optimization due to reactor split factors and maximum plant production rate, neglecting the substantially smaller catalyst mass compared to polymer mass. This causes the ratio of solids and fluids masses in the pre-polymerization and loop reactor basically be controlled by the propane inflow, see Eqs. (20)–(21) and Eqs. (42)–(46). Propane is inert, and is thus not consumed in the reactors. The inflow of propane to the pre-polymerization reactor is subsequently an inflow to the loop reactor. This gives the possibility to change fluids and solids masses in the loop

reactor by changing pre-polymerization reactor inflow. Altering masses in the reactors also change the masses of catalyst in the reactors, and subsequently the polymerization rate. To maintain a certain polymerization rate when e.g., mass of solids is increased, the ethylene molar concentration must be decreased. Thus, changing the mass gives a degree of freedom at optimization.

The optimal stationary point for grade B utilizes this degree of freedom as much as possible by having the propane inflow to the pre-polymerization reactor at its maximum constraint, yielding a small polymer mass in the pre-polymerization reactor. The propane inflow to the loop reactor is at the minimum value while no constraints are active in the GPR.

A similar stationary operating point is found for grade A if not considering constraints on the ethylene partial pressure in the GPR. However, to achieve correct total reaction rate in the GPR, this operating point violates the maximum allowed value of the ethylene partial pressure. To satisfy this constraint, the ethylene molar concentration must be decreased and thus, the catalyst increased, compared to the infeasible operating point. An increase in catalyst inflow requires less solids mass in the loop reactor, with the effect of propane inflow to the loop reactor not being at its lower limit at the optimal operating point for grade A.

8.2 Economically Optimal Grade Changes

Transitions from grade A to grade B and from grade B to grade A are considered where the stationary operating points from the stationary optimizations are used as start and end values in the transition optimization problems. For both transitions, the total optimization horizon is 30 normalized time units (t.u.) and the collocation element length is 0.5 t.u., giving a sufficiently dense grid for the dynamics to be well represented. The specified transition times t_T are at 9 t.u., while the time interval length T_c for constant control flows at the end of the interval, are 18 t.u. for the transition from grade A to B and 14.5 t.u. for the reverse transition.

In the cost function, p_j is set to 80% for both grades, i.e, at least 80% of the difference $E_j - E_{\text{off}}$ is added to the effective sell price when being on-grade compared to being off-grade, and the ideal on-grade function is approximated by $n_i = 10$ for all grade variables. For simplicity, no grade variable is considered more important than another, neither are the target values of the pressure and propane partial pressure in the GPR, yielding $p_{ji} = l_{jk} = (1 - p_j)/9$ in $\Omega_j(\mathbf{y}, \mathbf{z})$. The peak widths in $\Omega_j(\mathbf{y}, \mathbf{z})$ are set by $w_{ji} = (y_{ji}^{\max} - y_{ji}^{\min})/6$ for the grade variables and $h_{jk} = (P_{\max} - P_{\min})/6$ for the operation variables, where $P_{\min}$ and $P_{\max}$ are the limits for the GPR pressure. The weight matrix $\mathbf{U}_d$ is chosen from practical operating considerations and for smoothness of the inflows.

The resulting trajectories for the two economically optimal grade chang-

es are found in figures 3–17. In figures 3–5, the fresh inflows of fluids and catalyst to the three reactors are shown while Figure 6 shows the GPR flare flow and the propane and lights column off-gases. In figures 7–9 are the seven variables defining a grade found, while Figure 10 and 11 show the on-grade functions $\Pi_j(\mathbf{y}, \mathbf{z})$, approximate total profit $\tilde{V}_{\text{eco}}$ as function of time, plant production rate w_{s3} and relevant pressures in the GPR. The last six figures, i.e., 12–17, show the total reaction rate, fluid molar concentrations, solids masses and fluid masses in the three reactors. All trajectories are normalized such that the initial values are equal to 1.

Transition A to B. In the first transition, from grade A to B, $\overline{MI}_2$ and $\overline{MI}_{\text{mix}}$ are increased together with an increase in $\overline{\rho}_{\text{mix}}$. From the equations of melt indices i.e., Eqs. (50) and (79)–(80), and density, i.e., Eqs. (82)–(83), it is clear that the molar ratios X_{h2}/X_{e2}, X_{h3}/X_{e3} and X_{b3}/X_{e3} are to be increased. For the pre-polymerization reactor, the molar ratio X_{he1} is however to be decreased. The split factors are shifted such that the loop reactor produces more and the GPR less.

In the pre-polymerization reactor, it is desired to have slowly varying operating conditions due to e.g., catalyst sensitivity. Thus, the inflows are

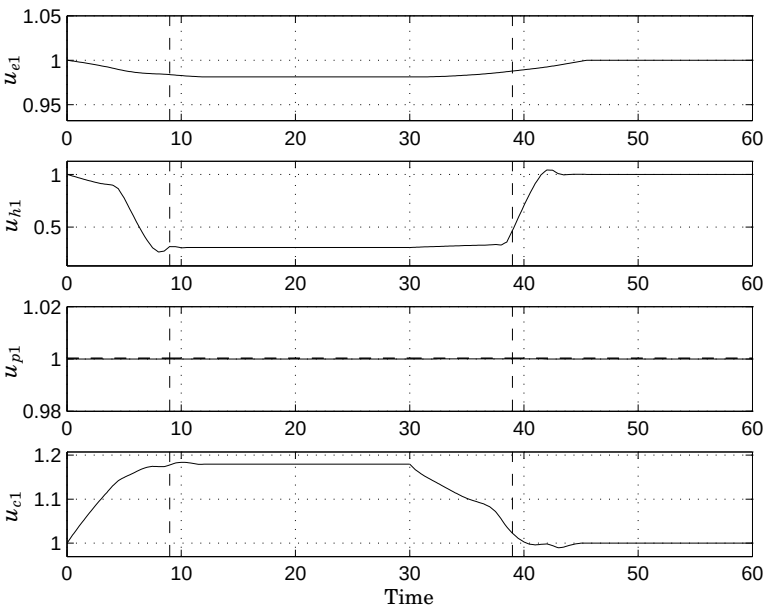

Figure 3. Inflows of ethylene, hydrogen, propane and catalyst to the pre-polymerization reactor, i.e., u_{e1}, u_{h1}, u_{p1} and u_{c1}. Vertical lines (--) show transition times and horizontal line (--) shows upper limit.

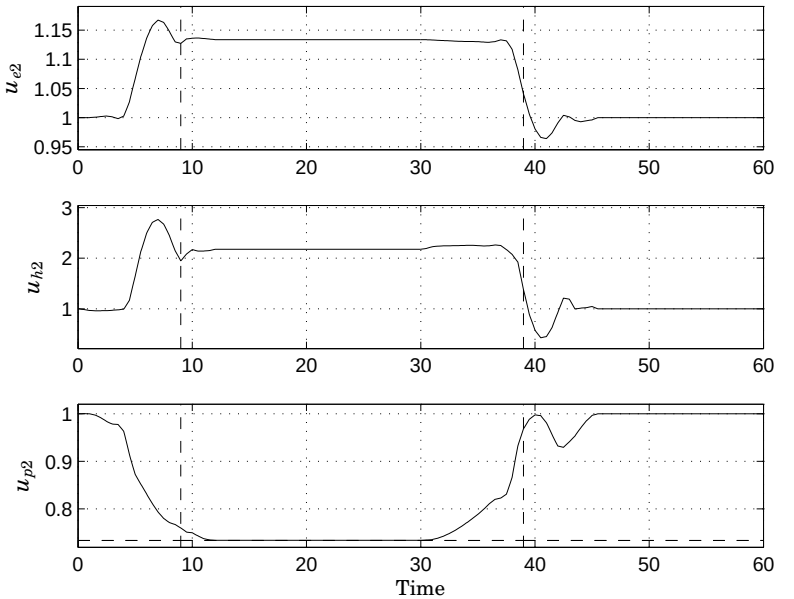

Figure 4. Inflows of ethylene, hydrogen and propane to the loop reactor, i.e., u_{e2}, u_{h2} and u_{p2}. Vertical lines (--) show transition times and horizontal line (--) shows lower limit.

not to be changed rapidly and all the weights in the matrix $\mathbf{U}_d$ considering pre-polymerization inflows are comparatively large. Changing ethylene and hydrogen molar concentrations in pre-polymerization reactor is easier than in the loop reactor and the GPR since no recycle flows are present. At stationary economical optimum, the total reaction rate in the pre-polymerization reactor is essentially determined from the maximum plant production rate and the pre-polymerization reactor split factor. For the two considered grades, both of these are equal, but with different catalyst inflows. As the catalyst flow and mass are negligible compared to polymer flow and mass, the total reaction rate in the pre-polymerization reactor are significantly the same for both grades. In the beginning of the optimization interval, the catalyst is increased slowly, and the inflow of ethylene is slightly decreased, resulting in an almost constant total reaction rate and decreasing ethylene molar concentration. To hold the molar ratio $\overline{X}_{he1}$ specified by grade A, the inflow of hydrogen is at the beginning slightly decreased as well, resulting in slowly decaying X_{h1}. Prior $t = 9$ t.u., the inflow of hydrogen is rapidly decreased to its end value with a small undershoot, thus changing the instantaneous molar ratio X_{he1} with an undershoot and the bed average value of the ratio

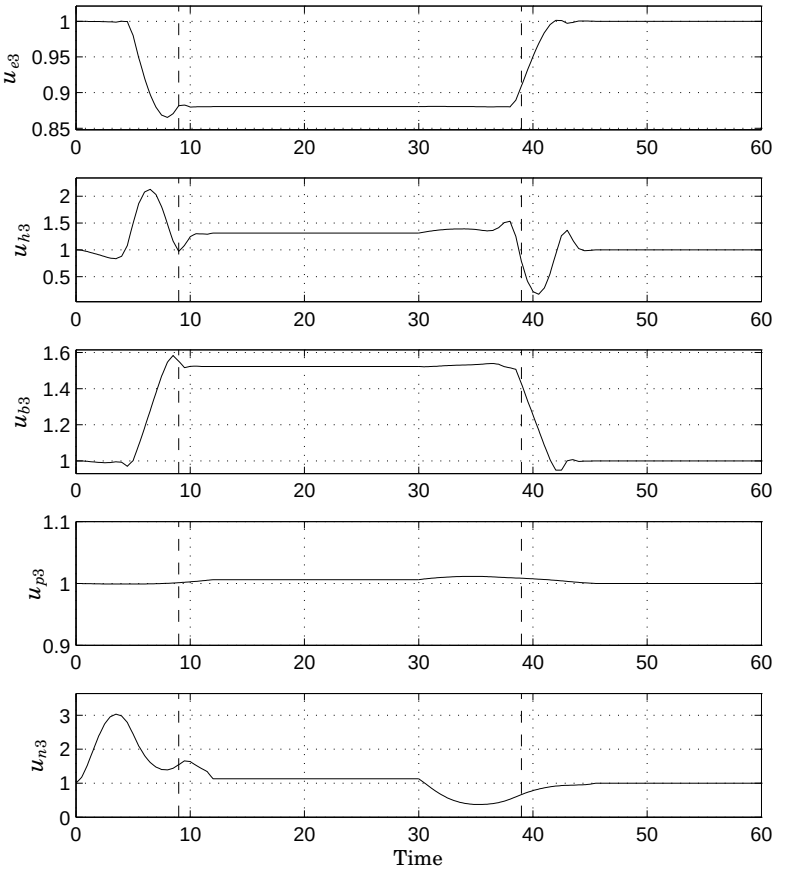

Figure 5. Inflows of ethylene, hydrogen, butene, propane and nitrogen to the GPR, i.e., u_{e3}, u_{h3}, u_{b3}, u_{p3} and u_{n3}. Vertical lines (--) show transition times.

fast. The propane inflow is close to its maximum value and not changed significantly, and since the total reaction rate is almost constant, the pre-polymerization reactor split is fulfilled during the whole optimization interval, as will be seen in the GPR, and the polymer and fluid masses are almost constant. The molar ratio $\overline{X}_{he1}$ leaves grade A at approximately $t = 5.5$ t.u. and grade B is reached at $t = 9$ t.u. From the inflows and molar ratios it is seen that grade B target value is reached prior stationarity and constant inflows.

For the loop reactor, as for the pre-polymerization reactor, if the total plant production rate is to be as high as possible with satisfied grade variables, the solids outflow from the loop reactor is essentially defined by the split factor and the maximum plant production, neglecting the catalyst

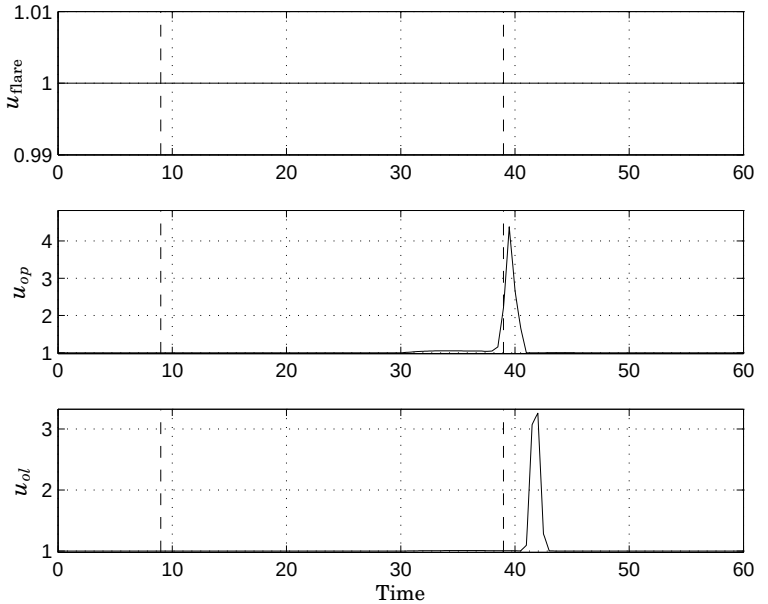

Figure 6. Flare flow from the GPR, i.e., u_{flare}, and off-gases on the propane and lights columns, i.e., u_{op} and u_{ol}. Vertical lines (--) show transition times.

mass as it is significantly smaller than polymer mass. The molar ratio X_{h2}/X_{e2} is defined from melt index grade value. The fluid outflow from the loop reactor is approximately equal to the total inflow of propane to the loop and since the inflow of propane from the pre-polymerization reactor is almost constant, the fluid outflow variations are due to fresh feed of propane and to a small extent also recycled propane. The propane inflow to the loop is to be decreased significantly, and thus also the fluid outflow, to reach grade B. In the beginning of the optimization interval, the inflow of propane is decreased, and if the polymer outflow should be constant and thus hold the grade B reactor split target, then the ratio between mass of solids and mass of fluids must increase. This is achieved since the inflow of catalyst is increased. Due to the increased conversion rate, almost not noticeable in the figure due to figure scale, the mass of ethylene, and also molar concentration, is decreased in the loop in the beginning. To produce polymer with correct melt index according to grade A, the total inflow of hydrogen is decreased by decreasing the fresh inflow and by a decreased recycle flow due to the higher conversion rate, but also since the hydrogen outflow from the pre-polymerization reactor is lower. The increased total reaction rate and the constant outflow of polymer causes the solids mass to increase in the reactor. Prior the transition time at

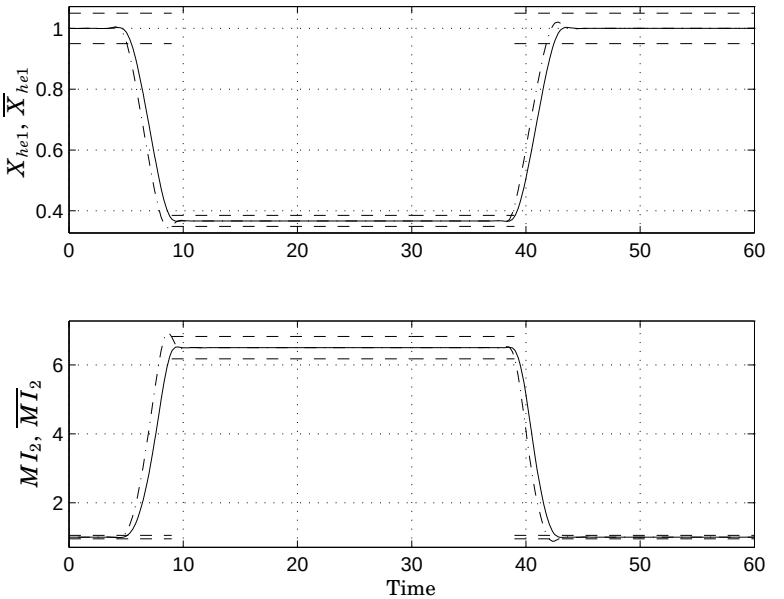

Figure 7. *Upper*: Instantaneous (- · -) and bed average (–) molar ratios X_{he1} and $\overline{X}_{he1}$ in pre-polymerization reactor. *Lower*: Instantaneous (- · -) and bed average (–) melt indices MI_2 and $\overline{MI}_2$ in loop reactor. Horizontal lines (--) show upper and lower limits of grade intervals.

$t = 9$ t.u., hydrogen and ethylene are changed rapidly, both with significant overshoots, resulting in overshoots in instantaneous melt index and loop split and a fast change of the bed average values. The hydrogen inflow also compensates for the rapid decrease of hydrogen coming from the pre-polymerization reactor. Prior to settling, the fresh feed of hydrogen makes an undershoot. This is because the prior overshoot of hydrogen is recycled and used as inflow to the loop again and this needs to be compensated for. For the ethylene, this compensation is not as pronounced since the recycle flow is considerably smaller than the fresh inflow. The propane inflow is not changed as rapidly as the other inflows, holding the outflow large and thus yielding the solid residence time small during the transition time and hence fast changes of bed average values. The polymer in the loop reactor leaves grade A at approximately $t = 5.5$ t.u. and enters grade B at $t = 9$ t.u. The inflows are changed such that the correct bed average melt index, and thus molar ratio of hydrogen and ethylene, is reached fast and thereafter held at its target value even though the individual molar concentrations change. Even after grade B is reached, the inflows are thus actively changed to reach stationarity.

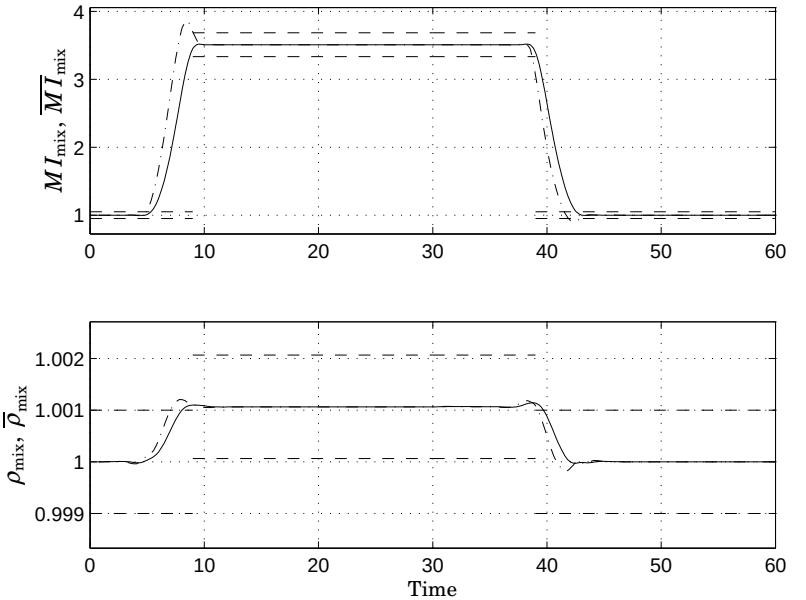

Figure 8. Instantaneous (- · -) and bed average (–) densities and melt indices in the GPR, i.e., ρ_{mix}, MI_{mix}, $\overline{\rho}_{\mathrm{mix}}$, and $\overline{MI}_{\mathrm{mix}}$. Horizontal lines (--) show upper and lower limits of grade intervals.

For the last reactor, i.e., the GPR, four out of the five grade variables are to be changed. At the starting point, the inflow of catalyst is increased and in order to maintain correct split according to the grade A specifications, the optimization changes the raw material fresh feeds such that raw material masses and concentrations are decreased in the reactor. The void is filled by nitrogen and the inflow of nitrogen has a comparatively large overshoot because the off-gas flow at the propane column removes a considerable amount. The melt index and density are not to be changed in the beginning, and accordingly, the molar ratios X_{h3}/X_{e3} and X_{b3}/X_{e3} are held constant by changing the inflows, and thus the molar concentrations in the reactor, in a coordinated manner. During the transition of grade variables to grade B target values, the inflow of polymer from the loop reactor increases. To reach the bed average split factors for grade B fast, production of GPR polymer is rapidly decreased with an undershoot of ethylene, causing the instantaneous split factors for the loop and the GPR to over- and undershoot, respectively. The bed average split factor for pre-polymerization reactor is slightly increased momentarily, but stays inside grade intervals. The inflows of hydrogen and butene are increased rapidly with overshoots, resulting in overshoots of the in-

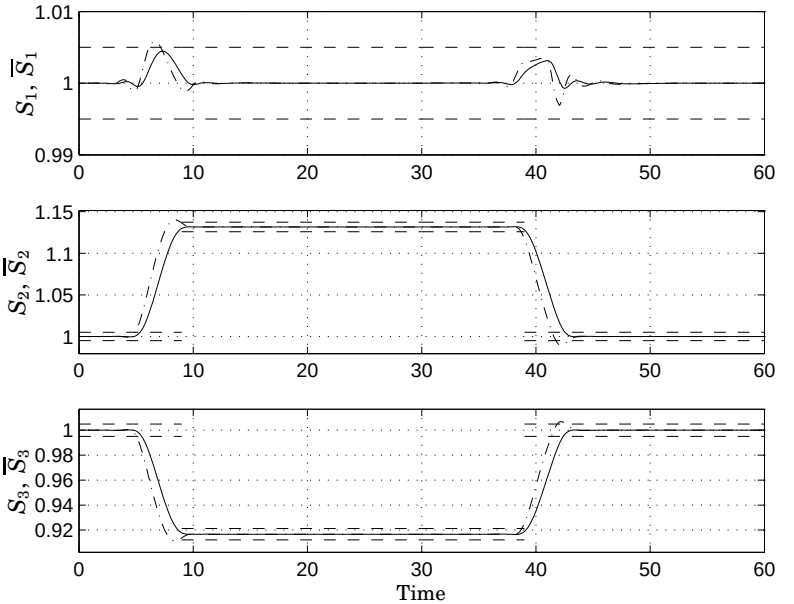

Figure 9. Instantaneous (- · -) and bed average (–) reactor split factors, i.e., S_1, S_2, S_3, $\overline{S}_1$, $\overline{S}_2$, and $\overline{S}_3$. Horizontal lines (--) show upper and lower limits of grade intervals.

stantaneous melt index and density, and in rapid changes of bed average properties. The propane inflow does not need to be changed considerably to hold the propane partial pressure close to its target value. This is since the other inflows are coordinated such that the sum of all molar concentrations, except for propane, is essentially constant. Additionally, the inflows are coordinated with the inflows of the loop reactor, and thus the loop polymer production, such that the bed volume controller of the GPR does not have to change the outflow from the GPR to hold the correct volume, i.e., the volumes of polymer and gas are not changed considerably during the transition. This yields the total plant production rate to be at maximum level, and the solid-phase residence time in the GPR is thus as small as possible, making the quality variables, i.e., bed average variables, to change fast. The grade variables for the polymer in the GPR leave grade A at approximately $t = 5.5$ t.u. and enters grade B at $t = 9$ t.u. At the latter point, some of the inflows are still actively changed, showing the driving-force to be on-grade as fast as possible and the importance of inflow synchronization.

For both the lights and the propane column, the off-gas flows are at minimum values. This is because the off-gas flows have high concentra-

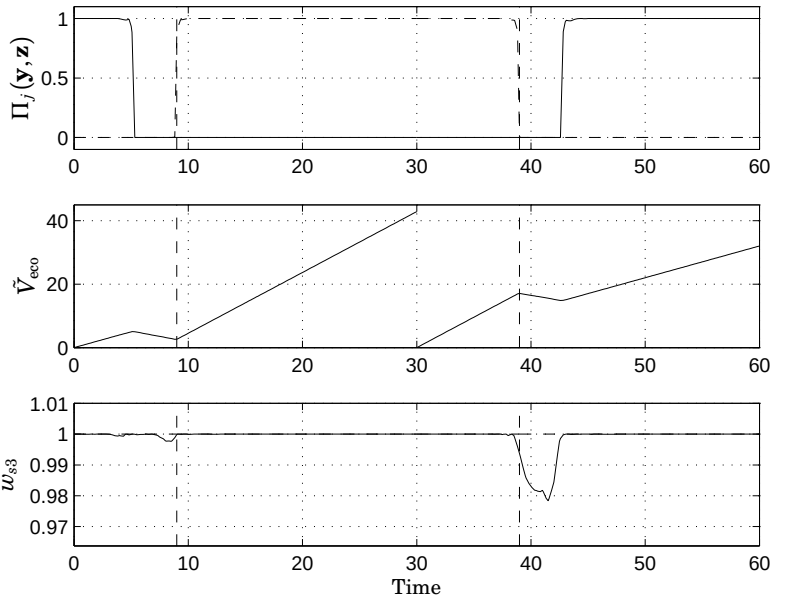

Figure 10. Approximate on-grade functions, i.e., $\Pi_{\text{A}}(\mathbf{y},\mathbf{z})$ (–) and $\Pi_{\text{B}}(\mathbf{y},\mathbf{z})$ (- · -), approximated total profit $\tilde{V}_{\text{eco}}$, and plant production rate w_{s3}. Vertical lines (--) show transition times and horizontal line (--) shows upper limit.

tions of light components such as hydrogen and nitrogen, and the hydrogen concentration is to be increased in both the loop reactor and the GPR and the nitrogen concentration is to be increased in the GPR. The flare of the GPR is also at its minimum value for the same reason and because of the fact that it is a pure economical loss to use it.

The total grade change takes about 3.5 t.u. to perform and the optimization renders the plant production to leave grade A such that grade B is reached at specified transition time. This is due to the maximization of approximate total profit $\tilde{V}_{\text{eco}}$ and the fact that the instantaneous profit for grade B is higher than for grade A, which is clearly seen in Figure 10 where the cumulative profit is shown. As the grade variables are transferred, they both leave and enter target values directly without the polymer being on-grade, but off target values, during a prolonged time period. This shows that the economical incentive provided by a peak in the effective sell price using $\Pi_j(\mathbf{y},\mathbf{z})$ is sufficient. The ratio between the two terms in the cost function is $V_{\dot{u}}/\tilde{V}_{\text{eco}} = 0.030$, showing that it is the criteria that expresses economy that clearly dominates the optimization.

Transition B to A In the transition from grade B to A, melt indices and density are to be decreased and thus the molar ratios X_{h2}/X_{e2}, X_{h3}/X_{e3}

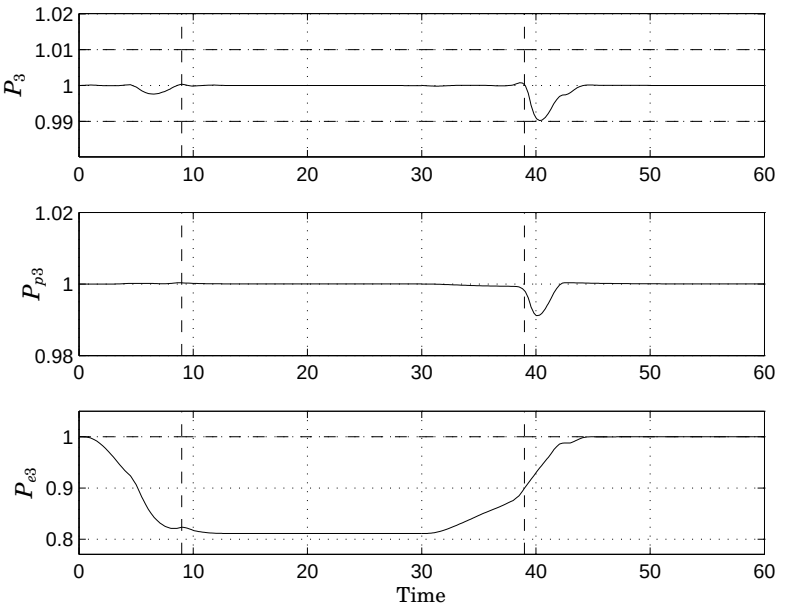

Figure 11. Pressure, propane partial pressure and ethylene partial pressure in the GPR, i.e., P_3, P_{p3} and P_{e3}. Vertical lines (--) show transition times and horizontal lines (--) show upper and lower limits.

and X_{b3}/X_{e3} should be decreased. This transition is considered harder since hydrogen must be removed from both the loop reactor and the GPR. The hydrogen in the reactors may only leave the system as part of the polymer or as off-gas. The reaction rates of hydrogen are very small compared to ethylene and butene, and a considerable amount of the hydrogen inflows to the loop reactor and the GPR come from the recycle area. Due to the column split factors, both the propane and lights column have higher ratios of light components in the off-gases than what is found in the reactors, and thus also the GPR flare flow. They are therefore powerful control flows for removing hydrogen. However, there is an economical loss in the off-gas flows due to the component pricing.

As for transition from grade A to B, inflows to pre-polymerization reactor are changed slowly. The catalyst flow starts to decrease in the beginning and the ethylene inflow is slightly increased, resulting in a nearly constant total reaction rate and an increased ethylene molar concentration in the reactor. The hydrogen compensates with an increased inflow so that $\overline{X}_{he1}$ is constant and on grade B target value. At the transition time $t = 39$ t.u., the hydrogen inflow is rapidly increased such that the instantaneous molar ratio X_{he1} changes with an overshoot and the bed

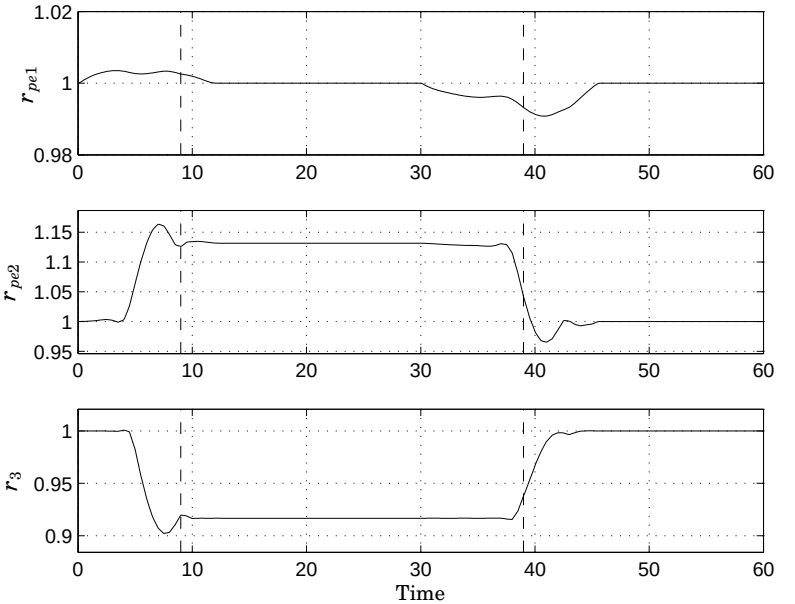

Figure 12. Total reaction rates in the pre-polymerization and loop reactor and the GPR, i.e., r_{pe1}, r_{pe2} and r_3. Vertical lines (--) show transition times.

average value $\overline{X}_{he1}$ reaches grade A approximately at time $t = 42.5$ t.u. The change in $\overline{X}_{he1}$ is not performed until after specified transition time. The propane inflow is nearly constant, yielding the polymer outflow from pre-polymerization reactor essentially the same over the whole optimization interval, and thus fulfilling the specification of the pre-polymerization split factor, as will be seen in the GPR.

In the beginning of the optimization interval, the outflow of polymer from the loop is constant in order to fulfill the loop reactor split factor of grade B. At the same time, the amount of catalyst is decreased due to the decreased inflow of catalyst to the pre-polymerization reactor. As the propane inflow is increased in the beginning, the ratio between polymer and fluid mass must decrease to hold outflow of polymer constant. The inflows are coordinated such that the total reaction rate is slightly decreased, resulting in decreasing polymer mass. At the same time, the fluid masses are increased to fill the void from the decreased polymer mass in such a way that the ethylene molar concentration is increased, partly compensating for the decrease of catalyst. The inflows are also coordinated so that the molar ratio X_{h2}/X_{e2} yields the specification of melt index of grade B to be fulfilled, i.e., the hydrogen inflow is slightly increased. The

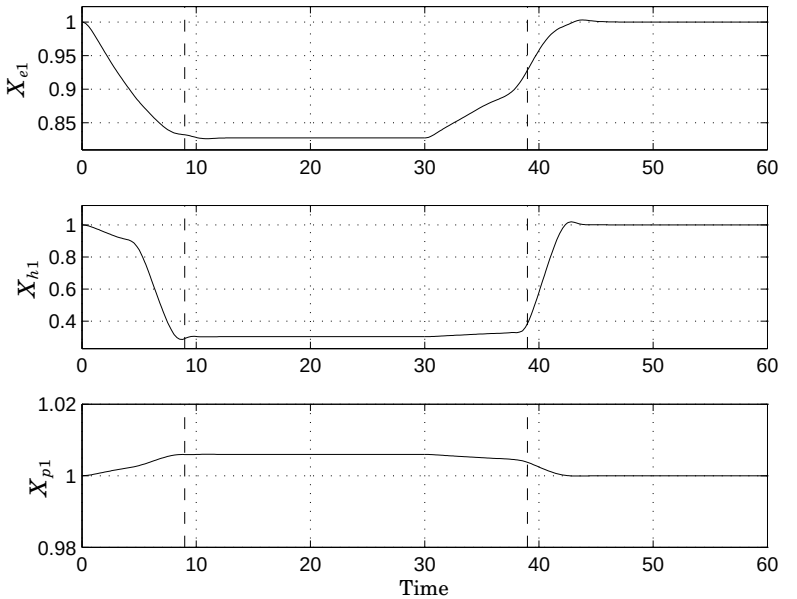

Figure 13. Molar concentrations in the pre-polymerization reactor, i.e., X_{e1}, X_{h1}, and X_{p1}. Vertical lines (--) show transition times.

grade B specifications are left at $t = 39$ t.u. and at this point, the inflow of ethylene is decreased rapidly with a large undershoot, resulting in an undershoot of the total reaction rate in the loop reactor. The instantaneous loop reactor split factor, calculated in the GPR, is subsequently undershot, making the bed average value to settle fast at grade A target value. To decrease melt index fast, and to compensate for the increased inflow of hydrogen from the pre-polymerization reactor, the fresh feed of hydrogen is undershot and the off-gas of the lights column is used to reduce the hydrogen flow from the recycle area. To recover from the hydrogen undershoot, the hydrogen inflow makes a small correction before it settles at the grade A target. The off-gas is only used at the end of the off-grade period, where the fresh inflow of hydrogen starts to increase to make its overshoot, keeping the total inflow of hydrogen low during the transition period. This results in undershoots of the molar ratio X_{h2}/X_{e2} and the instantaneous melt index. The total reaction rate undershoot and the rapid increase of propane inflow during the transition time are coordinated so that the polymer mass and polymer outflow undershoot with a resulting solid-phase residence time that is momentarily decreased during the off-grade period. This yields a faster change of bed average melt index,

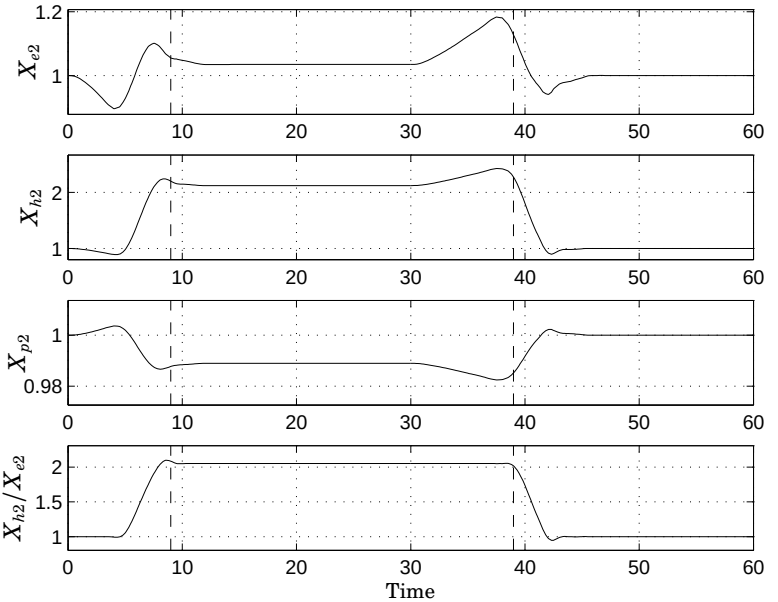

Figure 14. Molar concentrations in the loop reactor, i.e., X_{e2}, X_{h2}, and X_{p2}, and molar ratio X_{h2}/X_{e2}. Vertical lines (--) show transition times.

reaching on-grade target at approximately $t = 42.5$ t.u. After the loop polymer is on grade target, the fresh inflows are still used for corrections by the optimization to compensate for recycle flows and to reach correct stationary point. Thus, the component molar concentrations in the reactor change, but the molar ratio X_{h2}/X_{e2}, and thus melt index, are at grade A target values.

For the GPR in the optimization interval beginning, as the inflow of catalyst decrease, the molar concentration of ethylene must be increased to keep the correct total reaction rate, and thus correct split factor. This is accomplished by adjusting the fresh inflows so that the mass of nitrogen is decreased, masses of raw material for polymer is increased and the propane mass is almost kept constant. This yields the molar concentrations of raw material to increase while the molar concentration of inert nitrogen is decreased and both reactor pressure and propane partial pressure to be close to target values. The nitrogen inflow is changed slowly, since the off-gas on the propane column contains a high concentration of nitrogen. The molar concentrations of gases in the reactor are changed so that the melt index and density is on grade B targets, i.e., the molar ratios X_{h3}/X_{e3} and X_{b3}/X_{e3} are constant. The transition of grade vari-

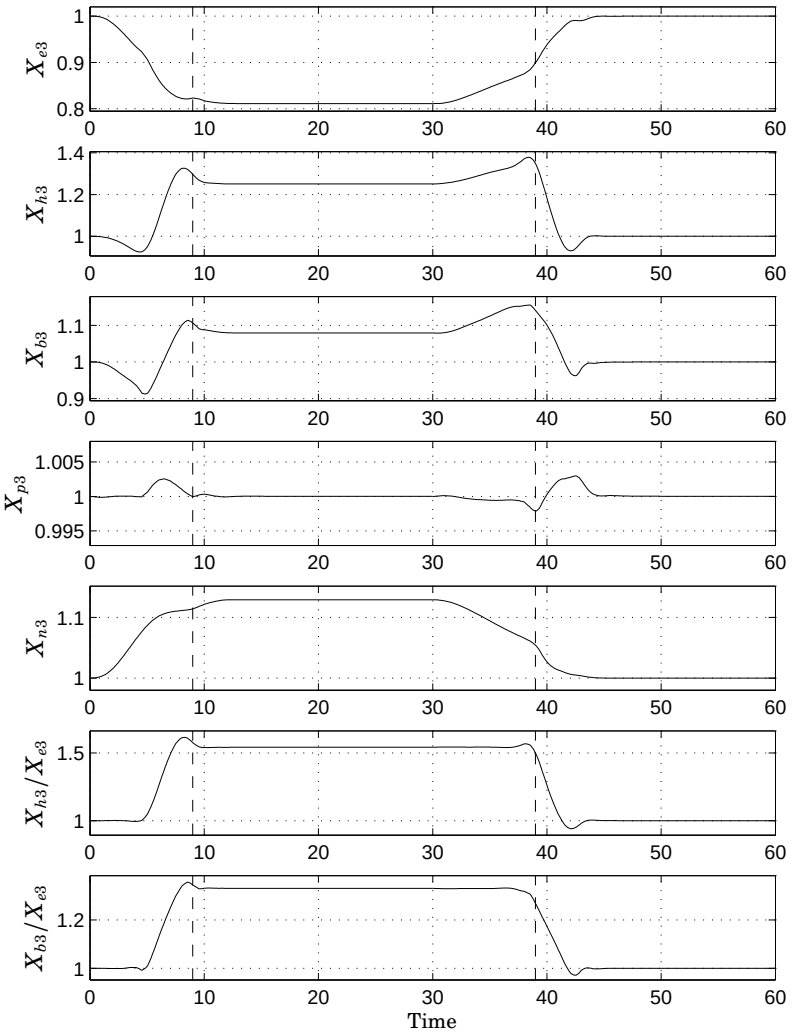

Figure 15. Molar concentrations in the GPR, i.e., X_{e3}, X_{h3}, X_{b3}, X_{p3} and X_{n3}, and molar ratios X_{h3}/X_{e3} and X_{b3}/X_{e3}. Vertical lines (--) show transition times.

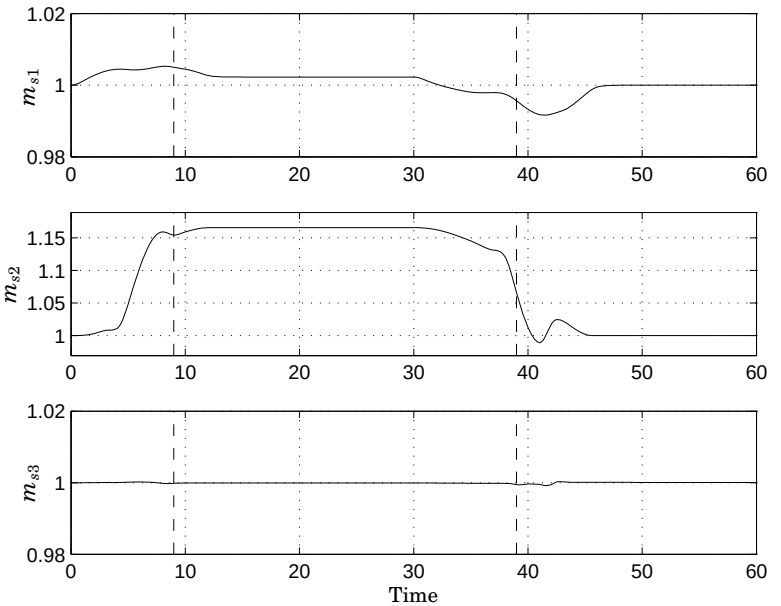

Figure 16. Solids masses in the pre-polymerization and loop reactor and the GPR, i.e., m_{s1}, m_{s2} and m_{s3}. Vertical lines (--) show transition times.

ables starts at $t = 39$ t.u. and at that point is the inflow of polymer from the loop reactor decreased with an undershoot and the production rate of polymer in the GPR is increased. However, the total reaction rate in the GPR cannot be increased with an overshoot since this would require the ethylene partial pressure to overshoot, violating its constraint. Therefore, the ethylene inflow is increased without any overshoot towards its grade A target. The undershoot of polymer inflow from the loop makes the split factor transitions faster, but the lack of polymer production overshoot in the GPR causes the total solids mass to begin to decrease. The bed volume controller then decreases the total volumetric outflow so that the bed volume is on its set-point. Thus, the total production rate of the plant is decreased during grade transition. However, the decrease is minor. The transitions of melt index and density, essentially controlled by the inflows of hydrogen and butene, are made by undershooting both fresh inflows, causing the instantaneous properties to have undershoots. The hydrogen inflow also makes a small increase prior settling at its correct value to compensate for the undershoot. For fast removal of hydrogen, the propane column off-gas is used at the transition start. This time instant is beneficial since the concentration of hydrogen is high, and so is

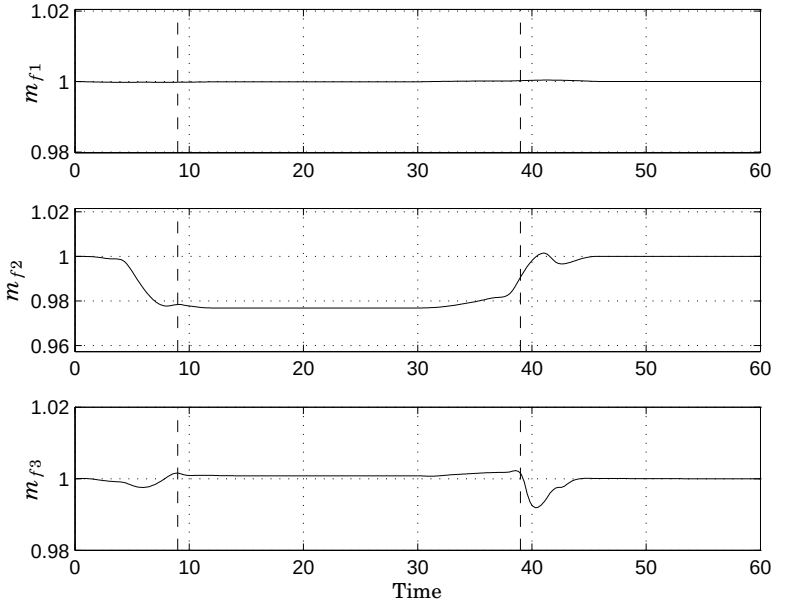

Figure 17. Fluids masses in the pre-polymerization and loop reactor and gas mass in the GPR, i.e., m_{f1}, m_{f2} and m_{f3}. Vertical lines (--) show transition times.

the concentration of inexpensive nitrogen, thus reducing the economical loss. The GPR flare flow is however not used for hydrogen removal due to its comparatively low hydrogen concentration and associated economical loss. The total pressure is held within limits and no significant change in the propane inflow is needed for holding the propane partial pressure close to its target value. Additionally, these operation variables differ only from their targets during the off-grade period where the approximated on-grade function is close to zero, and thus, no economical incentives for keeping target values exist. The polymer in the GPR is on grade A target at approximately $t = 42.5$ t.u. Several of the inflows continue to change after grade A target is reached, and stationary production is thus not reached until several time units later.

In total, the transition time is approximately 3.5 t.u. and as for the reverse transition, it is optimal to produce as much as possible of grade B, see Figure 10, in order to maximize the cumulative profit. The ratio between the two cost function terms is $V_{\dot{u}}/\tilde{V}_{\text{eco}} = 0.065$, showing that the economy term dominates the cost. And similar to the former transition, it is seen that the economical incentives from $\Pi_j(\mathbf{y}, \mathbf{z})$ to be on target values for quality and operation variables are sufficient.

8.3 Grade Change Characteristics

The economically optimal grade changes can each be divided into three different phases with distinguishable features.

Preparation Phase In the first phase, the reactors produce polymer on start grade target and at maximum production rate. However, since e.g., the catalyst start to change directly due to its heavy derivative penalty, the state of the reactors are continuously changed by adjusting the component inflows, and thus, the reactors are not in stationary production. The inflows to the three reactors are synchronized such that quality variables $\mathbf{y}$ and operation variables $\mathbf{z}$ do not change during this first phase.

Transition Phase The next phase, having a non-stationary initial condition, transfers the reactors from producing start grade to producing end grade. The transfer is performed by having significant inflow over- or undershoots depending on how the quality variables are to be changed, resulting in over- or undershoots of the instantaneous quality variables. This is made so that the bed average quality variables have fast transitions. The inflows are coordinated such that their effect on the outflow of the corresponding reactor, and thus also on the subsequent reactor or distillation column with recycle flow, are taken into consideration. Additionally, the off-gases on the propane and lights columns are used for removing hydrogen if desired. The phase ends when all quality variables are on end grade targets, but the reactors are not in stationary production.

Completion Phase The completion phase starts with non-stationary, but on-target, production and the inflows transfer the production into stationarity. This is performed as the quality and operation variables are on target values and having maximum plant production. Also in this phase, the synchronization between the different control flows is important since the component molar concentrations are to be changed to end grade values while the molar ratios are held constant. The last part of the completion phase contains constant control flows for stationary production of end grade.

Comparison to Current Practice at PE3 Today, a grade change at the plant PE3 at Borealis AB is performed manually by operators, following a time and action list. The list is specific for each transition and is updated after a performed transition. These lists often emphasize that preparation of the content in the reactors should be performed to make the transition fast and that over- and undershoots of the fresh inflows should be used. This aligns well with the optimization results. However, the completion phase is not as pronounced in the lists.

9. Summary and Conclusions

This paper has addressed optimization of stationary production and grade changes with regards to economy on a model of the PE3 plant at Borealis AB, incorporating three reactors and a recycle area consisting of three distillation columns. A Modelica library with models of the plant units has been constructed and used when building the plant model. The optimization problems were formulated using the JModelica.org platform. A direct collocation method was used for solving the resulting dynamic optimization problems. The cost function for the grade transition optimization problems was a smooth approximation of the ideal cost function with regards to economy, acknowledging that a produced polymer is considered on-grade if all the quality variables are inside certain intervals. The cost function also considered incentives for the quality and operation variables to be on targets. This was made by using an effective sell price that increased as the variables got closer to their target values, and full on-grade sell price was only received when all variables were at associated target values.

Two different grades were considered and transitions between them were optimized. In both cases, the optimization method succeeded in solving the transition problem with polymer quality variables being on grade targets both prior to and after the transition. The optimization results showed the importance of not starting the change of control inflows at defined transition time, which is the most common procedure in literature. A preparatory interval gives the opportunity to prepare the plant for a faster and economically better grade transition, similar to current practice at the PE3 plant at Borealis AB.

In the two transitions considered in this paper, the reactor operations during the preparatory time interval depend on the slow changes of the catalyst inflow, set by the relative large weight on the catalyst inflow derivative. This changed productivity with respect to the ethylene molar concentrations in the subsequent reactors and required a careful synchronization of the inflows for producing on-target polymer during the non-stationary production prior the actual grade transition. A similar situation was found after the quality variables changed from start grade to end grade targets, when end grade polymer was produced during non-stationary conditions. Thus, during these two time intervals the optimization rendered the inflows to change the molar concentrations in the reactors with respect to each other such that the molar ratios yielded on target non-stationary production at high production rate.

The actual transitions of the molar ratio of hydrogen and ethylene in the pre-polymerization reactor and the melt indices and density in the loop reactor and the GPR are essentially performed by over- and under-

shoots of hydrogen and butene. Transitions of the reactor split factors are performed mainly by, if allowed, over- and undershoots of ethylene inflows. The synchronization between fresh inflows, recycle flows, and contiguous reactor flows together with usage of off-gas flows showed to be important when making the transitions economically optimal.

The two time intervals with non-stationary on-grade production, high production rate during the full optimization interval, and that the optimization renders the plant to produce as much as possible of the grade with highest instantaneous profit, shows the impact of using a cost function that expresses the costs and revenues. The resulting trajectories correspond to almost pure optimization of the economy, as the approximations of the on-grade function are minor and not taken advantage of in the results. Additionally, the ratio $V_u / \tilde{V}_{\text{eco}}$ is very small in both transition cases. Thus, the results are close to the limits of performance when considering optimization of economical grade transitions on the plant PE3 at Borealis AB, regarding inflow costs and revenues from off-gases and produced polymer.

The transition optimization problem is large-scale and non-convex, and the results show that the method and tools used are highly applicable for solving it. However, compared to a quadratic optimization criteria, the optimization times are long, and the method and tools are not suitable for on-line usage in an iterative fashion as in e.g., NMPC. The resulting trajectories may instead be used for e.g.,

- comparison to other optimization criterias and strategies as a limit of performance.
- comparison to performed grade transitions on the actual plant regarding costs and revenues.
- as a planning tool for production order of different grades.
- as in indicator of how to synchronize different fresh inflows.

A drawback of the proposed cost function may be the inclusion of target values for operation variables. Incentives, related to the operational cost of not being on target, must be supplied and can be hard to quantize for a plant.

Future work includes modeling of ethane production at polymerization in the reactors, refinement of distillation column models and sensitivity analysis of optimal trajectories with respect to model and parameter uncertainties.

References

Åkesson, J. (2008): "Optimica—An Extension of Modelica Supporting Dynamic Optimization." In *6th International Modelica Conference 2008*. Modelica Association.

Åkesson, J., K.-E. Årzén, M. Gäfvert, T. Bergdahl, and H. Tummescheit (2010): "Modeling and Optimization with Optimica and JModelica.org — Languages and Tools for Solving Large-Scale Dynamic Optimization Problem." *Computers & Chemical Engineering*, **34:11**, pp. 1737–1749.

Andersson, B., C. Winberg, M. Gopalakrishnan, G. Cruey, and K. Lau (2002): "Enhanced ethylene plant planning model accuarcy by integrating with online optimizer." In *Proc. 2002 AIChE Spring National Meeting, 14th Annual Ethyelene Producers' Conference*. New Orleans, Louisiana, USA.

Andersson, N., P. Larsson, J. Åkesson, S. Haugwitz, and B. Nilsson (2011): "Calibration of a polyethylene plant for grade change optimizations." In *Proceedings of the 21st European Symposium on Computer-Aided Process Engineering*. Chalkidiki, Greece.

Backx, T., O. Bosgra, and W. Marquardt (1998): "Towards intentional dynamics in supply chain conscious process operations." In *Proc. Foundations of Computer-Aided Process Operations '98*. Snowbird, Utah, USA.

Biegler, L., A. Cervantes, and A. Wächter (2002): "Advances in simultaneous strategies for dynamic optimization." *Chemical Engineering Science*, **57**, pp. 575–593.

Binder, T., L. Blank, H. G. Bock, R. Bulitsch, W. Dahmen, M. Diehl, T. Kronseder, W. Marquardt, S. J., and O. von Stryk (2001): *Introduction to model based optimization of chemical processes on moving horizon*, chapter Online optimization of large scale systems. Springer.

Bonvin, D., L. Bodizs, and B. Srinivasan (2005): "Optimal Grade Transition for Polyethylene Reactors via NCO Tracking." *Chemical Engineering Research and Design*, **83:6**, pp. 692–697. 7th World Congress of Chemical Engineering.

Cervantes, A., S. Tonelli, A. Brandolin, J. Bandoni, and L. Biegler (2002): "Large-scale dynamic optimization for grade transitions in a low density polyethylene plant." *Computers & Chemical Engineering*, **26:2**, pp. 227–237.

Chatzidoukas, C., J. Perkins, E. Pistikopoulos, and C. Kiparissides (2003): "Optimal grade transition and selection of closed-loop controllers in a gas-phase olefin polymerization fluidized bed reactor." *Chemical Engineering Science*, **58:16**, pp. 3643–3658.

Debling, J., G. Han, F. Kuijpers, J. Verburg, J. Zacca, and W. Ray (1994): "Dynamic modeling of product grade transitions for olefin polymerization processes." *AIChE Journal*, **40:3**, pp. 506–520.

Dünnebier, G., D. van Hessem, J. Kadam, K.-U. Klatt, and M. Schlegel (2005): "Optimization and control of polymerization processes." *Chemical Engineering & Technology*, **28:5**, pp. 575–580.

Flores-Tlacuahuac, A., A. Biegler, and E. Saldívar-Guerra (2006): "Optimal grade transitions in the high-impact polystyrene polymerization process." *Industrial & Engineering Chemistry Research*, **45:18**, pp. 6175–6189.

Fritzson, P. (2004): *Principles of Object-Oriented Modeling and Simulation with Modelica 2.1*. IEEE Press, Wiley Interscience.

Kadam, J. V., W. Marquardt, B. Srinivasan, and D. Bonvin (2007): "Optimal grade transition in industrial polymerization processes via NCO tracking." *AIChE Journal*, **53:3**, pp. 627–639.

Larsson, P., J. Åkesson, and N. Andersson (2011a): "Cost Function Design for Economically Optimal Grade Changes for a Polyethylene Gas-Phase Reactor." In *Proceedings of the 50th IEEE Conference on Decision and Control and European Control Conference*. Orlando, Florida, USA. To appear.

Larsson, P., J. Åkesson, S. Haugwitz, and N. Andersson (2011b): "Modeling and optimization of Grade Changes for Multistage Polyethylene Reactors." In *Proceedings of the 18th IFAC World Congress*. Milano, Italy.

Larsson, P., N. Andersson, J. Åkesson, and S. Haugwitz (2010): "Modelica Based Grade Change Optimization for a Polyethylene Reactor." In *Proceedings of the 9th International Symposium on Dynamics and Control of Process Systems*. Leuven, Belgium.

McAuley, K. and J. MacGregor (1991): "On-line inference of polymer properties in an industrial polyethylene reactor." *AIChE Journal*, **37:6**, pp. 825–835.

McAuley, K. and J. MacGregor (1992): "Optimal grade transitions in a gas phase polyethylene reactor." *AIChE Journal*, **38:10**, pp. 1564–1576.

Reginato, A., J. Zacca, and A. Secchi (2003): "Modeling and simulation of propylene polymerization in nonideal loop reactors." *AIChE Journal*, **49:10**, pp. 2642–2654.

Richards, J. and J. Congalidis (2006): "Measurement and control of polymerization reactors." *Computers & Chemical Engineering*, **30:10-12**, pp. 1447–1463. Papers from Chemical Process Control VII - CPC VII.

Takeda, M. and W. Ray (1999): "Optimal-grade transition strategies for multistage polyolefin reactors." *AIChE Journal*, **45:8**, pp. 1776–1793.

The Modelica Association (2011): "The Modelica Association Home Page." `http://www.modelica.org`.

Touloupides, V., V. Kanellopoulos, P. Pladis, C. Kiparissides, D. Mignon, and P. Van-Grambezen (2010): "Modeling and simulation of an industrial slurry-phase catalytic olefin polymerization reactor series." *Chemical Engineering Science*, **65:10**, pp. 3208–3222.

Tousain, R. (2002): *Dynamic optimization in business-wide process control*. PhD thesis, Delft University of Technology.

van Brempt, W., T. Backx, J. Ludlage, and P. van Overschee (2001): "Optimal Trajectories for Grade Change Control: Application to a Polyethyelene Gas Phase Reactor." In *Proc. 6th IFAC Symposium on Dynamics and Control of Process Systems*. Jejudo Island, Korea.

van Brempt, W., P. van Overschee, T. Backx, C. Kiparissides, and C. Chatzidoukas (2004): "Plantwide Economical Dynamic Optimization: Appliaction on a Borealis Boreastar Process Model." In *Proc. 7th International Symposium on Advanced Control of Chemical Processes*. Hong Kong.

van Brempt, W., P. van Overschee, T. Backx, J. Ludlage, P. Hayot, L. Oostvogels, and S. Rahman (2002): "Economically Optimal Grade Change Trajectories: Application on a Dow Polystyrene Process Model." In *European Symposium on Computer Aided Process Engineering-12, 35th European Symposium of the Working Party on Computer Aided Process Engineering*, vol. 10 of *Computer Aided Chemical Engineering*, pp. 643–648. Elsevier.

van der Schot, J., R. Tousain, A. Backx, and O. Bosgra (1999): "SSQP for the solution of large-scale dynamic-economic optimization problems." *Computers & Chemical Engineering*, **23:Supplement**, pp. S507–S510.

Vinodograd, G. and A. Malkin (1980): *Rheology of Polymers – Viscoelasticity and Flow of Polymers*. Mir Publisher.

Wächter, A. and L. T. Biegler (2006): "On the implementation of an interior-point filter line-search algorithm for large-scale nonlinear programming." *Mathematical Programming*, **106:1**, pp. 25–58.

Wang, Y., H. Seki, S. Ohyama, A. Koji, M. Ogawa, and M. Ohshima (2000): "Optimal grade transition control for polymerization reactors." *Computers & Chemical Engineering*, **24:2-7**, pp. 1555–1561.

Xie, T., K. McAuley, C. Hsu, and D. Bacon (1994): "Gas phase ethylene polymerization: Production processes, polymer properties, and reactor modeling." *Industrial & Engineering Chemistry Research*, **33:3**, pp. 449–479.

Supplement A

PE3Lib – A Modelica Library for the Plant PE3 at Borealis AB

The model library for the plant PE3 at Borealis AB, denoted PE3Lib, has been used when formulating and solving the grade change and calibration optimization problems in Paper IV and VI, [Larsson *et al.*, 2010] and [Andersson *et al.*, 2011]. It is implemented in the Modelica language and several of the main features of the language described in Section 2.3 have been used. The following supplement will give details of the library contents.

A.1. Overview

The PE3 plant consists of six main units, i.e., the three reactors and the three distillation columns. This yields a natural structure of the library, where a Modelica component of each unit is constructed and means for connecting the components are given. The library is constructed with the aim of being easy to extend with additional components, and also to add models with lower or higher complexity compared to the currently available models.

The library is organized into five main packages,

1. Interfaces – contains connectors and models that define how the flows between the units are represented and what in- and outflows the different units have.
2. Components – contains models with equations describing the different units.
3. Templates – defines different topologies of the plant.
4. Experiments – contains models for calibration, optimization and simulation.
5. Miscellaneous – contains model parameters and constants, polymer grade definitions, stationary operating points for different grades, as well as minimum, maximum and nominal values for all variables in the packages in items 1–4 above.

In the forthcoming sections, the different packages will be explained in more detail.

A.2. Interfaces

One of the main parts of the Interface package is the Connector package. It defines how the material flows and properties are represented at the connection between two models. A connector model defining how the fluid flow is represented between two units, such as a reactor and a distillation column, has been custom made for the library. It contains the total fluid flow and flow fractions of the different components, see Listing A.1. A second connector type, also custom made for the library, considers the flow of solids, i.e., polymer and catalyst, and their properties, see Listing A.2. It contains the total flow and the flow fractions of polymer and catalyst. Additionally, the solids connector provides means to transfer catalyst properties, i.e., mean activity and deactivated sites, and also polymer properties such as density and melt index, used when defining polymer grades. The solids connector is used e.g., when transferring polymer from the loop reactor to the GPR. The third, and last, connector in the library is a connector considering both solids and polymer flows. It is constructed by using the object-oriented features of Modelica, by containing one fluids connector and one solids connector. It is used e.g., between the pre-polymerization and the loop reactor.

Apart from the connectors, the Interface package also contains interfaces for the reactor and distillation column models, implemented as partial models. The interfaces provide the in- and output structure of each unit and defines what, at the minimum, needs to be modeled for the unit. The interface models utilize the connectors above to define what in- and outflows the different units have, except for off-gases and flare which are modeled by inputs. For instance, the GPR interface model contains four different connectors and one input, see Figure A.1, where the interface is found together with the interfaces of the other units. One solids connector is used for the polymer transferred from loop reactor, one fluid connector considers the outflow of fluid to the propane column, one fluid connector is used for the recycle inflow from the propane column, one fluid connector is used for the fresh inflow of fluids, and lastly, the input represents the flare flow of the GPR. Additionally, the GPR interface may contain a connector for the solids outflow. As the subsequent units for e.g.,

```
connector Fluid
   //Total fluids flow
   flow Modelica.SIunits.MassFlowRate w_f(start=0,min=0,max=1,nominal=1);

   //Mass fractions
   Modelica.SIunits.MassFraction z_e(start=0,min=0,max=1,nominal=1);   //ethylene
   Modelica.SIunits.MassFraction z_h(start=0,min=0,max=1,nominal=1);   //hydrogen
   Modelica.SIunits.MassFraction z_b(start=0,min=0,max=1,nominal=1);   //butene
   Modelica.SIunits.MassFraction z_p(start=0,min=0,max=1,nominal=1);   //propane
   Modelica.SIunits.MassFraction z_n(start=0,min=0,max=1,nominal=1);   //nitrogen
end Fluid;
```

Listing A.1 Fluids connector in the PE3Lib library.

```
connector Solid
  //Total solids flow
  flow Modelica.SIunits.MassFlowRate w_s(start=0,min=0,max=1,nominal=1);

  //Mass fractions, polymer, formed in current component
  Modelica.SIunits.MassFraction ksi_pe1(start=0,min=0,max=1,nominal=1);  //C2 polymer
  Modelica.SIunits.MassFraction ksi_pb1(start=0,min=0,max=1,nominal=1);  //C4 polymer

  //Mass fractions, polymer, formed in previous component
  Modelica.SIunits.MassFraction ksi_pe2(start=0,min=0,max=1,nominal=1);  //C2 polymer
  Modelica.SIunits.MassFraction ksi_pb2(start=0,min=0,max=1,nominal=1);  //C4 polymer

  //Mass fraction, catalyst
  Modelica.SIunits.MassFraction ksi_c1(start=0,min=0,max=1,nominal=1);

  //Catalyst mean activation, deactivated sites
  Real c_a(start=0,min=0,max=1,nominal=1);
  Real c_d(start=0,min=0,max=1,nominal=1);

  //Melt index and density
  Real MI(start=0,min=0,max=1,nominal=1);
  Modelica.SIunits.Density rho(start=0,min=0,max=1,nominal=1);
end Solid;
```

Listing A.2 Solids connector in the PE3Lib library.

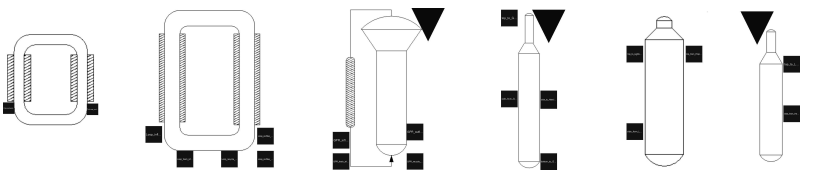

Figure A.1. Interface models of the three reactors and three distillation columns in the PE3Lib library. *From left to right*: Pre-polymerization reactor, loop reactor, gas-phase reactor, propane column, heavies column and lights column.

pelleting and packaging, are not included in the library, it was decided not to add this connector. However, it is straight forward to add it if desired.

Except for the connectors, the interface models also contain declaration of variables, which it is required to provide equations for when performing the modeling. Such variables are, for instance, the mass of ethylene and hydrogen in the reactors. The variables are given minimum, maximum and nominal values, which are important at optimization.

A.3. Components

The Components package contains the reactor and distillation column models, but also models used for routing flows.

The reactor and distillation column models extend the corresponding interfaces and implements the models, i.e., contain the equations describ-

```
//Fluids
der(m_e1)= u_e1 - w_f1*m_e1/m_f1 - r_e1;   //ethylene
der(m_h1)= u_h1 - w_f1*m_h1/m_f1 - r_h1;   //hydrogen
der(m_p1)= u_p1 - w_f1*m_p1/m_f1;          //propane
m_f1 = m_e1 + m_h1 + m_p1;                 //total fluids mass

//Solids
der(m_pe1) = r_pe1 - w_s1*m_pe1/m_s1;      //polyethylene
der(m_c1) = u_c1 - w_s1*m_c1/m_s1;         //catalyst
m_s1 = m_pe1 + m_c1;                       //total solids mass
```

Listing A.3 An excerpt from the pre-polymerization reactor model in the PE3Lib library.

ing the different plant units. Listing A.3 gives an excerpt of the pre-polymerization reactor model, showing the mass balances, and can be compared to the equations in Paper VI. The models must at least have equations for the variables specified in the interface models, but how detailed the models are depend on the modeler. The component models also introduce variables not found in the interfaces and they are given minimum, maximum and nominal values.

Different levels of model detail may be used for e.g., calibration, optimization and simulation. In the current library, only one level of detail for each plant unit is considered. However, since the library utilizes interface models for the units, it is straightforward to implement models of lower or higher complexity and use them interchangeably, as long as they adhere to the specified in- and output structures. The means to perform such extensions and direct changes of utilized models are main features of the library, valuable for its continued development.

The models used for flow routing are sources, sinks, an adder and multiplexers. The sources yield constant outflows of fluids and/or solids with different properties, while the sinks receive the flows. Both of these are useful when analyzing e.g., one reactor model at the time. The adder component adds two fluid flows that are described by the structure in the connectors, i.e., total flow and flow ratios for the different components. For instance, the top and bottom flow of the propane column are added together using the adder component before being fed into the GPR. The multiplexers have several fluid inputs, each with only one fluid component, and one fluid output connector. The inputs are transformed into one flow described by the structure in the fluid connector. The multiplexers are used when multiplexing the different fresh inflows before they are fed to the reactors.

A.4. Templates

Models in the Templates package define different plant topologies, such as what plant units and control flows to use when performing calibration,

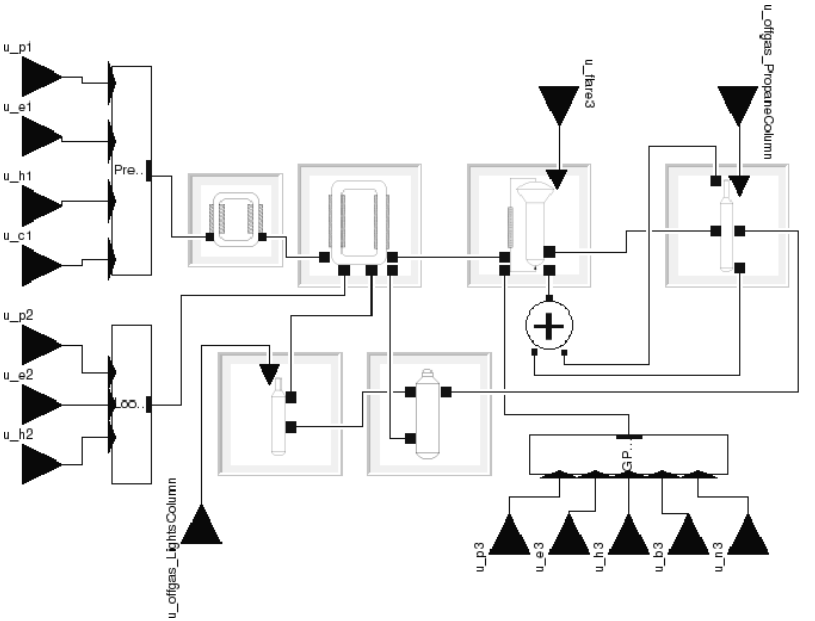

Figure A.2. Template in the PE3Lib library describing the topology of the plant PE3 at Borealis AB with three reactors, three distillation columns and 15 inputs.

optimization and simulation. The different template models use the interface models of the plant units as replaceable models. Figure A.2 shows the template model used in grade change optimizations in Paper VI. The template models, as they only contain the interface models, can not be simulated. It must be defined what model from the Components package is to be used for each unit, made by using the redeclare notation. Templates are useful as the plant topology is setup only once. It can then be used with unit models with different levels of detail as long as the unit models adhere to the in- and output structures defined in the Interfaces package. The library contains the template in Figure A.2 and a template for using only the three cascaded reactors without the distillation columns.

A.5. Experiments

The Experiments package contains three packages: Calibration, Optimization, and Simulation. The models in all three packages use the template models, i.e., setups of plant topologies.

The Calibration package contains models for calibration of stationary operating points using averaged plant data from stationary production. It

has also simulation models used at calibration with plant data recorded during transitions. For both calibration cases, models with and without the recycle area of the plant are included in the library.

The `Optimization` package include models for finding stationary points, stationary optimization, generation of initial guesses to the dynamic optimization problem, and dynamic optimization of grade changes. Each of these comes in two different versions, one where only the three cascaded reactors are used, as in Paper IV, and one where the three reactors and the three distillation columns are used, as in Paper VI. As the models use the templates, they must define which implemented models are to be used for the different units. This feature is, as noted previously, important in the future when models with different levels of detail are implemented.

In the optimization models, some parameter and variable values are set. For instance, in the models for finding stationary operating points and in the models used for optimization of stationary operating points, correct grade is set together with all derivatives equal to 0. The resulting operating points are used as initial values in the models for generating initial guesses for the dynamic optimizations and in the models for dynamic optimizations.

When working with large model libraries, it is advantageous to use a simulation and modeling software. Therefore, the reactor library has been built using the software Dymola, see [Dassault Systemes, 2011]. However, as the Optimica extension, used for formulation of optimization problems, is not an official extension of the Modelica language, it is not supported by Dymola. Accordingly, using Optimica constructs for expressing the optimization problems yield errors in Dymola. Therefore, models to be used in the optimization problem, not containing any Optimica constructs, are implemented in the library. They are subsequently extended by separate models, outside the library, that contain Optimica constructs to fully cover the optimization problems. These additional models, which are similar to the optimization model in Example 2.2, Section 2.5, contain e.g., the definitions of the cost functions to be used and the time intervals for the dynamic optimizations. One of the main reasons to implement as much as possible of the optimization models in the library is due to the use of Dymola, as it helps the user to find modeling errors by helpful messages at model compilation.

The `Simulation` package contains models with the same setups as in the `Optimization` package and are used for validation of optimization results. Inflow trajectories resulting from optimizations may be used as inputs to the models. For verification, Dymola or SUNDIALS through JModelica.org, are used for simulation of the models. See [Hindmarsh *et al.*, 2005] for an overview of SUNDIALS. The collocation based method used in the dynamic optimizations corresponds to a fixed step size Radau

solver, while both Dymola and SUNDIALS use more advanced solvers. Hence, if the simulation results and optimization results are equal within considered tolerances, it is likely that the optimization results fulfill the non-discretized dynamic constraints.

A.6. Miscellaneous

The Miscellaneous package contains various packages with parameters and constants used by the models in sections A.2–A.5.

Packages with reactor and distillation column parameters and constants, such as reaction kinetics parameters, distillation column split factors and reactor volumes, are found in the Miscellaneous package. Additionally, a package with physical constants, such as molar weights, is also implemented.

Minimum, maximum and nominal values for the variables in the different models in sections A.2–A.5 are found in associated packages.

For the different grades, packages containing grade definitions, i.e., target values and intervals for the different quality variables, are provided. Cost function parameters, both for optimization using a quadratic cost function and optimization regarding plant economy, are found in separate packages.

Several stationary operating points of the plant, corresponding to different polymer grades and found using the stationarity models in the Experiments package, are saved in associated packages. They are mainly used by the optimization and simulation models in the Experiments package as initial values and desired end values during grade changes.

References

Andersson, N., P. Larsson, J. Åkesson, S. Haugwitz, and B. Nilsson (2011): "Calibration of a polyethylene plant for grade change optimizations." In *Proceedings of the 21st European Symposium on Computer-Aided Process Engineering*. Chalkidiki, Greece.

Dassault Systemes (2011): "Dassault Systemes Home Page." `http://www.3ds.com/products/catia/portfolio/dymola`.

Hindmarsh, A., P. Brown, K. Grant, S. Lee, R. Serban, D. Shumaker, and C. Woodward (2005): "Sundials: Suite of nonlinear and differential/algebraic equation solvers." *ACM Trans. Math. Softw.*, **31**, September, pp. 363–396.

Larsson, P., N. Andersson, J. Åkesson, and S. Haugwitz (2010): "Modelica Based Grade Change Optimization for a Polyethylene Reactor." In *Proceedings of the 9th International Symposium on Dynamics and Control of Process Systems*. Leuven, Belgium.